

---

# **Understanding and controlling the collisions of ultracold polar molecules**

**Roman Bause**

---



München 2022



---

# **Understanding and controlling the collisions of ultracold polar molecules**

---

Dissertation  
an der Fakultät für Physik  
der Ludwig-Maximilians-Universität München

vorgelegt von

**Roman Bause**

München, den 11. Februar 2022

Erstgutachter: Prof. Dr. Immanuel Bloch  
Zweitgutachter: Prof. Dr. Olivier Dulieu  
Datum der mündlichen Prüfung: 30.03.2022

# Zusammenfassung

Ultrakalte polare Moleküle bieten eine Vielzahl von faszinierenden Möglichkeiten für physikalische Forschung. Die Vorschläge für ihre Nutzung reichen von Quantenchemie, wo sie detaillierte Untersuchung von Reaktionsprozessen erlauben, über Präzisionsspektroskopie zur Detektion von Supersymmetrie oder Dunkler Materie, bis hin zur Simulation stark wechselwirkender Quantenmaterie. Die hohe Anzahl von internen Freiheitsgraden der Moleküle, die all diese Anwendungen erst ermöglicht, bringt jedoch auch signifikante Schwierigkeiten mit sich. Entsprechend ist es eine nicht zu unterschätzende Aufgabe, ultrakalte Moleküle in Experimenten herzustellen und zu kontrollieren. Obwohl während der letzten Jahrzehnte große Anstrengungen unternommen wurden, experimentelle Techniken zu entwickeln und verbessern, ist die Kühlung von Molekülen noch immer schwierig und die tiefsten erreichten Temperaturen sind weit von dem entfernt, was mit atomaren Gasen möglich ist. Aus diesem Grund konnte bis heute die überwiegende Mehrzahl der vorhergesagten neuen Quantenphasen nicht realisiert werden. In den vergangenen zehn Jahren waren unverstandene und verlustbehaftete Stoßprozesse zwischen Molekülen das größte Hindernis. Sie machten evaporative Kühlung sehr schwierig und begrenzten die Lebensdauer stark wechselwirkender Gase mit hoher Dichte.

In dieser Dissertation berichte ich über Fortschritte bei der experimentellen Kontrolle von fermionischen polaren Molekülen der Spezies  $^{23}\text{Na}^{40}\text{K}$ , die es schließlich erlaubten, die Stoßprozesse zu regulieren und evaporative Kühlung zu demonstrieren. In Kapitel 1 gebe ich eine Einführung in die Molekülphysik. Ich erkläre dort die grundlegenden Eigenschaften zweiatomiger Moleküle und ihrer Quantenzustände sowie deren gruppentheoretische Beschreibung. Dies ermöglicht das Verständnis der Herausforderungen des Forschungsfeldes. Darauf folgt in Kapitel 2 eine chronologische Zusammenfassung der Entwicklungen dieses Feldes in den letzten Jahrzehnten. Diese soll nicht nur die erfolgreichen Pfade betrachten, sondern auch die Vielzahl an Sackgassen und Umwegen, ohne die der Erfolg nicht möglich gewesen wäre. Ab Kapitel 3 beschreibe ich neue Forschung. Kapitel 3 ist auf eine technische Verbesserung fokussiert: Es beschreibt ein neues Lasersystem für *stimulated Raman adiabatic passage* (STIRAP), das unser Team gebaut und getestet hat. Dieses Lasersystem hat die Effizienz der Molekülerzeugung verbessert und einen großen Beitrag zur Vereinfachung unserer Experimente geleistet. Kapitel 4 enthält eine Untersuchung des  $X^1\Sigma^+ \leftrightarrow b^3\Pi_0$ -Übergangs im  $^{23}\text{Na}^{40}\text{K}$ -Molekül. Es handelt sich hierbei um einen nahezu dipolverbotenen Übergang mit entsprechend schmaler Linienbreite, der außerdem im Spektrum der Übergänge relativ isoliert liegt. Dies erlaubt es, nahe am Übergang sowohl anziehende als auch abstoßende optische Dipolfallen zu erzeugen, ohne dabei hohe Photonenstreuaten in Kauf nehmen zu müssen. Außerdem kann durch kleine Änderungen der Wellenlänge die Wirkung der Dipolfalle auf bestimmte Rotationszustände gesteuert werden, was sich für viele Experimente als nützlich erwiesen hat. Kapitel 5 beinhaltet eine Untersuchung von Stößen zwischen zwei Molekülen im internen Grundzustand bei extrem geringer Lichtintensität. Mithilfe einer repulsiven, zylinderförmigen Dipolfalle konnte unser Team zeigen, dass die Verlustrate bei Zweikörperstößen von  $^{23}\text{Na}^{40}\text{K}$  nicht von der Lichtintensität abhängt. Diese Messung steht im Wider-

spruch mit theoretischen Vorhersagen sowie Beobachtungen an anderen Molekülspezies, wurde jedoch von Kollegen aus Hong Kong und Hannover bestätigt. Dieses Rätsel ist aktuell ungelöst. In Kapitel 6 beschreibe ich die erfolgreiche Demonstration einer Methode zur Unterdrückung der Zweikörperverluste. Mittels starker Mikrowellenfelder werden dabei Wechselwirkungen erzeugt, die bei ausreichend kurzem Abstand abstoßend wirken und Moleküle daran hindern, sich zu nahe zu kommen. Mit diesem Mikrowellenschild konnte unser Team evaporative Kühlung von polaren Molekülen durchführen und das derzeit kälteste molekulare Quantengas bei einer Temperatur von 21 nK herstellen. Eine Reihe an Vorhersagen, die bis jetzt nicht experimentell realisiert werden konnten, sind damit nun erreichbar geworden. Daher gebe ich schließlich in Kapitel 7 einen Überblick über diese neuen Möglichkeiten. Dieses Kapitel enthält Abschätzungen darüber wie realistisch die Umsetzung ausgewählter Vorhersagen ist und welche experimentellen Herausforderungen zu erwarten sind.

# Abstract

Ultracold polar molecules offer a multitude of fascinating possibilities for physical research. Proposals for their use reach from quantum chemistry, where they enable detailed studies of reaction processes, to precision spectroscopy for detecting supersymmetry or dark matter, to simulating of strongly interacting quantum matter. However, the large number of internal degrees of freedom, which enables these applications, also causes significant difficulties. Consequently, the task of preparing and controlling molecules in experiments is not to be underestimated. Though large efforts have been undertaken to develop and improve experimental techniques during recent decades, the cooling of molecules remains difficult, and the lowest reachable temperatures are still far higher than with atoms. Therefore, the majority of predicted new quantum phases could not be realised yet. During the last ten years, the main obstacle were lossy collision processes between molecules, which are still not understood. They have made evaporative cooling very difficult and have limited the lifetime of strongly interacting gases at high density.

In this dissertation, I report on progress in the experimental control of fermionic polar molecules of  $^{23}\text{Na}^{40}\text{K}$ , which allowed regulating the collisions and demonstrating evaporative cooling. In Chapter 1, I give an introduction to molecule physics. I explain the fundamental properties of diatomic molecules and their quantum states, as well as their group-theoretical description. This allows understanding of the challenges of the field. Chapter 2 follows with a chronological summary of the developments in ultracold-molecule research during recent decades. It focuses not only on the paths which turned out to be successful, but also sheds light on the many detours and dead ends without which success could not have been achieved. Beginning from Chapter 3, I describe original research. Chapter 3 is focused on a technical improvement: it describes a new laser system for *stimulated Raman adiabatic passage* (STIRAP), which our team built and tested. This laser system has improved the efficiency of molecule creation and has contributed greatly to simplifying our experiments. Chapter 4 contains an investigation of the  $X^1\Sigma^+ \leftrightarrow b^3\Pi_0$  transition in the  $^{23}\text{Na}^{40}\text{K}$  molecule. This transition is almost dipole-forbidden with a correspondingly small linewidth. Additionally, its position is relatively isolated in the transition spectrum. This allows the creation of both attractive and repulsive dipole traps near the transition. Furthermore, small wavelength changes can influence the effect of the dipole trap on specific rotational states, which has turned out to be useful for many experiments. Chapter 5 treats collisions between molecules in their internal ground state at extremely low light intensity. By using a repulsive, cylinder-shaped dipole trap, our team was able to show that the loss rate in two-body collisions of  $^{23}\text{Na}^{40}\text{K}$  is independent of light intensity. This measurement is in strong contradiction with theoretical predictions and with observations on other molecule species, but has been confirmed by colleagues in Hong Kong and Hannover. As of now, this riddle remains unsolved. In Chapter 6, I describe the successful demonstration of a method for suppressing these two-body losses. With strong microwave fields, interactions can be induced which become repulsive at sufficiently small distance and thereby prevent colliding molecules from coming too close to each other. This microwave shielding has enabled our team to demonstrate evaporative

cooling of polar molecules, and to create the currently coldest molecular quantum gas at a temperature of 21 nK. With this, a number of predictions, which were previously out of experimental reach have now become feasible. Therefore, in Chapter 7, I give an overview of these new possibilities. This chapter contains estimations about how realistic certain proposals are and which experimental challenges are to be expected.

# List of publications

The following articles have been published in the context of this dissertation:

- Frauke Seeßelberg, Xin-Yu Luo, Ming Li, Roman Bause, Svetlana Kotochigova, Immanuel Bloch, and Christoph Gohle: *Extending Rotational Coherence of Interacting Polar Molecules in a Spin-Decoupled Magic Trap*. Physical Review Letters 121, 253401 (2018). DOI: 10.1103/PhysRevLett.121.253401
- Roman Bause, Ming Li, Andreas Schindewolf, Xing-Yan Chen, Marcel Duda, Svetlana Kotochigova, Immanuel Bloch, and Xin-Yu Luo: *Tune-Out and Magic Wave-lengths for Ground-State  $^{23}\text{Na}^{40}\text{K}$  Molecules*. Physical Review Letters 125, 023201 (2020). DOI: 10.1103/PhysRevLett.125.023201
- Roman Bause, Andreas Schindewolf, Renhao Tao, Marcel Duda, Xing-Yan Chen, Goulven Quéméner, Tijs Karman, Arthur Christianen, Immanuel Bloch, and Xin-Yu Luo: *Collisions of ultracold molecules in bright and dark optical dipole traps*. Physical Review Research 3, 033013 (2021). DOI: 10.1103/PhysRevResearch.3.033013
- Roman Bause, Akira Kamijo, Xing-Yan Chen, Marcel Duda, Andreas Schindewolf, Immanuel Bloch, and Xin-Yu Luo: *Efficient conversion of closed-channel-dominated Feshbach molecules of  $^{23}\text{Na}^{40}\text{K}$  to their absolute ground state*. Physical Review A 104, 043321 (2021). DOI: 10.1103/PhysRevA.104.043321
- Xing-Yan Chen, Marcel Duda, Andreas Schindewolf, Roman Bause, Immanuel Bloch, and Xin-Yu Luo: *Suppression of Unitary Three-body Loss in a Degenerate Bose–Fermi Mixture*. Physical Review Letters 128, 153401 (2022). DOI: 10.1103/PhysRevLett.128.153401
- Marcel Duda, Xing-Yan Chen, Andreas Schindewolf, Roman Bause, Jonas von Milczewski, Richard Schmidt, Immanuel Bloch, and Xin-Yu Luo: *Transition from a polaronic condensate to a degenerate Fermi gas of heteronuclear molecules*. Arxiv preprint: <https://arxiv.org/abs/2111.04301>
- Andreas Schindewolf, Roman Bause, Xing-Yan Chen, Marcel Duda, Tijs Karman, Immanuel Bloch, and Xin-Yu Luo: *Evaporation of microwave-shielded polar molecules to quantum degeneracy*. Arxiv preprint: <https://arxiv.org/abs/2201.05143>
- Marcel Duda, Xing-Yan Chen, Roman Bause, Andreas Schindewolf, Immanuel Bloch, and Xin-Yu Luo: *Long-lived fermionic Feshbach molecules with tunable  $p$ -wave interactions*. Arxiv preprint: <https://arxiv.org/abs/2202.06940>



# Contents

<b>1. Fundamentals of molecular physics</b>	<b>1</b>
1.1. The structure of molecules . . . . .	1
1.1.1. Some intuition . . . . .	2
1.1.2. The symmetries of molecules . . . . .	9
1.1.3. Nomenclature and angular momentum . . . . .	14
1.1.4. Molecular transitions . . . . .	19
1.1.5. A note on dipole moments . . . . .	21
1.2. Fundamental problems of molecule cooling . . . . .	23
1.2.1. The laser-cooling conundrum . . . . .	23
1.2.2. The collision conundrum . . . . .	24
1.3. The NaK molecule . . . . .	25
<b>2. Ultracold molecules: A historical overview</b>	<b>29</b>
2.1. Before the 1990s: Moving towards the ultracold . . . . .	30
2.2. 1990–1999: A slow beginning . . . . .	31
2.3. 2000–2007: A field of its own . . . . .	38
2.3.1. Homonuclear alkali dimers and BEC-BCS crossover . . . . .	38
2.3.2. Towards associating polar molecules . . . . .	41
2.4. 2008–2011: Breakthroughs . . . . .	48
2.4.1. An ultracold Fermi gas . . . . .	48
2.4.2. Laser-cooling molecules . . . . .	51
2.4.3. Further developments . . . . .	53
2.5. 2012–2017: Hard times . . . . .	55
2.5.1. Associated molecules: Headfirst into the collision conundrum . .	55
2.5.2. The first molecule MOT . . . . .	59
2.5.3. New approaches to direct cooling . . . . .	61
2.6. 2018–2022: The second breakthrough? . . . . .	62
2.6.1. Quantum control at single-molecule level . . . . .	62
2.6.2. Collisions and evaporation . . . . .	64

2.6.3. Polyatomic and alkaline-earth molecules . . . . .	66
2.6.4. Fundamental physics with molecules . . . . .	67
2.7. Future directions . . . . .	69
<b>3. A new STIRAP setup</b>	<b>71</b>
3.1. Creation of Feshbach molecules . . . . .	71
3.1.1. Theoretical description . . . . .	71
3.1.2. Experimental procedure . . . . .	74
3.2. STIRAP setup . . . . .	77
3.2.1. Laser sources and locking . . . . .	77
3.2.2. Reference cavity . . . . .	79
3.2.3. Filtering and amplification . . . . .	81
3.3. Results . . . . .	83
3.3.1. Spectroscopy of the pump and Stokes transitions . . . . .	83
3.3.2. Determination of Rabi frequencies . . . . .	85
3.3.3. STIRAP and laser noise reduction . . . . .	88
<b>4. Near-resonant dipole trapping</b>	<b>93</b>
4.1. The $X^1\Sigma^+ \leftrightarrow b^3\Pi_0$ transition . . . . .	93
4.2. Experimental setup . . . . .	97
4.3. Tune-out frequency . . . . .	97
4.4. Magic frequency . . . . .	98
4.5. Intensity calibration . . . . .	101
4.6. Polarisability measurements . . . . .	102
4.7. Lifetime measurements . . . . .	106
4.8. Potential applications . . . . .	108
<b>5. Collisions of ground-state molecules</b>	<b>111</b>
5.1. Sticky complexes . . . . .	111
5.1.1. RRKM theory . . . . .	111
5.1.2. The recollision hypothesis . . . . .	112
5.2. Loss in a bright trap . . . . .	114
5.2.1. Data analysis . . . . .	114
5.2.2. Temperature dependence of collisions . . . . .	116
5.2.3. Dipolar collisions . . . . .	118
5.3. Temporally dark dipole trap . . . . .	119
5.4. The box trap . . . . .	123
5.4.1. Optical setup . . . . .	123
5.4.2. Electric-field levitation . . . . .	126

5.4.3. Residual intensity in the box . . . . .	126
5.5. Loss measurements in the box trap . . . . .	129
5.5.1. Data analysis . . . . .	129
5.5.2. Light-intensity dependence of collisional loss . . . . .	131
5.5.3. Dipolar collisions . . . . .	134
5.5.4. Enhanced sticking time due to p-wave barrier . . . . .	134
5.6. Discussion . . . . .	136
<b>6. Microwave shielding</b>	<b>139</b>
6.1. Motivation . . . . .	139
6.2. Operating principle . . . . .	140
6.3. Implementation with NaK . . . . .	141
6.4. Shielding effectiveness . . . . .	145
6.4.1. Data analysis . . . . .	145
6.4.2. Calibration measurements . . . . .	146
6.4.3. Elastic and inelastic collision rates . . . . .	147
6.5. Evaporative cooling . . . . .	149
6.5.1. Thermometry . . . . .	150
6.5.2. Evaporation procedure and results . . . . .	152
<b>7. Next steps for dipolar many-body physics</b>	<b>155</b>
7.1. Motivation . . . . .	155
7.2. Ground work . . . . .	156
7.3. Fermi-surface deformation . . . . .	158
7.4. Dipolar Wigner crystal . . . . .	159
7.5. Stripe phases and superfluidity in 2D bulk . . . . .	160
7.6. Rotational synchronisation . . . . .	161
7.7. Dipolar XY and XXZ models . . . . .	162
7.8. Checkerboard and stripe phases on a square lattice . . . . .	163
7.9. Supersolidity and superfluidity on cubic lattices or bilayers . . . . .	164
7.10. Topological superfluidity in 2D . . . . .	165
7.11. Conclusion . . . . .	166
<b>Appendix A. List of heteronuclear alkali dimers</b>	<b>167</b>
A.1. NaLi . . . . .	167
A.2. LiK . . . . .	169
A.3. LiRb . . . . .	170
A.4. LiCs . . . . .	171
A.5. NaK . . . . .	172

A.6. NaRb . . . . .	174
A.7. NaCs . . . . .	175
A.8. KRb . . . . .	176
A.9. KCs . . . . .	178
A.10. RbCs . . . . .	179
<b>Appendix B. Theory of dipolar many-body systems</b>	<b>181</b>
<b>Bibliography</b>	<b>183</b>
<b>Acknowledgements</b>	<b>233</b>





*The atoms may be compared to the letters of the alphabet, which can be put together into innumerable ways to form words. So the atoms are combined in equal variety to form what are called molecules.*

—W. H. Bragg, *Concerning the Nature of Things*

# 1. Fundamentals of molecular physics

## 1.1. The structure of molecules

A molecule is an electrically neutral state of multiple atoms, which is bound strongly enough to withstand at least some nudging without dissociating. In more formal terms, according to the *Compendium of Chemical Terminology*, a molecule is defined as “an electrically neutral entity consisting of more than one atom ( $n > 1$ ). Rigorously, a molecule, in which  $n > 1$  must correspond to a depression on the potential energy surface that is deep enough to confine at least one vibrational state” [1]. Molecular bonds can arise between almost any combination of elements. This is because in the vast majority of cases, the potential of two nuclei in close proximity allows more energetically favourable electron orbitals than that of one nucleus does.

In the grand scheme of things, only a small fraction of the matter in the universe consists of molecules, with most baryonic matter being either in the form of plasma or dilute atomic gases, at temperatures too high for molecules to be stable. However, from a human perspective, all the most interesting matter, such as life on earth, is made primarily of molecules. However, here I am interested in molecules for a different reason: diatomic molecules are the most complicated objects in nature that can be understood in full detail down to the quantum level at the current state of human knowledge. In this sense, they are at the frontier of fundamental physics, making them both a fascinating object of study in their own right, and an extremely versatile tool that opens up new possibilities in other areas.

A diatomic molecule can be described by the Hamiltonian [2, 3]

$$\begin{aligned} H = & -\frac{\hbar^2}{2m_e} \sum_i \nabla_i^2 - \frac{\hbar^2}{2m_a} \nabla_a^2 - \frac{\hbar^2}{2m_b} \nabla_b^2 \\ & - \sum_i \frac{Z_a e^2}{4\pi\epsilon_0 r_{ia}} - \sum_i \frac{Z_b e^2}{4\pi\epsilon_0 r_{ib}} + \sum_{i>j} \frac{e^2}{4\pi\epsilon_0 r_{ij}} + \frac{Z_a Z_b e^2}{4\pi\epsilon_0 r_{ab}} \\ & + H_{\text{rel}} + H_{\text{Lamb}} + H_{\text{HFS}}, \end{aligned} \quad (1.1)$$

where the index  $i$  runs over all the electrons in the molecule, and the two nuclei are

labelled  $a$  and  $b$  with nuclear charge numbers  $Z_a$  and  $Z_b$ . The symbols  $m_e$ ,  $m_a$ , and  $m_b$  denote the electron mass and the masses of the nuclei, respectively,  $\nabla^2$  are Laplace operators with respect to the coordinates of an electron or nucleus, and  $r$  stands for the distance between the two objects given by its indices. The first line of this Hamiltonian describes the kinetic energy of all constituent particles and the second line contains all of their respective Coulomb interactions. The third line contains approximate correction terms which account for relativistic effects, including spin-orbit and spin-spin coupling between electrons, and a hyperfine structure term which describes the interaction between the nuclear magnetic and electric moments and the electrons.

At first sight, this Hamiltonian looks completely intractable, and to some degree this is true: although diatomic molecules were some of the first systems that were investigated after the advent of quantum mechanics a century ago, there is still no end in sight. Even the most sophisticated numerical calculations available today are not able to predict the properties of diatomic molecules *ab initio* with the precision required for many tasks, making it necessary to develop theory and experiment step by step, using experimental results to determine theory parameters and vice versa. This process has now led to a situation where molecular physicists can be confident that any relevant question pertaining to a diatomic molecule *can* be answered, even though it might still take months or years to actually *do* it, depending on the details. In contrast, for the internal structure of atoms it is now fairly rare to find a relevant question that has not been answered yet (at least when limited to Standard Model physics), while for larger molecules, some problems remain practically impossible.

### 1.1.1. Some intuition

Luckily, there are approximations which can make the understanding of certain aspects of molecular structure much simpler and allow us to develop some intuition rather than having to perform complicated calculations at every turn. The most important one is the *Born–Oppenheimer approximation*. It makes use of the fact that the nuclei are much heavier than the electrons, such that coupling between nuclear and electronic motion can be ignored. The total wavefunction then neatly separates into a product of its electronic and nuclear parts. Essentially, the electronic motion is so fast that the nuclei can be assumed to be static and the electronic motion can be calculated for the Coulomb potential of two point charges at a fixed distance.

Because the true many-body wavefunction of all electrons in a molecule (or an atom) is a potentially very complicated object, it is basically impossible to visually imagine. However, by ignoring the interaction between the electrons, it becomes possible to think of the electron wavefunctions as being a fixed set of orbitals, which can be populated by electrons according to the Pauli principle. Hence, while ignoring electron-electron interactions is typically a very bad approximation in a quantitative sense, it is extremely helpful for visualisation.

With these two approximations, it becomes possible to calculate molecular orbitals, i.e., wavefunctions of electrons in the potential of the nuclei. Still, it is typically not possible to

find exact solutions to this problem. A conceptually simple way to calculate the orbitals is to approximate them as *linear combinations of atomic orbitals* of the constituent atoms. This is called the LCAO ansatz. With two atoms  $a$  and  $b$ , and their respective set of orbitals  $\psi_i^{a/b}$ , the set of molecular orbitals  $\psi_j^{\text{mol}}$  is then written as

$$\psi_j^{\text{mol}} = \sum_i \left( c_{ij}^a \psi_i^a + c_{ij}^b \psi_i^b \right). \quad (1.2)$$

In this formalism, one can think of the atomic orbitals as a basis for the space of molecular orbitals. The coefficients  $c_{ij}^{a/b}$  can sometimes be determined analytically using variational methods, but using numerical quantum-chemistry calculations is now much more common.

In principle, all atomic orbitals can contribute to a molecular orbital, but in the majority of cases, all but one or two of the  $c_{ij}^{a/b}$  are very small. If there is a molecular orbital which contains appreciable contributions from two or more atomic orbitals, it is said that the contributing atomic orbitals mix. Reasonable guesses about the mixing strength can be made with the following rules of thumb [4]:

1. Atomic orbitals with a larger overlap mix more strongly.
2. Atomic orbitals with similar energies mix more strongly.
3. Only symmetry-compatible atomic orbitals can mix. (This also follows from rule 1, as orbitals which are non-compatible are orthogonal and their overlap must vanish.)

As lower-lying atomic orbitals are situated closer to their nucleus and therefore have smaller overlaps with the orbitals of the other atom, they are influenced less and remain similar to the single-atom case. In many cases, only the highest populated orbitals have appreciable mixing, such that a molecule can be visualised as two atoms which share their valence electrons. Specifically in the case of bialkali molecules, a relatively good description can be reached by only considering two electrons, while all the others behave like in a free atom. In the homonuclear case, it is also reasonable to assume that strong mixing only exists between identical atomic orbitals.

Molecular orbitals are firstly characterised by their angular momentum. The main difference to the case of an atom is that an atom possesses spherical symmetry, such that the (orbital) angular momentum of an electron is a conserved quantity (also called a *good quantum number*). A diatomic molecule, in contrast, is cylindrically symmetric, which means that only the projection of angular momentum onto the internuclear axis is conserved. In analogy to the atomic case, the corresponding quantum number is called  $\lambda$ , and its values are labelled  $\sigma, \pi, \delta, \phi, \dots$ , just like atomic  $s, p, d, f, \dots$  orbitals. A further important characteristic of a molecular orbital results from the relative phase of the atomic wavefunctions: if it is such that the atomic orbitals interfere constructively in the area of their largest overlap, this leads to an energetically more favourable configuration as the electron density becomes higher in the area where the Coulomb attraction from both nuclei is relatively strong. Such states are called *bonding*. Conversely, if the interference

is destructive, there is a nodal plane of the wavefunction in this area, which results in an orbital energy that is typically higher than that of the sum of the unbound atoms. Such states are called *antibonding* and are marked  $\sigma^*, \pi^*, \delta^*, \phi^*, \dots$ . Sometimes a further label is added to mark which atomic orbitals are involved in the bond, such as  $\sigma_{1s}, \sigma_{2p}, \pi_{2p}$ , etc. Often, the bonding and antibonding orbitals are shown in a molecular orbital diagram (see Figure 1.1 a), which can be a very useful tool to determine some characteristics like the spin of the ground state, or make qualitative guesses about binding energies. Since each electronic state can contain a large number of different vibrational, rotational and hyperfine states, it is common to not speak of electronic “states”, but rather call them “manifolds” or “potentials”.

Figures 1.2 to 1.4 show three-dimensional visualisations of certain molecular orbitals and may help gaining an intuitive understanding of their properties. Though they are not quantitatively correct, they do convey the essential features of each orbital. As these figures show, the deformation of atomic orbitals by a molecular bond can be significant, and it results in correspondingly significant energy shifts on the order of  $10000\text{cm}^{-1}$ . (The inverse centimetre is a convenient unit to express molecular energy scales:  $1\text{cm}^{-1} \approx h \times 30.0\text{GHz} \approx 1.24 \times 10^{-4}\text{eV} \approx k_B \times 1.44\text{K} \approx 1.99 \times 10^{-23}\text{J}$ .) In a nutshell, these energy differences are the reason why chemistry exists.

Just as it was reasonable to assume the nuclei to be fixed when working out the electron wavefunction, the fast electron dynamics average out from the perspective of the nuclei in the Born–Oppenheimer approximation. The interaction between the nuclei can then again be modelled as a motion in a static potential. This results in molecular potential curves where the energy of a molecule in a given electronic state is plotted versus the internuclear distance (see Figure 1.1 b). The resulting nuclear motion can be separated into vibrational and rotational degrees of freedom. The vibrational motion is similar to a harmonic oscillator, such that its energy levels are approximately given by

$$E_{\text{vib}} = \hbar\omega(v + 1/2) \quad (1.3)$$

corresponding to the vibrational quantum number  $v$  and the vibrational spacing  $\omega$  (see Figure 1.1 c). Due to the strong binding, the level spacing is relatively large, typically  $\hbar\omega \sim 10\text{cm}^{-1}$ . The harmonic-oscillator approximation is often quite good, especially for low vibrational levels in deep electronic potentials.

In a similar fashion, the rotational motion of the nuclei can be approximated reasonably well as a quantum rigid rotor with energy levels

$$E_{\text{rot}} = B_{\text{rot}}R(R + 1) \quad (1.4)$$

with the rotational quantum number  $R$  and the rotational constant  $B_{\text{rot}}$  (see Figure 1.1 d). Typically, the rotational spacing is on the order of  $B_{\text{rot}} \sim 0.1\text{cm}^{-1}$ , becoming larger with smaller internuclear distance or higher mass of the nuclei. Within the rigid-rotor approximation

$$B_{\text{rot}} = \frac{\hbar^2}{2\mu r_0^2}, \quad (1.5)$$

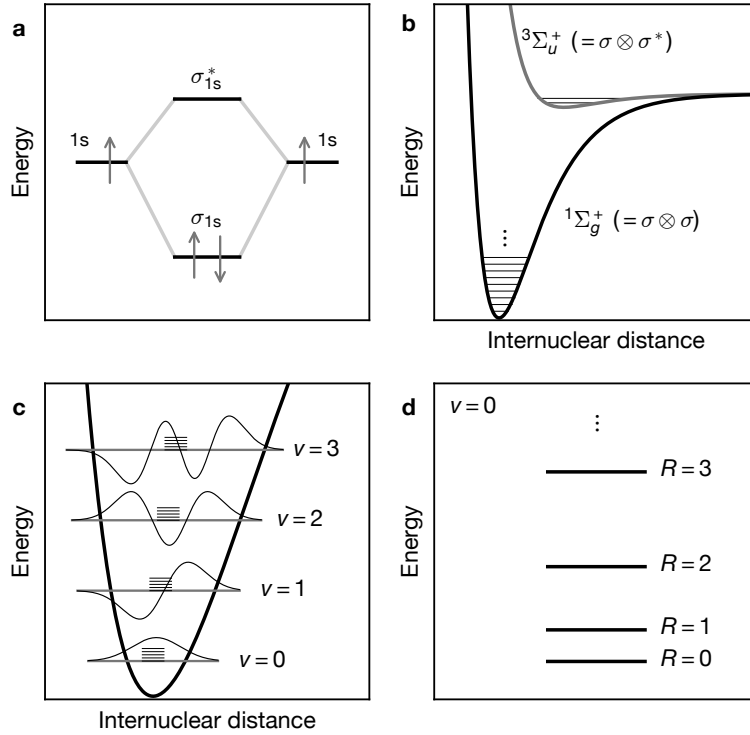


**Figure 1.1.:** Simplified model of molecular bonding and the energy scales of electronic and nuclear motion. **(a)** Molecular orbital diagram for the ground state of  $\text{H}_2$ . On the left and right are the  $1s$  orbitals of each hydrogen atom, in the centre are the two molecular orbitals formed from their combination. The bonding  $\sigma$  orbital is lowered in energy, while the antibonding  $\sigma^*$  is increased. **(b)** Molecule potentials for a homonuclear molecule of hydrogen-like atoms. For large internuclear distances, the energy asymptotically approaches that of two free atoms, while for very small distances, the Pauli repulsion between the electrons becomes dominating. In the middle, there is a sweet spot where molecular bonds occur. The electronic ground state with both electrons in the  $\sigma$  state is called  $^1\Sigma_g^+$ . The only other bound state belonging to the same atomic asymptote (i.e., constructed from the same atomic orbitals) is the  $^3\Sigma_u^+$ , where one electron is in  $\sigma^*$  and the electron-spin wavefunction is symmetric. Vibrational levels belonging to both electronic potentials are shown schematically. **(c)** Zoom-in into the lower vibrational levels. Close to the potential minimum, the vibrational wavefunctions resemble those of a harmonic oscillator. Rotational levels belonging to each vibrational level are shown schematically. **(d)** Zoom-in into the rotational levels belonging to a single vibrational state.

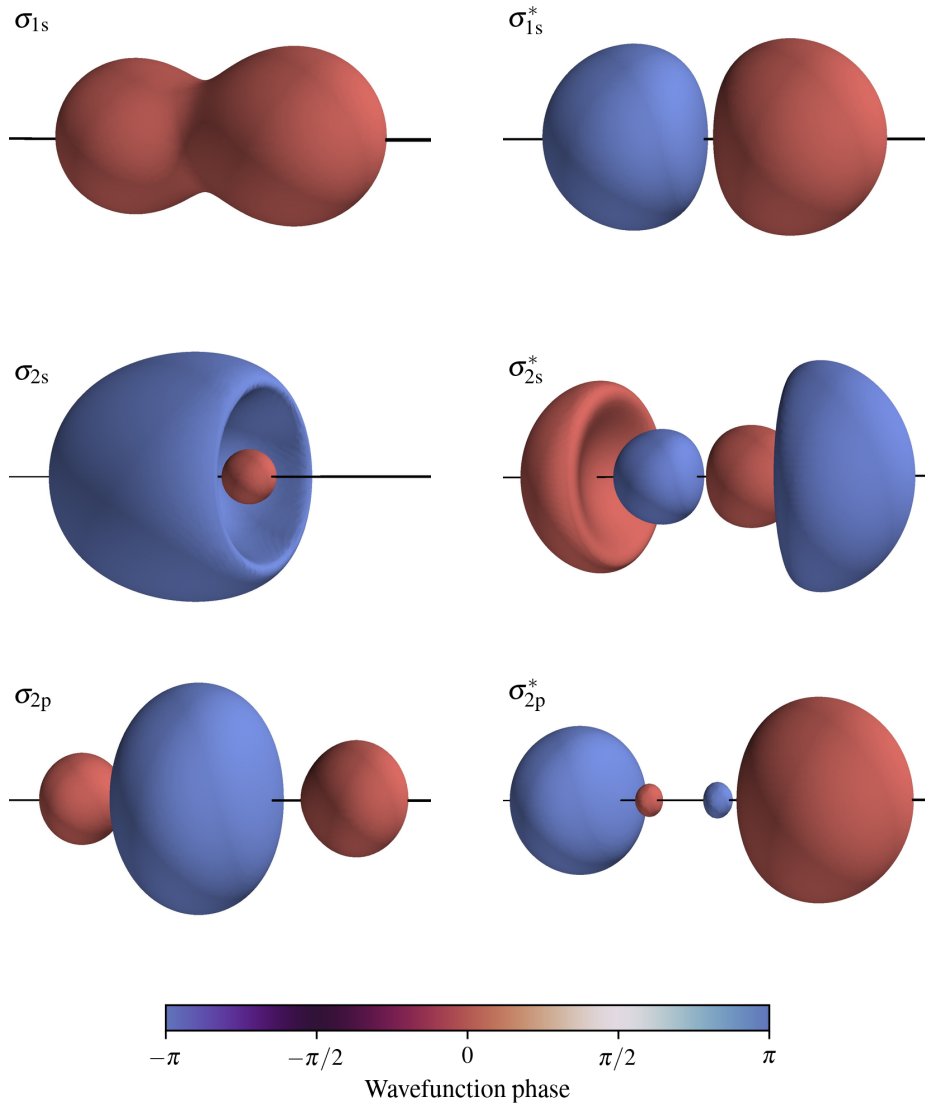


**Figure 1.2.:** Visualisations of selected molecular orbitals with  $\sigma$  character. The shapes correspond to isosurfaces of the electron probability distribution. The surface colour corresponds to the complex phase of the wavefunction at this position. The internuclear axis is shown as a black line. Note that these images are qualitative sketches, intended to help with intuitive understanding. The viewing angle, global phase, isosurface value and internuclear distance are adjusted for optimal visibility and are not necessarily consistent between different orbitals.

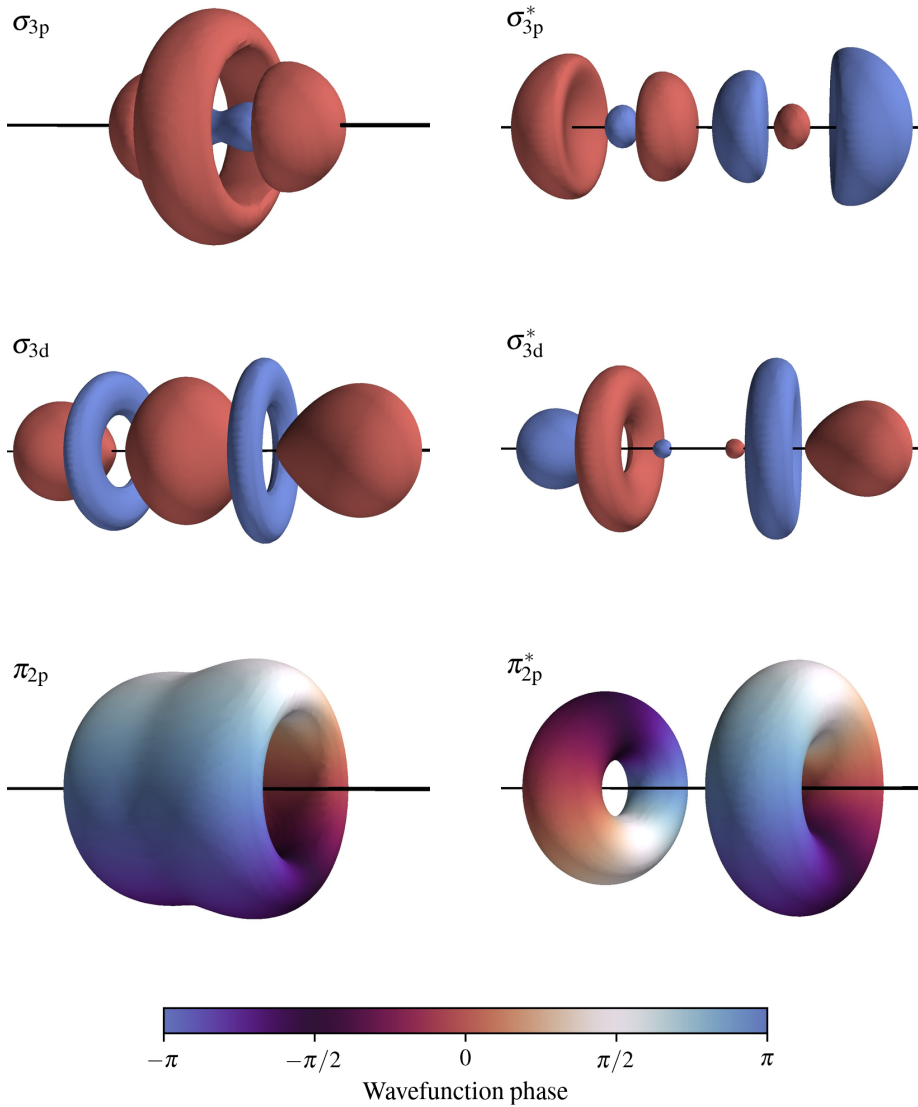


**Figure 1.3.:** Visualisations of selected molecular orbitals with  $\sigma$  and  $\pi$  character. The shapes correspond to isosurfaces of the electron probability distribution. The surface colour corresponds to the complex phase of the wavefunction at this position. The internuclear axis is shown as a black line. Note that these images are qualitative sketches, intended to help with intuitive understanding. The viewing angle, global phase, isosurface value and internuclear distance are adjusted for optimal visibility and are not necessarily consistent between different orbitals.

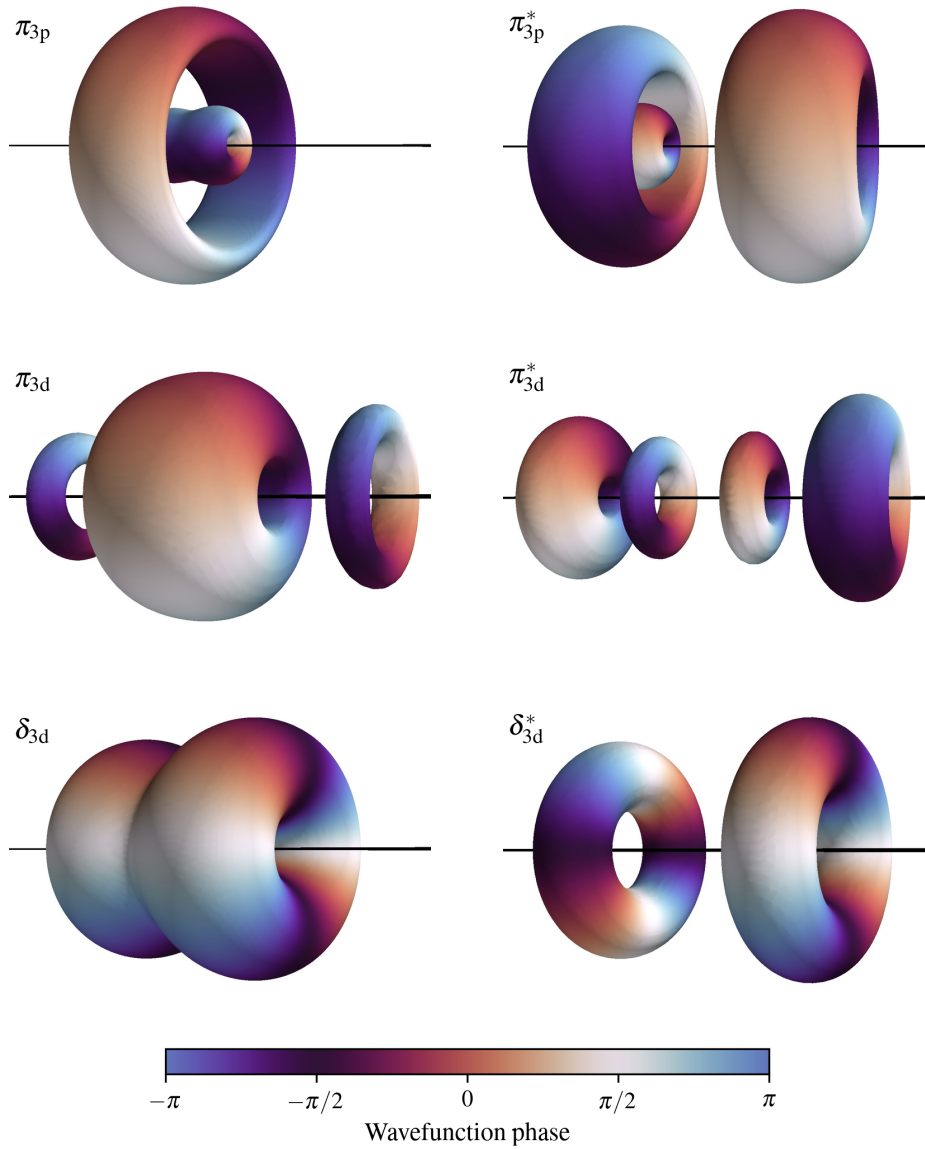


**Figure 1.4:** Visualisations of selected molecular orbitals with  $\pi$  and  $\delta$  character. The shapes correspond to isosurfaces of the electron probability distribution. The surface colour corresponds to the complex phase of the wavefunction at this position. The internuclear axis is shown as a black line. Note that these images are qualitative sketches, intended to help with intuitive understanding. The viewing angle, global phase, isosurface value and internuclear distance are adjusted for optimal visibility and are not necessarily consistent between different orbitals.

where  $\mu$  is the reduced mass of the nuclei and  $r_0$  the internuclear distance. Again, the rigid-rotor approximation is quite accurate especially for low rotational levels. Methods to predict rovibrational spectra more precisely as well as quantify the rotation-vibration interaction can be found, for example, in the textbooks by Herzberg [5] and by Demtröder [6]. The latter is also an excellent general introduction to molecule physics, but only available in German. An up-to-date overview of the rotational structure of molecules and its control in experiments can be found in Reference [7].

### 1.1.2. The symmetries of molecules

The electron wavefunctions shown in Figures 1.2 to 1.4 are highly symmetric objects. This is of course not a random occurrence, but a consequence of the underlying symmetry of the physical system. This symmetry is deeply connected to the physical properties of molecules and its understanding can form a foundation for the understanding of molecules. Because symmetry is a fundamental property of a molecule, the discussion in this section is very general and almost exact. There can be small symmetry-breaking effects caused by external fields or extremely small effects caused by non-symmetric terms of the Hamiltonian itself, which will be discussed later. By and large, however, the electromagnetic interaction within a molecule dominates over all external influences or other potentially symmetry-breaking forces. This means that the symmetries are almost perfectly realised in real molecules. Therefore, symmetries are ideal for obtaining fundamental understanding and for classifying molecular states.

The formal, group-theoretical<sup>1</sup> description of molecular symmetry begins with the fact that there is a set of symmetry operators  $\mathcal{S}$  under which the wavefunctions of a molecule are invariant in some sense [4, 9]. These operators must therefore commute with the molecular Hamiltonian  $H$ , and consequently also its unitary time evolution,  $e^{-iHt/\hbar}$ . Technically, the elements of  $\mathcal{S}$  are operators on an infinite-dimensional Hilbert space, but for single-electron states, they have a straightforward interpretation as transformations in position space, i.e., they map from  $\mathbb{R}^3$  to  $\mathbb{R}^3$ . As is typically the case for symmetry transformations, they fulfil all the properties of a group, which is called the *point group* of the molecule. Though this method also works for larger molecules, I will focus on the diatomic case here. For the case of a homonuclear diatomic molecule, the point group is called  $D_{\infty h}$ , and it contains the following symmetry transformations<sup>2</sup>:

1. The identity transformation  $E$ .
2. An infinite number of rotations  $C_n$ , which rotate by the angle  $2\pi/n$  about the internuclear axis.
3. An infinite number of reflections  $\sigma_v$  about any plane containing the internuclear axis.

---

<sup>1</sup>An excellent introduction to group theory, though not one specific to molecules, can be found in the textbook by Byron and Fuller [8].

<sup>2</sup>The transformations are named according to *Schoenflies notation*, the most commonly used convention in molecular physics.

4. The inversion transformation  $i$  with the midpoint of the internuclear axis as its centre.
5. An infinite number of rotation-reflection transformations  $S_n$ . Each of them consists of a rotation about the internuclear axis by the angle  $2\pi/n$  and a reflection on the plane orthogonal to this axis and through its midpoint. These are also called improper rotations.
6. An infinite number of 2-fold rotations  $C_2$ , about any axis orthogonal to the internuclear axis and through its midpoint.

To gain some intuition for these transformations, it may be helpful to visualise them with the states shown in Figures 1.2 - 1.4. In the case of a heteronuclear diatomic molecule, there is no inversion symmetry and the resulting point group, which is called  $C_{\infty v}$ , contains only the transformations (1)–(3) from the list above.

In order to effectively describe a point group, its elements can be categorised into *conjugacy classes*. They are the equivalence classes of the conjugation operation: if there exists a  $T$  in the group such that  $B = T^{-1}AT$ , then  $A$  and  $B$  belong to the same conjugacy class. This is strongly connected to our physical intuition about the symmetry operations. For example, reflections on a given plane all belong to the same class. Conversely, rotations and reflections, which we intuitively consider fundamentally different, are never in the same class. Hence, the conjugacy classes tell us how many fundamentally different transformations there are in the group.

In our specific case, the group  $D_{\infty h}$ , the classes are as follows: the identity  $E$  and the inversion  $i$  each form their own class with only one member. The  $C_n$  rotations are conjugate only if they rotate by the same angle, but regardless of direction. Hence, there is a class with two members (clockwise and counter-clockwise rotation) for every value of  $n$ . The same holds analogously for the improper  $S_n$  rotations. Finally, the  $\sigma_v$ -reflections and the  $C_2$ -rotations each have one class which contains all of these transformations. Both of these therefore have infinitely many members. For all the transformations which are also contained in  $C_{\infty v}$ , the conjugacy classes are the same.

Next, we need to describe how each class of transformations affects the wavefunction of a given molecular state. Some of them leave it completely invariant, while others might change its phase, leaving only the associated probability distribution invariant. As there are both infinitely many states and infinitely many transformations, one might expect the job of classifying each combination to be impossible, but in fact it turns out to be remarkably simple. This is because the states can also be sorted into equivalence classes, and the effect of each class of transformations on each class of states is the same. Hence, just the knowledge of a relatively small number of combinations is enough to gain lots of information about a molecular state. The equivalence classes of states are called the *irreducible representations* of the group, though some mental gymnastics is required to see why this makes sense.

In general, a representation of a group  $G$  is a map  $t : G \rightarrow GL$  which preserves the group structure, i.e.  $t(T \circ S) = t(T) \circ t(S)$  for  $S, T \in G$  with the group operation  $\circ$ . Here,  $GL$  stands for some set of linear transformations of a vector space, i.e.,  $n \times n$  matrices

in the finite-dimensional case or invertible operators in the infinite-dimensional case. In informal terminology it is common to refer to not only the map itself but also the set of matrices or operators it maps to as a representation. The most obvious representation of a point group is the one which maps to  $\mathcal{S}$ , the set of symmetry operators, but there are also infinitely many others. Importantly, for a map to be a representation, it is not required to carry over the entire complexity of the group: for example, for any group there is a trivial representation which maps every element to a unit matrix. A representation is called irreducible if it does not permit any nontrivial invariant subspaces of its underlying vector space. A nontrivial invariant subspace in this sense is a subspace of the vector space with dimension higher than one, which every vector remains inside under the action of any transformation. In matrix language, this corresponds to the statement that there is no basis in which every matrix in the representation has block-diagonal form.

From the group-theoretical point of view, the significance of irreducible representations comes from the fact that any possible representation can be uniquely decomposed into a direct sum of irreducible representations [9]. In other words, for any representation there is a basis in which it has block-diagonal form, and all the non-zero blocks in this matrix are irreducible representations. Hence, the vector space the representation acts upon is divided into invariant subspaces, each of which corresponds to one irreducible representation.

Now some magic happens: each irreducible representation can be identified with the vectors in its invariant subspace. As all the symmetry operators commute with the molecular Hamiltonian, there is a simultaneous eigenbasis of both, and the invariant subspaces correspond to degenerate eigenspaces of the Hamiltonian. Though the Hilbert space of all possible wavefunctions of a molecule is an astoundingly complicated thing, this method remarkably makes it possible to sort all the elements of this space into just a few intuitively understandable types. The correspondence between states and representations is not one-to-one; there can be many degenerate eigenspaces which correspond to the same irreducible representation, but every degenerate eigenspace belongs to exactly one irreducible representation of the point group. In other words, states of different energy *can* have the same symmetry properties, but states of the same energy *must* have the same symmetry properties. An important exception here is *accidental degeneracy*, where states from two uncoupled subspaces of the Hamiltonian happen to have the same energy but different symmetry properties.

This is where the physical significance of irreducible representations comes from: they give us an equivalence relation on the Hilbert space of molecular wavefunctions, which categorises them into subspaces according to their symmetry. This also shows a connection between degeneracy and symmetry: a symmetry operator can never change the energy of a state, therefore every state must belong to an irreducible representation with dimension equal to its degeneracy. The irreducible representations are named according to the following scheme:

1. By symmetry under rotation around the principal axis:  $\Sigma$  for representations which are invariant under any rotation, then capital Greek letters  $\Pi, \Delta, \dots$  for ones which are invariant under rotations by integer multiples of  $2\pi/n$ . A  $\Pi$  representation is

invariant only under rotations by  $2\pi$ , a  $\Delta$  also under rotations by  $\pi$ , and so on.

2. By symmetry under inversion  $i$ : An index  $g$  denotes symmetric representations under  $i$ , an index  $u$  antisymmetric ones. The letters  $g$  and  $u$  stand for the German words *gerade* and *ungerade*, meaning even and odd.
3. By symmetry under  $\sigma_v$ -reflections: symmetric representations get an index  $+$ , antisymmetric ones a  $-$ . Note that only  $\Sigma$  representations are purely symmetric or antisymmetric, all other ones receive complex phase shifts.

To understand the action of a symmetry operator on a given state, it is not necessary to know the explicit form of the operator. Instead, everything of importance can be encoded in a single number, the *character* of the representation. It is defined as the trace of the representation, i.e., the sum of the diagonal elements of the corresponding matrix. As the trace is invariant under conjugation, the character is the same for all transformations in a conjugacy class. The physical meaning of the character becomes clear when looking at the effect of operators in  $\mathcal{S}$  on eigenstates of the Hamiltonian: In the case of a one-dimensional representation, the character is equal to its expectation value with respect to the corresponding state. In the higher-dimensional case, the expectation values with respect to all basis states are added up. Visually, one can imagine the one-dimensional case as follows: if a state is transformed by a certain symmetry operator, then how much overlap does it have with the original version of itself? For states that remain completely invariant, this is 1, for antisymmetric states, it is  $-1$ , and for rotations, the overlap will depend on the angle. In the higher-dimensional cases, it is instead the sum of overlaps with all the transformed versions of the state.

All this information can be compiled into *character tables* for each symmetry group, which are an essential tool of molecule physics. The character tables for  $D_{\infty h}$  and  $C_{\infty v}$  are given in Tables 1.1 and 1.2. In these tables, the  $C_n$  and  $S_n$  rotations are only represented by a single column, which is the general case of a rotation by the angle  $\phi$ . Is it denoted  $2C_\infty^\phi$  or  $2S_\infty^\phi$ . The numbers in front of the conjugacy class names are a reminder of the number of elements in this class.

Now it should become clear what this digression into mathematics was good for: we now have a powerful tool which allows us to capture a large amount of information about a molecular state by just stating which irreducible representation it belongs to. The behaviour of the state under any symmetry transformation can then be read off from the corresponding character table.

Here are some examples for what can be learned from Table 1.1. The behaviour under the identity transformation in the first column tells us the degeneracy of a state: all  $\Sigma$  states are nondegenerate, whereas all other states are two-fold degenerate. This comes about because the direction of phase-rotation (i.e., the angular momentum) can be either parallel or antiparallel with the internuclear axis. Next, the  $C_\infty^\phi$  rotations by an angle  $\phi$  around the internuclear axis lead to an overlap proportional to  $\cos n\phi$ . Hence,  $\Sigma$  states are invariant under all rotations, since their phase does not depend on rotations. Note that the imaginary part of the overlap is cancelled out because the expectation values for clockwise and counter-clockwise rotations are added up. Applying  $\sigma_v$ -reflections to a  $\Sigma$  state can

**Table 1.1.:** Character table of the point group  $D_{\infty h}$ , the symmetry group of a homonuclear diatomic molecule. Each column stands for a conjugacy class, each row for an irreducible representation.

	$E$	$2C_{\infty}^{\phi}$	...	$\infty\sigma_v$	$i$	$2S_{\infty}^{\phi}$	...	$\infty C_2$
$\Sigma_g^+$	1	1	...	1	1	1	...	1
$\Sigma_g^-$	1	1	...	-1	1	1	...	-1
$\Pi_g$	2	$2\cos\phi$	...	0	2	$-2\cos\phi$	...	0
$\Delta_g$	2	$2\cos 2\phi$	...	0	2	$2\cos 2\phi$	...	0
...	...	...	...	...	...	...	...	...
$\Sigma_u^+$	1	1	...	1	-1	-1	...	-1
$\Sigma_u^-$	1	1	...	-1	-1	-1	...	1
$\Pi_u$	2	$2\cos\phi$	...	0	-2	$2\cos\phi$	...	0
$\Delta_u$	2	$2\cos 2\phi$	...	0	-2	$-2\cos 2\phi$	...	0
...	...	...	...	...	...	...	...	...

**Table 1.2.:** Character table of the point group  $C_{\infty v}$ , the group of symmetry operations of a heteronuclear diatomic molecule. Each column stands for a conjugacy class, each row for an irreducible representation.

	$E$	$2C_{\infty}^{\phi}$	...	$\infty\sigma_v$
$\Sigma^+$	1	1	...	1
$\Sigma^-$	1	1	...	-1
$\Pi$	2	$2\cos\phi$	...	0
$\Delta$	2	$2\cos 2\phi$	...	0
...	...	...	...	...

**Table 1.3.:** Direct products of the irreducible representations of the point groups  $D_{\infty h}$  and  $C_{\infty v}$ . The inversion symmetry obeys the rules  $g \times g = u \times u = g$ ,  $g \times u = u \times g = u$ . Table adapted from [4].

	$\Sigma^+$	$\Sigma^-$	$\Pi$	$\Delta$	...
$\Sigma^+$	$\Sigma^+$	$\Sigma^-$	$\Pi$	$\Delta$	...
$\Sigma^-$		$\Sigma^+$	$\Pi$	$\Delta$	...
$\Pi$			$\Sigma^+, \Sigma^-, \Delta$	$\Pi, \Phi$	...
$\Delta$				$\Sigma^+, \Sigma^-, \Gamma$	...
...	...	...	...	...	...

either lead to an unchanged state or flip the sign, which is indicated by an upper index  $\pm$ . This may at first seem puzzling, because looking at the wavefunctions in Figures 1.2 to 1.4, it is clear that no single-electron wavefunction can actually be antisymmetric under this operation. However it is possible with two electrons in  $\pi$  or higher states, where their orbital angular momenta can cancel out, to form an antisymmetric  $\Sigma^-$  state. On the other hand, all non- $\Sigma$  states are orthogonal to their  $\sigma_v$ -reflected versions, and they consequently do not receive the  $\pm$  index. The  $i$ -reflections leave  $g$  states completely invariant but cause a sign change for  $u$  states. The improper  $S_\infty^\phi$ -rotations are quite similar to rotations, but in some cases receive an additional sign flip from the reflection. Finally, the  $C_2$  rotations lead to no change for  $\Sigma_g^+$  and  $\Sigma_u^-$  states, a sign flip for  $\Sigma_g^-$  and  $\Sigma_u^+$  states, and orthogonal states for everything else.

The group-theoretical description is valid for states with any number of electrons, but it is often not obvious how the one-electron orbitals shown above combine into states. This can be read off the *direct product table*, see Table 1.3. As one might expect, a  $\sigma$  state has  $\Sigma$  symmetry, a  $\pi$  state has  $\Pi$  symmetry, and so on. In the homonuclear case, the antibonding orbitals have  $u$ -symmetry, while the bonding ones have  $g$ -symmetry. Then, the symmetry of the combination of two one-electron states can simply be read off the table. For example, two  $\sigma$  orbitals can only combine into a  $\Sigma^+$  state. When combining states of higher angular momenta, multiple combinations are sometimes allowed. For example, in a combination of two  $\pi$  states, the angular momenta can either cancel out to  $\Sigma$  or add up to  $\Delta$ . This scheme works not only for combining single-electron states, but any states whatsoever can be built up step by step.

### 1.1.3. Nomenclature and angular momentum

In principle, the full quantum state of a molecule could be described by listing the occupation of each molecular orbital and the nuclear quantum numbers. However, even for simple molecules, this description contains a lot of redundant information, such as angular momenta which cancel out. Conversely, relevant characteristics such as the total electronic angular momentum can not be seen directly. Therefore, molecular states are instead characterised by a system that is based on the group-theoretical description of their

**Table 1.4.:** Nomenclature of molecular quantum numbers according to [3, 4, 11]. Here, “projection” always means the projection of the corresponding angular momentum vector onto the quantisation axis.

Total electronic spin	$S$
Total electronic orbital angular momentum	$L$
Total electronic angular momentum	$J_a = L + S$
Total nuclear spin	$I$
Total nuclear orbital angular momentum	$R$
Total angular momentum	$F = R + L + S + I$
Total angular momentum exclusive of nuclear spin	$J = R + L + S$
Total orbital angular momentum	$N = R + L = J - S$
Total angular momentum exclusive of nuclear spin and electronic angular momentum	$O = J - L = R + S$
Magnitude of the projection of total electronic orbital angular momentum $L$	$\Lambda \in \{\Sigma, \Pi, \Delta, \dots\}$
Projection of total electronic spin $S$	$\Sigma$
Magnitude of the projection of total electronic angular momentum $J_a$	$\Omega =  \Sigma + \Lambda $

symmetry. This system was originally proposed by Mulliken in 1930 [10] and has found widespread use since, with only minor modifications. There are excellent overviews of this topic by Herzberg [5] and by Lefebvre-Brion and Fields [3]. The nomenclature used here (see Table 1.4) is identical to the one in References [3, 4, 11], but differs in a few minor points from the original one by Mulliken. The operators are always labelled in boldface, and their eigenvalues are written in roman letters, for example  $J|\psi\rangle = \hbar J|\psi\rangle$ .

When giving the quantum numbers in a transition, primes are used to distinguish the states. By convention, the initial state is not primed, the second state gets one prime, and so on. For example, a transition could go  $J = 0 \rightarrow J' = 1 \rightarrow J'' = 0$ . (There is also a conflicting convention where electronically excited states get a single prime, and all other states get double primes.) It is important to remember that certain quantum numbers are named differently by different authors, as this can easily cause confusion. This is most notoriously the case for the operators called  $R$ ,  $N$ , and  $O$  in the nomenclature used here. It has also been noted that one symbol can sometimes have different meanings depending on context, for example  $\Sigma$  stands for states with electronic angular momentum  $\Lambda = 0$ , but also for the projection of electronic angular momentum onto the quantisation axis. On the other hand, the advantage of this system is that it is a close analogy to the atomic case, where for example  $S$  is double-used in exactly the same way.

Though the nomenclature is comprehensive, it is important to keep in mind that it is based on approximations: molecules are still complicated many-body systems and do not fit into our categories as neatly as we might perhaps like. For example, for any two

non-zero angular momenta in a molecule, there is always some coupling between them, which means that the two corresponding quantum numbers are not strictly conserved. In some cases where the coupling is sufficiently weak, the uncoupled quantum numbers are still useful, but for stronger coupling, it may be necessary to use only their sum. Hence, which quantum numbers are a good basis to use depends strongly on the properties of the molecule under consideration. That being said, there are two commonly used methods to label the electronic states of diatomic molecules. Both of them are somewhat idiosyncratic, but given the equally idiosyncratic nature of molecules themselves, maybe this is just appropriate. The most common nomenclature is this:

$$2S+1 \Lambda_{\Omega, g/u}^{\pm}. \quad (1.6)$$

It is typically used in all those cases where  $\Lambda$  is a good quantum number. The labels  $g/u$  and  $\pm$  stand for the symmetries under inversion and reflection as described in the previous section. The quantum number  $\Omega$  is often omitted in spin-singlet states, where it is trivially equal to  $\Lambda$ .

Of course, this nomenclature does not uniquely identify states, as one molecule can, for example, have many different  ${}^1\Sigma^+$  states. To avoid ambiguity, the states are additionally enumerated according to the energy of their lowest rovibrational levels (i.e., the minimum of the electronic potential). For historical reasons, the enumeration uses latin letters, beginning with  $X$  for the ground state, then continuing in parallel with  $A, B, C, \dots$  and  $a, b, c, \dots$ . The upper-case letters are used for states with the same spin multiplicity as the ground state, and the lower case letters for those with different spin multiplicity. Sometimes this approach is abandoned and the states are instead just enumerated  $1, 2, 3, \dots$ . Importantly, in this case, the enumeration proceeds separately both for states with different spin multiplicity and with different  $\Lambda$ . For example,  $2{}^1\Pi$  is the second-lowest  ${}^1\Pi$  state, not the second-lowest singlet. The nomenclature with numbers is commonly used in molecules where many electronic potentials overlap, such that it becomes difficult to decide their order. Occasionally, letters are used initially, and then numbers for the higher-lying excited states once they become too dense. In some cases, the conventions used for the nomenclature of a certain molecule seem to make very little sense, which is often a relic from times in which the electronic structure was not yet completely understood.

In the naming of states according to  $\Lambda$ , we see a connection to the irreducible representations discussed in the previous section. Indeed, it is precisely the  $\Sigma$  states which belong to those irreducible representations that are completely invariant under rotations, as their phase does not depend on the angle. Similarly, the higher-angular-momentum states correspond to those irreducible representations which behave accordingly under rotations: a phase rotation of  $2\pi$  per full rotation for  $\Pi$  states,  $4\pi$  for  $\Delta$  states, and so on. The same analogy also holds for the  $g/u$  labels.

For those cases where  $\Lambda$  is not a good quantum number, there is an alternative labelling system:

$$\Omega_{g/u}^{\pm}. \quad (1.7)$$

The  $g/u$  and  $\pm$  labels are used just as described above. With this nomenclature, latin

**Table 1.5.:** Relative strength of interactions in the different Hund's cases. In the list of good quantum numbers,  $n$  always stands for other state labels, such as vibration and electronic configuration. Table adapted from [12].

case	interaction strength			good quantum numbers
	electron-axis	spin-orbit	rotational	
(a)	strong	intermediate	weak	$n, J, S, \Omega, \Lambda, \Sigma$
(b)	strong	weak	intermediate	$n, J, S, N, \Lambda$
(c)	intermediate	strong	weak	$n, J, \Omega$
(d)	intermediate	weak	strong	$n, J, L, S, N, R$
(e)	weak	intermediate	strong	$n, J, R$
(e')	weak	strong	intermediate	$n, J, R$

letters are still sometimes added to uniquely identify states, but most commonly this is omitted.

The next question is, how do we know what the good quantum numbers are? Already in the 1920's, it was recognised that there are some classes of diatomic molecules with similar couplings, which can be grouped together to understand them more easily. These classes are called *Hund's coupling cases*, after Friedrich Hund who first described them. In-depth treatments of Hund's cases and the underlying physics can be found, for example, in the publications by Nikitin and Zare [12], Bransden and Joachain [13], Lefebvre-Brion and Fields [3], and Wörner and Merkt [4]. Of course, Hund's cases are merely limiting cases to the real behaviour, and every real molecule falls somewhere between them, but they are often useful to facilitate conceptual thinking about molecular states.

Excluding the hyperfine interactions, whose energy scales are much smaller than those of the electronic and nuclear motion, there are three relevant couplings in a diatomic molecule: first, the electrostatic coupling between the nonspherical component of the electric field of the nuclei and the electron motion. This is the interaction that breaks spherical symmetry and destroys the conservation of  $L$ . It is strongest in molecules with very different nuclei, and much weaker in homonuclear molecules, where the axial component of the electric field of the nuclei vanishes. This is called electron-axis-coupling, because it describes how strong the influence of the direction of the internuclear axis is on the electrons. Second, spin-orbit coupling of the electrons. This can be thought of as an interaction between the magnetic fields associated with the electron's spin and its circular motion, which causes  $L$  and  $S$  to precess about  $J$ . When it is strong enough, spin-orbit coupling breaks the conservation of  $\Lambda$  and  $S$ . Third, coupling between nuclear rotation and electron motion. The relative importance of these three interactions determines the appropriate Hund's case as shown in Table 1.5. Figure 1.5 shows how one can imagine the different angular momenta precessing either about the internuclear axis or about each other, in each coupling case.

In Hund's case (a), the electrostatic coupling of the electronic motion to the internuclear axis dominates. Therefore,  $L$  precesses around the internuclear axis, such that  $\Lambda = |m_L|$ ,

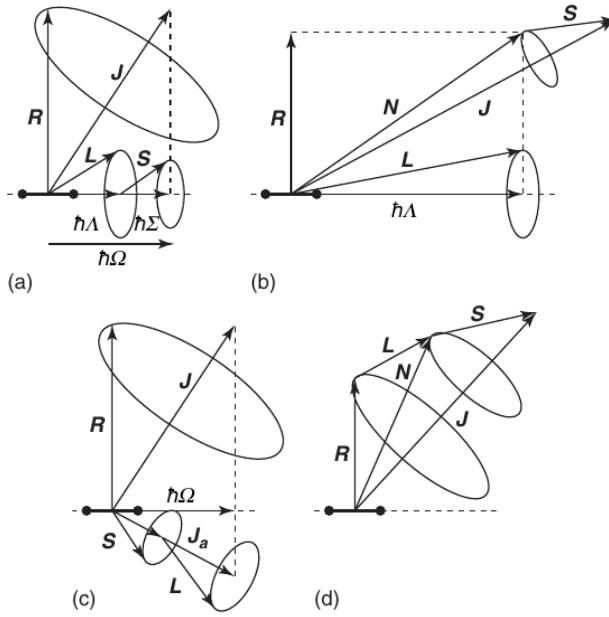


**Figure 1.5.:** Vector precession models of Hund's cases (a) to (d). Figure adapted from [4].

the magnitude of the projection of  $\mathbf{L}$  onto the axis, remains a good quantum number. The spin-orbit interaction is caused by the magnetic field of the rotating electrons, which points along the internuclear axis. Hence, this is also the quantisation axis for the precession of  $\mathbf{S}$ , resulting in the good quantum number  $\Sigma$ , the projection of  $\mathbf{S}$  onto the axis. Obviously, also  $\Omega = |\Lambda + \Sigma|$  is a good quantum number. However, the spin-orbit interaction is not strong enough to destroy the conservation of  $S$ . Just as for all other Hund's cases, the influence of the nuclear spin is weak, such that the total angular momentum exclusive of nuclear spin  $J$ , is also a good quantum number. In Hund's case (a), the  $^{2S+1}\Lambda_{\Omega,g/u}^\pm$  convention is typically used.

Hund's case (b) describes molecules where the spin-orbit interaction is much weaker than the electron-axis coupling, which is typically the case for  $\Sigma$  states. The electronic spin  $\mathbf{S}$  then does not precess about the internuclear axis, such that  $\Sigma$ , and consequently also  $\Omega$ , are not well-defined. On the other hand, the rotational coupling is strong enough to couple the nuclear rotation and electron rotation, giving  $N$  as a good quantum number. States are labelled in the  $^{2S+1}\Lambda_{g/u}^\pm$  convention, identical to the notation in Hund's case (a), but with  $\Omega$  omitted.

In Hund's case (c), the spin-orbit interaction is the dominant one. Here, the coupling between  $\mathbf{S}$  and  $\mathbf{L}$  is so strong that  $S$  and  $L$  separately are no longer good quantum numbers, but  $\Omega$  remains conserved. States corresponding to Hund's case (c) are typically

labelled in the  $\Omega_{g/u}^\pm$  convention.

Hund's cases (d), (e), and (e') are much less common than the previous ones. They describe molecules where the electron-axis coupling is relatively weak, which can be the case for Rydberg molecules with very weakly bound valence electrons. In case (d), the spin-orbit interaction is also weak, such that the rotational interaction becomes the dominant term. In this case,  $\mathbf{L}$  couples directly with  $\mathbf{R}$  to form  $\mathbf{N}$ , but  $L$  and  $S$  remain good quantum numbers due to the weak spin-orbit coupling. In cases (e) and (e'), even this is no longer the case and only  $R$  and  $J$  remain good quantum numbers. There is no generally accepted nomenclature for these cases [12].

### 1.1.4. Molecular transitions

Having discussed the multitude of different quantum numbers and states that exist in molecules, the next question is how to experimentally interact with them. Since molecules are fundamentally governed by electromagnetic interactions, the answer is simple: with electromagnetic fields, which can induce transitions between states. Because of this, transitions are arguably more relevant than states to an experimentalist. In most transitions, a molecule absorbs or emits a single photon. Such one-photon transitions are also called *dipole transitions*, since the field of a single photon contains only dipole contributions. Not all transitions are equal: some states are coupled very strongly, while others are not connected at all via dipole transitions. This can be seen from the dipole operator, which is given by [14]

$$\mathbf{d} = \sum_i q_i \mathbf{x}_i, \quad (1.8)$$

where the summation is over all the constituent particles of the system in question,  $q_i$  are their charges, and  $\mathbf{x}_i$  are their position operators. By sandwiching the dipole operator between the initial and final states of the transition, we find the *transition dipole moment*

$$M_{if} = \langle \psi_i | \mathbf{d} | \psi_f \rangle, \quad (1.9)$$

which is a measure of the transition strength, i.e. the number of photons that are absorbed and re-emitted in a given light field per unit of time is proportional to  $|M_{if}|^2$ . Quantitatively determining a transition dipole moment requires precise knowledge of the initial and final states and can therefore usually only be done numerically, using known spectroscopic data about the molecule in question.

However, there are ways to gain qualitative understanding via *selection rules*, which can give a good intuitive idea of transition strengths. As dipole transitions always involve the exchange of a photon (with spin 1), angular-momentum conservation leads to some selection rules, most importantly

$$\Delta J = 0, \pm 1, \quad (1.10)$$

$$J = 0 \nrightarrow J' = 0. \quad (1.11)$$

This selection rule holds quite generally; the only case in which it can be violated occurs

when a unit of angular momentum is transferred to a nuclear spin degree of freedom via rotational-hyperfine coupling. However, this coupling is typically very weak, such that nuclear spins are almost always conserved. There are a number of corollaries to this selection rule, which follow from the relative coupling strengths in the molecule. For example, for vanishing spin-orbit coupling,  $S$  becomes conserved as well, such that the selection rules become

$$\Delta\Lambda = 0, \pm 1, \quad (1.12)$$

$$\Delta S = 0. \quad (1.13)$$

For light molecules (where spin-orbit coupling is weak), this leads to the emergence of distinct spin-multiplet substructures. For example, in the bialkali case, there are singlets ( $S = 0$ ) and triplets ( $S = 1$ ), and transitions between them are strongly suppressed. With increasing spin-orbit coupling, the strength of transitions which violate this selection rule grows. There are many other, similar selection rules which are valid only in certain Hund's cases, see for example Chapter 5 of Herzberg's textbook [5].

There is also a number of other selection rules which are only indirectly related to angular momentum. The most important one of these is the *parity rule*. Note that the term “parity” is used to mean multiple different things in the literature, which can often lead to confusion.<sup>3</sup> Here, parity ( $P$ ) means the operation that flips the sign of all spatial coordinates, i.e.  $P\psi(x) = \psi(-x)$ . In contrast to the molecular inversion  $i$ , which flips the coordinate signs in the molecule-fixed frame, the operation  $P$  does this in the laboratory frame. This leads to different effects of the two transformations, depending on the rotational state of the molecule. The parity operation  $P$  is the same that is also discussed in the context of  $P$ - or  $CP$ -violation on a fundamental-physics level.

States which remain unchanged under  $P$  are said to have positive (+) parity, while states which obtain a sign flip are said to have negative (−) parity. This is similar to the notation of symmetry for  $\Sigma^\pm$  states for a good reason: it turns out that the previously discussed  $\pm$  symmetry of  $\Sigma$  states under  $\sigma_v$ -reflections is closely related to parity symmetry. They can both be considered equivalent to a  $\sigma_v$ -reflection, however the parity operation changes all signs in the rotational, vibrational, and electronic parts of the wavefunction, while only the electronic part is relevant for the labels  $\Sigma^\pm$ . Explicitly working out the parity of a given state is somewhat complicated; the details can be found in Reference [3]. Suffice it to say that the parity rule is always obeyed, and is often relevant for direct optical cooling schemes, where it can be used to avoid transitions to unwanted states.

One of the fundamental properties of the dipole operator is that it flips the parity of any eigenstate of  $P$  that it acts upon. In addition,  $P$  commutes with any molecular Hamiltonian  $H$  as long as there are no external fields, such that any eigenstate of  $H$  is also an eigenstate of  $P$ . This is because there is no  $P$ -violation in the electromagnetic interaction. Hence, according to Equation (1.9), dipole transitions can only occur between states with different parity. For a similar reason, dipole transitions must also change the  $g/u$  symmetry in the homonuclear case.

---

<sup>3</sup>For a detailed discussion, see Reference [3], Chapter 3.2.2, and Reference [11], Chapter 2.

### 1.1.5. A note on dipole moments

The reason why heteronuclear diatomic molecules are considered interesting is simple: homonuclear diatomic molecules have a mirror-symmetry plane orthogonal to the internuclear axis, but heteronuclear molecules do not. The distribution of electrons is then skewed towards one side, making the heteronuclear diatomic the simplest molecule with a *body-fixed electric dipole moment*. This constitutes the main reason that ultracold molecules are studied today, as they are an ideal basic building block for dipolar quantum matter. Dipolar interactions are fundamentally different from the usual van-der-Waals interactions found in ultracold atoms, because they exhibit much longer range and are spatially anisotropic, i.e., the strength and the sign of the interaction depends on the relative orientation of the dipoles. Specifically, the van-der-Waals potential is given by

$$V_{\text{vdW}} = \frac{C_6}{r^6}, \quad (1.14)$$

with the interaction coefficient  $C_6$  and the distance  $r$ . Due to its fast decay with distance, the low-energy dynamics caused by this interaction can be fully described by a single parameter, the  $s$ -wave scattering length. In contrast, the interaction between two particles with dipole moment  $d$  when the dipole moments are oriented in parallel and the interparticle axis is at an angle  $\theta$  relative to the dipole moment is

$$V_{\text{dd}} = \frac{d^2(1 - 3\cos^2\theta)}{4\pi\epsilon_0 r^3}. \quad (1.15)$$

This interaction has a much longer range, which means that higher partial waves contribute significantly to the scattering dynamics even at low energies. More details about this can be found, for example, in Baranov *et al.*'s review paper [15] and further references therein. Hence, the behaviour of ultracold dipolar gases is qualitatively different from the case with only short-range interactions, making a large dipole moment very interesting and desirable for experiments. However, the origin of the dipole moment is not trivial, and there are some common difficulties and misunderstandings associated with it. This makes it worth looking at the fundamental physics of dipolar particles in some detail.

First, a word about terminology: Especially in chemistry, it is common to say that heteronuclear molecules exhibit a “permanent electric dipole moment”. This name might suggest that a molecule always behaves as an electric dipole, but this is not actually the case. Viewed from the lab frame, a heteronuclear diatomic molecule in the ground state (or any other eigenstate) is a perfectly spherically symmetric object as long as there is no external electromagnetic field. This can be visualised as the molecule being in a superposition state of all spatial orientations. This is analogous to a hydrogen atom, which would be strongly dipolar in a coordinate frame where the proton and the electron lie on a line, but in the lab frame, the wavefunction is spherically symmetric and there is no dipole moment. The situation changes only once the symmetry is broken, typically by an external dc electric field. Though each of the eigenstates of the molecule in the field-free case is rotationally symmetric, an external field mixes them in such a way that a dipole moment

emerges in the lab frame. This is called the *lab-frame* or *effective* dipole moment. This also means that the orientation of molecules in a dipolar system is not a dynamic quantity like a spin in a magnetic field. It only exists by virtue of symmetry breaking caused by the external field and is therefore static. Hence, what is typically called the “permanent” electric dipole moment of a molecule is permanent only in the body-fixed reference frame of the molecule. In the following, I will therefore use the word “body-fixed dipole moment” to distinguish this quantity from, for example, the hypothesised electric dipole moments of certain atoms and elementary particles, which are also called “permanent”, but with a different meaning.

Another misunderstanding may result from the fact that whether a particle features a dipole moment is not directly related to the type of Stark effect<sup>4</sup> it experiences in an external electric field. One might think that a linear Stark effect always corresponds to a permanent dipole moment, whereas a quadratic Stark effect always corresponds to an induced dipole moment. However, the truth is more subtle: the energy shift depends on the details of the internal structure of the particle as well as on the magnitude of the external field.

Importantly, no eigenstate of any isolated atom or molecule possesses a nonzero dipole moment. By “isolated”, I mean here that there are no external fields or close-by objects which could break the isotropy of space. This is because the Hamiltonian of any such system obeys  $P$ -symmetry up to very small deviations (originating from the weak interaction, or from hypothetical beyond-Standard Model physics), and any eigenstate of such a Hamiltonian is also an eigenstate of the parity operator. Since the dipole operator reverses the parity of any state it acts on, its expectation value for any parity eigenstate must vanish. Therefore, strictly speaking, a molecule can not possess a permanent electric dipole moment [18].

However, there are three ways in which the requirements for this statement to be true, can be circumvented, such that a particle can indeed obtain a dipole moment:

1. By breaking the isotropy of space with an external electric field as described above. For systems where no eigenstates of opposite parity are degenerate, perturbation theory shows that there is a quadratic Stark shift. If there are degenerate eigenstates of opposite parity, this will lead to a linear Stark shift as can be seen by applying degenerate perturbation theory. This is, for example, the case for the  $2s$  hydrogen atom, which is, up to relativistic corrections, degenerate with a  $2p$  state of opposite parity. The fact that the states are not precisely degenerate leads to a quadratic Stark shift for weak fields, which only becomes linear once the field is strong enough to overwhelm the splitting between the unperturbed states. The same is true for molecules, where there is a quadratic Stark shift for weak external fields, which becomes linear at stronger fields.

---

<sup>4</sup>I would like to point out here that the Stark effect is named after Johannes Stark, who discovered it and was awarded the 1919 Nobel prize partially for this discovery. Stark was an early supporter of Hitler and the national socialist movement. He devoted a considerable part of his life to the cleansing of “German physics” from supposed “Jewish influences” such as the works of Einstein [16]. His thoughts, laid out for example in a 1938 article in *Nature* [17], make for quite appalling reading.

2. By exciting the particle into a superposition of two states of opposite parity. Since this is not an eigenstate of the Hamiltonian, the argument above does not hold. In this case, the breaking of  $P$ -symmetry is induced by a small background bias field, which is necessary to create a well-defined quantisation axis, and by the polarisation of the field which creates the superposition. Such a superposition state always experiences a linear Stark shift.
3. By a breaking of  $P$ -symmetry on the level of fundamental physics. Such a  $P$ -violation is known to exist for the weak interaction, but is extremely small compared to the energy scales relevant for atoms and molecules. On the other hand, it is indeed highly relevant for the search of beyond-Standard Model physics, where some models predict  $P$ -violations which are still very weak, but much stronger than in the Standard Model, and possibly strong enough to be measured with the most precise methods available today.

## 1.2. Fundamental problems of molecule cooling

I hope that it has become clear that molecules are rich and fascinating objects, which offer an enormous variety of interesting physics to study. However, this complexity is of course not only an advantage. It also makes the task of controlling molecules in experiments a difficult one. For many applications, experiments must be performed at extremely low temperature, where quantum effects start to dominate over thermal fluctuations and new phases of matter like Bose–Einstein condensates and degenerate Fermi gases emerge. Today, this can be done easily enough with atoms, and the wealth of knowledge that ultracold atoms have brought is impressive. Unfortunately, molecules have not yet come this far. This is for the following two reasons.

### 1.2.1. The laser-cooling conundrum

The most important technology in the preparation of ultracold atoms is laser cooling. There are a variety of different laser-cooling methods, but they are all based on the principle that a sample of atoms is illuminated with laser light in such a way that atoms with higher velocity are more likely to absorb photons coming towards them. If the atom undergoes spontaneous emission afterwards, the photon can be re-emitted into any direction, thus slowing the atom down on average. This can also be thought of as a transfer of entropy from the atoms into the laser field, whose photons are initially coherent, but are then randomly scattered around while the atoms are cooled down.

Alkali atoms are ideally suited to this method because they are close to being ideal two-level systems. Hence, the majority of spontaneous emission events will bring the atom back to its initial state, where it can then scatter further photons. This is referred to as a *closed transition*. There typically are a few other weak decay channels available

too, but with the use of a single “repumper” laser, the vast majority of atoms falling into these channels can be brought back into circulation. In this way, an atom that is being laser-cooled can scatter on the order of  $10^6$  photons before being lost.

On the other hand, molecules may have dozens or hundreds of decay channels due to their vibrational structure. The branching ratio, i.e. the probability of a molecule to spontaneously decay back into the state addressed by the cooling laser, is therefore very low. For most molecules, the laser system required to repump all the relevant decay channels would be prohibitively complicated. As I will show in the next chapter, the laser-cooling conundrum has shaped the last two decades of research on ultracold molecules. Especially since 2008, enormous progress has been made, and many ways have been found to either circumvent it or push through it. However, this effort is not yet complete, and laser cooling of molecules is still one of the most significant challenges we face today.

### 1.2.2. The collision conundrum

The natural limitation of laser cooling is the recoil energy: a particle can not become colder than the temperature corresponding to the momentum that a scattered photon imparts on it. As this is still much hotter than the required temperatures in most cases, atoms are typically cooled down further by evaporative cooling. The idea here is to weaken the trap that contains the atoms until those at the high end of the thermal distribution have enough energy to escape. The remaining atoms then thermalise by elastically colliding with each other, refilling the tail of the distribution. This process can be extremely efficient, because every lost atom removes a lot more than the average entropy from the sample. It is typically limited by density: at low densities, most collisions involve only two atoms. If both atoms are in their internal ground states, two-body collisions must necessarily be elastic, since there is no other way to satisfy energy and momentum conservation. Three-body collisions, however, can lead to the formation of a diatomic molecule, while the third atom carries excess energy and momentum away. Such an event causes the loss of all three atoms from the trap, and three-body collisions become more and more likely with higher density, until their detrimental effect outweighs the gains from evaporation. Still, the densities where this happens are quite high for some atoms, and evaporative cooling of atoms is generally a robust and effective method.

For a long time, it was expected that evaporation would also work with molecular gases. Considerable effort was therefore invested into finding molecules which can collide without undergoing chemical reactions or change their internal states. However, every time a molecular species reached the point where evaporative cooling could have become viable, it was found that no elastic collisions occurred. Instead, all the colliding molecules were lost, even in two-body collisions. Serious efforts are still ongoing to achieve evaporative cooling of molecular samples. While they have had some success, the efficiency is still nowhere near as good as with atoms, despite many sophisticated methods being used to improve it. The reasons for the lack of elastic collisions have baffled researchers for years, and still remain partially unclear. Some possible explanations are discussed later in this thesis.

## 1.3. The NaK molecule

The most important molecule in the context of this thesis is of course  $^{23}\text{Na}^{40}\text{K}$ . Though it contains a total of 30 electrons, most of these are in strongly bound atomic orbitals, which are only weakly influenced by the molecule bond. Only the  $3s$  and  $4s$  valence electrons of Na and K, respectively, play an important role for the molecule's properties. This makes its electronic structure relatively simple, as can be seen in the potential curves shown in Figure 1.6. More detailed spectroscopic data can be found in [20–24]. The two-electron structure makes this molecule similar to alkaline-earth atoms such as strontium in that it features distinct spin-singlet and triplet states, with transitions that change the multiplicity being strongly suppressed. This leads to a quite interesting electronic structure with both very strong and very weak transitions. The most important state for our work and the starting point of all our experiments with polar molecules is the absolute ground state in the  $X^1\Sigma^+$  manifold. This means that for example  $b^3\Pi_0$  states can only be reached via very weak and narrow transitions, a fact that has turned out to be extremely useful for much of the work described later.

NaK is an ideal candidate to be associated from atoms for multiple reasons: first, it is made up of two alkali species, which can be laser-cooled with relatively little effort. Sodium and potassium specifically are well-suited for this task because their interactions, both intra- and interspecies, make it possible to mix and associate them easily. Sodium is also a particularly good choice as a sympathetic coolant for potassium, because large samples of it can be created easily [25, 26], and because it is trapped less strongly than potassium in dipole traps, making it evaporate earlier. This is especially important when working with the fermionic isotope  $^{40}\text{K}$ , which is hard to obtain in large numbers due to its small natural abundance of  $10^{-4}$ . The NaK molecule is also chemically stable in the ultracold regime, which means that there are no possible exothermic reactions between two NaK molecules. This property was expected to be very important for a long time, because it was thought it would help avoid the collision conundrum. It has later turned out to be somewhat irrelevant, because even chemically stable molecules are still lost in collisions with almost 100% probability.

Once molecules can be prepared with high efficiency and at low temperature, the most important performance indicator is their lab-frame dipole moment. This quantity determines the strength of dipolar interactions, and it depends both on the body-fixed dipole moment and the rotational constant. The body-fixed dipole moment determines the absolute maximum lab-frame dipole moment that can be reached, however whether this is practically possible depends on the required strength of the electric field. This scales with the rotational constant  $B_{\text{rot}}$ , since the mixing of rotational states is easier if they are energetically closer to each other. For molecules with very high rotational constants, the necessary field can be on the order of 100 kV/cm, which is very challenging to realise experimentally. Favourably low rotational constants are found in molecules with large internuclear distances (i.e., weak bonds) and high mass. Of course, large internuclear distances also lead to weaker body-fixed dipole moments, so some tradeoff has to be made. Among bialkali molecules, NaK offers a reasonable compromise with a body-fixed dipole

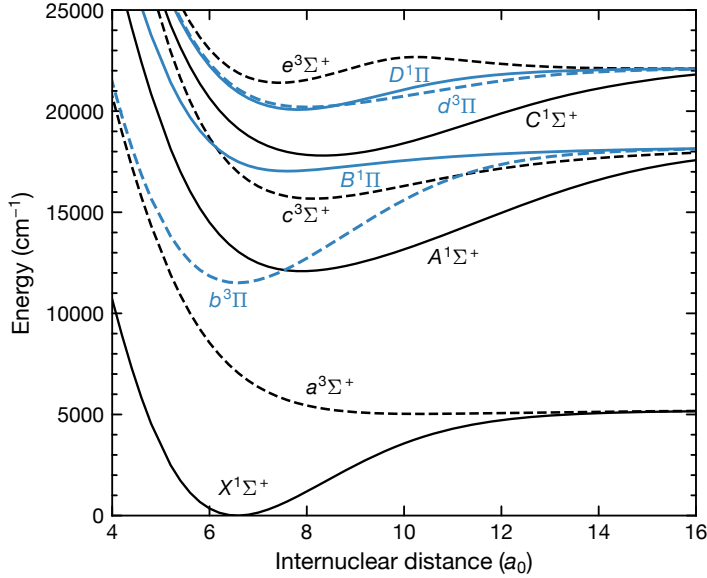


**Figure 1.6.:** Molecular potential curves for NaK, according to calculations from Reference [19]. Internuclear distances are given in units of the Bohr radius  $a_0$ . Solid lines correspond to singlet states, dashed lines to triplets.  $\Sigma$  states are shown in black,  $\Pi$  states in blue. For the work shown here, the most relevant curves are  $X^1\Sigma^+$  (the ground state),  $a^3\Sigma^+$  (the Feshbach state),  $b^3\Pi$  (to create near-resonant dipole traps),  $B^1\Pi \sim c^3\Sigma^+$  (the STIRAP intermediate state), and  $d^3\Pi \sim D^1\Pi$  (the former STIRAP intermediate state).

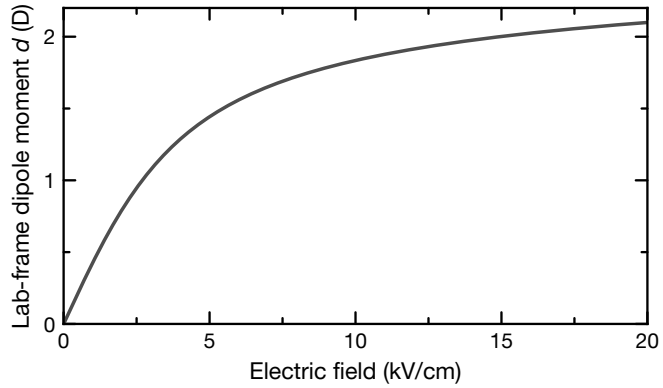


**Figure 1.7.:** Lab-frame dipole moment of NaK depending on the magnitude of the external electric field. The Stark shift is quadratic at low fields, then becomes linear at high fields when the dipole moment reaches saturation. For intermediate fields, which are the most important case in experiments, the behaviour is between these limiting cases.

moment of 2.7 D and a rotational constant of about  $h \times 5.6$  GHz. (The Debye is the cgs unit of electric dipole moment. 1 D =  $3.34 \times 10^{-30}$  Cm.) This means that at a realistically reachable field of 10 kV/cm, a strong dipole moment of 1.85 D can be realised (see Figure 1.7). Finally, potassium has long-lived bosonic and fermionic isotopes, so that NaK can be made in a bosonic and a fermionic variant. As I will discuss later, each of these bring their own distinct challenges and possibilities.



*It is probably unfortunate that physics and chemistry ever were separated.*

—J. C. Slater [28]

## 2. Ultracold molecules: A historical overview

Reading through the introductory paragraphs of ultracold-molecule papers from the last decade, one could come to the conclusion that the field began in 2008 with the seminal experiment of Ni *et al.* [27], which for the first time brought ground-state molecules within reach of quantum degeneracy. The rapid growth we are seeing today makes it seem natural to view our field as beginning a few years ago at a singularity, followed by a period of accelerated expansion. Even though we of course know that this is not strictly true, it is, for the most part, a useful approximation. However, it also means that the important and fascinating developments that led to the breakthrough of 2008 sometimes do not get the attention that they deserve. Here, I hope to follow the development of the field beginning at an earlier point, attempting to shed some light on the steps that led to the creation of the first ultracold molecular quantum gases, and how the field has evolved since then. Even in a relatively small field like this, I can of course not hope to give a complete and comprehensive overview. I merely attempt to cover the most important developments to the best of my knowledge.

The story I will tell is one of the connection of two previously quite different parts of physics, namely chemical physics and ultracold-atom physics. In chemical physics, the interaction between atoms and the properties of molecules have been investigated for almost a century. The defining characteristic of this field is that its objects of study are the molecules themselves and their reactions. Highly sophisticated methods have been developed to this end, including Raman spectroscopy, X-ray diffraction imaging, nuclear magnetic resonance spectroscopy, and many more. In order to obtain more precise results, it has often been necessary to use molecule samples at low temperatures to avoid confounding effects, prompting the development of a variety of cooling techniques.

The second direction is that of quantum many-body systems with ultracold atoms, born from the successful creation of Bose–Einstein condensates and quantum-degenerate Fermi gases in the mid to late 1990s. Due to the unprecedented low temperatures which can be reached in such systems, they allow studying quantum effects which would otherwise be hidden under thermal fluctuations. Researchers in this field aspire to understand the collective behaviour of large quantum systems, their quantum phase transitions and their microscopic evolution.

One might think of the distinction of the two fields as one of energy scales: in chemical

physics, one usually thinks on the order of binding energies or transitions between molecular states, i.e. 0.1 to  $10\,000\,\text{cm}^{-1}$ . These correspond to temperatures of 0.1 to 10 000 K. In contrast, ultracold atom samples are typically confined in traps of a depth equivalent to a few  $\mu\text{K}$ , and reaching even significantly lower temperatures is often necessary in order to see quantum behaviour.

These two fields came in contact when the cooling of atoms had been understood to a degree where it became reasonable to consider associating them into molecules. Simultaneously, the techniques used to cool down molecules directly were also beginning to push into temperature ranges close to those of ultracold atoms. These two approaches were still different in terms of methods, but they had a common goal: to make the coldest possible molecules. It has now become clear that reaching this goal requires an unprecedented level of understanding of the details of molecular structure and collisions. Many times, physicists have found their ultracold molecules behaving in complicated and unexpected ways. In some cases, these observations have led to a better understanding of molecular physics. In other cases, we are still working on solutions to the puzzles found there.

## 2.1. Before the 1990s: Moving towards the ultracold

Before the days of laser cooling, the best way of studying molecules under well-controlled conditions was by using a molecular beam. Such beams can be created in a strikingly simple way: a gas of molecules at high pressure expands through a small hole in its container into a vacuum, where the molecules are then velocity-selected and subsequently used for experiments. This method has been in use since the 1920s and still remains useful due to its simplicity and applicability to a wide range of different molecules. Over the decades, molecular beams have helped physicists understand many aspects of molecular structure and the response of molecules to electromagnetic fields. Perhaps the most well-known among the many groundbreaking discoveries that made use of molecular beams was that of the maser, which worked by shooting a focused beam of ammonia molecules into a microwave cavity, where they became a gain medium [29, 30]. These discoveries are highly interesting in their own right and are treated in an excellent open-access book edited by Friedrich and Schmidt-Böcking [31]. The review articles [32–34] are also highly recommended.

While molecular beams allowed probing the properties of molecules far more precisely than would be possible in liquids or gas clouds, in the 1980s they were still quite far away from being the temperature regimes we today call “ultracold”. Molecule beams could be focused, but slowing them down was much more difficult, and trapping molecules in a three-dimensional potential minimum was not yet possible. This meant that, for example, spectroscopy was still limited by Doppler broadening caused by the broad velocity distribution of molecules. Ideas like producing pure samples of many molecules in a single quantum state or controlling quantum many-body systems of molecules were no more than a dream at this point.

The journey of molecules into the ultracold regime began only when laser cooling and trapping of atoms became possible in the 1980s. Over just a few years between 1980 and 1987, laser cooling of atoms was developed and grew from its infancy to an enormously influential technique. The demonstration of optical molasses [35], the Zeeman slower [36] and the magneto-optical trap (MOT) [37] brought atoms down to microkelvin temperatures and enabled a level of control previously unheard of. These fascinating developments are described for example in the Nobel lectures of Chu, Phillips, and Ketterle [38–40], which are not only insightful but also make for very enjoyable reading. More detailed and complete discussions can be found in References [41–44].

In the late 1980s, the continuing success of atom cooling and trapping provoked some cautious curiosity about whether molecule research might profit from this progress, too. The first concrete idea in this direction was published by Thorsheim *et al.* [45] in 1987: they proposed that a laser beam resonant with a transition from an unbound state of two atoms to a molecular state could be used to associate  $^{23}\text{Na}_2$  molecules in a cloud of  $^{23}\text{Na}$  atoms in a MOT. During a collision, a photon could be absorbed by the colliding atoms, turning them into an excited molecule in a process called photoassociation. The interest in this direction came mostly from a quantum-chemistry perspective, where it had been a long-standing research goal to more deeply understand the reaction processes that occur when two atoms meet down to the quantum level.

This experiment would open up a completely new regime: up to this point, the de-Broglie wavelengths of colliding particles had been much smaller than the range of the interaction potential, such that the dominating reactions could be described semi-classically by reaction rates which scale exponentially with temperature. Thorsheim *et al.* suggested that with ultracold atoms, it would be possible to enter a regime where the de-Broglie wavelength was actually larger than the interaction range. At such low energies, reactions could only happen through tunnelling, making chemistry at these temperature scales a completely quantum phenomenon. It was expected that the efficiency of the photoassociation process would depend strongly on the photon energy, allowing it only on resonance with a molecular transition. With sufficiently cold samples, spectroscopy of photoassociation lines could then reveal molecular structure with extremely high resolution.

Less than one year later, the same group succeeded in making the first step towards their proposal and demonstrated the first observation of molecules formed from laser-cooled atoms. They detected the creation of  $^{23}\text{Na}_2^+$  molecular ions from collision events between two excited Na atoms in optical molasses [46], marking the first time that quantum collisions were observed. In their two papers, the authors specifically cite the development of optical molasses, the magneto-optical trap, magnetic and optical trapping of atoms [47, 48], as well as the improvement of slowing techniques for atomic beams [49, 50] as crucial for their success.

## 2.2. 1990–1999: A slow beginning

The predictions and experiments of Thorsheim *et al.* were not immediately met with enthusiasm: out of the 269 citations listed by the American Physical Society for their 1987

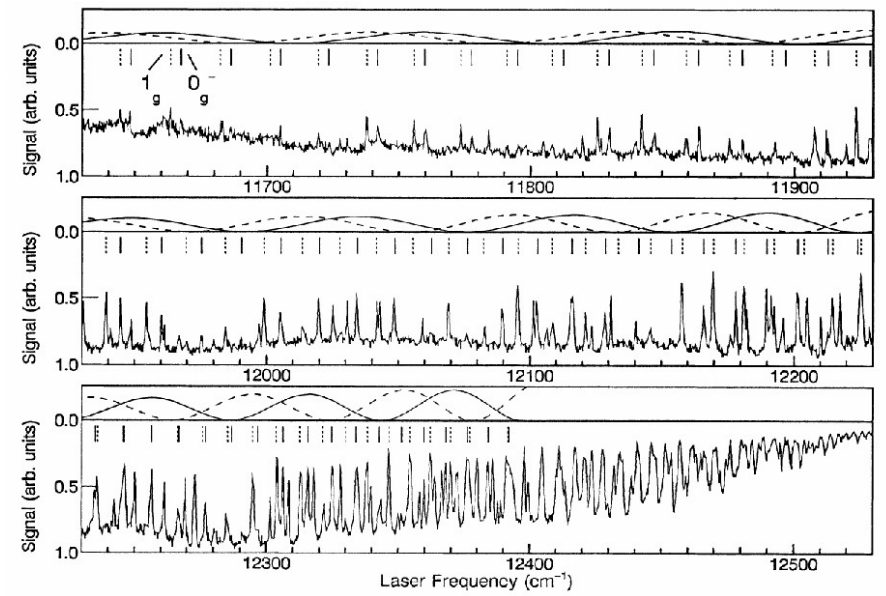


**Figure 2.1.:** The first observed photoassociation spectrum of  $^{85}\text{Rb}$  as shown in Figure 2 of Miller *et al.*'s 1993 paper [54]. The distinct peaks that can be seen here were an impressive confirmation of the predictions made by Thorsheim *et al.* [45].

paper, only eight date to the first five years after its publication. It appears that during the early 1990s, the creation of molecules was mostly considered a nuisance that limited lifetimes and reachable temperatures in atom traps, as it could cause loss or heating due to the molecular binding energy released into the atomic cloud.

This was investigated for example by Julienne *et al.* [51] and by Tiesinga *et al.* [52]. In 1993, this view slowly began to change as the first experimental investigations into photoassociation were published. These came from a team in Maryland, again working with  $^{23}\text{Na}$  atoms and another in Texas, which used  $^{85}\text{Rb}$ . Within three days of each other, they sent papers to Physical Review Letters in which they showed photoassociation spectra, obtained by illuminating atomic samples with a tunable laser beam [53, 54]. Their results confirmed that photoassociation spectra taken with ultracold atoms indeed showed sharp and distinct lines, in contrast to the very broad features of semi-classical chemistry (see Figure 2.1). As Miller *et al.* remarked in their paper, “another dramatic possibility first discussed by Thorsheim, Weiner and Julienne [...], is that colliding, ultracold atoms could display a resolved photoassociation spectrum” [54]. The work done in these studies can be called the first true experimental investigation of ultracold molecules, as they aimed to understand molecular physics in its own right, rather than to better control trapped atoms. For example, Miller *et al.* wrote that “our results clearly demonstrate the potential of photoassociative spectroscopy as a new probe of molecular structure” [54].

Until 1998, interest in ultracold molecules grew only slowly, with most of the experimental progress reported in this time related to photoassociation spectroscopy. For ex-

ample, molecular hyperfine structure was observed for the first time [55], further alkali species like lithium and potassium were investigated [56, 57], and two-photon photoassociation was used to probe high-lying vibrational levels which were hard to reach with previous techniques [58–60]. The review articles [61–63] give a good overview of the many experiments performed on this topic at the time. Other than this, little experimental progress was reported. As Bahns *et al.* noted in 1996: “There has been tremendous progress in atomic laser cooling in recent years, but progress at manipulating even simple molecules during the same period has been comparatively minimal” [64]. Even though molecules were certainly considered interesting objects of study, the laser-cooling conundrum meant the experimental effort was much larger than what was needed for atoms, making molecules seem unappealing at a time where rapid progress was made with atoms.

Still, a number of noteworthy theoretical proposals on how to circumvent this problem were published between 1995 and 1997. For example, Doyle *et al.* [65] suggested a combination of the established techniques of buffer-gas cooling and magnetic trapping. According to their proposal, certain paramagnetic molecules could first be cooled by letting them thermalise with a buffer gas of  ${}^3\text{He}$  atoms at a temperature of a few hundred millikelvin, cold enough to be confined in a magnetic trap for evaporative cooling. Around the same time, Band *et al.* [66] and Côté *et al.* [67] suggested that photoassociation might not only be a tool to probe molecular structure, but could also be used to produce molecules from ultracold atoms. Molecules created in this way would inherit the low temperature from the atoms, making it easier or even unnecessary to cool the molecules themselves.

Another proposal by Bahns *et al.* [64] went a step further and suggested that it might be possible to push through the laser-cooling conundrum rather than avoid it, making direct laser cooling of molecules possible. Instead of impractically many repumping lasers, their scheme employed a single laser with a large number of sidebands which is chirped to cool down rotational, translational and vibrational degrees of freedom, one after the other. This method proved to be too complex to be practical and has never been implemented (see, e.g., Reference [68] for a more recent discussion of the topic).

On the other hand, buffer-gas cooling and magnetic trapping of CaH molecules was accomplished by Weinstein *et al.* [69] in 1998, quite shortly after the publication of the initial idea. This was achieved by first creating a gas of molecular CaH via laser ablation. Then, as proposed by Doyle *et al.* three years earlier, this gas was thermalised with cryogenic helium and trapped in a quadrupole magnetic trap generated by a pair of superconducting coils in anti-Helmholtz configuration (the experimental setup is shown in Figure 2.2). The authors remarked that “removal of the buffer gas after trapping should lead to evaporative cooling.” However, in the following years, this turned out to be quite difficult.

At the same time, the creation of ultracold molecules via photoassociation was also successfully implemented: after Fioretti *et al.* [70] had first measured photoassociation spectra of  ${}^{133}\text{Cs}_2$  molecules, Takekoshi *et al.* [71, 72] demonstrated that  ${}^{133}\text{Cs}_2$  molecules created in this way could be trapped in an optical dipole trap<sup>1</sup> and detected using a ph-

---

<sup>1</sup>The principle of optical dipole traps is explained in the review article [73].

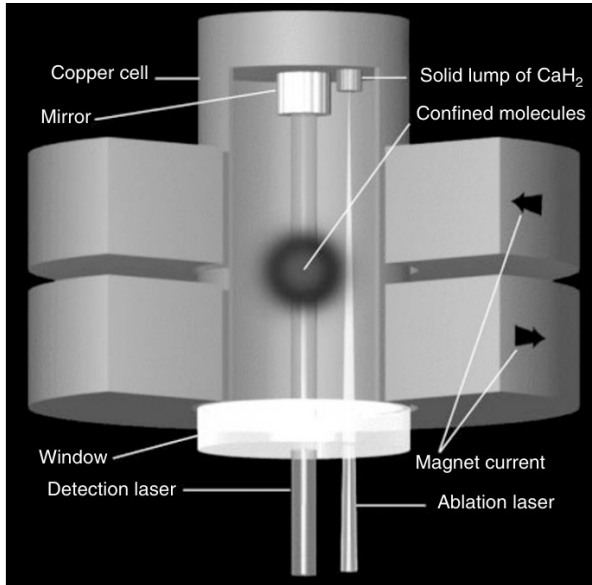


**Figure 2.2.:** The magnetic trap setup used for the first successful cooling and trapping of molecules as shown in Figure 1 of Weinstein *et al.*'s 1998 paper [69].

toionisation scheme. In another remarkable coincidence, the completely different experiments by Weinstein *et al.* and by Takekoshi *et al.* were published within three months of each other. Together, they mark the first time ultracold molecules could be trapped in three-dimensional potentials. However, the samples created with both methods were still small, relatively hot, and far from pure; they contained molecules in many different quantum states as the methods used could not control vibrational, rotational, or hyperfine degrees of freedom.

This was not the only way in which important progress was made in 1998: this year also saw the first theoretical investigations of atom-molecule collisions by Balakrishnan *et al.* [74] (see also the review articles on ultracold collisions and chemistry [63, 75]) as well as the first experimental observation of a Feshbach resonance by Inouye *et al.* [76]. Since Feshbach resonances soon became one of the most important tools in the field of ultracold gases, a more detailed explanation is in order.

Feshbach resonances had been predicted to exist between alkali atoms as early as 1993 [52]. They occur when a free and a bound state of a two-body quantum system are close to each other in energy. These states are typically called the *open channel* and the *closed channel*, respectively. Close to a Feshbach resonance, the proximity of the closed channel influences the scattering properties of the open channel, see Figures 2.3 and 2.4. For atomic species with unpaired spins, such as alkali metals, the energy of the open channel can be tuned by changing the background magnetic field, moving its relative energy with respect to the closed channel. In the vicinity of the energy crossing, the resonance influences the collision dynamics, increasing the scattering length  $a$  on one

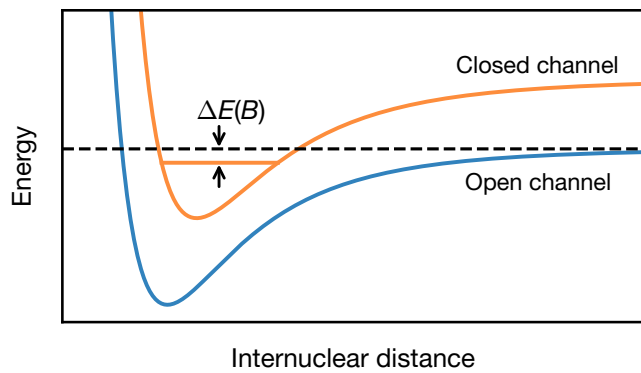


**Figure 2.3.:** Working principle of a Feshbach resonance. The open channel (blue) represents the energy of two unbound atoms in a collision, while the closed channel (orange) is a molecular bound state. The energy available in a collision is indicated by the dashed line. The difference  $\Delta E$  between it and the bound state can be tuned by changing the external magnetic field.

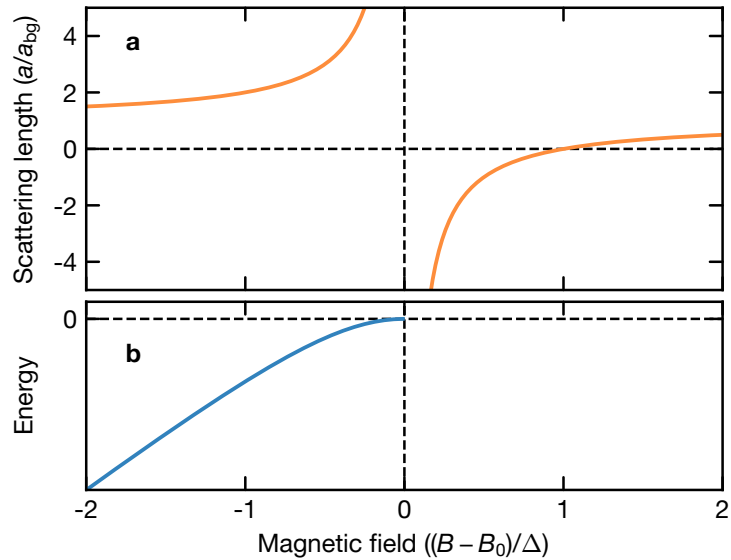


**Figure 2.4.:** A Feshbach resonance. **(a)** Dependence of scattering length  $a$  on the magnetic field for a resonance of width  $\Delta$  at a background scattering length  $a_{bg}$ . On the left side, the interaction becomes more repulsive ( $a > 0$ ), on the right side it becomes more attractive ( $a < 0$ ). **(b)** Energy of the molecular state corresponding to the closed channel. On the attractive side, this state is unbound, but on the repulsive side, it smoothly becomes more and more deeply bound. Thus, a Feshbach resonance can serve as a bridge between the worlds of atoms and molecules.

side and decreasing it on the other.

Almost immediately, the influence of Feshbach resonances on collisions and their relation to molecular physics were investigated [77–80]. As Stenger *et al.* noted, “the observed losses of atoms near Feshbach resonances indicate molecular and many-body physics which is not yet accounted for by any theory” [78]. Using Feshbach resonances to control the scattering length has since become a staple technique, allowing a great number of fascinating discoveries. However, they are arguably even more important for molecular physics than atomic physics: since they occur at a coincidence of free and bound states, they represent a gateway between unbound atoms and molecules. Indeed, the most common methods used today to create ultracold molecules from atoms make use of Feshbach resonances. Further information on Feshbach resonances can be found in Chin *et al.*’s famous review paper [81].

The next big step came once again from the efforts of direct molecule cooling: in 1999, Bethlem *et al.* [82] and Maddi *et al.* [83] first demonstrated slowing of molecular beams. As Doyle and Friedrich exclaimed in a short news article summarising these results: “Molecules are cool” [84]. The principle of both experiments is similar: A beam of low-field-seeking molecules goes through a series of alternating electric fields (see Figure 2.5). Whenever they go into a region of increasing electric field, they have to climb up a potential slope, converting kinetic into potential energy. The electric field is then turned off quickly, such that the energy is absorbed by the field rather than being turned back into kinetic energy. The process can be repeated, slowing the molecule down bit by bit. This technique became known as *Stark deceleration* or *alternating gradient deceleration* and has seen widespread use over the following decades, often in combination with trapping [85]. Among the molecules cooled with these methods were carbon monoxide [82, 86], ammonia [87–89], OH radicals [90], ytterbium fluoride [91], lithium hydride [92], and many more. A more complete description of the endeavours in this field can be found in the review articles [32, 33, 93].

Photoassociation was also further developed: only a few months after the first trapping of photoassociated  $^{133}\text{Cs}_2$ , Nikolov *et al.* [94] reported the creation of ultracold  $^{39}\text{K}_2$  in low vibrational levels of the electronic ground state which had previously not been reachable due to the small wavefunction overlap between free and deeply bound states. Subsequently, the same group demonstrated a new two-step photoassociation technique in which they employed an additional laser to reach specific excited states chosen for their large overlap with the electronic ground state [95]. This technique attempted to mitigate the fundamental problem of photoassociation as a method of creating ultracold molecules: its reliance on spontaneous emission to transfer molecules from reachable excited states into the target states. In this process, it is not possible to control in which exact rovibrational level a molecule ends up, such that a random mixture of many states is created. The method by Nikolov *et al.* enabled significantly increased production rates of molecules in low vibrational states compared to previous experiments, but was not yet suitable for creating large samples in a single quantum state. Still, a certain optimism about photoassociation is clearly visible in articles from this time: for example Stwalley and Wang [62] mention its unique potential in probing long-range molecular potentials and for creation of both homonuclear and heteronuclear bi-alkali molecules.

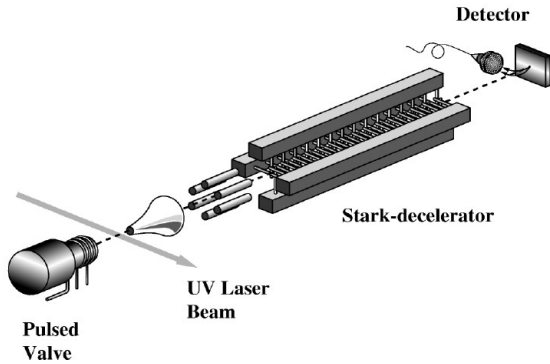


**Figure 2.5.:** Experimental apparatus used for Stark deceleration of CO molecules as shown in Figure 1 of Bethlem *et al.*'s 1999 paper [82].

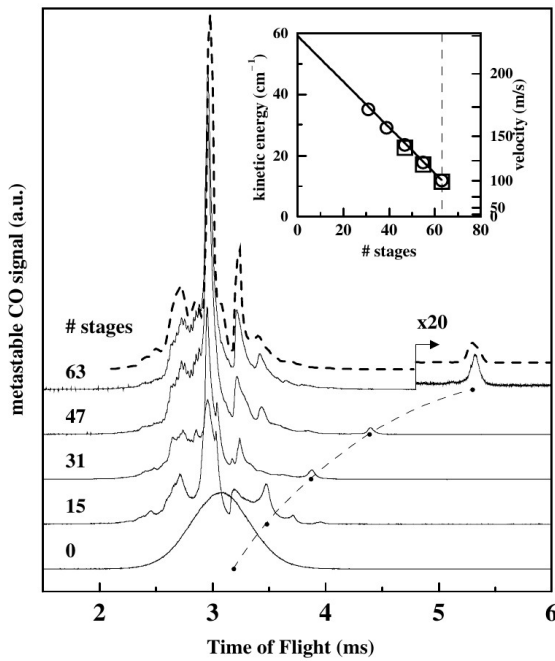


**Figure 2.6.:** Velocity distribution of CO molecules with various numbers of Stark-deceleration stages. The signal of the decelerated molecules (marked by the solid points on the baseline of each curve) move towards longer flight times and therefore smaller velocity as the number of stages is increased. Figure taken from Reference [82].

## 2.3. 2000–2007: A field of its own

### 2.3.1. Homonuclear alkali dimers and BEC-BCS crossover

Following the decisive progress at the end of the 1990s, the new millennium began with enthusiasm and high expectations. Ever since Bose–Einstein condensation of alkali atoms had been achieved in a number of seminal experiments since 1995 [44, 96–99], there had been some theoretical investigation into the formation of molecular Bose–Einstein condensates (BECs) using atomic BECs as a starting point [100–103]. From the year 2000 and onwards, this led to a fast growth of experiments attempting to observe a BEC of homonuclear molecules. Wynar *et al.* [104] made the start, observing  $^{87}\text{Rb}$  dimers in a single weakly bound rovibrational state of the  $a^3\Sigma_u^+$  potential. Due to their small binding energy on the order of  $h \times 600 \text{ MHz}$  and the fact that the free and bound state show predominantly the same spin and orbital angular momentum character, these molecules could be created relatively easily by means of a Raman process, illuminating a BEC of Rb atoms with two lasers offset from each other by the binding energy.<sup>2</sup> Two years later, McKenzie *et al.* [106] demonstrated formation of  $^{23}\text{Na}$  dimers from an atomic BEC via single-photon photoassociation.

While these experiments were well-suited for spectroscopic studies and for understanding collision dynamics in BECs, they were not able to create molecules as quickly and easily as was desirable: for example, the Raman process used in Wynar *et al.*'s experiment took hundreds of milliseconds, during which loss and heating could occur. One alternative proposal suggested that an optical lattice<sup>3</sup> could be used in order to achieve discrete energy levels for the unbound atoms, which would allow making free-bound Raman transitions much more efficient [108].

However, it quickly turned out that the use of Feshbach resonances provided a much simpler way to efficiently create molecules than optical pathways. This was demonstrated by Donley *et al.* [109] who, working with a gas of  $^{85}\text{Rb}$  atoms, ramped a background magnetic field close to a Feshbach resonance, approaching from the molecular side. This way, they tuned the free and bound states very close to each other in energy without actually crossing, leading to oscillations between atomic and molecular populations (see Figure 2.7). The crucial limitation of this experiment was caused by the use of  $^{85}\text{Rb}$ , whose negative background scattering length would make a BEC collapse due to attractive interactions anywhere on the atomic side of the resonance. Thus, with this atom, ramping over the resonance was not feasible and no permanent population transfer into molecules could occur.<sup>4</sup>

<sup>2</sup>Even though this method was called STIRAP in a later review [105], it should rather be called a Raman transition. This is because here, both Raman beams are turned on simultaneously and no pulse sequence is involved, requiring large detuning to avoid resonant excitation.

<sup>3</sup>See the review article [107] for more information on optical lattices.

<sup>4</sup>There were later experiments by Thompson *et al.* [110], where a magnetic field modulation led to permanent molecule formation with  $^{85}\text{Rb}$ , but this method never found widespread use.

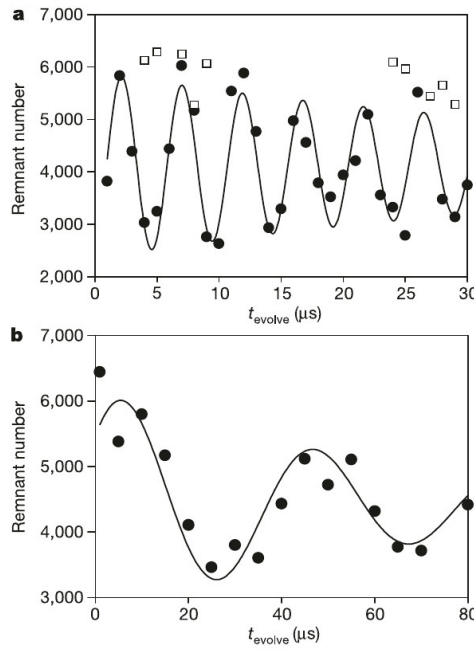


**Figure 2.7.:** Atom-molecule oscillations observed in a gas of  $^{85}\text{Rb}$  after ramping the background magnetic field close to a Feshbach resonance situated at 155 G from the attractive side. (a) shows the behaviour at  $B = 159.69(4)$  G, (b) at  $B = 157.60(4)$  G. This marks the first creation of molecules by means of a Feshbach resonance, though it was not yet permanent. Figure taken from Reference [109].

Still, the experiment proved that the formation of molecules near Feshbach resonances was possible in principle, and soon multiple groups investigated this topic in more detail, creating dimers of  $^{133}\text{Cs}$ ,  $^6\text{Li}$ , and  $^{40}\text{K}$  [111–115] (see also the excellent reviews [105, 116]). The method developed in these experiments was simple and effective, and it remains essential to many experiments today: molecules are formed from atoms by ramping the background magnetic field adiabatically from the attractive to the repulsive side of a Feshbach resonance. They then enter a bound state, which is typically the highest vibrational level of the interaction potential. With homonuclear bi-alkali atoms in identical states, this is typically the  $a^3\Sigma_u^+$  potential [117]. Today, this method is called magnetoassociation, and the molecules created with it are colloquially known as Feshbach molecules.

Even in the first demonstration of this technique, it was already highly efficient, for example Regal *et al.* [114] were able to create 250000  $^{40}\text{K}_2$  molecules via magnetoassociation. Notably, in contrast to the bosonic atoms  $^{23}\text{Na}$ ,  $^{85}\text{Rb}$  and  $^{133}\text{Cs}$ ,  $^6\text{Li}$  and  $^{40}\text{K}$  are fermions, but this makes no difference for the quantum statistics of the dimers since when pairing two fermionic atoms, the resulting molecule is also a boson. Indeed, it had been theorised that near a Feshbach resonance, it should be possible to create a phase transi-

tion between a degenerate Fermi gas on the attractive side and a molecular BEC on the repulsive side, a phenomenon known as *resonance superfluidity* or *BEC-BCS crossover*, described in more detail in References [118–123].

At last, nearing the end of 2003, there was a veritable explosion of experiments in which molecules approached or reached the BEC phase. Within few months, no less than seven different groups from around the world reported the successful creation of ultracold, high phase-space density samples of homonuclear molecules created from  $^6\text{Li}$ ,  $^{23}\text{Na}$ ,  $^{40}\text{K}$ ,  $^{87}\text{Rb}$ , and  $^{133}\text{Cs}$  atoms [124–132]. All these experiments employed magnetoassociation, starting from deeply degenerate atomic samples, and were able to keep the phase-space density high throughout the association process due to its high efficiency and small heating.<sup>5</sup>

The main difficulty here was the thermalisation of molecules: for example, the team working on  $^{23}\text{Na}_2$  emphasised in their paper that they did not consider their system a BEC, as “in our opinion, BEC requires thermal equilibrium. High phase-space density is necessary, but not sufficient” [126]. Thermalisation was not possible in their system because the molecules were situated in a dense background of atoms and were lost in inelastic atom-molecule collisions too quickly to reach equilibrium. Attempts to address this limitation were made by Herbig *et al.* in Innsbruck [129] and by Dürr *et al.* at MPQ [128, 136] who successfully separated their  $^{133}\text{Cs}_2$  and  $^{87}\text{Rb}_2$  molecules, respectively, from the atoms, thus creating pure molecular samples. Still, even inelastic molecule-molecule collisions alone were strong enough to severely limit lifetimes and preclude thermalisation.<sup>6</sup>

It was soon theoretically explained by Petrov *et al.* [137, 138] that the less-than-ideal collisional properties of sodium and rubidium dimers were actually not random occurrences, but a consequence of the bosonic quantum statistics of the constituent atoms. In fact, in the weakly bound molecules of  $^6\text{Li}$  and  $^{40}\text{K}$ , the atoms retain some of their fermionic character and prevent close-range collisions by a *p*-wave barrier, even though this is not the case for more deeply bound molecules [139]. Therefore, in an ironic turn of events, the first molecular BECs were actually created from fermionic atoms. For  $^6\text{Li}_2$ , this was achieved by Jochim *et al.* in Innsbruck [115, 124] and by Zwierlein *et al.* at MIT [125]. With this isotope, it was not even necessary to ramp over the Feshbach resonance; the field could just be held at the resonance and molecules would form. With  $^{40}\text{K}_2$ , a normal magnetoassociation procedure was used and a BEC was reported by Greiner *et al.* at JILA [127] (see Figure 2.8). The observations made with fermionic atoms were very positively received in the ultracold-atom community, mostly due to their connection with BEC-BCS crossover and superfluidity. In this story, they are relevant for a different reason: molecules had become quantum degenerate for the first time.

---

<sup>5</sup>There were also some remarkable experiments that demonstrated the condensation of atom pairs on the attractive side of the resonance [133–135].

<sup>6</sup>The experiment by Dürr *et al.* is also noteworthy because it required magnetoassociation of  $^{87}\text{Rb}$ , an isotope whose first Feshbach resonance is situated at a magnetic field of 1007 G. Only few machines were ever built to make use of this resonance, as fields of this magnitude are not easy to reach. The enormous copper current leads and coils that were necessary for this job are present in the machine to this day, and are a sight to behold.

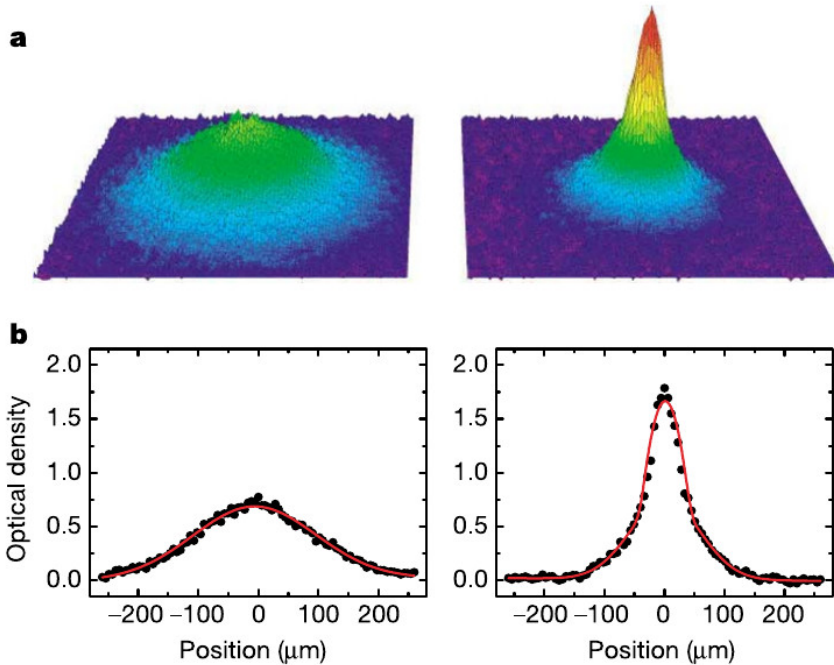


**Figure 2.8.:** Spatial profile of the first BEC of  $^{40}\text{K}_2$  molecules as shown in Figure 1 of Greiner *et al.*'s 2003 paper [127]. At a temperature of 250 nK in the left graphs, there is no condensate. In the right graphs at a temperature of 79 nK, a condensate has begun to emerge.

### 2.3.2. Towards associating polar molecules

In the midst of the impressive experiments with homonuclear molecules, interest in heteronuclear molecules also gradually began to grow. Consisting of two different atoms, they exhibit unique properties, especially in the presence of external electric fields, where they orient themselves and obtain an electric dipole moment (see Section 1.1.5). For this reason, they are often called *polar* molecules.

It was already suspected that there were a number of fascinating possibilities to be explored with ultracold polar molecules: for example, if they could be cooled down far enough, they would be the ideal material to make quantum many-body systems with dipole-dipole interactions. A number of predictions already existed, mostly for bosonic particles, for example dipolar BECs were theoretically investigated in References [140–143], and Reference [144] predicted the phase diagram for polar bosons on a lattice.<sup>7</sup> First progress in describing dipolar fermions was also made, see for example [149] and the overview by Baranov *et al.* [150]. DeMille [151] even suggested that polar molecules

<sup>7</sup>Most of the body of work on dipolar BECs turned out to be more interesting for the community working with ultracold magnetic atoms, where it has become a very productive research area. Overviews of this field can be found in References [145–148].

could become the building blocks of a quantum computer.

Another possibility was to use polar molecules to measure quantities typically associated with high-energy physics: it had been hypothesised for a long time that the electron could possess a non-zero electric dipole moment, a so-called eEDM. This idea is connected to the violation of charge- and parity-reversal (*CP*) symmetry and can be used to probe beyond-standard-model physics, because the Standard Model predicts a vanishingly small eEDM, but many other theories expect it to be significant. Excellent and detailed explanations of this effect and its consequences can be found in the review papers by Safronova *et al.* [152] and by Chupp *et al.* [153]. Certain molecules offer a unique advantage in measuring the eEDM, as they provide electric fields on the order of  $10^{12}$  V/m between the nuclei, far out of reach of conventional methods. As the electrons in the molecule interact with this large field, the spin states get split up, not only by the electron's magnetic moment, but also by its electric dipole moment, which could then be observed in the molecular spectrum [154]. Such experiments had been proposed as early as 1978 [155], but finally, in 2000, technology had advanced sufficiently to begin experimental work, using PbO and YbF molecules [156–159].

Experimentally studying ultracold polar molecules was still considered a very difficult challenge, mainly because it was unclear how one could create sufficiently large, cold and pure samples of them. This was less of a problem for the dipole-moment searches, as they could be done with relatively hot samples. However, the requirements for studying dipolar quantum many-body systems were far more stringent: for dipolar interactions to overpower thermal fluctuations at the typical densities and interaction strengths reached in experiments, molecules would have to be fully polarised at temperatures around 100 nK. The coldest samples available via direct molecule cooling were scalding hot in comparison, reaching only a few millikelvin. Atoms could be cooled down easily enough, but creating polar molecules from atoms required solving a whole series of new problems: how to mix different species of ultracold atoms together? How to then associate them while keeping the temperature low? And would the resulting molecules be stable enough to survive thermalisation or the onset of new quantum phases? It would take two decades until these problems were solved.

The problem of mixing multiple species was tackled first: in 2001, Mosk *et al.* [160] succeeded in trapping two different elements together in one optical dipole trap, in this case  $^6\text{Li}$  and  $^{133}\text{Cs}$ . They were soon followed by Modugno *et al.* [161] with a  $^{41}\text{K} + ^{87}\text{Rb}$  mixture, Hadzibabic *et al.* [162] using  $^6\text{Li} + ^{23}\text{Na}$ , and many more. As the scattering properties of mixtures were studied, it was soon verified that Feshbach resonances also exist between atoms of different species with the first ones found in the  $^6\text{Li} + ^{23}\text{Na}$  and  $^{40}\text{K} + ^{87}\text{Rb}$  systems [163, 164] (see Figure 2.9). Thus, a path to associating heteronuclear Feshbach molecules seemed to be open.

However, this path would only lead to weakly bound  $a^3\Sigma^+$  molecules, whose large internuclear distance caused them to behave almost like unbound atoms. This had not hindered the previous homonuclear-molecule experiments for which the internal molecular structure was mostly irrelevant, but was a dealbreaker for creating polar molecules, as the dipole moment of Feshbach molecules is vanishingly small. It was also believed that the weakly bound molecules were going to be unstable in collisions, where they could

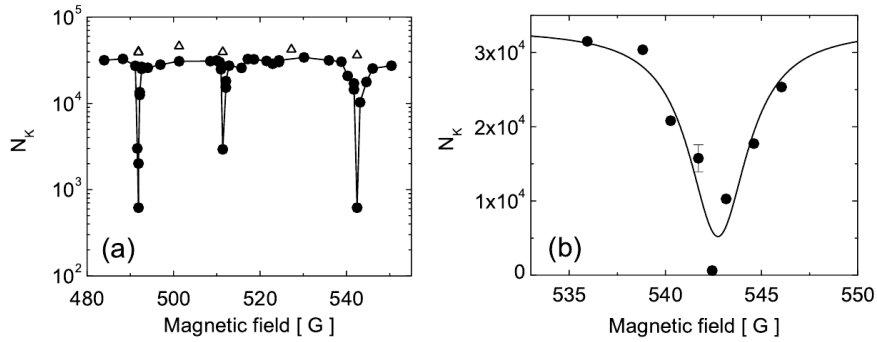


**Figure 2.9.:** First observation of an interspecies Feshbach resonance in the  $^{40}\text{K} + ^{87}\text{Rb}$  system as shown in Figure 3 of Reference [164]. **(a)** Remaining number of  $^{40}\text{K}$  atoms after holding the mixture for a given time (circles). Dips were observed at magnetic fields close to resonances where the scattering length becomes large. The triangles are comparison measurements without rubidium atoms. **(b)** Higher resolution view of the right-most resonance.

relax into more deeply bound states, releasing enormous energies. To get an idea of the magnitude of such a process, consider that the binding energy of a typical alkali dimer is on the order of  $k_B \times 10^4 \text{ K}$ , and a significant fraction of this might be released in a single collision. It thus seemed clear that sufficiently long lifetimes would only be achievable with a sample of molecules in the rovibrational ground state in the  $X^1\Sigma^+$  manifold.<sup>8</sup>

Due to the much smaller internuclear separation in such a state, the molecules would also obtain a more strongly polar character and a much larger electric dipole moment. Owing to the energy scales involved, creating ground-state molecules could only be done using optical methods. The only heteronuclear  $X^1\Sigma^+$ -molecule that had been created previously was  $^6\text{Li}^7\text{Li}$  in 2001, where Schloeder *et al.* [166] had used photoassociation from a dual-species MOT. However, due to the similarity between the two nuclei, the dipole moment of  $^6\text{Li}^7\text{Li}$  was very weak, and, since the association was performed directly from a MOT, the molecules were neither very cold nor could they be in a single rovibrational state.

Even though further improvements were still being made in the efficiency of photoassociation [167], it was at this point clear that the fundamental problem of the method, its reliance on (or, at least, susceptibility to) random spontaneous emission events, made it unsuitable for the more demanding tasks in dipolar many-body physics. Nonetheless, photoassociation was the only available way to learn more about deeply bound states of polar molecules at the time and efforts continued: on the theoretical side, better predictions were made for the association rates that could be achieved in bi-alkali mixtures [168, 169], and in 2004, experiments finally succeeded in the photoassociative creation of multiple two-species dimers, namely  $^{39}\text{K}^{85}\text{Rb}$  [170–172],  $^{85}\text{Rb}^{133}\text{Cs}$  [173] and  $^{23}\text{Na}^{133}\text{Cs}$  [174].

<sup>8</sup>It was later found that this pessimistic view was not entirely justified. There are indeed regimes in which Feshbach molecules can be more stable than ground-state molecules [165].

The review articles [175, 176] describe these developments in more detail.

The point where ultracold-polar-molecule research started to stake its own claim within the molecule community came in the end of 2004, when the European Physical Journal D published a special issue on ultracold polar molecules. It began with a fascinating editorial by Doyle *et al.* [177], fittingly titled “Quo vadis, cold molecules?”, where polar molecules were called a target of “intense interdisciplinary interest” from physical chemistry and ultracold quantum gas researchers. Many of the experts in the young field contributed to the special issue, and the result was a remarkably far-sighted collection of papers. The list of research goals given there could just as well be found in the introduction of a paper written today, 18 years later. But also going down to the details, many ideas which later became highly successful were published here for the first time: for example DiRosa [178] made the first proposal of a molecule MOT and DeMille *et al.* [179] proposed a microwave trap which was finally realised in 2019 [180].

Another very important idea put forth in this issue was Stwalley’s suggestion to use *stimulated Raman adiabatic passage* (STIRAP) to transfer heteronuclear Feshbach molecules into the ground state [181]. STIRAP had first been demonstrated a few years prior [182] and, as shown in a number of highly interesting review papers [183–186], had already found uses in many fields. Though STIRAP is not difficult to describe formally, it has no classical analogue and it can be difficult to wrap one’s head around it.

The idea is to consider a three-level system with two low-lying states  $|G_1\rangle$  and  $|G_2\rangle$  and one excited state  $|E\rangle$ , where laser light is used to introduce Rabi couplings  $|G_1\rangle \leftrightarrow |E\rangle$  (*pump*) and  $|E\rangle \leftrightarrow |G_2\rangle$  (*Stokes*) with Rabi frequencies  $\Omega_p$  and  $\Omega_s$ , respectively (see Figure 2.10). Even though  $|G_1\rangle$  and  $|G_2\rangle$  are not coupled to each other, this method allows transferring population between them without ever populating  $|E\rangle$ . This is possible with a pulse sequence often called “counter-intuitive”: by turning on  $\Omega_s$  first, while all molecules are in  $|G_1\rangle$ , they begin their time evolution in a dark state of the system. Next,  $\Omega_s$  is ramped down and  $\Omega_p$  is ramped up adiabatically. As a calculation of the eigenstates of the three-level system shows, it is possible for the population to always remain in the dark state, while it slowly changes its character from purely  $|G_1\rangle$ , to a superposition of  $|G_1\rangle$  and  $|G_2\rangle$ , to purely  $|G_2\rangle$ .

By taking  $|G_1\rangle$  to be the Feshbach-molecule state,  $|G_2\rangle$  a lower-lying state in the  $X^1\Sigma^+$  manifold, and choosing a suitable  $|E\rangle$ , this method solves a number of issues simultaneously: first, it overcomes the limitations of photoassociation by fully controlling which state the transfer goes to. In the process, no molecules are excited into the short-lived excited states above the dissociation threshold, avoiding spontaneous emission completely. In contrast to strongly detuned Raman transitions, STIRAP can achieve this on resonance, making it ideally suited for molecules where detuning strongly from one resonance typically means hitting another. By choosing a suitable intermediate state with strong mixing between spin-triplet and spin-singlet character, STIRAP would also allow bridging the gap between the initial  $a^3\Sigma$  and the final  $X^1\Sigma$  manifolds where the different spin multiplicity otherwise forbids optical transitions.

The only remaining problem was how to get a high enough transfer efficiency. It had previously been suggested to use STIRAP to directly transfer free atoms into deeply bound states, but it was unclear whether or not this could work [100, 103, 187–189].

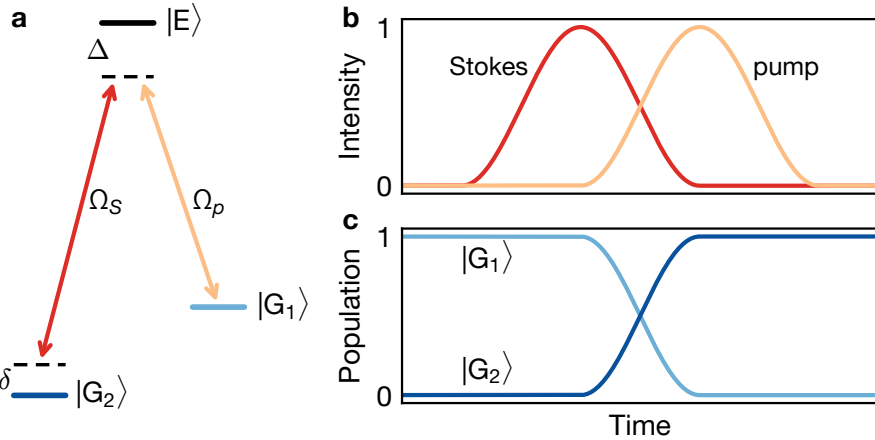


**Figure 2.10.:** Working principle of STIRAP. (a) Three-level system. The *upleg* or *pump* beam with Rabi frequency  $\Omega_p$  connects the initial state  $|G_1\rangle$  with the intermediate state  $|E\rangle$ ; the *downleg* or *Stokes* beam with Rabi frequency  $\Omega_S$  connects  $|E\rangle$  with the final state  $|G_2\rangle$ . The one-photon and two-photon detunings are denoted  $\Delta$  and  $\delta$ , respectively. (b) “Counter-intuitive” STIRAP pulse sequence. By turning on the Stokes transfer first, the population always remains in the dark state of the system. (c) Population transfer. In the beginning, all population is in the initial state  $|G_1\rangle$ . As the dark state is adiabatically transferred, the population follows and is moved into  $|G_2\rangle$ . In the ideal case,  $|E\rangle$  remains unpopulated throughout, thus avoiding losses caused by spontaneous emission.

Stwalley’s proposal, in contrast, was to first use magnetoassociation to efficiently reach a bound state, then use STIRAP from this point, where the spatial overlap between initial and final states would already be much larger. Whether or not it would be large enough was still unclear, but it seemed a worthwhile thing to try. Even though it took a few more years for it to be fully realised, this was precisely the idea that made possible the creation of the first dipolar quantum gas and it is used in many labs around the world to this day.

Only one month later, Sage *et al.* [190] published their demonstration of a scheme that could be described as “almost-STIRAP” with  $^{85}\text{Rb}^{133}\text{Cs}$ . They first created molecules in a highly vibrationally excited state in the  $a^3\Sigma^+$  manifold using photoassociation, then used a short “pump” light pulse to excite molecules into a state with mainly  $c^3\Sigma_1^+$  character and admixtures of  $B^1\Pi_1$  and  $b^3\Pi_1$ . With a delay of 7 ns, a “dump” pulse then transferred the population into multiple rotational sublevels of the  $X^1\Sigma^+, v = 0$  state. The short duration of the procedure allowed populating the short-lived excited level with little spontaneous emission, but also limited the transfer efficiency to only 6% due to the large spectral width of the laser pulses. Crucially, however, this was the first experiment that demonstrated that the ground state could be reached without the need for spontaneous emission.

Shortly afterwards, Winkler *et al.* [191] demonstrated the first transfer of ultracold molecules via actual STIRAP. They brought Feshbach molecules of  $^{87}\text{Rb}_2$  from the least bound into the second-to-least bound vibrational state, covering an energy difference of

$h \times 637$  MHz. Even though this may seem like a small step relative to the ground-state binding energies on the order of  $h \times 100$  THz, the efficiency of the transfer into a single molecular state was up to 87%, an enormous improvement over all previous methods.

Following this successful demonstration, only two things remained to be done to realise Stwalley's proposal: creating heteronuclear Feshbach molecules and finding a viable STIRAP pathway to  $X^1\Sigma$  states. Up to this point, though it was known that Feshbach resonances exist between different atomic species, Feshbach association had not been demonstrated yet. Two factors had contributed to this: first, constructing an experiment that can produce cold samples of two atomic species in the same trap is quite difficult and expensive. Second, the dynamics of a system of two different species of particles is much more complex than a single-species gas because there are three different scattering lengths (two intra-species and one inter-species), which can not be tuned independently from each other. If, for example, any of these scattering lengths were large and negative, the mixture would collapse under the attractive interaction. Conversely, a strongly repulsive inter-species interaction would make it impossible for the two species to mix, leading to phase separation or other more complicated effects [192].

With Feshbach resonances being very difficult to predict, there was therefore significant risk involved in attempting to create heteronuclear Feshbach molecules. In 2006, a remarkable series of papers by Silke and Christian Ospelkaus and their coworkers at the University of Hamburg shed light on the case of the Bose–Fermi mixture of  $^{40}\text{K} + ^{87}\text{Rb}$ . They described in detail the design of an experiment and the optimisation procedure necessary to obtain large dual-species quantum gases [193, 194], explained under which conditions the mixture was stable [195], how to tune the inter-species interaction [196], and investigated effects of this interaction on the mixture dynamics [197]. Finally, they succeeded in creating the first sample of stable heteronuclear Feshbach molecules<sup>9</sup> using a radio-frequency sweep to transfer unbound atom pairs in the sites of a three-dimensional optical lattice into molecules [199]. In combination with the investigations on the same mixture at JILA and at the University of Florence [200–203], this *tour de force* made  $^{40}\text{K} + ^{87}\text{Rb}$  the best-understood mixture available, providing an ideal stepping stone to advance the field further.

With these developments, there was great hope in the community that it would soon be possible to discover the physics of strongly dipolar gases of ultracold molecules. This is perhaps best exemplified by the number of theory publications which came out between 2006 and 2008, investigating properties of dipolar systems that were now thought to be within experimental reach. It was predicted, for example, that a high-density sample of strongly dipolar bosons under two-dimensional confinement could undergo a transition from a gas to a crystalline phase with triangular symmetry due to the interplay between high density and dipolar repulsion [204–207] (see Figure 2.11).

Fermionic dipolar systems were also studied, both in 3D and effective 2D confinements [208, 209]. While previous investigations of 2D-confined dipoles had focused on a purely repulsive interaction potential, in the fermionic case also attractive interactions were studied and found to potentially give rise to pairing and superfluidity. Multiple

---

<sup>9</sup>There was also an almost simultaneous result by Papp and Wieman [198], who associated  $^{85}\text{Rb}^{87}\text{Rb}$ .

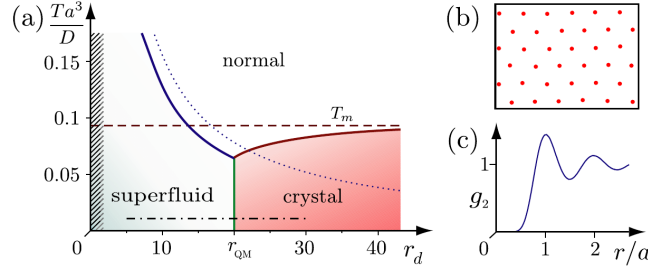


**Figure 2.11.:** Theoretical prediction of triangular dipole crystal as shown in Figure 3 of Büchler *et al.*'s 2007 paper [204]. (a) Phase diagram for dipolar bosons in 2D confinement, with density on the  $x$ -axis and temperature in units of interaction strength on the  $y$ -axis. (b) Lattice of the triangular crystal. (c) Density-density correlation function of the crystalline phase.

suggestions were made as to how dipolar particles could serve as building blocks for quantum computers or quantum memories, for example by using self-assembled dipolar crystals [210], specially engineered lattices [211, 212], or using them as interfaces to couple light to solid-state quantum processors [213].

Finally, with experimental efforts to measure the electron dipole moment with molecules well underway, new proposals came out for the next step towards using molecules as probes of beyond-Standard Model physics. Flambaum and Kozlov [214] found that certain molecules exist where the effects of the nuclear mass on the fine structure and the vibrational splitting almost cancel each other, leading to very close-lying levels whose energy separation is sensitive to the electron-proton mass ratio and the fine-structure constant. Microwave spectroscopy could then be used to probe spatial or temporal variations of these constants with extremely high precision. In a similar vein, DeMille *et al.* [215] put forth the idea that experiments with molecules could measure certain electroweak couplings between electrons and nuclei which would induce parity violation, but are forbidden by the Standard Model, so that measuring such an effect might give hints at new physics.

Compared to the previously described experimental avenues which were to become the basis of today's ultracold-molecule labs, there was also a number of other attempts [216], which in hindsight turned out to be less successful, but are nevertheless interesting in their own right. One of these was to use helium nanodroplets as a basis for forming bialkali molecules like LiCs, NaCs, and KRb [217, 218]. A helium nanodroplet is a cluster of  ${}^4\text{He}$ , containing a few thousand atoms [219], which can be formed using supersonic expansion techniques. Alkali (and other) atoms can stick to the droplet surface and, as the droplet automatically cools down to a temperature of 380 mK through evaporation, those atoms are cooled with it and are able to form molecules on the surface. Therefore, in contrast to helium buffer gas cooling, the technique can be used not just to cool already existing molecules, but also to create them in a cold environment. However, just like buffer gas cooling, the method is ultimately limited by the presence of the helium itself. To reach

significantly lower temperatures, the helium would have to be removed, but this was not possible in any practical way.

Another attempt was aimed at improving the efficiency of photoassociation by removing its dependence on spontaneous emission, in a similar way as had been shown in Sage *et al.*’s “almost-STIRAP” scheme. It was expected that, instead of relying on an adiabatic transfer, it should be possible to engineer short laser pulses with intensity and frequency profiles optimised to improve the efficiency of a nonadiabatic transfer. Put simply, a pump pulse could be used to generate a time-dependent excited state. If left alone, this state would eventually decay into one of many different bound states, but a dump pulse of the right shape could catch it and steer it deterministically into a target state. Following the proposal of the method [220, 221], it was experimentally attempted with less-than-ideal results: to achieve the necessary short laser pulse duration, the pulses had to be so spectrally broad that some frequency components became resonant with molecular transitions, leading to decreased transfer efficiency [222]. While some of the shortcomings of the technique were later fixed [176, 223], high efficiencies could never be realised. Though there are still unanswered questions and untested proposals on how to improve short-pulse photoassociation, there has been little experimental interest in it for the past decade. A recent and comprehensive overview can be found in Reference [224].

These episodes, while perhaps not highly relevant for understanding the current state of the field, can serve to show that the path to ultracold polar molecules was by no means as obvious as it might seem. With the benefit of hindsight, it looks surprising that the techniques which later became successful were not attempted earlier and with more focus, but it is a good reminder of how complicated and surprising molecules can be and how many failed attempts it took until success could finally be achieved.

## 2.4. 2008–2011: Breakthroughs

### 2.4.1. An ultracold Fermi gas

The stage was now set for some the greatest breakthroughs of the field, which paved the way to bringing it to where it is today. The first of these was the creation of an ultracold sample of heteronuclear molecules in the rovibrational ground state. Since her ground-breaking work on  $^{40}\text{K}+^{87}\text{Rb}$  mixtures, Silke Ospelkaus had become a postdoc at JILA in Colorado, working with, among others, Kang-Kuen Ni, Debbie Jin, and Jun Ye on  $^{40}\text{K}^{87}\text{Rb}$ . In 2008, this team reported the first creation of heteronuclear Feshbach molecules in an optical dipole trap [225–227]. Their magnetoassociation scheme turned out to be highly efficient, allowing them to create 25 000 molecules, more than double of what had previously been achieved. The Feshbach molecules were also found to be long-lived, even without a 3D lattice for protection. Next, they demonstrated the first STIRAP of a heteronuclear alkali dimer with some of the highest vibrationally excited states of the  $X^1\Sigma^+$  manifold as targets, reaching binding energies on the order of  $h \times 10\text{GHz}$ .

In a bold move, they then decided to attempt STIRAP directly into the absolute ground state, 96 vibrational levels and a binding energy of  $h \times 125\text{THz}$  below the previous

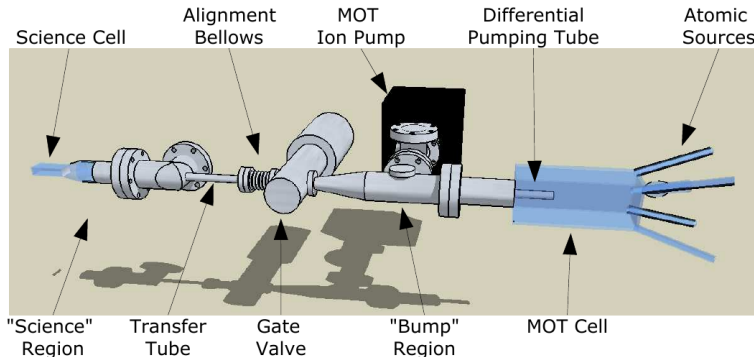


**Figure 2.12.:** Vacuum chamber of the first-generation KRb setup at JILA, where the first ultracold ground-state molecule gas was created. Figure taken from Reference [227].

record [27, 228]. As a STIRAP intermediate state,  $2^3\Sigma^+, v = 23$  was chosen due to its admixture of a close-lying  $1^1\Pi$  state, which gave it the necessary singlet component (see Figure 2.13). This could be addressed with diode lasers at 970 nm for the pump and 690 nm for the Stokes transition, which were locked to a frequency comb to reach the required small linewidths.

Despite initial worries about wavefunction overlap and laser coherence, the scheme worked incredibly well; to put it in Kang-Kuen Ni's words: "In 2008, to the surprise of the community and to our own delight, we were able to perform a single-step of STIRAP to transfer 90% of Feshbach molecules to the absolute ground state" [229]. The influence of this achievement can hardly be overstated: previously, the coldest ground-state molecules had been created from a MOT at temperatures around 100  $\mu\text{K}$ ; now 350 nK was suddenly possible. Phase-space densities made an even bigger leap, from previously  $10^{-14}$  to 0.02. On top of this, the methods applied by the JILA team were relatively simple, requiring "only" the creation of a mixture, a magnetic field ramp, and two well-stabilised STIRAP lasers. The mixture of  $^{40}\text{K}$  and  $^{87}\text{Rb}$  was also comparatively easy to create: the two species could be laser-cooled with similar lasers and could remain together throughout the cooling cycle. Furthermore, no Zeeman slower was needed, making it possible to do the experiment in the surprisingly small and simple vacuum setup shown in Figure 2.12.

With the molecule-creation process established, the JILA team lost no time in using it: over the next two years, they published fascinating studies about control of hyperfine levels [230], imaging techniques [231], and collisions between molecules [232–235]. This also marks the first observation of dipolar interactions in a molecule gas, since it was clearly observed that the collision properties changed with the application of an external electric field.

At this point, there was no competition in sight. There was an attempt made by Aikawa *et al.* [236, 237] at the University of Tokyo, which succeeded in finding a STIRAP pathway to the ground state of bosonic  $^{41}\text{K}^{87}\text{Rb}$ . However, they could only do this with much hotter molecules made via photoassociation directly from a MOT.

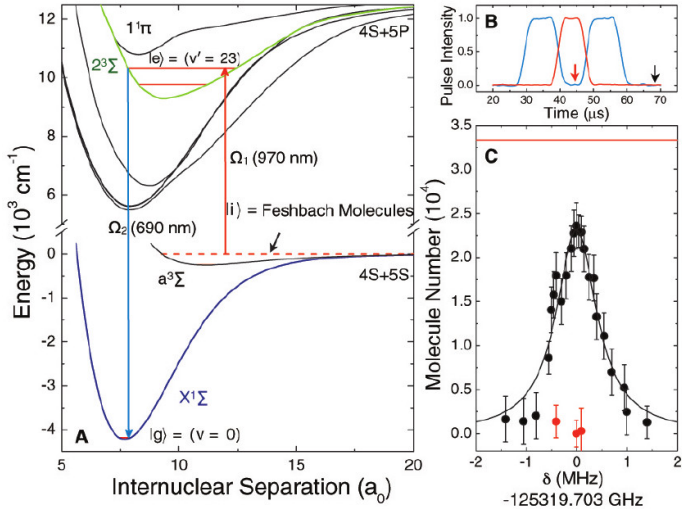


**Figure 2.13.:** Overview of the first successful STIRAP scheme to reach the absolute ground state of a molecule as shown in Figure 5 of Ni *et al.*'s 2008 paper [27]. **(a)** Molecular potentials, indicating the STIRAP pathway as red and blue arrows. **(b)** Pulse shapes for both STIRAP pulses. **(c)** Transfer efficiency depending on the detuning from the two-photon resonance, after the transfer to the ground state (red) and after the transfer back (black).

The JILA team also quickly encountered some limitations: the role of quantum statistics and many-body effects in magnetoassociation had not yet been studied, and it was unclear how to make the procedure work with degenerate atoms. This limited the reachable phase-space density. It had been initially hoped that it would be possible to produce quantum-degenerate molecules via evaporative cooling, the same way it had been done with atoms a decade earlier. Evaporative cooling depends strongly on collisions: doing it efficiently requires the lifetime of a sample to be much longer than it takes to thermalise. This is because efficient evaporation relies on losing only the particles on the high end of the energy distribution from the trap, thereby removing as much entropy per particle as possible. Once the tail of the energy distribution is gone, it must be refilled quickly, or the cooling process stops. However, in the first collision studies, it was found that collisions between two ground-state KRb molecules were inelastic in almost all cases, destroying both molecules in a chemical reaction



This not only made evaporative cooling essentially impossible. Even if it was somehow possible to create colder, higher-density samples of molecules, they would destroy themselves too quickly to be of much use. Luckily, a theoretical investigation by Żuchowski *et al.* [238] showed that not all bialkali molecules are chemically reactive in this way. Instead, five out of ten (NaK, NaRb, NaCs, KCs, and RbCs) were predicted to be stable

against all possible chemical reactions in two-body collisions.

### 2.4.2. Laser-cooling molecules

Despite the success of the JILA experiment, their method had some significant drawbacks, most prominently that it could only be used to make molecules out of laser-coolable atoms. This limited the accessible candidates basically to bialkalies and a small number of other dimers containing metals and rare earths. To go beyond this limitation, it was going to be necessary to further develop direct cooling methods. This field had seen quite limited progress between the early 2000s and 2007, though certainly not for lack of trying. In fact, a multitude of highly creative ideas were tried out or developed, including buffer-gas cooling with cold helium [239–241], Stark deceleration [90, 91, 242–244], velocity-selection using electric fields [245], reflection of molecules by moving mirrors [246], vibrational cooling with short laser pulses [247], magnetic traps [248–251], and combined magneto-electric traps [252, 253]. As ingenious as these approaches were, they were still limited to temperatures in the range of 10 mK or more, and only very gradual improvements could be made during a decade of work.

Despite its known difficulties, direct laser cooling of molecules seemed to be the only way to overcome this limitation. Multiple ways to deal with the laser-cooling conundrum were therefore discussed. One of these suggested using an optical cavity to assist with getting an almost-closed cooling transition [254]. The presence of the cavity was expected to strongly increase the probability of the molecule to decay via transitions resonant with a cavity mode, thus avoiding spontaneous emission into unwanted states for a well-tuned cavity. However, this was soon found to be more complicated than expected [255], and was never implemented.

The approach that finally turned out to be practical was the one originally suggested by DiRosa in 2004 [178]: a magneto-optical trap. It was clear that not just any molecule could be cooled in such a way, but for certain ones with some special properties, there was hope. The problem was how a molecule could scatter enough photons without going into a dark state. As a quite high scattering rate was needed, only electronic transitions were considered practical for this purpose. In principle, losses could then occur by decay into unwanted electronic, vibrational, rotational, or hyperfine levels. It was clearly impractical to use repumping lasers on tens or hundreds of transitions, so the key was to reduce the number of relevant loss channels. Avoiding loss to other electronic channels was no problem, this could be achieved simply by choosing the cooling transition to be the lowest dipole-allowed one. Decay into other electronic states could then only occur through dipole-forbidden transitions and would be naturally suppressed. Rotational losses were similarly easy to deal with, as they are also subject to a selection rule. There are at most three possible rotational decay channels for any given excited state, since angular-momentum conservation can not be satisfied otherwise. Going even further, a 2008 proposal by Stuhl *et al.* [256] suggested choosing a molecule with a  ${}^3\Delta$  ground state and a  ${}^3\Pi$  excited state. In this case, selection rules forbid all but one decay from  $R' = 0$ , such that the transition  $R = 1 \rightarrow R' = 0$  is rotationally closed. Hyperfine decay could be

similarly controlled by clever use of selection rules, or even completely avoided by using molecules with zero nuclear spin. However, vibrational decays constituted a much bigger problem.

The ingenuity of DiRosa's proposal was that it suggested using a class of molecules with *highly diagonal Franck–Condon factors*. A Franck–Condon factor is an overlap integral between two vibrational wavefunctions, and it determines the strength of the transition between these two states. Within one electronic state, the vibrational levels are mutually almost perfectly orthogonal, since the potential is similar to a harmonic oscillator. This is no longer the case between two different electronic states, especially because the minima of their electronic potentials are not necessarily at the same internuclear separation. However, in cases where two electronic potentials are similar both in shape and position of the minimum, transitions also predominantly occur between levels with the same vibrational quantum number [257]. Hence, a matrix of the Franck–Condon factors between all initial and final vibrational levels is almost diagonal. For the molecules most suited to laser cooling, the decay probability into unwanted vibrational states is on the order of 1%, and the vast majority of this probability is into the nearest-neighbour level. In this situation, only two repump lasers can be enough to scatter an average of  $10^4$  photons on a molecule before it becomes dark.

Following this theoretical work, laser cooling of a molecule was finally demonstrated for the first time in 2010 by Shuman *et al.* [258, 259] at Yale. This experiment used the species  $^{88}\text{Sr}^{19}\text{F}$ , a particularly good choice for multiple reasons: first, the strontium atom has two valence electrons, while fluorine has a single empty spot in its valence orbital and attracts electrons very strongly. This means a bond between the two is almost ionic, with one of the strontium's valence electrons becoming part of the fluorine atom. The resulting molecule then effectively has only a single valence electron, making its electronic structure relatively simple. Second, SRF has highly diagonal Franck–Condon factors, making it possible to control the vibrational branching. Third, the isotope  $^{88}\text{Sr}$  has nuclear spin  $I = 0$ , and  $^{19}\text{F}$  has  $I = 1/2$ , resulting in comparatively few hyperfine components. The cooling transition  $X^2\Sigma^+ \rightarrow A^2\Pi_{1/2}$  simplifies this further by using an excited state where the hyperfine splitting is smaller than the linewidth, such that the hyperfine structure is unresolved. Hence, it is only the hyperfine structure of  $X^2\Sigma^+$  which needs to be considered. The Yale team did this with an effective scheme which used sidebands of a single laser to address all the hyperfine levels (see Figure 2.14). The problem of rotational branching was solved by using a  $R = 1 \rightarrow R' = 0$  transition.<sup>10</sup> The resulting cooling method was not yet very effective, did not provide trapping, and worked only in one spatial direction at a time, but it worked. After many years of work, this proved that reaching microkelvin temperatures with direct molecule cooling was possible. With these two breakthroughs, ultracold molecules finally emerged as a truly promising platform for quantum physics.

---

<sup>10</sup>The reason why decays to other rotational levels are forbidden is the parity selection rule. This is in contrast to the scheme proposed in Reference [256]. More details can be found in the PhD theses of John Barry [260] and Benjamin Stuhl [261].

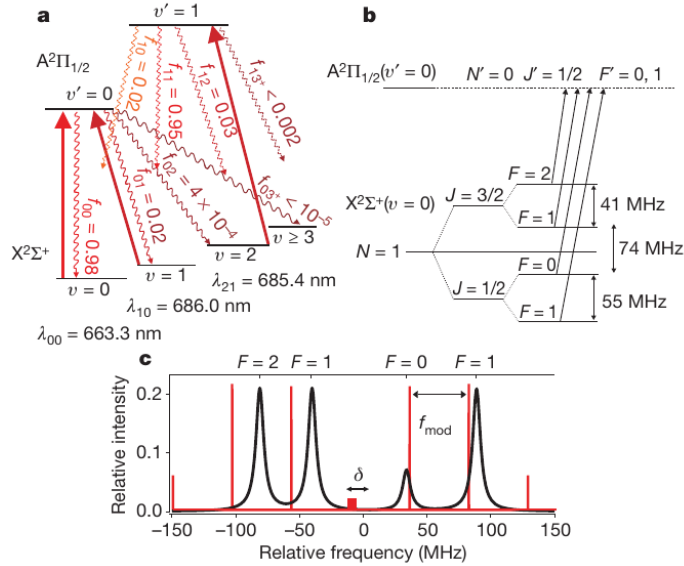


**Figure 2.14.:** Overview of the first successful laser cooling scheme for a molecule as shown in Figure 1 of Shuman *et al.*'s 2010 paper [259]. (a) Vibrational structure and branching ratios of the  $^{88}\text{Sr}^{19}\text{F}$  molecule. The wiggly arrows indicate spontaneous decay channels, and the straight arrows are the transitions addressed by the cooling and repumping lasers. The highly diagonal Franck–Condon factors lead to strongly suppressed decay in vibrational states other than  $v = 0$ . (b) Hyperfine structure of the cooling transition. The hyperfine structure of the excited state is unresolved and not shown. (c) Scheme for addressing all the hyperfine components with laser sidebands.

### 2.4.3. Further developments

Another great advancement was reported in 2011 by Hudson *et al.* [262], who achieved the most precise measurement of the eEDM to date, using a cold beam of  $\text{YbF}$  molecules. In comparison to the previous best measurement [263], which had been done with tellurium atoms, the molecule allowed an improvement of sensitivity of almost one order of magnitude. The molecules were prepared in a superposition of hyperfine states and sent through a homogeneous external electric field. Even tiny shifts in the relative energy of the hyperfine levels could then be detected in the emerging molecule beam as a phase shift between the components. If there was a finite eEDM, this phase shift would change when the sign of the applied electric field was flipped, but no such effect was found. This was arguably the first time that the rapid advancement in the control of molecules was actually useful for a task not directly related to molecule physics.

Somewhat overshadowed by the enormous success of associating heteronuclear molecules, serious efforts were also ongoing to create ultracold samples of ground-state homonuclear molecules. Compared to the heteronuclear case, this was expected to be even more difficult due to additional selection rules concerning the  $g/u$  symmetry. In

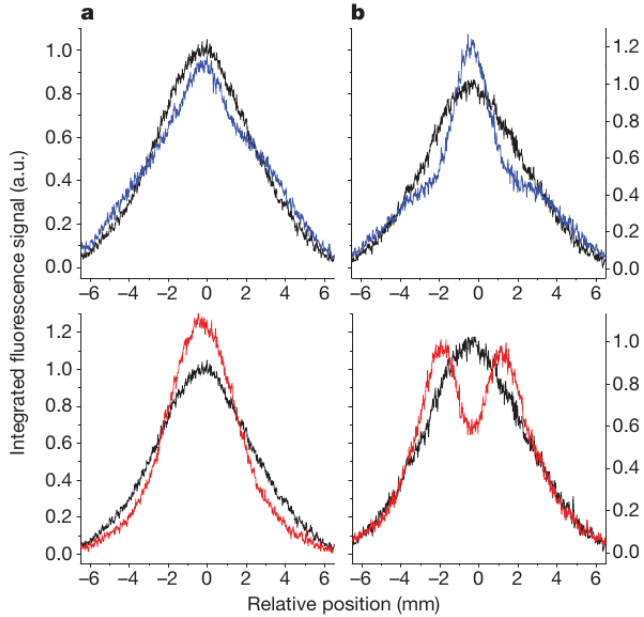


**Figure 2.15.:** Laser cooling of SrF molecules as shown in figure 2 of Shuman *et al.*’s 2010 paper [259]. The black lines are taken without laser cooling, the blue and red lines are taken with blue- or red-detuned cooling and repumping lasers, respectively. Depending on the detuning and magnetic field configuration, either cooling or heating is observed.

2008, STIRAP was reported for Rb<sub>2</sub> and for Cs<sub>2</sub> dimers [264, 265], though the ground state was not yet reached. Instead, the Rb<sub>2</sub> experiment targeted the rovibrational ground state of the  $a^3\Sigma_u^+$  manifold, such that the transfer changed only the vibrational level. For Cs<sub>2</sub>, the  $X^1\Sigma_g^+, v = 73$  state was populated, bridging an energy gap of  $h \times 30\text{ GHz}$ . Two years later, the same group reported a successful double-STIRAP scheme where they added another transfer from  $v = 73$  to  $v = 0$  [266, 267]. It was hoped that this technique would lead to a BEC of ground-state molecules, as well as fascinating studies of collisional properties in short order. However, there were significant difficulties, resulting both from the technical complexity of the experiments, and from mysterious molecule losses described in Reference [268], which are also the topic of Chapter 5. Until today, no BEC of homonuclear or heteronuclear ground-state molecules has been produced.<sup>11</sup>

Though the advancements made in the time between 2008 and 2011 were mostly technical in nature, they were no less important. With the problem of creating ultracold molecules solved, there was now strong interest in new physics that could finally be accessed. This is evidenced by a number of review articles written in 2009 [270–272]. Out of these, the one by Carr *et al.* [270] is especially significant, as it gives the most complete

<sup>11</sup>However, the creation of a BEC of highly rovibrationally excited Cs<sub>2</sub> molecules from a BEC of Cs atoms was reported in 2021 [269]. This can be seen as a bosonic counterpart to the BEC-BCS crossover experiments discussed in Section 2.3.1.

overview of the wide range of cold and ultracold molecule research at the time. Reading it today is a surprising experience, with most of its content feeling shockingly up-to-date more than a decade later. This is a testament to the greatness of the discoveries made between 2008 and 2011, but also to the severity of the problems encountered since then.

## 2.5. 2012–2017: Hard times

### 2.5.1. Associated molecules: Headfirst into the collision conundrum

Once the exothermic chemical reactions of KRb had been identified as a problem, a major experimental and theoretical effort began to either control the chemical reactions or to create ultracold gases of chemically stable molecules. In 2011, Debbie Jin and Jun Ye, the leaders of the JILA team, remarked that “With an understanding of inelastic and elastic collisions, one can tackle the goal of creating and studying novel quantum matter with ultracold polar molecules. The next steps include evaporative or sympathetic cooling to create a quantum degenerate gas and investigation of many-body or collective effects in the gas” [273].

It was clear that this could only be achieved with some understanding of loss rates and collision dynamics. The most recent results suggested that chemically reactive molecules could be made stable by avoiding all short-range collisions, which could be done by creating a purely repulsive potential between them [274–277]. If the tunnelling rate through the repulsive barrier was small enough, this should suppress chemical reactions. This was to be achieved by trapping molecules in a strong 2D confinement orthogonal to their dipole moment [278–281]. An alternative proposal suggested that the quantum Zeno effect could reduce reaction rates in three-dimensional optical lattices [282]. A thorough overview of the underlying theory of collisions can be found in References [283–285].

In parallel, a number of other experiments began studying some stable bialkali molecules, initially with  $^{87}\text{Rb}^{133}\text{Cs}$ . There was a clear expectation that this path would lead to the solution of the collisional-loss problem. For example, Lercher *et al.* remarked: “This molecule belongs to a class of dimer molecules chemically stable under two-body collisions, i.e., the reaction  $\text{RbCs} + \text{RbCs} \rightarrow \text{Rb}_2 + \text{Cs}_2$  is endothermic when  $\text{RbCs}$  is in its rovibronic ground state. As a consequence,  $\text{RbCs}$  dipolar quantum gases are expected to be stable. [...] In general, we expect that at ultralow temperatures, and in the lowest hyperfine sublevel of the rovibronic ground state of the  $\text{RbCs}$  molecule, only molecular three-body collisions present a possible limitation in experiments with dipolar many-body systems” [286].  $\text{RbCs}$  in particular seemed a reasonable choice as some properties of the  $^{87}\text{Rb} + ^{133}\text{Cs}$  mixture were already known from earlier studies [286–289]. Being the heaviest bialkali,  $\text{RbCs}$  also required the smallest electric field to be polarised. Two groups, one in Innsbruck and one in Durham, had already been working on the creation of Feshbach molecules [290–292]. In 2014, they almost simultaneously succeeded in creating ultracold samples of ground-state molecules [293, 294], using the same Feshbach

resonance near 197 G and subsequent STIRAP.

Though the fundamental principle was the same as with KRb, RbCs turned out to be much more difficult to work with for three reasons: first, ultracold mixtures of  $^{87}\text{Rb}$  and  $^{133}\text{Cs}$  can not be stable. In order to make spin-changing collisions impossible, all atoms should be in their hyperfine ground state, however  $^{133}\text{Cs}$  in this state has a large and positive background intraspecies scattering length. The repulsion is so strong that a caesium BEC can only exist at certain fields near a resonance, notably around 20 G or 894 G. On top of this, the interspecies scattering length of the mixture must be small enough to allow mixing. This can be done, but only at magnetic fields where a caesium BEC is unstable. Second, the structure of intraspecies Feshbach resonances is much more complicated than in the case of KRb. Not only is the density of resonances much higher, they are also all quite narrow, making very precise control of the magnetic field necessary. Third, the structure of molecular excited states of  $^{87}\text{Rb}^{133}\text{Cs}$  is less conducive to finding a STIRAP intermediate state which offers large overlaps with both the Feshbach and the ground-state molecule states. This made a careful investigation of the electronic manifolds necessary before STIRAP could be achieved. Together, these factors meant that it took more than two years from the first successful Feshbach association until a ground-state sample could be made. Similar surprising findings would keep coming up over the following years: while some bialkali combinations were well-behaved and easy to work with, others unexpectedly caused significant trouble, and some were completely impractical. Even today, there is no good method to predict these phenomena, and every combination must be painstakingly tested during years of experimental work.

It is instructive to look in more detail at the ways in which the difficulty of mixing rubidium and caesium was addressed in the two experiments (see Figures 2.16–2.17). The Durham team went for a very simple method: they chose to work at relatively high temperatures on the order of 1  $\mu\text{K}$ . The kinetic energy of atoms is then high enough to overpower interaction effects, such that mixing of the two species becomes possible even when they repel each other strongly. To achieve lower temperatures, the Innsbruck team chose to use a much more complicated method to mix the species [295]. They used an optical lattice, where Rb and Cs were first moved to two separate locations, then overlapped later, exploiting the fact that the heavier Cs atoms can be frozen in the lattice, while Rb remains able to move. The price to pay for the lower reachable temperature was the increased effort for the construction and maintenance of the setup.

Other bialkali molecules were also studied at the time. In fact, the enthusiasm was so great that out of the ten possible bialkali combinations, there was only a single one, namely NaCs, which was not yet seriously investigated.<sup>12</sup> The degree of success varied wildly, with some molecules being created in the ground state within few years while others never went beyond photoassociation in MOTs. I will here treat only the most successful ones in more detail. An overview and a list of references about the efforts with all the bialkalies can be found in Appendix A.

After  $^{87}\text{Rb}^{133}\text{Cs}$ , the next molecule which could be transferred to the ground state was  $^{23}\text{Na}^{40}\text{K}$ . It was studied at the time by Martin Zwierlein's group at MIT, as well as at

---

<sup>12</sup>In a bitter twist, NaCs was later found to be one of the best possible combinations.

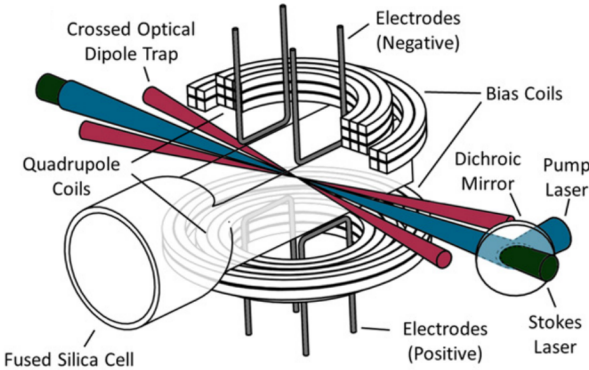


**Figure 2.16.:** Experimental setup used for the creation of an ultracold gas of ground-state  $^{87}\text{Rb}^{133}\text{Cs}$  at the University of Durham. Figure taken from [296].

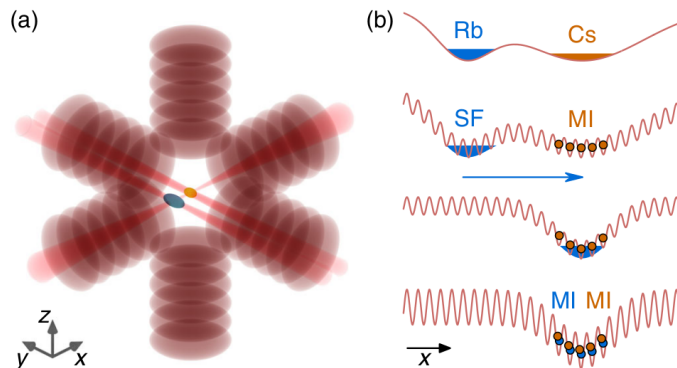


**Figure 2.17.:** Method used for the efficient association of  $^{87}\text{Rb}^{133}\text{Cs}$  in the Innsbruck experiment as shown in the 2017 paper by Reichsöllner *et al.* [295] (a) Lattice and dipole trap setup. There are two dipole traps along the y-direction. (b) Overlapping scheme. Rb and Cs clouds are first created in separate dipole traps, then the lattice is turned on to a depth where Rb forms a superfluid (SF) and Cs becomes a Mott insulator (MI). In this phase, the Cs atoms are bound so strongly by the lattice potential that they cannot move, and changing the magnetic field no longer leads to an explosion of the cloud. Only then can the two species be moved to the same position and associated.

MPQ. Being both fermionic and chemically stable, this species was expected to give new insights. The MIT team was consistently ahead, achieving the first Feshbach association [297, 298] and the first STIRAP to the ground state [24, 299]. It quickly became clear that the combination of  $^{23}\text{Na}$  and  $^{40}\text{K}$  was a lucky choice: sodium has an ideal, small and repulsive, intraspecies background scattering length and exhibits no Feshbach resonances at fields below 900 G. In addition,  $^{40}\text{K}$  is approximately noninteracting at any field due to its fermionic statistics. This means that the magnetic field can be chosen to optimise the interspecies properties without worrying about stability. Two broad interspecies Feshbach resonances are situated at 78.3 G and 89.7 G, such that Feshbach association requires neither particularly high fields nor very precise field control.

In 2016 and 2017, the now established method of associating Feshbach molecules in an optical dipole trap, followed by STIRAP, was also applied to  $^{23}\text{Na}^{87}\text{Rb}$  at the Chinese University of Hong Kong [300–302], and to  $^{23}\text{Na}^6\text{Li}$  at Harvard [303–306]. The experiment working with  $^{23}\text{Na}^6\text{Li}$  was unique in the sense that it did not target the ground state with its STIRAP, but rather the lowest rovibrational level in the  $a^3\Sigma^+$  potential (sometimes confusingly called the “triplet ground state”).

With every new species that became available at ultracold temperatures, researchers hurried to check if it was stable against two-body loss. The answer was the same for all of them: no. Instead, the probability of loss in two-body collisions was found to be near 100% for each of these molecules, despite their predicted chemical stability. When such a result was first found with RbCs [293], it seemed hard to believe. Maybe it was just an experimental error? Indeed, a 2015 paper by the NaK team at MIT seemed to show that a loss probability slightly below unity was possible [299]. However, within a few years, results with  $^{23}\text{Na}^{87}\text{Rb}$  and  $^{23}\text{Na}^{40}\text{K}$  indicated the presence of strong loss more and more clearly.<sup>13</sup> The presence of loss proved quite devastating: it not only made evaporative cooling of molecules impossible, but even if a dense and cold sample of molecules could somehow be made, it would be unable to survive. Most of the recent proposals involving dipolar physics required much lower temperatures, which now seemed unreachable. Where just a few years earlier, the field had been thought on the verge of another breakthrough, it had now hit a wall. Beginning around 2017, the focus of many experimentalists therefore shifted towards controlling the losses and making molecules stable.<sup>14</sup>

That is not to say that there was no progress with bialkali molecules during this time. In fact, despite the severe limitations imposed by two-body losses, some interesting discoveries were made. Broadly, the successes fell into two categories: Lattice physics and rotational-state control. The direction of lattice physics was mostly the focus of the KRb team at JILA. Since they had not expected their molecules to be collisionally stable in the first place, they had begun to look for way to protect them earlier than other groups. A three-dimensional optical lattice is one way to achieve this: if there is at most one molecule sitting on each lattice site, and the lattice is strong enough to suppress tun-

<sup>13</sup>A later study showed that the two-body loss coefficient of  $^{23}\text{Na}^{40}\text{K}$  is indeed consistent with unit loss [307].

<sup>14</sup>It is interesting to note that the majority of ultracold-bialkali experiments in operation today were constructed during a time where chemical stability was still considered to be highly important. As a consequence, KRb remains the only non-stable species which has been investigated in the ground state.

nelling between sites, then collisions become impossible. With this method, they demonstrated lifetimes of 25 s, limited only by off-resonant scattering of lattice photons [308, 309]. While the molecules in the lattice could not move, their rotational excitations certainly could: dipolar exchange interactions were found in 2013 with molecules where long-range interactions between neighbouring lattice sites allowed rotational excitations to jump [310]. A number of interesting review articles summarise these results [311–314].

There was also hope that lattices could help not only with stabilising molecules, but with creating them as well [309]. Typically, with mixtures in dipole traps, it was difficult to effectively overlap the different species due to differences in mass, polarisability, or quantum statistics. It had been suggested that this could be fixed by creating overlapping Mott or band insulators with near-unit filling in a deep lattice and then associating a molecule on every site [199, 315]. While the implementation with  $^{87}\text{Rb}^{133}\text{Cs}$  had been made difficult by the unfavourable interactions, this was not necessarily the case for other combinations [316]. This approach has had limited success until today, but there is no fundamental reason it should not work, and it may yet turn out to be the optimal way to create low-entropy samples of bosonic molecules.

Another problem that was addressed at JILA at this time was that of controlling electric fields. With the typical distances between charged electrodes on the order of a few centimetres, the required voltages could be tens of kilovolts to achieve full polarisation of molecules. There was not yet an established technique for creating such high voltages in a safe, stable and repeatable manner, making this a hit-and-miss thing. For example, in the original setup built at JILA beginning in 2003, it was found that glass parts of the vacuum chamber could become electrically charged, leading to uncontrollable offsets in the field [226, 317]. This was recognised quickly as a serious problem, but multiple attempts to fix it failed. Only the construction of a completely new setup with conductively coated glass surfaces, which was finished in 2016, solved the charging issue and allowed the creation of stable and precise fields [318].

The topic of controlling rotational states was also first studied at JILA [319, 320], however as they began focusing more on lattice physics and their new vacuum setup, other teams took over. Within a few years, the rotational transitions of  $^{87}\text{Rb}^{133}\text{Cs}$ ,  $^{23}\text{Na}^{40}\text{K}$ , and  $^{23}\text{Na}^{87}\text{Rb}$  were mapped out in detail, providing a starting point for further investigation [321–323]. Due to the coupling between rotational and hyperfine degrees of freedom, this also allowed coherent changes of the hyperfine state of molecules with relatively little effort. In 2017, the NaK team at MIT used this to create superpositions of hyperfine states, which, due to the weak coupling of hyperfine degrees of freedom to the environment, could remain coherent for multiple seconds [324].

### 2.5.2. The first molecule MOT

The efforts on direct laser cooling of molecules were somewhat more successful. After the basic principle had been demonstrated in 2010, teams at Yale, Harvard, Imperial College London, and JILA got to work on making a fully functional magneto-optical trap. Though achieving laser cooling had already been an enormous technical challenge, making a MOT

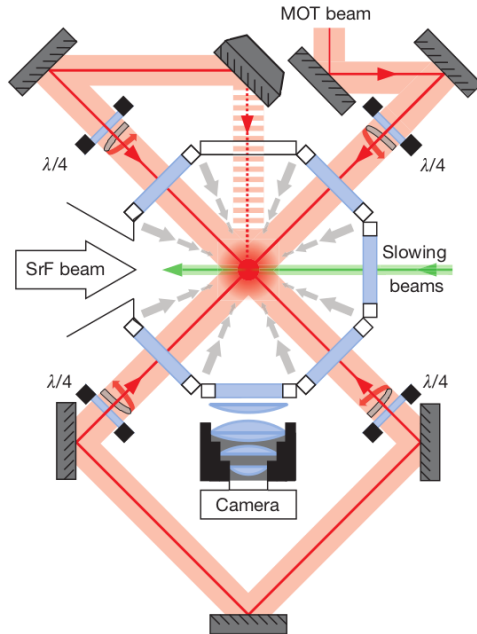


**Figure 2.18.:** Schematic of the setup used to create the first 3D MOT of molecules. Figure taken from Reference [329].

was going to be even harder. The difficulty was a direct consequence of the cooling transitions used in the MOT: as discussed above, in order to avoid rotational losses, it was required that  $R' = R - 1$ . This implies that the MOT cooling must be done on a  $F \rightarrow F' = F - 1$  transition, a so-called type-II MOT [258, 261, 325]. The problem with these is that the spin-stretched (i.e.,  $m_F = \pm F$ ) magnetic sublevels of the ground state are effectively dark states, so that any molecule that enters such a state will be lost. Multiple solutions to solve this problem were considered, all with the goal of mixing different  $m_F$ -levels such that molecules could not remain in the dark state long enough to leave the trap. Tools suggested for this purpose included magnetic fields, pulsed electric fields, microwave fields, or modulating the polarisation of the cooling light [256, 258, 326–328].

The first full-blown 3D MOT of a molecule was achieved by the Yale group in 2014 [329], using  $^{88}\text{Sr}^{19}\text{F}$  with the same cooling scheme as in their previous work. However, the cooling was now applied from all three spatial dimensions in combination with magnetic trapping and beam-slowing to facilitate loading (see Figure 2.18). Initially, the efficiency was extremely poor, with only a few hundred molecules trapped at a temperature of 2.5 mK. Over the next years, follow-up experiments demonstrated significant improvements, leading to molecule numbers up to 6000 at sub-millikelvin temperatures [325, 330–333]. In parallel, MOTs of  $^{89}\text{Y}^{16}\text{O}$  were developed at JILA [327, 334], while the teams at Imperial College and Harvard chose  $^{40}\text{Ca}^{19}\text{F}$  [335–339]. Both of these species exhibit similar properties to SrF, with a single valence electron and a total

nuclear spin of 1/2. Overviews of the advancements in laser-cooling of this time can be found in References [340, 341].

With the MOTs working reasonably well, the next important setup was to load the laser-cooled molecules into a conservative trap, where they no longer scatter photons. This is required in order to ensure that they are in a single quantum state, as well as to reach temperatures below the recoil-limit. In 2018, this was demonstrated both with magnetic traps [342, 343] and with optical dipole traps [344]. Importantly, since all laser-coolable molecules have a single unpaired electron, they possess a non-zero electron spin, making magnetic trapping possible. In contrast, magnetic trapping of bialkalies is impossible, because their ground state has an electron spin of zero, resulting in an extremely small magnetic moment.

### 2.5.3. New approaches to direct cooling

Though the demonstration of MOTs was a major success, it also highlighted the method's limitations. The range of valid species was perhaps even smaller than for associated molecules. Working with a new species also required building immensely complicated vacuum and laser setups and painstakingly developing an understanding of the molecular structure. As these things typically cost multiple millions of dollars and took the better part of a decade, attempts were only undertaken by the most dedicated research groups. So, while it was precisely their specialised nature which allowed both MOT and associated-molecule experiments to be successful, it was now more and more recognised that this was also their big limiting factor. What new and exciting research opportunities could be found if we had simpler and more general methods? If we could cool any molecule we wanted? A large number of ideas were investigated in the pursuit of this goal:

- Gerhard Rempe's group at MPQ developed a new method of electrostatically trapping molecules, beginning in 2011 [345, 346]. They used microstructured electrodes to create trapping potentials, leveraging the Stark effect. In this trap, a specially developed laser-cooling method was then used to cool fluoromethane ( $\text{CH}_3\text{F}$ ) molecules down to about 30 mK. In 2016, formaldehyde ( $\text{H}_2\text{CO}$ ) was also cooled in the same setup, demonstrating the versatility of the method [347, 348]. This was the first experiment to demonstrate temperatures below one millikelvin for a polyatomic species.
- The same group also invented a new beam-slowing technique which utilised electrostatic quadrupole guides inside a mechanically rotating centrifuge [349–351]. This yielded beams at velocities below 20 m/s for multiple polyatomic species such as fluoroform ( $\text{CHF}_3$ ). A schematic of the setup is shown in Figure 2.19. Despite the method's success, the MPQ group remains the only one to use it, perhaps owing to the high complexity of building the centrifuge machinery.
- An improvement to the well-established method of buffer-gas cooling was demonstrated by John Doyle's group at Harvard in 2011 [352]. For this, they used two

buffer-gas cells with different collision rates to achieve a better compromise between efficient slowing and high molecule numbers.

- A number of proposals were made to make laser cooling easier and more versatile by reducing the number of required photon-scattering events. This could be achieved by transferring molecules from an untrappable to a trappable internal state of a constant potential at the right moment [353, 354]. Another approach was to apply carefully timed sequences of fast laser pulses to avoid spontaneous emission into dark states [355].
- A group led by Edvardas Narevicius at Weizman Institute of Science investigated beam-slowing by moving magnetic traps [251, 356]. Molecules coming from a buffer-gas cell are typically too fast to be trapped in a stationary magnetic trap, but an initially co-moving trap can be slowed down adiabatically, so that it can catch the molecules. This was first demonstrated with O<sub>2</sub> molecules in 2015.
- Multiple groups, notably at Weizman Institute, ETH Zürich, and the University of British Columbia, developed a Zeeman decelerator; essentially a magnetic analogue to the electrostatic Stark decelerator. Note the fundamental difference to Zeeman slowers, which are based on laser cooling, while this type of device uses only dc magnetic fields. While this had already been investigated in 2008 [357], the method gained some popularity around 2012 and was used for O<sub>2</sub> and He<sub>2</sub> [358–360]. It also allowed the simultaneous deceleration of an atom-molecule mixture [361].
- In 2012, Jun Ye’s team at JILA claimed to have achieved the first evaporative cooling of molecules, specifically OH radicals [362]. In their experiment, molecules were trapped in a quadrupole magnetic potential, with radiofrequency fields performing the job of transferring the hottest particles into untrapped states, leading to evaporative cooling. A temperature of 5 mK could be reached. Later investigations cast some doubt onto this result when it was found that a significant part of the observed effect was caused by unwanted spin-flip losses rather than radiofrequency transfer [363].

## 2.6. 2018–2022: The second breakthrough?

### 2.6.1. Quantum control at single-molecule level

Up to this point, all ultracold-molecule experiments had worked with samples of at least hundreds of molecules, with no or very little control over single particles. This began to change around 2018, when techniques for controlling individual molecules were implemented for the first time. The method of choice were optical tweezers, essentially tiny dipole traps of which there could be a few hundred in an experiment, each one containing

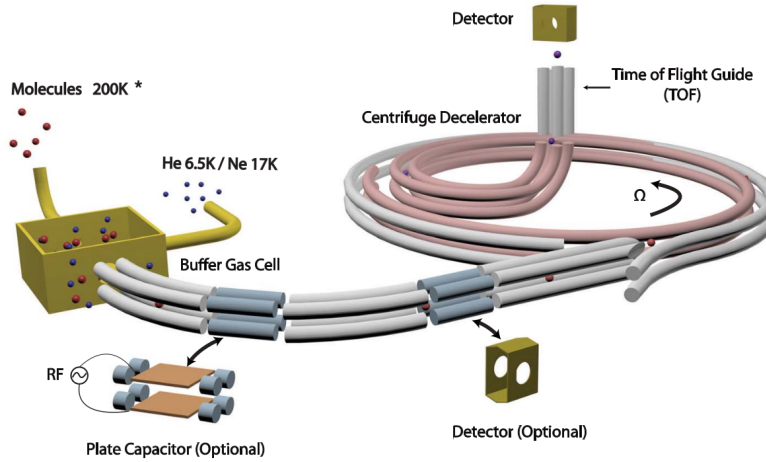


**Figure 2.19.:** Schematic of the centrifuge decelerator developed at MPQ. Figure taken from Reference [350].

a single atom or molecule. This technique had been introduced about a decade earlier for atoms and had quickly become very influential, see for example the review article [364]. There were two major advantages of tweezers over the larger conventional dipole traps and lattices: first, due to their much smaller size, they could reach enormously strong confinement, such that even relatively hot particles could be in well-defined motional states of the trap potential. This could reduce the complexity of cooling significantly. Second, the ability to move individual tweezers around enabled direct control over single molecules, which had never been possible before.

The first molecules in tweezers were realised by Kang-Kuen Ni's group. In their experiment, they first trapped  $^{133}\text{Cs}$  and  $^{23}\text{Na}$  atoms in separate tweezers, then merged them and used the strong confinement to reach high conversion efficiency into molecules [365–371]. A similar method was also used to associate  $^{85}\text{Rb}^{87}\text{Rb}$  [372]. Notably, this method of molecule creation circumvented all potential problems of miscibility, three-body loss and other such undesired effects, which had long plagued molecule association. On the other hand, this method only allowed the creation of up to a few hundred molecules, whereas bulk association had been demonstrated with tens of thousands. Soon after, Anderegg *et al.* demonstrated the trapping of  $^{40}\text{Ca}^{19}\text{F}$  in optical tweezers [373]. These molecules were laser-cooled in a MOT and loaded into the tweezers after an intermediate step of a new sub-Doppler cooling technique [374]. This method also allowed non-destructive detection of single molecules without dissociating them, a major improvement for quantum control.

With tweezers being established, there was no shortage of ideas on how to use them, for example for quantum computation, with hyperfine or rotational states of molecules as qubits [375–378]. Hyperfine levels specifically had the advantage that they could be controlled using rotational transitions, but were otherwise coupled weakly to the environ-

ment, enabling long coherence times [322, 379, 380]. Rotational coherence times had also been improved significantly, but were still on the order of a hundred milliseconds or less, at least an order of magnitude smaller than for hyperfine states [381–383].

## 2.6.2. Collisions and evaporation

In July 2018, the KRb team at JILA again surprised the community when they reported the first creation of a degenerate gas of molecules [384]. They claimed to have brought 30 000 ground-state molecules to 30% of their Fermi temperature. Probably the most unexpected thing about their paper was that they did not require any fundamentally new methods to achieve this. Simply starting out with more and colder atoms in combination with a better association efficiency was enough. However, the result also stirred some doubt: critics argued that even when starting out with perfectly degenerate atoms, some holes would be created in the phase space during association. Without any elastic collisions, thermalisation was impossible, such that these holes could never reach the Fermi surface. A gas in such a non-equilibrium state could not reasonably be called “degenerate” or even “cold”, as its temperature was, strictly speaking, undefined. Even more crucially, with the holes distributed uniformly over the phase space, it was impossible to detect this from the cloud shape, leading to a false impression of degeneracy. The JILA team soon published a second paper with improved data analysis [385], but could not fully address all doubts.

The NaK team at MPQ began developing an improved method of Feshbach association for degenerate mixtures of  $^{23}\text{Na}+^{40}\text{K}$  soon afterwards, but quickly realised that two- and three-body losses as well as previously not understood quantum many-body effects had a strong influence on the efficiency. Following an investigation of loss processes [165, 386], they managed to create a doubly-degenerate Bose–Fermi mixture of atoms with equal density of both species, allowing a quantum phase transition from a strongly-interacting polaronic phase to a low-entropy molecular phase [387]. However, just as in the JILA experiment, the resulting molecules could not elastically collide and remained in a nonequilibrium state. A watertight claim to degeneracy was only going to happen with molecules that could thermalise.

Of course this was easier said than done. At this time, there was finally no longer any doubt about the two-body losses of chemically stable molecules. These were not experimental errors or some unusual edge cases, but had been repeatably found with every investigated species [388–390]. They were also not a mere nuisance, but almost completely stopped progress towards colder samples and the possibility to create dipolar quantum many-body systems. But how could it be possible for chemically stable ground-state molecules to be lost in two-body collisions? Changes to their internal state, which would make the molecules untrappable or invisible can not occur because they require extra energy, which is not available in ultracold collisions. There are no possible chemical reactions which could provide this energy, either. Finally, two molecules entering a bound state indefinitely is forbidden due to energy and momentum conservation in the collision. It seemed to make no sense at all.

This caused renewed interest in a proposal by John Bohn and coworkers from 2012.

They had suggested that colliding diatomic molecules could form a four-body entity, later fittingly dubbed a “sticky complex” [391–393]. These predictions were refined by Christianen *et al.* in 2019 [394–396]. Sticky complexes could of course not be stable, but might live long enough for other processes, such as photon scattering, to cause loss. This can be understood as follows: when two molecules get close enough to each other, they sample a part of the four-body interaction potential where the binding energy is quite large. Though the molecules can not enter any bound states, this energy can temporarily go into other degrees of freedom, leading to rotational and vibrational excitations of both molecules. However, they can not leave the well of the interaction potential until they have both reached the initial state again. This leads to a collision in which the two molecules chaotically go through a large number of states, remaining trapped until they randomly come back to their respective two-body ground states. This opened up an exciting possibility: if photon scattering was indeed responsible for the loss, then molecules could be made stable in a sufficiently dark environment. There were methods for studying collisions in low light intensity, such as by merging molecular beams to create a low-energy collider [397–400]. However, the ultracold regime, where the sticky collisions really started playing an important role, had previously only been reached in optical dipole traps at very high light intensity. So how could this be done?

The RbCs team at Durham came up with an ingenious idea: the dipole trap did not need to be on all the time. Due to the inertia of the molecules, the trap could be periodically switched off for hundreds of microseconds without any effect on the trapping potential. Because the loss was saturated (i.e., every sticky complex got destroyed before dissociating) during the bright phases of the trap, the average two-body loss should be reduced in such a “chopped” dipole trap. Indeed, they found a longer lifetime of  $^{87}\text{Rb}^{133}\text{Cs}$  [401, 402], prompting other teams to begin similar efforts. The first came from Kang-Kuen Ni’s group at Harvard: they had constructed an experiment using  $^{40}\text{K}^{87}\text{Rb}$  that actually allowed the detection of arbitrary molecules via mass spectroscopy and ion detection [403]. With this setup, it was possible to see the reaction products rather than just missing molecules. They could indeed observe sticky complexes, though they were much shorter-lived due to chemical reactions, and confirmed that they can be excited by light [404].

However, three other teams working with  $^{23}\text{Na}^{39}\text{K}$ ,  $^{23}\text{Na}^{40}\text{K}$ , and  $^{23}\text{Na}^{87}\text{Rb}$  failed to find any influence of light intensity on complex lifetime [307, 405]. What had seemed like a solution had instead made the problem even more confusing: some molecules behaved as expected while others did not, and nobody understood why. A number of subsequent theory publications [406–413] attempted to solve this problem, but to date a complete explanation of this puzzling phenomenon is missing. A more detailed explanation is given in Chapter 5.

Luckily, it soon turned out that understanding the sticky-collision puzzle was not so important after all, at least from a practical perspective: the blocking of close-range interactions via repulsive interaction could finally be experimentally implemented. The first evaporative cooling of a pure molecule sample was reported by Valtolina *et al.* in 2020 [414]. This was done with  $^{40}\text{K}^{87}\text{Rb}$  confined in a 2D “pancake” trap with an electric field parallel to the strong confinement. However, despite the relatively strong suppres-

sion of two-body loss, only 60% of the Fermi temperature could be reached, mostly due to the difficulty of efficiently removing hot molecules from 2D planes. In the next year, a significant improvement was made by choosing a specific value of the electric field where the shielding was resonantly enhanced by a crossing of two rotational levels [415–418]. This *resonant shielding* had two advantages: first, it worked not only in collisions orthogonal to the electric field, and could therefore be done in 3D traps [419]. Second, the shielding in a 2D geometry was more effective than previously shown [420].

Another approach was to apply strong ac fields to create superpositions of rotational states in such a way that the molecule-molecule interaction becomes repulsive at close range [421–428]. The first demonstration of this effect was done with CaF molecules in optical tweezer traps [429, 430]. In this system, the lifetime was increased by a factor six with an optimally tuned, highly intense microwave field. Motivated by this success, the NaK team at MPQ used the same method and achieved efficient evaporative cooling in 3D (see Chapter 6).

With molecule-molecule collisions being lossy, it was also natural to wonder if molecules could thermalise with atoms instead. This would allow evaporatively cooling an atom-molecule mixture, and removing the atoms afterwards. A number of experiments revealed that this was indeed possible, but the efficiency depended strongly on the species combination [431, 432]. For example,  $^{23}\text{Na}^{39}\text{K} + ^{23}\text{Na}$  collisions were very lossy, but  $^{23}\text{Na}^6\text{Li} + ^{23}\text{Na}$  worked well. With this combination, the first sympathetic cooling of a molecule-atom mixture was demonstrated by Wolfgang Ketterle's group at MIT [433]. Soon, Feshbach resonances between molecules and atoms were found [434–437], specifically with the combinations  $^{23}\text{Na}^{40}\text{K} + ^{40}\text{K}$  and  $^{23}\text{Na}^6\text{Li} + ^{23}\text{Na}$ . Up to now, the resonances have not been used to improve sympathetic cooling, but there is hope that this may soon be possible, especially if a model can be found that accurately predicts the collision properties of a given combination.

### 2.6.3. Polyatomic and alkaline-earth molecules

With very few exceptions, previously cooled molecules were diatomics, specifically either made of two alkali atoms, or of an alkaline-earth-like atom and a halogen, such as CaF. Experience had shown that developing more general cooling techniques was very difficult, but why would it not be possible to extend working techniques to a few more types of molecules?

There was one type that had already been investigated for a while: alkaline-earth + alkali combinations. Their advantage was that the mixtures needed for association were almost as easy to make as bialkali mixtures. In fact, over the past decade, certain alkaline-earth atoms, namely strontium and ytterbium, had become almost as commonly used as rubidium and potassium in ultracold-atom experiments. Hence, it seemed quite natural to attempt the creation of molecules like RbYb, CsYb, and RbSr. Molecules of this type are basically three-electron systems with a total electron spin  $S = 1/2$  in the ground state. In contrast to bialkali molecules with  $S = 0$ , they have a magnetic moment in addition to their electric dipole moment. This allows additional degrees of freedom for quantum

simulation, but also has more practical advantages like allowing magnetic trapping.

First studies on such molecules had been done as early as 2009 [438–440], however the field started picking up momentum around 2018 [441–446]. The main problem was achieving Feshbach association: the coupling between free and bound states is quite weak for these systems [447], leading to narrow Feshbach resonances, which in turn makes very precise magnetic-field control necessary. Some resonances in the systems  $^{87}\text{Rb}+^{87}\text{Sr}$  and  $^{87}\text{Rb}+^{88}\text{Sr}$  have been experimentally found [448], and investigation is ongoing on further combinations [449], as well as on association methods which do not require Feshbach resonances [450, 451]. However, to date no molecule formation other than by photoassociation has been reported in any of these systems.

Meanwhile, some teams working on direct laser cooling realised that a certain class of polyatomic molecules have an electronic structure very similar to diatomics, and were potentially amenable to the same cooling methods. This seems hard to believe at first glance, but actually makes sense. For example, the hydroxide ligand (OH) behaves very similar to a single fluorine atom: the O-H bond is strong and the electrons involved in it basically don't interact with the rest of the molecule. The ligand is also strongly electronegative and attracts one electron from an alkaline-earth atom, forming an almost ionic bond. In this sense, CaOH is not so different from CaF. The same argument holds also for many other ligands like OCH<sub>3</sub>, CH<sub>3</sub>, and NH<sub>2</sub>, as described in References [452–455].

John Doyle's group quickly took the lead in this field, both from the theoretical and experimental side. Within few years, they reported laser cooling of SrOH, YbOH, CaOH, and CaOCH<sub>3</sub> [456–462]. In 2021, the first MOT of a polyatomic molecule, CaOH, was realised in the same group [463]. Once under control, polyatomic molecules might be used for new quantum computing schemes [464], but mostly for probing fundamental physics, where they are expected to open up many new possibilities as described in the following section.

## 2.6.4. Fundamental physics with molecules

Since 2011, precision measurement in the pursuit of probing fundamental physics with molecules had made steady progress. Two new records on the upper bound of the eEDM had been published in 2013 and in 2018, both by the ACME collaboration [465, 466]. The latest iteration reached an astonishingly precise result of  $d_e < 1.1 \times 10^{-29} e\text{cm}$ , using ThO molecules in an  $H^3\Delta_1$  excited state. Similar to previous eEDM measurements, a superposition of two states, in this case two different directions of the electron spin, was created before letting the molecules propagate through an external electric field (see Figure 2.20). This resulted in a Ramsey sequence where an energy shift between the spin states caused by the electric field could be detected as a phase shift in the superposition. Both the species and the electronic state were carefully chosen to reduce the impact of possible systematic effects as described in detail in Reference [467]. Another experiment confirmed this result, also finding a eEDM consistent with zero, using trapped HfF<sup>+</sup> ions [468]. So despite many predictions to the contrary, no *CP*-violating physics was found. This meant that precision measurements with ultracold molecules were now

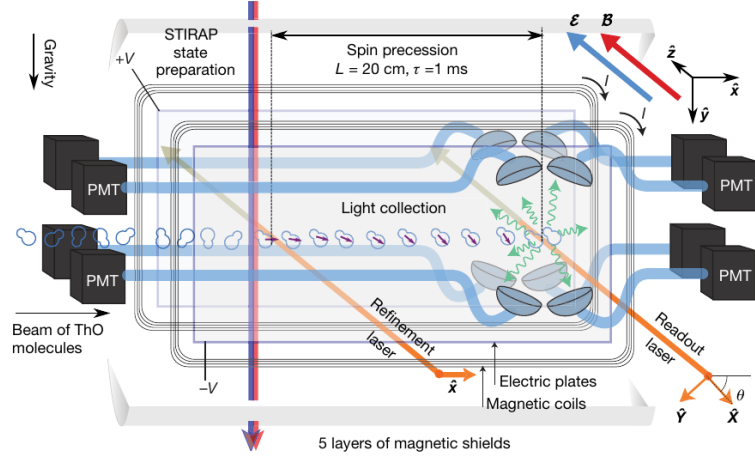


**Figure 2.20.:** Schematic of the method for measuring eEDM in the ACME II experiment. ThO molecules in a superposition of two spin directions travel through an area of precisely controlled electric and magnetic fields for Ramsey spectroscopy. Figure taken from Reference [465].

able to exclude beyond-Standard Model physics at energy levels never probed by colliders [469, 470].

Unsurprisingly, this caused a lot of excitement, both in high-energy and AMO physics. Proposals were brought forward to detect many kinds of new physics, such as variations in the electron-proton mass ratio [471–475], ultralight dark matter [476, 477], and *PT*-violating effects like axions [478]. More details can be found in the review articles [152, 479, 480]. A significant number of these proposals suggested the use of polyatomic molecules, for example SrOH due to its sensitivity to ultralight dark matter [477].

Further improvements of eEDM measurements were also suggested: a team at Imperial College attempted to improve the performance of YbF by increasing the interrogation time and brightness [481–484], while some other groups, notably at the University of Groningen and at Columbia University, looked at BaF and BaH instead [485–492]. Again, polyatomics like YbOH or YbOCH<sub>3</sub> were considered, as they offer strong coupling to *CP*-violating terms and long potential coherence times [493–495]. It was also suggested to use hydride molecules like BaH and CaH as an intermediate step in the creation of an ultracold gas of hydrogen, which could then be used for precision tests of quantum electrodynamics [496].

Another, yet more radical, idea was to use associated molecules with even heavier nuclei, like YbAg, FrAg, RaAg or LrO [497–501]. Especially the species <sup>223</sup>Fr<sup>107</sup>Ag promised high sensitivity, however creating it certainly posed a challenge. Though both francium and silver have been laser-cooled [502, 503], the half-life of <sup>223</sup>Fr is a mere 22 minutes, meaning that working with this isotope requires a particle accelerator on site. Despite this, some considered francium-containing molecules to be a promising research

project [504, 505].

To date, these ideas are still a few years away from being experimentally realised, and for now, the next improvement of the lower bound of the eEDM will likely come from ACME III, following the same method as previous iterations, but with many technical improvements.

## 2.7. Future directions

Having worked our way through 35 years of ultracold-molecule history, we have now arrived in the present and should have a look into the near future of the field. What are its most promising developments and what is likely to be achieved soon? At this point, both of the fundamental problems of molecule cooling, the laser-cooling conundrum and the collision conundrum, have been solved. Though the solutions are complicated and only applicable to certain species, they are nonetheless available and will allow ultracold molecules to finally fulfil their potential after decades of struggle.

For 20 years, quantum systems with strong dipolar interactions have been studied theoretically, with the expectation that experimental realisations were just around the corner. A plethora of new quantum phases have been predicted, including charge-density waves, dipolar superfluids and supersolids, Wigner crystals, and many more. With the development of collisional shielding and evaporation techniques, quantum-degenerate molecules are now finally available, bringing many of these predictions into experimental reach. An overview of theoretical predictions is given in Appendix B, and a more thorough look into the challenges of experimentally implementing them can be found in Chapter 7. Though previously, there have been realisations of quantum systems with dipolar interactions, mostly using magnetic atoms [147, 148, 506–510] and Rydberg atoms [511], ultracold molecules can extend and improve the possibilities of these systems. Between magnetic atoms, which can be long-lived and very cold, but have quite weak dipolar interactions, and Rydberg atoms, which have very strong interactions but very short lifetimes, dipolar molecules can fill important niches in quantum simulation of dipolar quantum matter.

Which species are the most promising candidates for this endeavour? On the bosonic side,  $^{23}\text{Na}^{133}\text{Cs}$  has recently been associated for the first time in bulk by Sebastian Will's group at Columbia University. The combination of sodium and caesium has been found to be unexpectedly well-controllable, and the molecule has already been made at very low temperatures by overlapping two atomic BECs [512, 513].  $^{23}\text{Na}^{87}\text{Rb}$  also remains a strong candidate, as it is simple to work with and has recently been used in the first molecular quantum-gas microscope, where single molecules on the sites of an optical square lattice can be resolved [514]. With some improvements in association efficiency, the long-sought BEC of polar molecules may soon become reality.

Looking at fermions,  $^{40}\text{K}^{87}\text{Rb}$  was the undisputed leader for a decade, but I think it is fair to say that  $^{23}\text{Na}^{40}\text{K}$  has now closed the gap and is beginning to open up new possibilities with its larger dipole moment. The other bialkali combinations (NaLi, LiK, LiRb, LiCs, KCs, and RbCs) are likely to be used rather in niche applications, either due to their complicated association procedure or small dipole moment. Looking one step

further ahead, with the discovery of molecule-atom Feshbach resonances [434–437] and the recent proposal of photoassociation of larger molecules [515, 516], it may soon be possible to assemble polyatomic molecules step by step from atoms.

Laser-cooled molecules have made enormous strides in the past decade, with the phase-space density record going up by eleven orders of magnitude over eight years [517–519]. However, the highest value achieved to date is still only on the order of  $10^{-6}$  with 1200 molecules [520]. At least five orders of magnitude more would be necessary for directly cooled molecules to reach a regime where they can be used for quantum simulation. Though improvements are still being made, it seems certain that the progress is going to slow down, with many simple problems having been solved already. Nonetheless, many great things can be done with directly cooled molecules, especially in the areas of probing fundamental physics and quantum computing in tweezer arrays. With recent proposals on cooling more complicated molecules like  $C_2$  or  $CaSH$ , the field of direct laser cooling may also soon widen up further [454, 521]. Without a doubt, interesting times are ahead.

*The craftsman who wishes to do his work well, must first sharpen his tools.*

—Kong Fuzi, Analects 15

## 3. A new STIRAP setup

The STIRAP system is our gateway to the molecule ground state and one of the most crucial parts of the experimental setup. However, STIRAP is quite technically challenging. Until 2020, the pathway we used was based on the intermediate state  $|d^3\Pi_1, v = 5\rangle$ , which has a 2% admixture of  $|D^1\Pi_1, v = 6\rangle$ . The laser system to address this state and the resulting transfer are described in [522–525]. After a few years, we decided it had to be replaced due to two significant shortcomings: first, its one-way efficiency was limited to about 60% even under optimal conditions, due to the unresolved hyperfine structure of the excited state leading to unwanted interference effects between multiple overlapping transitions [524, 525]. This problem occurs specifically for excited states with no  $\Sigma$  contribution, because the wavefunction overlap between valence electrons and nuclei is extremely small. This is sometimes called “missing Fermi contact interaction”. Despite significant efforts in understanding the detrimental effects of the hyperfine structure, we were unable to achieve efficiencies comparable to other pathways. Second, the required laser wavelengths were 488 nm and 652 nm. 488-nm light can be produced with diode lasers, but the diodes are unreliable and hard to work with, particularly when stabilising to the required narrow linewidths. 652-nm light can not be produced at sufficient power with diode lasers, prompting us to use a dye laser instead. This met the power and stability requirements, but only with a significant maintenance effort.

For these reasons, we decided to switch to a different intermediate state which was already in use by the MIT and USTC teams, and had proven to be efficient [299, 526]. During this project, the old setup was completely disassembled and replaced. With improved Feshbach association, we were also able to demonstrate a significant simplification of the setup compared to previous implementations. This chapter is based on the publication [527], and describes the new setup and the improvements it enabled.

### 3.1. Creation of Feshbach molecules

#### 3.1.1. Theoretical description

The two most common ways to associate weakly bound Feshbach molecules from atoms are magnetoassociation and radiofrequency (rf) association. For rf association, the atomic mixture is prepared at a magnetic field slightly below the desired Feshbach resonance,

where a bound state exists. However, the mixture is initially in a different hyperfine state which does not exhibit a resonance at this field. An rf  $\pi$ -pulse is then used to transfer the atoms into the target hyperfine state, moving some of them directly into the molecular bound state. This has been the method of choice for  $^{23}\text{Na}^{40}\text{K}$  [24, 297, 526], and was used in our experiment, too. For this, the combination  $\text{Na} |F = 1, m_F = 1\rangle + \text{K} |9/2, -7/2\rangle$  is prepared at a magnetic field of 85.4 G, after which the K atoms are transferred to  $|9/2, -9/2\rangle$ , creating molecules in  $|11/2, -7/2\rangle$ .

Radiofrequency association is essentially instantaneous compared to the time scale of collisions in the gas. Hence, its efficiency is limited by the phase-space overlap between the two species in the weakly interacting case, far away from resonances. This is a significant problem because  $^{23}\text{Na}$  and  $^{40}\text{K}$  exhibit different quantum statistics. Once the bosons start condensing, a significant number of them are in the ground state of the trap, while the Pauli exclusion principle prevents fermions from doing the same. In the extreme case of no interaction and zero temperature, this means that only a single molecule can be formed because all bosons are in the same state, which can only contain one fermion. In the opposite case of high temperatures, the overlap is also very low, limited by the small phase-space density of both species. There is a compromise between these extremes for near-degenerate samples, but the best efficiencies that have been achieved are 10 to 15% [297, 524].

In contrast, magnetoassociation requires an atomic mixture that is initially already in the state where the binding will happen. Instead of changing the hyperfine state, the magnetic field is ramped from the attractive to the repulsive side of the resonance, slowly enough that the atoms can adiabatically follow. This can be more technically challenging because it requires magnetic-field control that is simultaneously fast and precise. The great advantage of this method is that it allows multiple elastic collisions to occur during the transfer. This way, the phase-space overlap can increase bit by bit and much higher efficiency can be reached. Instead of phase-space overlap, it is inelastic collisions which are the limiting factor to this approach.

In pursuit of creating a degenerate gas of polar molecules, our team decided to switch from rf association to magnetoassociation. This project included a careful characterisation of the Feshbach resonances at 78.3 G and 89.7 G, the two- and three-body loss during association, and the many-body physics of balanced, strongly-interacting Bose-Fermi mixtures. This work was carried out primarily by Marcel Duda and Xing-Yan Chen, and is described in detail in References [165, 386, 387]. Here, I will only briefly describe the association procedure, insofar as it is relevant to understand the STIRAP results.

To perform efficient magnetoassociation, it is important to precisely understand the relevant resonances. An overview of resonances in our system is shown in Figure 3.1. As described in the supplemental material of Reference [386], the width and position of the resonances were determined from binding-energy measurements, following Reference [528]. The binding energy  $E_b$  can be measured precisely via rf-association spectroscopy, and it is related to the Feshbach-resonance shape via the formula

$$\frac{\sqrt{2\mu E_b}}{\hbar} = \frac{1}{a_{\text{bg}} - \bar{a}} + \frac{1}{\bar{a}} \sum_{i=1,2} \frac{C_i}{E_b + E_i}, \quad (3.1)$$

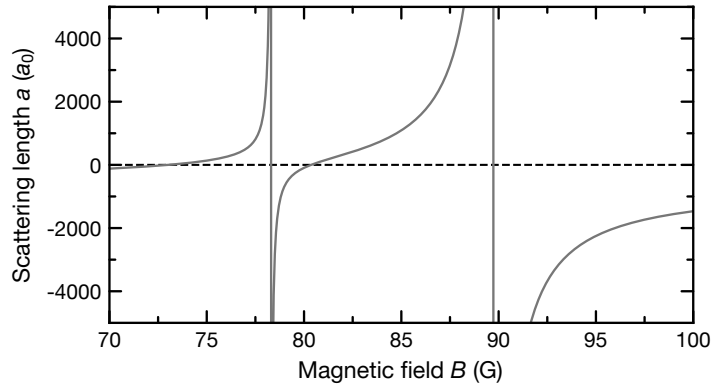


**Figure 3.1.:** Feshbach resonances between  $^{23}\text{Na}$   $|F = 1, m_F = 1\rangle$  and  $^{40}\text{K}$   $|9/2, -9/2\rangle$ . The resonance widths and positions are taken from Reference [386].

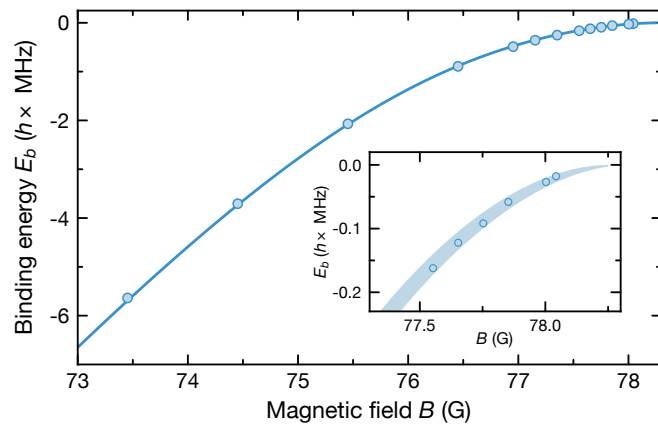


**Figure 3.2.:** Binding energy  $E_b$  of Feshbach molecules in the  $|\text{FB}\rangle$  state, depending on the magnetic field  $B$ . The inset is a close-up to the same data very close to the resonance. The data points result from fitting rf association spectra. The resonance parameters used in Figure 3.1 were determined from these data using Equation (3.1), as described in Reference [386].

where  $\mu$  is the reduced mass,  $E_i$  and  $C_i$  are the energies of the bare molecular state and the Feshbach coupling strengths for the two resonances, respectively,  $a_{\text{bg}} = 619(31) a_0$  is the background scattering length [529], and  $\bar{a} \approx 51 a_0$  is the mean scattering length [528]. Figure 3.2 shows the measured binding energy and a fit of this model. The scattering length in the vicinity of the two relevant resonances is then given by

$$\frac{1}{a - \bar{a}} = \frac{1}{a_{\text{bg}} - \bar{a}} + \frac{1}{\bar{a}} \sum_{i=1,2} \frac{C_i}{E_i}. \quad (3.2)$$

Though all previous experiments worked on the repulsive side of the 89.7-G resonance,<sup>1</sup> this is not particularly well-suited for magneto-association. This is because the resonance is quite broad with a width of 9.3 G, meaning that ramping over it, even with a fast magnetic-field control system, takes a significant time during which inelastic collisions can occur. Choosing the resonance at 78.3 G, which is 5.3 G wide, reduces this effect. In addition, on the right side of the 78.3-G resonance, the interspecies interaction can be tuned to be moderately repulsive, which is better suited for sympathetic cooling than the much stronger and attractive interaction on the right side of the 89.7-G resonance. Finally, there is another advantage to the lower-lying resonance: as there are no further resonances directly below it, the field can easily be ramped into the regime of more deeply bound molecules.

The Feshbach-molecule state  $|\text{FB}\rangle$  can be described as a superposition of the open-channel part, which corresponds to two unbound atoms, and the closed-channel part, which corresponds to the least-bound vibrational level of the electronic  $a^3\Sigma^+$  manifold. As shown in Figure 3.3, the relative weight of the open- and closed-channel contributions depend on the magnetic field, with the closed-channel fraction becoming larger for the more deeply-bound Feshbach molecules far below the resonance. This is important for the STIRAP transfer because the Franck–Condon overlap between (unbound) continuum states and the (bound) intermediate states is negligible. Rather, it is only the closed-channel part of the Feshbach-molecule state which is coupled by the STIRAP light. Consequently, the transition dipole moment can be increased by using closed-channel-dominated Feshbach molecules.

### 3.1.2. Experimental procedure

In order to create Feshbach molecules, we first need atoms. The creation of an atomic mixture of  $^{23}\text{Na}$  and  $^{40}\text{K}$  in our setup has previously been described in the PhD theses of Nikolaus Buchheim, Zhen-Kai Lu, and Frauke Seeselberg [522, 523, 525], but a few key aspects have been upgraded since then. The process begins with metallic samples of sodium and potassium which are heated to sufficient vapour pressure in two separate ovens inside an ultrahigh-vacuum chamber. The sodium subsequently passes through a

---

<sup>1</sup>The same resonance was often quoted to be at 88.2 G, following Reference [298]. The results given there are likely to contain systematically underestimated resonance positions, as they are based on loss measurements rather than more reliable binding-energy measurements.

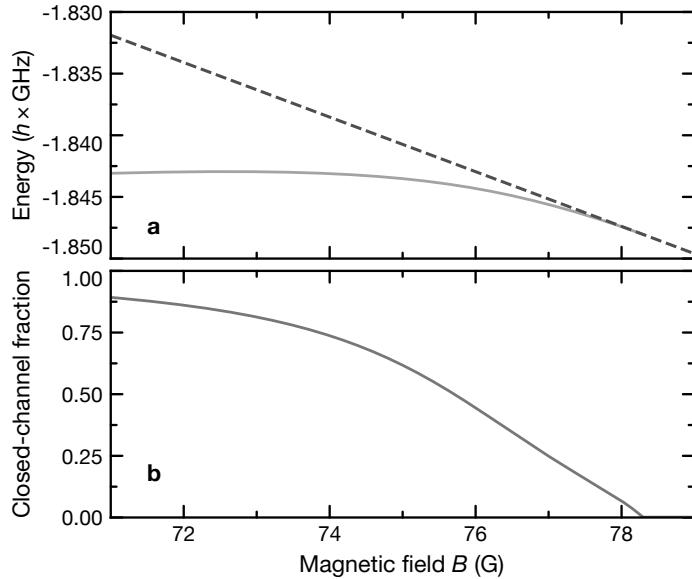


**Figure 3.3.:** Magnetic-field dependence of atomic and molecular states. **(a)** Zeeman shift of atoms and Feshbach molecules. The dashed line shows the energy of an unbound pair of Na  $|1, 1\rangle$  + K  $|9/2, -9/2\rangle$ , relative to the hyperfine centre of mass. The solid line which branches off at the resonance position shows the energy of the Feshbach molecule. At  $B = 72.4\text{G}$ , the energy of the Feshbach state becomes first-order insensitive to field changes. **(b)** Closed-channel fraction of Feshbach molecules. Large values can be achieved at magnetic fields significantly below the resonance.

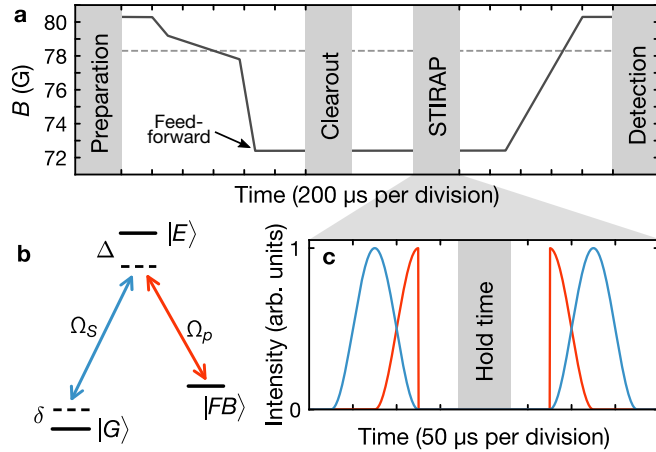


**Figure 3.4.:** Experimental sequence. (a) Field ramps for magnetoassociation and subsequent dissociation. “Clearout” stands for a 20-ms magnetic field gradient pulse to remove unassociated atoms. The dashed grey line indicates the resonance position. (b) Three-level system used for STIRAP. The pump beam is shown in red, the Stokes beam in blue. (c) STIRAP pulse shapes for the pump and Stokes beams. A pulse duration of 50  $\mu$ s is assumed here. The typical peak intensities of the beams are 200 W/cm<sup>2</sup> for the pump beam and 0.3 W/cm<sup>2</sup> for the Stokes beam. This corresponds to powers of 10 mW and 15  $\mu$ W, respectively.

Zeeman slower and is captured in a 3D MOT. The same is done with the potassium, but a 2D MOT is used instead of a Zeeman slower. The 3D MOT captures both species simultaneously, cooling down about  $5 \times 10^9$  Na atoms and  $1.4 \times 10^7$  K atoms to 300  $\mu$ K. This is too hot for loading directly into an optical trap, so evaporative cooling to 6  $\mu$ K is first performed in a magnetic trap. Afterwards, the mixture is loaded into a 1064-nm optical dipole trap and transported from the MOT chamber to a glass cell, where all further experimental steps are done. The dipole trap consists of two beams intersecting under a small angle, which helps to create the axial confinement necessary for transport. Once the sample has arrived in the glass cell, the dipole trap is ramped down for further evaporative cooling until the desired temperature is reached. Notably, the sodium is confined much less strongly in the dipole trap, such that almost no potassium gets evaporated, and it is only sympathetically cooled by the sodium. During the evaporation, an additional dipole-trap beam at 1550 nm is turned on, orthogonal to the transport beam, keeping the density close to the optimal value where a good compromise between three-body loss and thermalisation time is reached.

For the case of the experiments described in this chapter, the dipole-trap evaporation is stopped with  $1 \times 10^5$  sodium atoms in the state  $|1, 1\rangle$  and  $2 \times 10^5$  potassium atoms in  $|9/2, -9/2\rangle$ . At this point, the trap frequencies of the crossed-beam optical dipole trap are  $2\pi \times (50, 72, 191)$  Hz for Na and  $2\pi \times (54, 88, 223)$  Hz for K in the  $(x, y, z)$  directions, respectively. At the end of the evaporation, the temperature is typically 300 nK.

The association of Feshbach molecules begins at a magnetic field of 80.3 G, where the interspecies scattering length vanishes. We then ramp over the 78.3 G-resonance in three steps to create about  $4 \times 10^4$  molecules, corresponding to 40% transfer efficiency of sodium. The association procedure is shown in Figure 3.4. The first part is a quick ramp to 79.2 G, slightly above the resonance, which takes 100  $\mu$ s. Because there is not yet any association at this time, doing the ramp this fast has no detrimental effects, but does reduce losses. The second ramp, where the actual association takes place, changes the field to 77.8 G within 470  $\mu$ s. The duration and end point of this ramp are chosen to optimise the association efficiency. At 77.8 G, the molecules are highly unstable against collisions with residual atoms and with each other, so we perform a third ramp to a final field of 72.4 G within 100  $\mu$ s to minimise inelastic atom-molecule collisions.

The final value is chosen because the energy of the curve of energy versus magnetic field for the Feshbach state has an extremum here, meaning that the following STIRAP transfer is least sensitive to field fluctuations, see Figure 3.3. To achieve optimal stability for STIRAP and the following experiments, the final ramp is performed with a feed-forward procedure, which is designed to minimise the effect of eddy currents in conductive parts of the apparatus close to the molecule sample. This is achieved by changing the current through the magnetic-field coil in such a way that the known eddy currents are compensated, following [530]. Finally, we apply a “clearout” magnetic-field gradient of 40 G/cm for 20 ms. This pulls residual atoms out of the dipole trap, but leaves molecules unaffected due to their small magnetic moment.

## 3.2. STIRAP setup

### 3.2.1. Laser sources and locking

The intermediate excited state  $|E\rangle$  used for the new STIRAP scheme contains strong components of  $|c^3\Sigma^+, v = 35\rangle$  and  $|B^1\Pi, v = 12\rangle$ , with 64% triplet and 36% singlet fraction. The contribution of different hyperfine states is given in Table 3.1. This state was first characterised in Reference [24], and subsequently used by the MIT and USTC groups with consistent results [299, 526].

The setup is based on two external-cavity diode lasers (DLPro, Toptica) at wavelengths of 1134 nm and 805 nm. An overview is shown in Figure 3.5. As a description of the technical details can be found in Akira Kamijo’s master thesis [531], I will give a more general account here.

To achieve the low laser linewidth necessary for STIRAP, both lasers are stabilised to a single, dual-wavelength reference cavity (Stable Laser Systems) which is described in Section 3.2.2. To do this, a small amount of power is split off from each laser beam, sent through a single-mode optical fibre, and coupled into the reference cavity. This light is power-stabilised with acousto-optical modulators, because the heating of the cavity mirror coatings by absorbed light causes frequency shifts. By positioning the photodiodes used for stabilisation close to the cavity, we reduce the power fluctuations caused by optics in between.

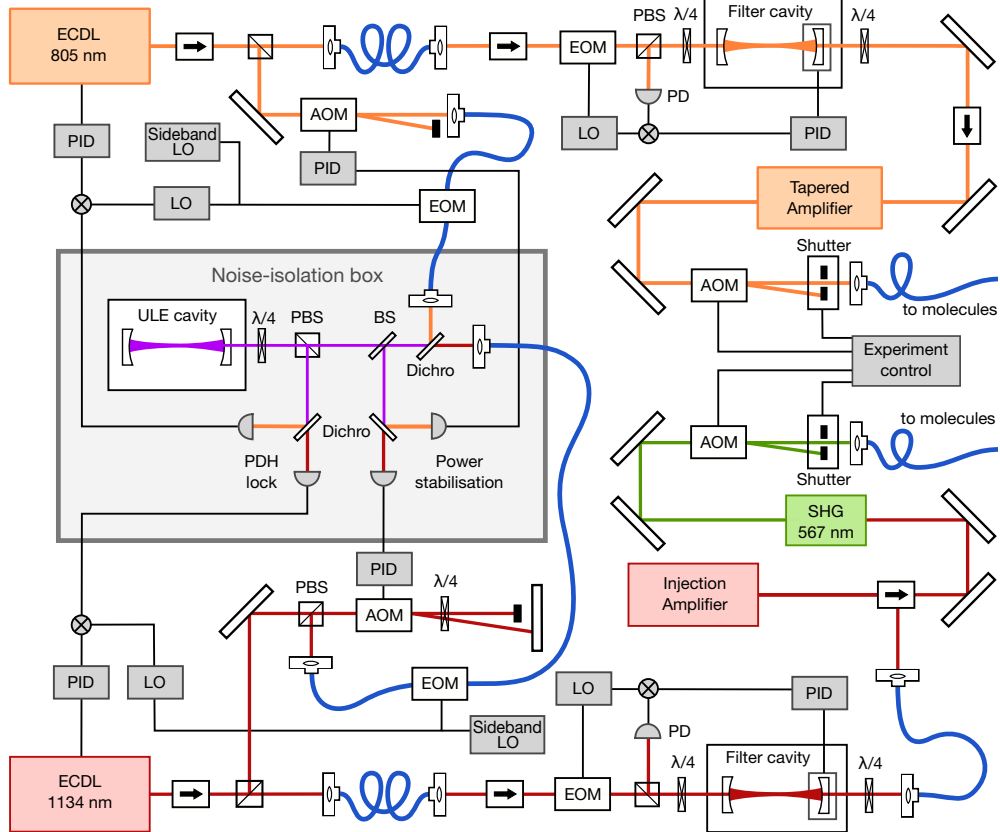


**Figure 3.5.:** The STIRAP setup. Laser light is generated by two external-cavity diode lasers, which are stabilised to a dual-colour ULE cavity. Faraday isolators prevent unwanted backreflection of light into the lasers. Sidebands are modulated onto the light to allow stabilisation to arbitrary wavelengths. The light of both colours is sent through additional filter cavities to reduce phase noise. The 1134-nm light is then amplified and frequency-doubled in a periodically-poled lithium niobate SHG module. A tapered amplifier can optionally be inserted to increase the available power of the 805-nm light. Acousto-optical modulators and shutters are used to control the pulse shape and ensure that no unwanted leakage light gets to the molecules.

Abbreviations: AOM—acousto-optical modulator, BS—beam splitter, ECDL—extended-cavity diode laser, EOM—electro-optical modulator, LO—local oscillator, PBS—polarising beam splitter, PD—photodiode, PID—proportional-integral-differential loop filter, SHG—second-harmonic generation.

**Table 3.1.:** Quantum numbers of the STIRAP intermediate state,  $|E\rangle$ . The projections of the nuclear spin of the atoms are labelled  $m_{I,\text{Na}}$  and  $m_{I,\text{K}}$ . Only the eight strongest contributions, which together make up 99.2% of the weight, are shown.

Manifold	$m_J$	$m_{I,\text{Na}}$	$m_{I,\text{K}}$	weight
$B^1\Pi$	0	1/2	-3	0.0145
	0	3/2	-4	0.0754
	1	-1/2	-3	0.0098
	1	1/2	-4	0.258
$c^3\Sigma^+$	0	1/2	-3	0.0257
	0	3/2	-4	0.133
	1	-1/2	-3	0.0173
	1	1/2	-4	0.458

The light is overlapped on a dichroic mirror, and sent into the cavity to create Pound-Drever-Hall (PDH) error signals for each colour [532, 533]. Fibre-coupled electro-optical modulators (EOM; PM830 and PM1170, Jenoptik) are used to provide phase modulation to create the PDH signal as well as to add sidebands for frequency offsets. By locking a sideband instead of the carrier to the cavity, this allows generating arbitrary offsets of the target frequency within the EOM’s bandwidth. Though the EOMs themselves remain efficient up to frequencies of many gigahertz, the direct digital synthesisers we use to generate the driving signal can only reach up to 400 MHz. With the 1.5-GHz free spectral range of the cavity, this means that the frequency-shift caused by the power-stabilisation AOMs must also be used in order to cover all possible lock frequencies. To reach the desired lock point of the 1134-nm laser, this requires a double-pass AOM configuration. By combining these shifts, the full frequency range given by the coating of the cavity mirrors can be covered. In comparison to free-space EOMs, the fibre-coupled EOMs have the advantage of significantly larger bandwidth, allowing higher sideband frequencies. They also exhibit much lower residual amplitude modulation, which could cause slow, uncontrolled frequency drifts [534]. To avoid disturbances from acoustic noise, the entire reference-cavity assembly is protected by a noise-isolation box made of wood and polymer foam.

### 3.2.2. Reference cavity

The reference cavity is essentially a hollow cylinder made of ultralow-expansion (ULE) glass with two highly reflective mirrors optically contacted to its ends at a distance of 10 cm. Its finesse is  $\mathcal{F}_{1134} = 3.530(6) \times 10^4$  and  $\mathcal{F}_{805} = 4.58(12) \times 10^4$  at the two wavelengths, respectively. ULE material exhibits a very low thermal expansion coefficient and high mechanical stiffness compared to most other materials, allowing the construction of cavities that are extremely stable against external perturbations. At a specific temperature, there is a zero-crossing of the thermal expansion coefficient, which is where

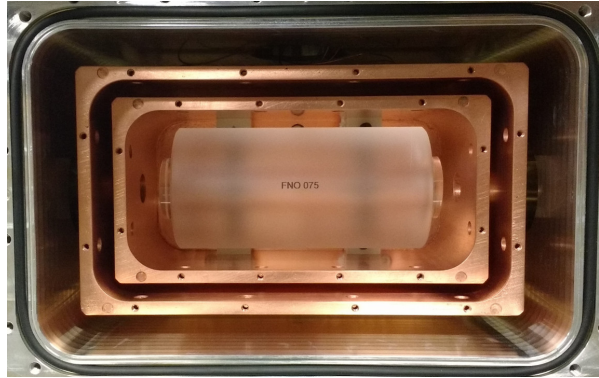


**Figure 3.6.:** The reference cavity inside its housing. The two-layer copper shield enables high stability against temperature drifts and gradients. Picture courtesy of Akira Kamijo.

optimal stability is reached. To take advantage of these properties, the cavity must be temperature-stabilised, with as little thermal gradients as possible, and must be isolated from mechanical noise.

This is achieved in our experiment by mounting it inside an aluminium vacuum chamber, which contains two layers of copper shielding (see Figure 3.6). The pressure inside the chamber is  $1.3 \times 10^{-6}$  mbar. The outer copper layer sits on top of a Peltier element, which is connected to the aluminium chamber. With this, the outer copper layer is stabilised to the zero-expansion point, however, there can still be significant temperature gradients in this layer, especially if the zero-expansion point is far away from room temperature. This problem is solved by the second copper layer, which is thermally connected to the outer layer only at a single point. While the thermal gradients can not be reduced to zero because of black-body coupling between the two layers, the additional layer reduces the gradient strongly. In combination, the copper shielding increases the time constant for temperature changes of the cavity to 6.5 hours and allows us to reach the zero-expansion point of  $30.74(10)$  °C to a precision of 0.01 K. By mounting the cavity at two nodal points of its strongest mechanical vibration mode, its coupling to acoustic vibrations is also reduced to a minimum.

These techniques allow us to reach a long-term stability limited by the ageing of the cavity spacer itself. It is initially in a glassy state, but slowly crystallises, approaching equilibrium over years [535, 536]. By measuring the shift of the sideband frequency corresponding to the STIRAP resonance, we mapped out this ageing process, finding a frequency drift which is described well by the formula

$$\Delta\omega(t) = 2\pi \times 3.2 \text{ MHz} \times \left(1 - \exp\left(-\frac{t}{441 \text{ d}}\right)\right), \quad (3.3)$$

as shown in Figure 3.7. To get some appreciation for the astounding level of precision that is routinely achieved with such cavities, it may be helpful to visualise it in terms of length changes: over hours and days, the 10-cm cavity length is stable up to about a nanometre,

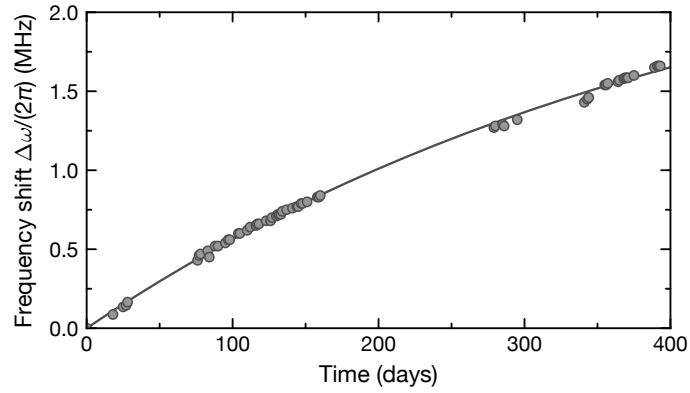


**Figure 3.7.:** Drift of STIRAP two-photon detuning over time due to cavity ageing. The solid line corresponds to Equation (3.3).

and even over years, it only changes by less than a micrometre.

### 3.2.3. Filtering and amplification

The power spectral density (PSD) of a laser can typically be described as the sum of a narrow central peak (the carrier), and a broad but much lower Lorentzian noise pedestal. The quality of a laser lock is determined by the achieved phase-noise spectrum. Locking the laser to a narrow reference can make the carrier extremely narrow and its position extremely stable, however it also causes additional phase noise at the edges of the lock bandwidth [537]. These zones of increased phase noise are called *servo bumps*. Depending on the application, different frequency ranges are important: while for optical clocks, it is mostly the low-frequency phase noise (Hz-level and below) that matters, coherent addressing of qubits is often limited by phase noise at much higher frequencies [538–540].

As STIRAP efficiency is strongly influenced by phase noise, understanding and optimising it requires knowledge of the laser performance. In our case, this is measured via the power spectrum of the in-loop PDH error signal. From this, the phase-noise power spectral density  $\mathcal{L}(\omega)$  can be determined as described in [541]. At sufficiently high frequencies and small modulation, the integral of  $\mathcal{L}(\omega)$  is equal to the total power in the phase-noise pedestal  $P_\phi$ . This method of measuring phase noise is fundamentally limited for two reasons: first, it is based on the in-loop error signal, which is created by the reference cavity. This means that any errors caused by the cavity itself can not be seen. Second, at sufficiently low frequencies, the actual signal is overwhelmed by  $1/f$ -noise of the lock electronics. This means that the method is only reliable at frequencies down to roughly 10 kHz. However, measuring phase noise in a manner that avoids these problems requires significant effort, e.g., constructing two identical lasers to create a beat signal, and is not necessary for our application.

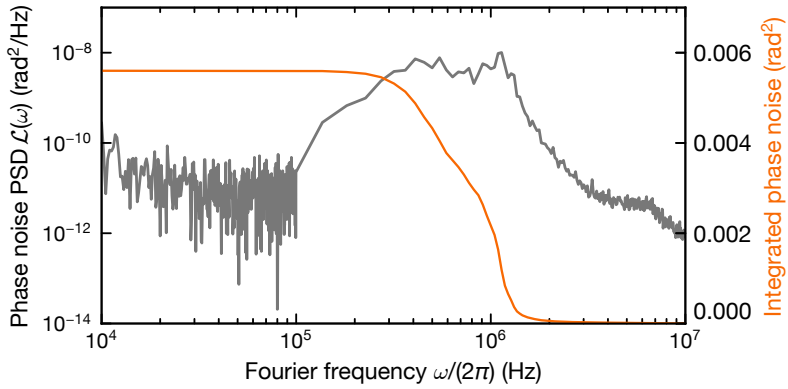


**Figure 3.8.:** Power spectral density (PSD) of phase noise of the pump laser,  $\mathcal{L}(\omega)$ , relative to the ULE reference cavity. This was determined from the measured power spectral density of the PDH error signal. The PSD is shown in grey. The orange line corresponds to the integrated PSD, with the integration beginning at high frequencies.

Figure 3.8 shows the result of the phase-noise measurements on the 805-nm laser. The servo bumps are situated at frequencies of  $2\pi \times 1.2$  MHz. The integrated power of the laser's phase noise pedestal is almost exclusively in these servo bumps and is about 0.6% of the total laser power. Due to the limitations mentioned above, we are not able to determine the carrier linewidth, however judging from previous measurements on similarly stabilised lasers, 1 kHz is a reasonable estimate.

The servo bumps are located in an especially problematic frequency range, see also Section 3.3.3. Hence, it is important to suppress them, which we achieve by sending the light through two optical filter cavities. These have a medium finesse of  $\mathcal{F} = 4430(14)$  and  $\mathcal{F} = 5110(30)$  for the 1134-nm and the 805-nm light, respectively. This offers a compromise between noise reduction and simplicity of locking. Using piezo-driven mirrors, the filter cavities are PDH-locked to be resonant with the laser frequency. A Faraday isolator before the input of each filter cavity reduces detrimental back-reflection into the ULE-cavity setup. Theoretically, a reduction of the servo-bump noise power by 22 dB is expected. On the downside, the filter cavities reduce the available laser power by about 50%, as not all light can be coupled through them. They also increase intensity noise because acoustic vibrations of the cavity can not be completely compensated by the lock.

After filtering, the 1134-nm light is injection-amplified to a total power of 105 mW using an anti-reflection-coated gain chip (GC-1180-100-TO-200-B, Innolume). It is then sent into a second-harmonic-generation module, which contains a single-pass periodically-poled lithium-niobate waveguide (HC Photonics). It produces 3 mW of 567-nm laser power. Optionally, the 805-nm light can also be amplified using a tapered amplifier (EYP-TPA-0808, Eagleyard). Though this is not necessary, as sufficient power can be reached without amplification, it does allow for larger STIRAP beam sizes and reduces intensity noise caused by the filter cavity.

Finally, both beams are sent to the experimental chamber through acousto-optical modulators, which allow us to create the desired pulse shape for STIRAP. Shutters are additionally used to completely block the beams while they are not needed, as even very small leakage could otherwise lead to reduced molecule lifetime. As shown in Figure 3.4, the STIRAP pulse shape is given by

$$I(t) = \begin{cases} I_0 \cos^2(\pi t / 2\tau), & -\tau < t < \tau \\ 0 & \text{otherwise} \end{cases} \quad (3.4)$$

with the peak intensity  $I_0$ . The beam intensities are independently chosen to achieve comparable Rabi frequencies of around  $2\pi \times 2.5$  MHz. For the transfer to the ground state, the Stokes pulse precedes the pump pulse by  $\tau$ , for the reverse transfer they are interchanged. For both pump pulses, one half is cut off, which simplifies our experimental control without disturbing the transfer. Immediately after each transfer, we quickly change the dipole-trap power in order to compensate for the smaller ac polarisability of ground-state molecules compared to Feshbach molecules. Otherwise, the sudden change in trap confinement would lead to breathing oscillations and subsequent heating of the molecule sample. With this procedure, we can reduce the sudden change in the trapping potential to a point where the recoil momentum imparted by the STIRAP itself becomes the dominant source of heating.

## 3.3. Results

### 3.3.1. Spectroscopy of the pump and Stokes transitions

In the first step of our experiments, we identified the intermediate state  $|E\rangle$  by photoassociation spectroscopy on Feshbach molecules, as demonstrated in Reference [24]. Because the target state has  $m_F = -5/2$  character, the pump beam was  $\sigma^-$ -polarised. Consistent with previous measurements, we located the dip corresponding to this state at  $2\pi \times 372\,554\,391(1)$  MHz. This number was determined by beating the laser with an optical frequency comb. In the following, the pump laser frequency is given as a detuning  $\Delta_p$  relative to this transition.

To find the Stokes frequency, we performed dark-state spectroscopy of the ground state by illuminating Feshbach molecules with both lasers simultaneously for  $200\,\mu\text{s}$ . The idea of this measurement is that the Stokes beam causes a light shift on the excited state, which is sufficient to prevent photoassociation at the frequency where the pump beam would otherwise be resonant with the  $|FB\rangle \leftrightarrow |E\rangle$  transition. By keeping the pump light on the unperturbed resonance and scanning the Stokes frequency, a narrow peak in molecule number can be observed when the Stokes beam becomes resonant. Our measurements were performed with intensities of  $5\,\text{W/cm}^2$  and  $4\,\text{mW/cm}^2$  for the pump and Stokes beam, respectively. Depending on the frequency and polarisation of the two beams, dif-

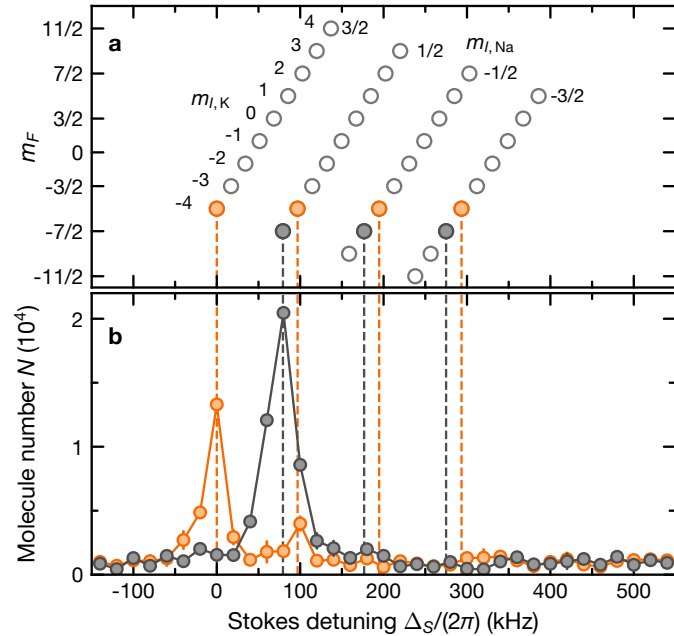


**Figure 3.9.:** Dark-state spectroscopy of the ground state. **(a)** Hyperfine structure of the rovibrational ground state. States with  $m_F = -5/2$  (orange) can be reached from  $|E\rangle$  via  $\pi$ -transitions. States with  $m_F = -7/2$  (grey) can be reached via  $\sigma^-$ -transitions. **(b)** Two-photon spectra for parallel polarisation of the Stokes beam, corresponding to  $\pi$ -transitions (orange), and for orthogonal polarisation, corresponding to  $\sigma^\pm$ -transitions (grey). Frequencies are given as a Stokes detuning  $\Delta_S$ , i.e., relative to the  $|E\rangle \leftrightarrow |G\rangle$  transition which corresponds to  $2\pi \times 528\,805\,718$  MHz.

ferent hyperfine states of the rovibrational ground state can be seen.

The absolute ground state of  $^{23}\text{Na}^{40}\text{K}$  is unusual in that it is not a hyperfine-stretched state: due to the inverted hyperfine structure of  $^{40}\text{K}$ , the energetically lowest  $m_F$ -level of this isotope is the most negative one, while it is the opposite for  $^{23}\text{Na}$ . Therefore, to reach the absolute ground state, with  $m_F = -5/2$ , from  $|\text{E}\rangle$ , a  $\pi$ -transition is needed. Figure 3.9 shows an overview of the hyperfine states as well as the results of the dark-state spectroscopy, both for a  $\pi$ - and a  $\sigma^-$ -polarised Stokes beam. The Stokes transition frequency to reach the absolute ground state  $|\text{G}\rangle$  was found to be  $2\pi \times 528\,805\,718(1)$  MHz. The detuning of the Stokes laser from this frequency is denoted by  $\Delta_S$ . Throughout this measurement, the pump detuning remained constant, such that the two-photon detuning  $\delta = \Delta_S - \Delta_p$  was changed together with the Stokes detuning and the one-photon detuning  $\Delta = \Delta_p$  was always zero. From these results, we found a binding energy of  $5212.04443(3)\text{ cm}^{-1}$  for  $|\text{G}\rangle$ , relative to the hyperfine centre of mass of the free atoms, again consistent with the value found in [24].

### 3.3.2. Determination of Rabi frequencies

Next, we determined the Rabi frequencies associated with the two transitions. This was done with two-photon spectroscopy of Feshbach molecules with a high Stokes-beam intensity of  $50\text{ W/cm}^2$  at  $\Delta_S \approx 0$ . Hence, for this measurement, the condition  $\delta = \Delta$  was always fulfilled. While the Stokes beam remained on, the pump beam was added for  $50\mu\text{s}$  and its detuning  $\Delta_p$  was scanned. In contrast to the dark-state spectroscopy, which is done by scanning  $\Delta_S$ , and with much lower Stokes power, this results in spectra with two distinct dips and a revival in between, as shown in Figure 3.10. At the two-photon resonance ( $\delta = \Delta = 0$ ), the molecules are preserved, but this becomes less efficient for stronger pump detunings until the molecule number again goes to zero at a detuning equal to half the Rabi frequency. The shape of the feature is given by [524, 542]

$$N = N_0 \exp \left( -t \Omega_p^2 \frac{4\Gamma\delta^2}{|\Omega_S^2 + 2i\delta(\Gamma + 2i\Delta)|^2} \right), \quad (3.5)$$

where  $N$  and  $N_0$  are the remaining and initial molecule numbers,  $\Gamma$  is the natural linewidth of  $|\text{E}\rangle$ , and  $t$  is the duration of the pump pulse. This shows that the width of the broad loss feature and the revival peak is related to the Rabi frequencies of the two beams, which can therefore be determined accurately by fitting this equation to the spectra. The equation describes the lineshape both in the regime of electromagnetically induced transparency (EIT), which is purely an interference effect between the two beams, and Autler–Townes splitting, which does not require interference. Since in our case  $\Gamma \approx \Omega_S$ , we are in an intermediate regime between the two [542]. Here, we keep the convention of naming the transitions “pump” and “Stokes”, as is typical for STIRAP, even though in the context of the measurements in this section, they are usually called “probe” and “coupling” [542].

We repeated this measurement at multiple values of the magnetic field to determine the dependence of the Rabi frequencies on the closed-channel fraction of the Feshbach molecules. For this, an additional  $B$ -field ramp was performed after the completion of the

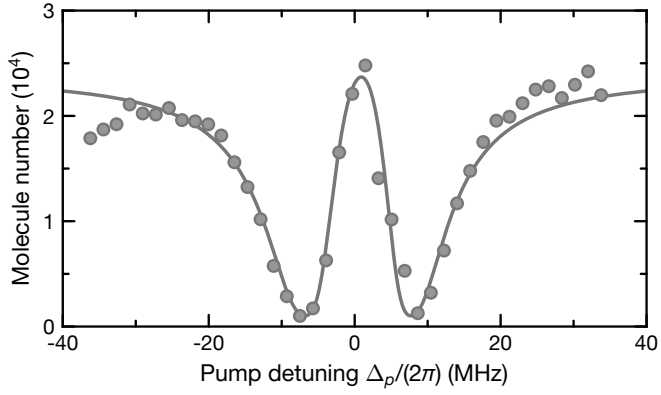


**Figure 3.10.:** Two-photon spectrum for determining Rabi frequencies with  $\Delta_S \approx 0$  at  $B = 72.4\text{G}$ . The solid line is a fit of Equation (3.5), which yields  $\Omega_p = 2\pi \times 0.29(1)\text{MHz}$ ,  $\Omega_S = 2\pi \times 17.1(3)\text{MHz}$ , and  $\Gamma = 2\pi \times 11(1)\text{MHz}$ .

clearout. After this, we determined the normalised Rabi frequencies  $\bar{\Omega}_p = \Omega_p / \sqrt{I_p}$  and  $\bar{\Omega}_S = \Omega_S / \sqrt{I_S}$  by fitting Equation (3.5) to the obtained spectra. Here,  $I_p$  ( $I_S$ ) stands for the intensity of the pump (Stokes) beam. The normalised Rabi frequencies are directly proportional to the respective transition dipole moments, with  $1\text{kHz}/\sqrt{\text{mW/cm}^2}$  corresponding to a transition dipole moment of  $9.00 \times 10^{-4} ea_0$ . As expected, we found that  $\bar{\Omega}_p$  is proportional to the closed-channel fraction, but  $\bar{\Omega}_S$  is almost independent of it (see Figure 3.11). This confirms that  $|\text{E}\rangle$  and  $|\text{G}\rangle$  are only weakly affected by  $B$ -field changes, but in the vicinity of the resonance, small changes of  $B$  can greatly affect  $|\text{FB}\rangle$ , changing its coupling to  $|\text{E}\rangle$ .

Extrapolating our results to the case of a closed-channel fraction near zero, we found  $\bar{\Omega}_p = 2\pi \times 0.8\text{kHz}/\sqrt{\text{mW/cm}^2}$  is consistent with previous measurements of the pump transition dipole moment where rf association was used [24]. However, at  $B = 72.4\text{G}$ , which corresponds to a closed-channel fraction of 84%, we found  $\bar{\Omega}_p = 2\pi \times 6.3(4)\text{kHz}/\sqrt{\text{mW/cm}^2}$ , which is 14 times larger. Considering that the Rabi frequency scales with the square of the light intensity, this means that the same STIRAP efficiency can be achieved with less than 1% of the laser power. Hence, while previous implementations of STIRAP with the same intermediate state required the use of either a Ti:sapphire laser [299] or a tapered amplifier [543], we have the possibility to work directly with unamplified light from a diode laser. Amplification can still be used to allow larger beam sizes, for example to perform STIRAP during time of flight rather than on a trapped sample.

The measured excited-state linewidth,  $\Gamma = 2\pi \times 11(1)\text{MHz}$ , is also consistent with the value found by Park *et al.* [299], however this is surprisingly not the case for the normalised pump Rabi frequency. We found this to be  $\bar{\Omega}_S = 2\pi \times 142(8)\text{kHz}/\sqrt{\text{mW/cm}^2}$ , which is six times larger than reported there, though the results should be similar. There is not yet a satisfactory answer to this question, but measurements made at USTC are con-

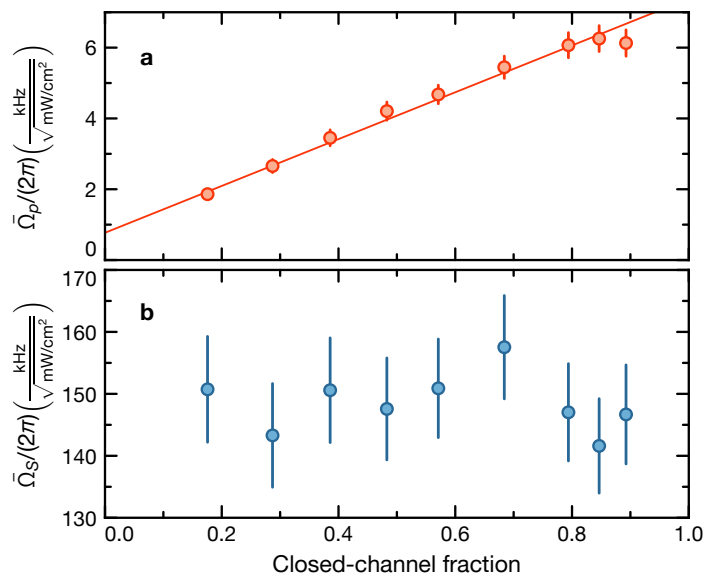


**Figure 3.11.:** Rabi frequencies depending on closed-channel fraction, determined from two-photon spectra. **(a)** Normalised pump Rabi frequency  $\bar{\Omega}_p$ . The solid line is a linear fit, which yields a slope of  $2\pi \times 6.6 \text{kHz}/\sqrt{\text{mW/cm}^2}$  and an offset of  $2\pi \times 0.8 \text{kHz}/\sqrt{\text{mW/cm}^2}$ . **(b)** Normalised Stokes Rabi frequency  $\bar{\Omega}_S$ . Error bars represent one standard deviation of the fit.

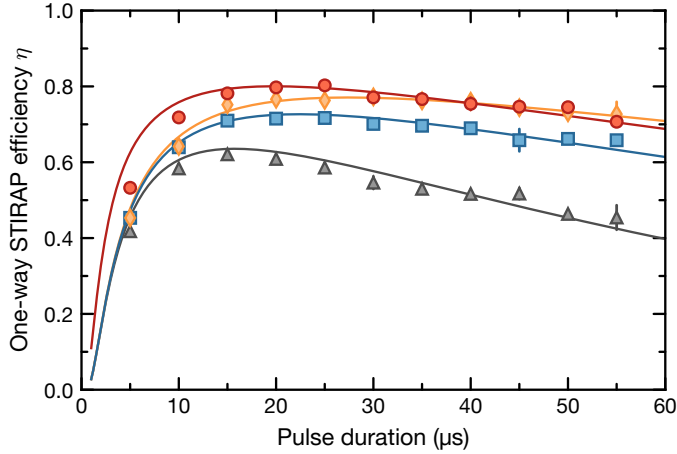


**Figure 3.12.:** One-way STIRAP efficiency  $\eta$  depending on pulse duration, Rabi frequencies, and presence of filter cavities. The lines are fits of Equation (3.6). Grey triangles were taken with no filter cavities, orange diamonds with both filter cavities, blue squares with only the pump filter cavity. In all the datasets above, the Rabi frequencies were  $\Omega_p = \Omega_S = 2\pi \times 2.2\text{MHz}$ . Red circles were taken at  $\Omega_p = \Omega_S = 2\pi \times 2.8\text{MHz}$  with both filter cavities. Here,  $\eta = 80\%$  was achieved. Error bars denote the standard error of the mean of three repetitions. For the fit results, see Table 3.3.

sistent with our results [543]. Table 3.2 gives an overview of transition dipole moments, excited-state linewidths and efficiencies which have been achieved in similar systems, providing some context to this result.

### 3.3.3. STIRAP and laser noise reduction

With knowledge of the pump and Stokes transition frequencies, we used the STIRAP pulse sequence (see Figure 3.4) to transfer Feshbach molecules into the absolute ground state  $|G\rangle = |X^1\Sigma^+, v = 0, J = 0, m_{I,\text{Na}} = 3/2, m_{I,\text{K}} = -4\rangle$ . For this, the lasers were tuned to  $\Delta = \delta = 0$ . Initially, we attempted STIRAP without any filtering, and observed a strong dependence of the one-way STIRAP efficiency  $\eta$  on the pulse duration  $\tau$ , as well as an overall low one-way efficiency of  $\eta = 64\%$ . As seen in Figure 3.12, the filter cavities improved the transfer efficiency up to 80%.

The relatively low efficiency obtained with the unfiltered lasers can be explained with the theoretical framework developed by Yatsenko *et al.* [544, 545] to describe the effect of laser noise on STIRAP. From a simplified version of their results, we expect

$$\eta = \exp\left(-\frac{\pi^2\Gamma}{\Omega^2\tau} - \frac{\tau}{4}(D_p + D_S + \Gamma_p + \Gamma_S)\right). \quad (3.6)$$

Here,  $D_{p/S}$  are the FWHM laser linewidths, and  $\Gamma_{p/S}$  are effective linewidths correspond-

**Table 3.2:** Overview of experimentally investigated STIRAP schemes from Feshbach states to  $X^1\Sigma^+$  rovibrational ground states of alkali molecules. The pump and Stokes laser wavelengths are denoted by  $\lambda_p$  and  $\lambda_s$ , respectively. Note that STIRAP has not yet been demonstrated for some of the listed transition pairs.

Molecule	Intern. state	$\lambda_p$ (nm)	$\lambda_s$ (nm)	$\frac{\bar{\Omega}_p}{2\pi} \left( \frac{\text{kHz}}{\sqrt{\text{mW/cm}^2}} \right)$	$\frac{\bar{\Omega}_s}{2\pi} \left( \frac{\text{kHz}}{\sqrt{\text{mW/cm}^2}} \right)$	$\frac{\Gamma}{2\pi}$ (MHz)	$\eta$	Sources
${}^6\text{Li}^{40}\text{K}$	$A^1\Sigma^+$ <sup>a</sup>	1119	665	2.7(2)	12(2)	5	–	[546]
${}^{23}\text{Na}^{39}\text{K}$	$c^3\Sigma^+ \sim B^1\Pi$	816	572	–	65.2	6	70%	[547, 548]
${}^{23}\text{Na}^{40}\text{K}$	$c^3\Sigma^+ \sim B^1\Pi$	805	567	0.45(10)	25(5)	9(1)	78%	[24, 299, 549]
${}^{23}\text{Na}^{40}\text{K}$	$d^3\Pi \sim D^1\Pi$	652	487	0.6	6	20	50%	[524]
${}^{23}\text{Na}^{40}\text{K}$	$c^3\Sigma^+ \sim B^1\Pi$	805	567	6.3(4)	142(8)	11(1)	80%	[527]
${}^{23}\text{Na}^{87}\text{Rb}$	$b^3\Pi \sim A^1\Sigma^+$	1248	769	1.01	23.2	0.67	93%	[301, 302, 389]
${}^{23}\text{Na}^{87}\text{Rb}$	$B^1\Pi \sim c^3\Sigma^+$	803	574	3.4	100	6	–	[550]
${}^{23}\text{Na}^{133}\text{Cs}$	$c^3\Sigma^+ \sim B^1\Pi$	922	635	10.1(13)	257(3)	120	82% <sup>b</sup>	[370]
${}^{40}\text{K}^{87}\text{Rb}$	$2^3\Sigma^+ \sim 1^1\Pi$	968	689	6(2)	13(3)	–	89%	[27, 229, 309]
${}^{87}\text{Rb}^{133}\text{Cs}$	$b^3\Pi \sim A^1\Sigma^+$	1557	977	0.84(24)	2.76(67)	0.135(10) <sup>c</sup>	92%	[293, 551]

<sup>a</sup> A Feshbach state with a strong singlet contribution was used, avoiding the need for singlet-triplet mixing in the intermediate state.

<sup>b</sup> This efficiency was achieved with off-resonant Raman scattering rather than with STIRAP.

<sup>c</sup> Reference [551] reported a different value of  $\Gamma = 2\pi \times 35(3)$  kHz.

**Table 3.3.:** Results of the fits of Equation (3.6). The values for  $P_{\text{tot}}$  are determined using Equation (3.7).

Filter cavities	$\Omega_p = \Omega_S$	$\Gamma_{\text{tot}}$	$P_{\text{tot}}$
None	$2\pi \times 2.2 \text{ MHz}$	$2\pi \times 7.2 \text{ kHz}$	$4.6 \times 10^{-2}$
Only pump	$2\pi \times 2.2 \text{ MHz}$	$2\pi \times 2.5 \text{ kHz}$	$1.6 \times 10^{-2}$
Both	$2\pi \times 2.2 \text{ MHz}$	$2\pi \times 1.0 \text{ kHz}$	$6.5 \times 10^{-3}$
Both	$2\pi \times 2.8 \text{ MHz}$	$2\pi \times 1.6 \text{ kHz}$	$6.7 \times 10^{-3}$

ing to the broadband phase-noise pedestals of the two lasers. The first term inside the exponential function corresponds to loss caused by non-perfect adiabaticity of the transfer.

The terms  $\Gamma_p$  and  $\Gamma_S$  can be analytically calculated under the assumption of a specific shape of the noise pedestal. For the case of a Lorentzian shape, they are given by [545]

$$\Gamma_i = \frac{\Omega_i^2 G_i P_i}{4G_i^2 + 2G_i \Gamma + \Omega_i^2}, \quad (3.7)$$

where  $i$  is replaced by  $p$  or  $S$ . Here,  $\Omega$  stands for the peak Rabi frequency,  $G$  for the FWHM of the laser noise pedestal, and  $P$  for the total noise power fraction, i.e., the sum of the phase and intensity noise power fractions of the respective laser. In our case, we expect this description to be only qualitatively correct, since the shape is dominated by the servo bumps and is far from being Lorentzian. In the following, we assume that  $D_p = D_S = 2\pi \times 1 \text{ kHz}$ , a typical value likely limited by fibre noise and vibrations of the ULE cavity, which affect the two lasers similarly [552].

According to this model, the transfer efficiency is affected most strongly for pedestal widths near the Rabi frequency. This effect becomes stronger for longer pulse durations, creating a tradeoff with the adiabaticity criterion. This makes intuitive sense, as noise far above  $\Omega$  will average out over typical pulse time scales, and noise far below  $\Omega$  will show up as a constant frequency offset. This problem can be reduced by increasing  $\Omega$ , however the line-broadening caused by this can create other problems such as unwanted addressing of off-resonant hyperfine levels [549]. The most promising option for increasing  $\eta$  should therefore be to reduce phase-noise contributions at frequencies close to  $\Omega$ , i.e., to remove the servo bumps from the laser spectra.

As the data in Figure 3.12 shows, this was indeed the case in our system: By adding filter cavities, we could not only increase  $\eta$ , but also the optimal value of  $\tau$ , which went from  $15 \mu\text{s}$  to  $25 \mu\text{s}$ . While filtering only the pump laser already showed some effect, the best results were found with both filter cavities. By fitting Equation (3.6) to our data, using the known peak Rabi frequencies and the excited-state linewidth, we determined  $\Gamma_{\text{tot}} = \Gamma_p + \Gamma_S$ . The results are shown in Table 3.3.

A comparison of these results to the prediction of Equation (3.7) shows that the expected and measured efficiencies agree qualitatively. Though for a laser lineshape that is dominated by servo bumps,  $G$  is not a well-defined quantity, it is reasonable to use

$G = 2\pi \times 1.2 \text{ MHz}$ , because the noise power decays very quickly beyond the servo bumps. From this and the fitted values of  $\Gamma_{\text{tot}}$ , we obtained the total noise power fraction  $P_{\text{tot}} = P_p + P_S$  as shown in Table 3.3. For each laser without filter cavity, we expect a phase-noise power fraction  $P_\phi = 6 \times 10^{-3}$  as well as a contribution from intensity noise which is of similar magnitude. The fitted value of  $P_{\text{tot}} = 4.6 \times 10^{-2}$  thus agrees reasonably well with the model for the case without filter cavities. The filter cavities appear to provide less than the expected 22 dB reduction of total phase noise power. This could be due to the additional intensity noise that they cause. Alternatively,  $D_p$  or  $D_S$  might be larger than  $2\pi \times 1 \text{ kHz}$ , which would lead to an underestimation of the effect of the filter cavities. In this case, fibre-noise cancellation as described in Reference [552] would be desirable.



*Examined in sufficient detail, the spectrum of every diatomic molecule is full of surprises.*

—H. Lefebvre-Brion and R. W. Field [3]

## 4. Near-resonant dipole trapping

Optical dipole traps are an enormously important tool for experiments. They are easily and precisely controllable, both in shape and depth, which is often not the case for other trap types. They also work for a wide variety of atomic or molecular species because their function only depends on the existence of electric-dipole transitions in the spectrum of the trapped particle. This chapter describes the development and testing of a near-resonant dipole trap for molecules, which allowed us to realise well-controlled, rotational-state-dependent dipole potentials. It is based on the publication [553].

### 4.1. The $X^1\Sigma^+ \leftrightarrow b^3\Pi_0$ transition

In principle, optical dipole traps can be realised at any frequency, but using large detunings, on the order of many terahertz below the lowest optical dipole transition, is most common. The response of an atom or molecule to an external laser field can be described by two quantities: the polarisability and the photon-scattering rate. For a given state, we can enumerate all electric dipole transitions by an index  $i$ , each with a resonance position  $\omega_i$  and a linewidth  $\Gamma_i$ . Then, in the rotating-wave approximation, the polarisability is given by [73]

$$\alpha = \frac{U_{\text{dip}}}{I} = - \sum_i \frac{3\pi c^2}{2\hbar\omega_i^3} \frac{\Gamma_i}{\Delta_i}, \quad (4.1)$$

where  $I$  is the laser intensity, and  $\Delta_i$  its detuning from the transition  $i$ .  $U_{\text{dip}}$  denotes the trap potential.

In contrast to the polarisability, the photon-scattering rate scales inversely quadratically with the detuning:

$$\gamma_{\text{sc}} = \frac{\Gamma_{\text{sc}}}{I} = \sum_i \frac{3\pi c^2}{2\hbar\omega_i^3} \left( \frac{\Gamma_i}{\Delta_i} \right)^2. \quad (4.2)$$

This means that, at sufficiently high power and large detuning, deep traps can be realised with a low scattering rate. For molecules, this typically implies working far red-detuned from the lowest electronic transition, which means there is no need to worry about the complex level structure. Otherwise, reaching large detuning from any one transition would only lead to approaching another. Then, the condition  $\Delta_i \gg \Gamma_i$  is fulfilled, meaning that the polarisability is almost independent of the laser frequency.

While this simplifies working with dipole traps both conceptually and practically, this comes at the cost of control over some important degrees of freedom: when working with multiple internal states of a molecule, the polarisability of these can not be chosen independently by changing the dipole-trap laser frequency as long as the smallest  $\Delta_i$  is much larger than the separation between these states.

However, the ability to independently control the trap depth for multiple states is highly desirable. For example, it allows creating a *magic* trapping condition, where the polarisability of two internal states is equal [319, 554–556]. This is a requirement for long coherence time in Ramsey experiments, which is important, e.g., for atomic and molecular clocks [557–559]. Another relevant case is the *tune-out* condition, where the polarisability of one state vanishes while the other remains finite [560, 561]. Such highly state-dependent potentials allow independent control of the two states, a useful ability in a wide variety of experiments [562–564]. Tune-out wavelengths also enable novel cooling schemes [565], and precision measurements of atomic structure [566–571].

For polar molecules, one of the most important and difficult experimental challenges is manipulating their rotational states, because this allows controlling the dipole-dipole interactions. The difficulty arises from the anisotropic coupling between molecules and the laser field. This means that in Equation (4.1), the linewidths  $\Gamma_i$  depend on the light polarisation and this dependence can be different for each rotational level. Hence, at a given polarisation, the polarisability of two rotational levels can be completely different, even if the energy difference between them is much smaller than the detuning. On top of this, there are additional higher-order terms such that the energy shift no longer scales linearly with  $I$ . These effects have previously been used to engineer magic conditions, however this comes at the cost of high sensitivity to fluctuations of the polarisation angle or intensity, which limits rotational coherence [319, 381, 572–574]. Tune-out conditions have previously not been demonstrated at all for polar molecules.

We have demonstrated a simple, versatile, and stable way to achieve arbitrary rotational-state-dependent optical dipole traps for molecules. This is enabled by the use of light at a detuning comparable to the rotational splitting of 5.6 GHz. Such detunings, which are about 10000 times smaller than usual, can only be realised near a transition with small  $\Gamma_i$  that is also isolated with no other transitions nearby. Luckily, such transitions exist in  $^{23}\text{Na}^{40}\text{K}$  because the minimum of the  $b^3\Pi$  electronic potential is significantly below the minimum of  $A^1\Sigma^+$  (see Figure 1.6). Due to the different electronic spins, transitions from  $X^1\Sigma^+$  to  $b^3\Pi_0$  are nominally dipole-forbidden, and it is only the presence of spin-orbit coupling that allows them to occur. As spin-orbit coupling is quite weak in this molecule, these transitions are extremely narrow.

Under these conditions,  $\alpha$  becomes strongly frequency-dependent. This allows us to create tune-out and magic conditions for rotational states of molecules by controlling the laser frequency. Any intermediate polarisation ratio can be achieved in between these two extreme cases. In addition, the scheme is first- and second-order insensitive to the polarisation angle and intensity of light, which are both much harder to precisely control than the laser frequency.

In our experiments, we use  $^{23}\text{Na}^{40}\text{K}$  in its rovibrational ground state  $|X^1\Sigma^+, v = 0, R = 0\rangle$  as well as the first rotationally excited state,  $|R = 1, m_R = 0\rangle$ . In the fol-

lowing, they will be called  $|0\rangle$  and  $|1\rangle$ , respectively. The rotational-state dependent dipole trap is realised with laser light slightly detuned from the  $|X^1\Sigma^+, v=0, R=0\rangle \leftrightarrow |b^3\Pi_0, v'=0, R'=1, m'_R=0\rangle$  transition (subsequently called the  $X \leftrightarrow b$  transition), which was previously studied in References [23, 575]. This transition is located at  $\omega_0 = 2\pi \times 346.12358(7)$  THz, corresponding to a wavelength of  $\lambda = 866.1428(3)$  nm. Its linewidth is  $\Gamma = 2\pi \times 301(10)$  Hz. As Figure 4.1 shows, tune-out conditions for both states as well as a magic condition can be achieved here within a frequency range of less than 10 GHz.

The polarisabilities  $\alpha_0$  and  $\alpha_1$  of a molecule in  $|0\rangle$  or  $|1\rangle$ , respectively, at a small detuning  $\Delta$  from the  $X \leftrightarrow b$  transition can be described by

$$\alpha_0 = -\frac{3\pi c^2 \Gamma}{2\omega_0^3 \Delta} + \alpha_{\text{iso}}, \quad (4.3)$$

$$\alpha_1 = -\frac{3\pi c^2}{2\omega_0^3} \left( \frac{\Gamma \cos^2 \theta}{\Delta + 2(B+B')/\hbar} + \frac{1}{5} \frac{\Gamma(\cos^2 \theta + 3)}{\Delta - 2(2B'-B)/\hbar} \right) + \alpha_{\text{iso}} + \alpha_{\text{ang}}(\theta), \quad (4.4)$$

if  $\Delta$  is much larger than the hyperfine structure of the resonance. Here, all the terms corresponding to other, far-detuned transitions have been consolidated into the two background terms  $\alpha_{\text{iso}}$  and  $\alpha_{\text{ang}}(\theta)$ , which are approximately frequency-independent over the relevant frequency range. The terms which are independent of light polarisation are collected in  $\alpha_{\text{iso}}$ , all others in  $\alpha_{\text{ang}}(\theta)$ , where  $\theta$  denotes the angle between the light polarisation and the quantisation axis, which is given by the direction of the dc electric field. The rotational constants of the ground and excited state are denoted  $B_{\text{rot}}$  and  $B'_{\text{rot}}$ , respectively.

The background polarisability terms can be expressed as [381, 555, 576]

$$\alpha_{\text{iso}} = \frac{1}{3} (\alpha_{\text{bg}}^{\parallel} + 2\alpha_{\text{bg}}^{\perp}), \quad (4.5)$$

$$\alpha_{\text{ang}} = \frac{2}{15} (3\cos^2(\theta) - 1) (\alpha_{\text{bg}}^{\parallel} - \alpha_{\text{bg}}^{\perp}), \quad (4.6)$$

where  $\alpha_{\text{bg}}^{\parallel}$  and  $\alpha_{\text{bg}}^{\perp}$  are the background parallel and perpendicular polarisabilities. The photon-scattering rate per unit intensity of molecules in  $|0\rangle$  near the  $X \leftrightarrow b$  transition is given by

$$\gamma_{\text{sc}} = \frac{3\pi c^2 \Gamma \Gamma_e}{2\hbar \omega_0^3 \Delta^2}. \quad (4.7)$$

Here,  $\Gamma_e$  is the *natural linewidth* of the excited state, which is the inverse of its lifetime. Note the difference to  $\Gamma$ , the *partial linewidth*, which is a measure of the decay rate into a specific state. Strictly speaking, there is also a constant background term in this expression, but it is not significant at the detunings studied here.

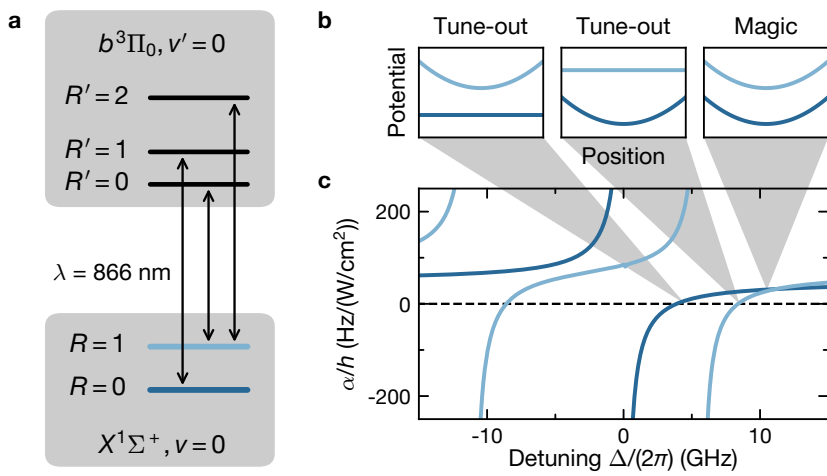


**Figure 4.1.:** Overview of the rotational-state dependent trapping scheme near the  $X \leftrightarrow b$  transition. (a) Level diagram of the NaK molecule near the  $X \leftrightarrow b$  transition and two transitions to the same vibrational state from  $|1\rangle$ . (b) Sketches of the potential experienced by  $|0\rangle$  (dark blue) and  $|1\rangle$  (bright blue) in a dipole trap at a tune-out condition for  $|0\rangle$  (left panel), a tune-out condition for  $|1\rangle$  (center panel) and a magic condition (right panel). (c) Polarisability versus laser frequency for  $|0\rangle$  (dark blue) and  $|1\rangle$  (bright blue), assuming parallel light polarisation. Each pole corresponds to one of the transitions shown in (a).

## 4.2. Experimental setup

The measurements described in this chapter were all taken with an older version of the apparatus, without the upgrades described in Chapter 3. In this setup, molecule association is performed after preparing a mixture of about  $10^5$   $^{23}\text{Na}$  and  $^{40}\text{K}$  atoms each, at a temperature of 300 nK. In contrast to the measurements taken with later versions of the setup, we perform radiofrequency association at the 89.9-G Feshbach resonance. The radiofrequency pulse is applied at a magnetic field of 85.4 G in the vertical ( $z$ ) direction, creating about  $10^4$  molecules in the Feshbach state  $|\text{FB}\rangle$ . We then use STIRAP as described in Reference [524] to bring them to the rovibrational ground state  $|0\rangle$ . Note that this method yields molecules in the hyperfine state  $|m_{I,\text{Na}} = -1/2, m_{I,\text{K}} = -4\rangle$ , which is not the absolute ground state. After STIRAP, we remove all unassociated atoms with short pulses of resonant light.

The molecules can be created either in a far-detuned crossed-beam optical dipole trap or in a 1D or 3D optical lattice. The crossed dipole trap consists of a 1064-nm and a 1550-nm laser beam intersecting orthogonally in the horizontal ( $x$ - $y$ ) plane. The 1D lattice is formed by a retroreflected 1550-nm laser beam and is magic for the  $|0\rangle \leftrightarrow |1\rangle$  transition. The magic condition is achieved by tilting the lattice polarisation by  $54^\circ$  with respect to the electric field, which points along the  $y$ -direction [381]. The electric field of 86 V/cm serves to decouple the rotational and hyperfine structure from the trapping light field. It is generated by four rod electrodes inside the ultra-high vacuum chamber which are connected to ultrastable high-voltage amplifiers (see Reference [525] for more details on the electrodes). The 3D lattice is used to suppress collisional loss in experiments that require long molecule lifetimes. It is formed by two retroreflected 1064-nm beams in the  $x$ - $y$ -plane in addition to the 1550-nm beam along the  $z$ -axis.

To probe the response of molecules to light near-detuned from the  $X \leftrightarrow b$  transition, we focus an additional beam at a corresponding frequency onto the molecules along the  $z$ -direction, with a small  $1/e^2$  beam radius of 75  $\mu\text{m}$ . In the following, this is called the 866-nm beam. It is provided by a Ti:sapphire laser (MBR-110, Coherent), which allows simple tuning of the frequency over many gigahertz. For frequency stabilisation, the laser is locked to a wavelength meter (WS-7, HighFinesse) with a systematic frequency error of 50 MHz. This is the dominating source of error for most frequency measurements described in this chapter. Except in the measurements to determine the polarisation dependence of the differential polarisability, the polarisation of the 866-nm beam is always at an angle of  $4(2)^\circ$  to the  $y$ -direction, almost parallel to the dc electric field.

## 4.3. Tune-out frequency

We first measured the tune-out detuning  $\Delta_0^{(0)}$  for the  $|0\rangle$  state with molecules in the crossed dipole trap by parametric heating. In addition to the trap, the 866-nm beam was turned on for 160 ms with a strong intensity modulation at a frequency of 110 Hz. As this is the strongest heating resonance of the trap, the modulation heats the sample, which is easily

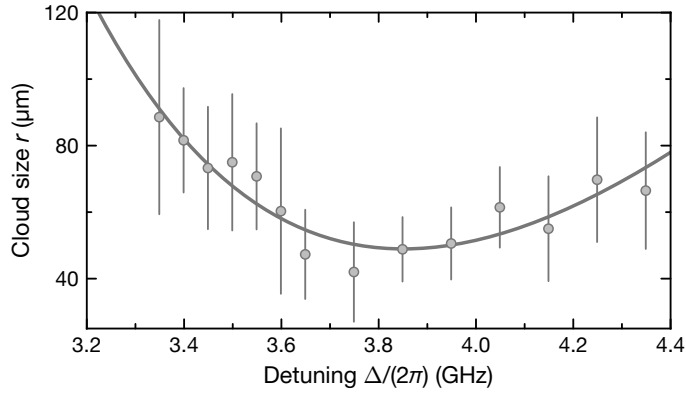


**Figure 4.2.:** Determination of the tune-out detuning for  $|0\rangle$  by measuring cloud size after parametric heating. The solid line is a fit of Equation (4.8) used to find the minimum.

detectable. At the tune-out frequency, this effect must vanish. After heating, we measured the molecule cloud size by determining the root-mean-squared size of the density distribution,  $r$ , after 0.6 ms time of flight. The heating process depends on the sample temperature as well as the modulation amplitude and modulation frequency. When the temperature of the molecules is much smaller than the trap depth and the modulation is weak, the effect of heating can be described as a linear increase in the sample's energy at a rate  $S\alpha_0^2(\Delta)I_{\text{mod}}^2$ , where  $S$  depends on the modulation frequency and initial temperature and  $I_{\text{mod}}$  is the intensity-modulation amplitude [577]. For the case of strong heating, the temperature quickly saturates to an equilibrium where the heating is balanced by hot molecules escaping from the trap. However, for  $\alpha_0(\Delta) \approx 0$ , the linear model is still valid. The expression for the cloud size  $r$  after modulating the 866-nm beam power at a given modulation frequency for a fixed time then reads

$$r(\Delta) = r_0 + \chi \left( \frac{1}{\Delta} - \frac{1}{\Delta_0^{|0\rangle}} \right)^2. \quad (4.8)$$

Here,  $r_0$  is the initial cloud size and  $\chi$  is a constant which contains the dependence on intensity, modulation time and modulation frequency. As shown in Figure 4.2, we used this expression with  $r_0$ ,  $\chi$ , and  $\Delta_0^{|0\rangle}$  as fit parameters to determine the detuning at which the minimum of heating occurs and thereby found the tune-out detuning  $\Delta_0^{|0\rangle} = 2\pi \times 3.85(8)$  GHz.

## 4.4. Magic frequency

The magic detuning was measured via Ramsey spectroscopy of the  $|0\rangle \leftrightarrow |1\rangle$  transition, which consists of two resonant  $\pi/2$  microwave pulses separated by a free evolution period

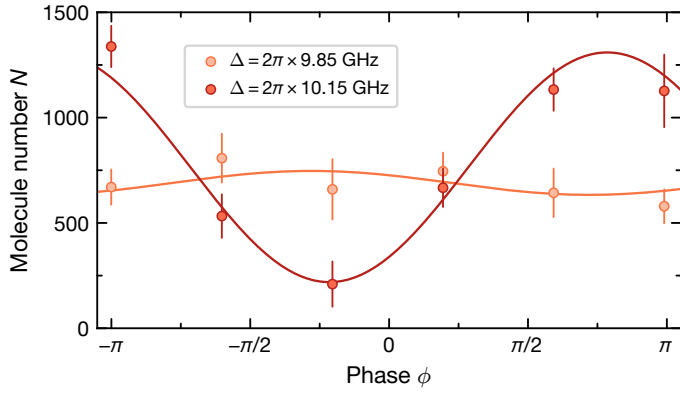


**Figure 4.3.:** Example data for determination of the magic detuning via Ramsey spectroscopy. Data were taken after 0.4 ms free evolution time at detunings  $\Delta = 2\pi \times 9.85 \text{ GHz}$  (bright circles) and  $\Delta = 2\pi \times 10.15 \text{ GHz}$  (dark circles). Error bars denote the standard error of the mean. The solid lines are fits of Equation (4.9).

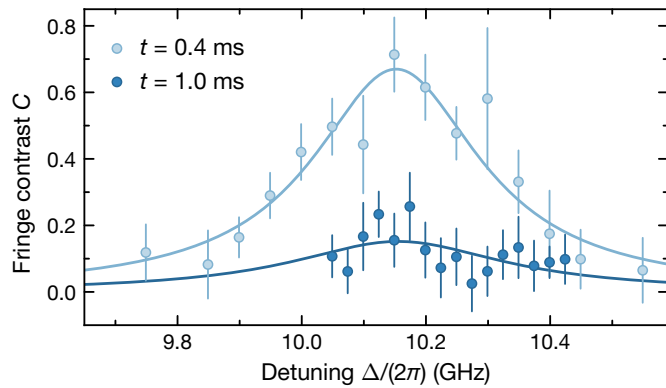


**Figure 4.4.:** Determination of the magic detuning  $\Delta_m$  via Ramsey spectroscopy. Bright (dark) blue circles are experimentally measured contrast after free evolution time  $t = 0.4 \text{ ms}$  (1.0 ms) in the presence of 866-nm light. Lines are Lorentzian fits to the respective data sets, used to determine the centre. Error bars denote one standard deviation of the fit.

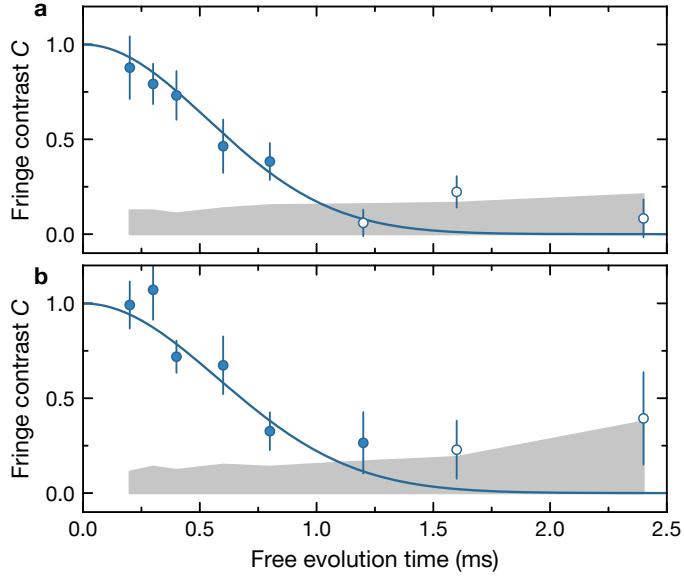


**Figure 4.5.:** Contrast in Ramsey spectroscopy after variable free evolution time. **(a)** With 866-nm light turned on, **(b)** with 866-nm light turned off. Blue points denote contrast data, blue lines are Gaussian fits used to determine the  $T_2$  coherence time. The grey shaded area indicates the contrast bias caused by molecule-number fluctuations. Open circles denote data points that were ignored in the fit due to this bias (see Reference [381]).

with duration  $t$ . We varied the phase  $\phi$  of the second microwave pulse for a given  $t$  to obtain Ramsey fringes. During the free evolution period, the 866-nm beam was turned on, such that a differential light shift caused by it reduced the observed coherence time. The fringe contrast  $C$  and initial phase  $\phi_0$  were determined by fitting the function

$$N(\phi) = \frac{N_{\text{tot}}(t)}{2} (1 - C(t) \cos(\phi + \phi_0)) \quad (4.9)$$

where  $N$  is the number of molecules in  $|0\rangle$ , to the measured molecule numbers (see Figure 4.3). This allowed us to determine the magic point by measuring the remaining fringe contrast after  $t = 0.4\text{ ms}$  and  $t = 1.0\text{ ms}$ . By fitting a Lorentzian to the contrast data as shown in Figure 4.4, we determined the magic detuning to be  $\Delta_m = 2\pi \times 10.15(6)\text{ GHz}$ .

Figure 4.5 shows the reduction of contrast over time due to the influence of various sources of decoherence. The time constant for a superpositon of  $|0\rangle$  and  $|1\rangle$  to evolve into a mixed state, such that the coherence disappears, is called the  $T_2$  time. For the case of dipolar particles in a trap, the contrast decay over time is expected to be Gaussian [381]. The  $T_2$  times extracted from these data in presence and absence of 866-nm beam are  $0.75(4)\text{ ms}$  and  $0.81(7)\text{ ms}$ , respectively. This shows that the dephasing is dominated by

factors not related to the presence of the 866-nm light. The strongest factor is instead electric-field inhomogeneity, which would limit  $T_2$  to 1.3 ms in the best-case scenario. The precision of this estimate is limited, because it is difficult to measure the actual electric-field distribution at the molecule position. Hence, the agreement with the measurements is reasonable. There are also a number of other sources of decoherence, including errors of the frequency and polarisation angle, second-order polarisability, and dipolar interaction, which have a much smaller effect. More details about these can be found in supplemental material of our paper [553].

In comparison, in our earlier publication [381] we realised a much longer coherence time of about 5 ms under comparable conditions. This was possible due to an additional set of electrodes, which were used to compensate electric field gradient and curvature. In the experiments shown here, these electrodes were no longer present, leading to much larger inhomogeneity.

## 4.5. Intensity calibration

Accurate determination of  $\alpha$  and  $\gamma_c$  at arbitrary frequencies, rather than only at zero-crossings, requires knowledge of the intensity of the 866-nm beam. As this beam goes through a complicated imaging setup and its shape can not be measured *in situ*, this requires a calibration of the intensity using the molecular response. However, with an unknown polarisability, it is not obvious how to obtain that. For this purpose, we determined another intensity-independent point on the polarisability curve, specifically the detuning  $\Delta^*$  where molecules in the Feshbach-molecule state  $|FB\rangle$  and the rovibrational ground state  $|0\rangle$  experience the same light shift. Knowing two points on the curve of  $\alpha_0(\Delta)$  then uniquely determines  $\Gamma$  and  $\alpha_{\text{iso}}$ .

To do this, we first measured the resonant STIRAP two-photon detuning with the 866-nm light turned off. We then observed the reduction of STIRAP efficiency caused by adding 866-nm light at various values of  $\Delta$ , which has an effect on both the  $|FB\rangle$  and  $|0\rangle$  states. As the shift of  $|FB\rangle$  is constant, but that of  $|0\rangle$  is strongly frequency-dependent, there exists a point at which they cancel out, which means the STIRAP efficiency is maximal. Because  $|FB\rangle$  is a very weakly bound state, its polarisability can be computed as  $\alpha_{FB} = h \times 76.26 \text{ Hz}/(\text{W/cm}^2)$  by summing the polarisabilities of the constituent atoms [73, 578, 579]. To determine  $\Delta^*$  from the data, we modelled the drop in conversion efficiency due to the shift of the STIRAP two-photon resonance as

$$N = N_0 \frac{\Gamma_s^2/4}{\Gamma_s^2/4 + (I(\alpha_0(\Delta) - \alpha_{FB})/\hbar)^2}, \quad (4.10)$$

where  $N_0$  is the molecule number at resonant STIRAP, and  $\Gamma_s$  is the linewidth of the STIRAP two-photon resonance. To obtain a fit function, the general form  $\alpha_0(\Delta) = A/\Delta + \alpha_c$  was inserted into Equation (4.10), and  $N_0$ ,  $\Gamma_s$ ,  $A$ , and  $\alpha_c$  were used as fit parameters (see Figure 4.6). We found  $\Delta^* = -2\pi \times 6.78(17) \text{ GHz}$ .

From the values of  $\Delta^*$ ,  $\Delta_0^{|0\rangle}$ , and  $\omega_0$ , we then computed the partial linewidth of the  $X \leftrightarrow$

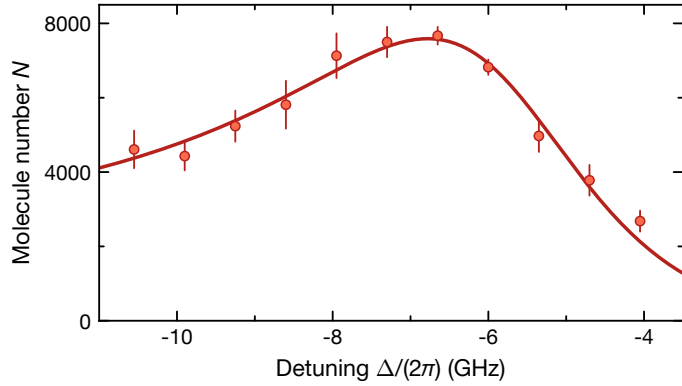


**Figure 4.6.:** Magic condition for  $|\text{FB}\rangle$  and  $|0\rangle$ . The STIRAP two-photon detuning was set to the resonance frequency as determined with no 866-nm light. Data points were taken with 866-nm light turned on at various values of  $\Delta$  during STIRAP. The solid line is a fit of Equation (4.10). Error bars denote the standard error of the mean.

$b$  transition  $\Gamma$ , as well as the isotropic background polarisability  $\alpha_{\text{iso}}$  via Equation (4.3). To find the background polarisability terms  $\alpha_{\text{bg}}^{\parallel}$  and  $\alpha_{\text{bg}}^{\perp}$ , we used the known form of  $\alpha_0(\Delta)$  as well as Equations (4.5)–(4.6) and required the differential polarisability  $\alpha_{0\leftrightarrow 1}(\Delta_m) = 0$ . This allowed us to compute the expected frequency of the two tune-out points of  $|1\rangle$ , one on the left side and one on the right side of the  $R = 1 \leftrightarrow R' = 2$  transition. From  $\Gamma$  and the background polarisability terms, we expect these points to be at  $\Delta_0^{(1),l} = -2\pi \times 8.93(15) \text{ GHz}$  and  $\Delta_0^{(1),r} = 2\pi \times 7.95(15) \text{ GHz}$ .

With  $\alpha_{\text{iso}}$  known,  $I$  can be determined from the shift of the STIRAP transition in the presence of the 866-nm beam at varying power settings. We did this at a large detuning  $\Delta = 2\pi \times 80 \text{ GHz}$ ,  $\alpha_0$  to avoid confounding frequency errors. Specifically, we used the value  $\alpha_0(2\pi \times 80 \text{ GHz}) = h \times 47(1) \text{ Hz}/(\text{W}/\text{cm}^2)$ . The intensity was then determined via the relation

$$\hbar\delta\omega_{\text{FB}\leftrightarrow 0}(I, \Delta) = (\alpha_{\text{FB}} - \alpha_0(\Delta))I. \quad (4.11)$$

This yielded the result  $2700(100) \text{ W}/\text{cm}^2$  at 100% relative power.

## 4.6. Polarisability measurements

In the next step, we confirmed the shape of the  $\alpha_0(\Delta)$  curve by measuring ground-state polarisability at varying detunings. This was again done by observing the shift of STIRAP two-photon detuning that occurred when turning the 866-nm beam on during one of the STIRAP pulses. Example data is shown in Figure 4.7(a). The shift of two-photon detuning is equal to the differential light shift  $\hbar\delta\omega_{\text{FB}\leftrightarrow 0}(I, \Delta)$  between the  $|\text{FB}\rangle$  and  $|0\rangle$

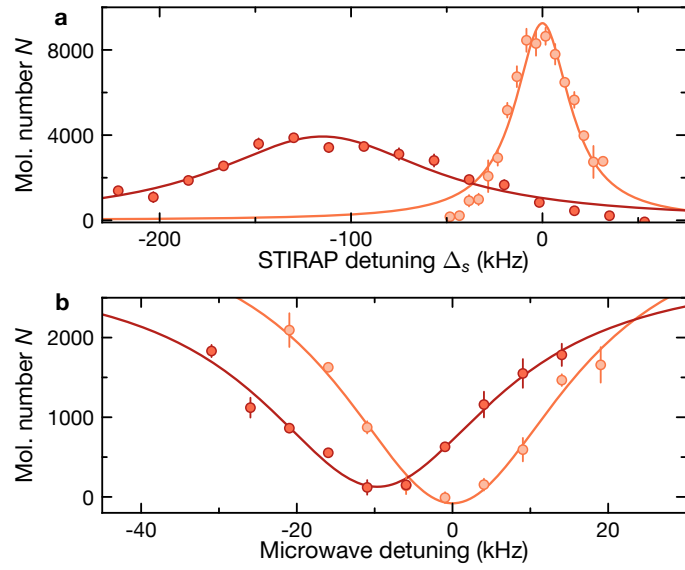


**Figure 4.7.:** Example data for polarisability measurements. **(a)** Determination of  $\alpha_0$  via STIRAP two-photon resonance shift. The 866-nm beam was turned on during STIRAP. Dark red points were taken at  $\Delta = -2\pi \times 2\text{GHz}$  and  $I = 1200\text{W/cm}^2$ . **(b)** Determination of differential polarisability  $\alpha_{0\leftrightarrow 1}$  via microwave spectroscopy. Dark red points were taken at  $\Delta = 2\pi \times 3\text{GHz}$  and  $I = 69\text{W/cm}^2$ . In both (a) and (b), the bright points are calibration measurements taken without 866-nm light. Solid lines are Lorentzian fits. Error bars denote the standard error of the mean.

**Table 4.1.:** Properties of the  $X \leftrightarrow b$  transition and the  $b^3\Pi_0$  state.

Quantity	Value
$\omega_0$	$2\pi \times 346.12358(7)$ THz
$\Gamma$	$2\pi \times 301(10)$ Hz
$\Gamma_e$	$2\pi \times 13.0(5)$ kHz
$\alpha_{\text{bg}}^{\parallel}$	$h \times 105(3)$ Hz/(W/cm <sup>2</sup> )
$\alpha_{\text{bg}}^{\perp}$	$h \times 20(1)$ Hz/(W/cm <sup>2</sup> )
$B'_{\text{rot}}$	$h \times 2.79(2)$ GHz
$\Delta_0^{[0]}$	$2\pi \times 3.85(8)$ GHz
$\Delta_0^{[1],l}$	$-2\pi \times 8.93(15)$ GHz
$\Delta_0^{[1],r}$	$2\pi \times 7.95(15)$ GHz
$\Delta_m$	$2\pi \times 10.15(6)$ GHz
$\Delta^*$	$-2\pi \times 6.78(17)$ GHz

states. From this, we obtained  $\alpha_0(\Delta)$  via

$$\alpha_0(\Delta) = \alpha_{\text{FB}} - \hbar\delta\omega_{\text{FB}\leftrightarrow 0}(I, \Delta)/I. \quad (4.12)$$

The precision of this method was limited by drifts of the STIRAP laser frequency, which we compensated as far as possible by regular calibration measurements without 866-nm light.

The differential polarisability  $\alpha_{0\leftrightarrow 1}(\Delta)$  was measured in a more stable way, namely microwave spectroscopy. After the association of molecules in the state  $|0\rangle$  in the magic 1D lattice, their rotational state can be changed to  $|1\rangle$  via a resonant microwave  $\pi$ -pulse with a duration of 35  $\mu$ s. This can be observed as molecule loss because molecules in  $|1\rangle$  are not resonant with the reverse STIRAP. The light shift  $\hbar\delta\omega_{0\leftrightarrow 1}(\Delta)$  of the  $|0\rangle \leftrightarrow |1\rangle$  transition caused by the presence of 866-nm light during the microwave pulse then yields  $\alpha_{0\leftrightarrow 1}(\Delta)$  by

$$\alpha_{0\leftrightarrow 1}(\Delta) \equiv \alpha_1(\Delta) - \alpha_0(\Delta) = \hbar\delta\omega_{0\leftrightarrow 1}(\Delta)/I. \quad (4.13)$$

Example data from a scan of the microwave transition frequency is shown in Figure 4.7(b).

For all polarisability measurements, the intensity of the 866-nm light was chosen in order to achieve a compromise between the magnitude of the light shift and the inhomogeneous broadening caused by the finite size of the 866-nm beam. For the measurements of  $\alpha_0$ , intensities between 360 W/cm<sup>2</sup> and 2200 W/cm<sup>2</sup> were used. The measurements of  $\alpha_{0\leftrightarrow 1}$  were performed at intensities between 69 W/cm<sup>2</sup> and 550 W/cm<sup>2</sup>. The obtained results, both for the ground-state and differential polarisabilities, match well with the expected curves as can be seen in Figure 4.8. The location of the poles of Equation (4.4) and the known ground-state rotational constant  $B_{\text{rot}}$  were used to determine the excited-state rotational constant  $B'_{\text{rot}}$ . A summary of all the measured quantities is given in Table 4.1.

Finally, the polarisation dependence of the background term  $\alpha_{\text{ang}}(\theta)$  was determined

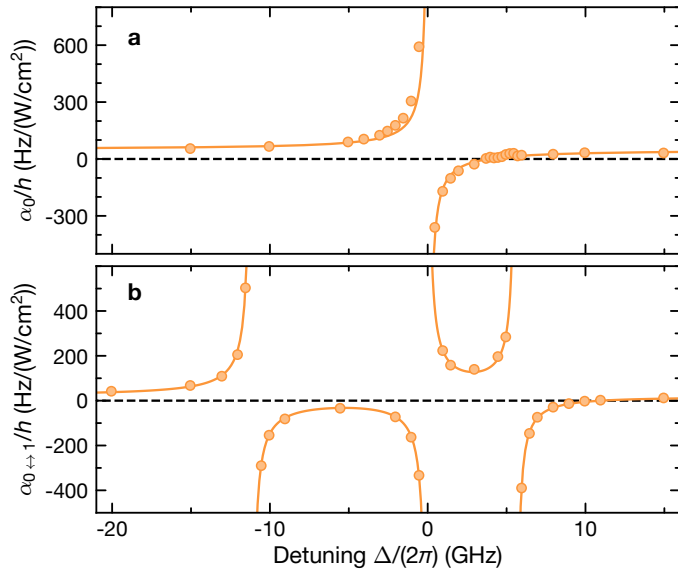


**Figure 4.8.:** Ground-state and differential polarisability. (a) Experimental data for polarisability  $\alpha_0(\Delta)$  and theoretical curve determined using parameters from intensity-independent measurements. The black dashed line indicates zero. (b) Differential polarisability  $\alpha_{0\leftrightarrow 1}$  measured by microwave spectroscopy and fit to the data. The fit function is a combination of three resonances each described by Equation (4.3), with a constant offset as well as the linewidths and positions for each resonance as fit parameters.

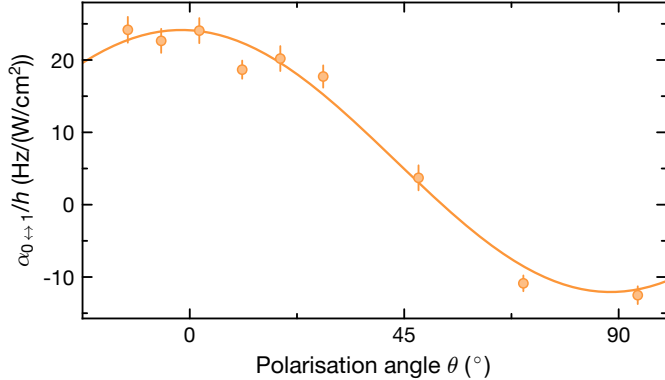


**Figure 4.9.:** Dependence of differential polarisability  $\alpha_{0\leftrightarrow 1}$  on the angle  $\theta$  between laser polarisation and electric field. Measurements were performed at  $\Delta = 2\pi \times 80$  GHz. Error bars denote the standard error of the mean. The solid line is a fit of Equation (4.6).

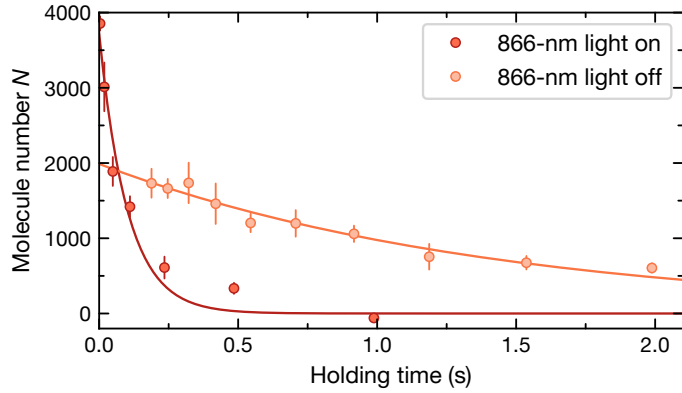


**Figure 4.10.:** Example data for lifetime measurements in a 3D lattice in the presence of 866-nm light at a detuning  $\Delta = -2\pi \times 1.5 \text{ GHz}$  and intensity  $I = 1150 \text{ W/cm}^2$  are shown in dark red. The measurement of the background loss rate in the deep 3D lattice is shown in bright red. Error bars denoting the standard error of the mean of three to four data points, and the solid lines are exponential fits to determine the  $1/e$  lifetime.

by measurements of  $\alpha_{0\leftrightarrow 1}$  at a constant detuning  $\Delta = 2\pi \times 80 \text{ GHz}$  and at various angles between the laser polarisation and the electric field, see Figure 4.9. At this detuning,  $\alpha_{0\leftrightarrow 1} = \alpha_{\text{ang}}(\theta)$  is a good approximation. The results agree with the prediction of Equation (4.6) as well as with the values determined for  $\alpha_{\text{bg}}^{\parallel}$  and  $\alpha_{\text{bg}}^{\perp}$  in Table 4.1.

## 4.7. Lifetime measurements

In order to obtain long lifetimes for molecules in an optical dipole trap, the photon-scattering rate must be sufficiently low. We measured the radiative lifetime by illuminating  $|0\rangle$ -molecules in a deep 3D lattice with 866-nm light. The lattice served to freeze the molecules, thus avoiding confounding collisional loss. The one-body loss rate  $\Gamma_L$  caused by the 866-nm beam was determined by fitting an exponential decay curve to the measured molecule numbers, see example data in Figure 4.10. While inelastic collisions between molecules in the ground band are strongly suppressed in deep lattices, there is still heating caused by intensity and frequency noise of the lattice light. This can excite molecules into higher bands where they are able to move through the lattice more freely, resulting in inelastic close-range collisions. To compensate for this as well as for off-resonant scattering of lattice photons, the loss rate measured in the respective lattice configuration in absence of 866-nm light was subtracted for each data point. From the lifetime data, we determined the resonance position  $\omega_0$ . To ensure that this was not shifted by the presence of far off-resonant dipole trap light, we performed additional loss measurements for small values of  $\Delta$  with all far-detuned trapping light turned off and found a shift in resonance frequency of less than 20 MHz. The results are shown in Figure 4.11.

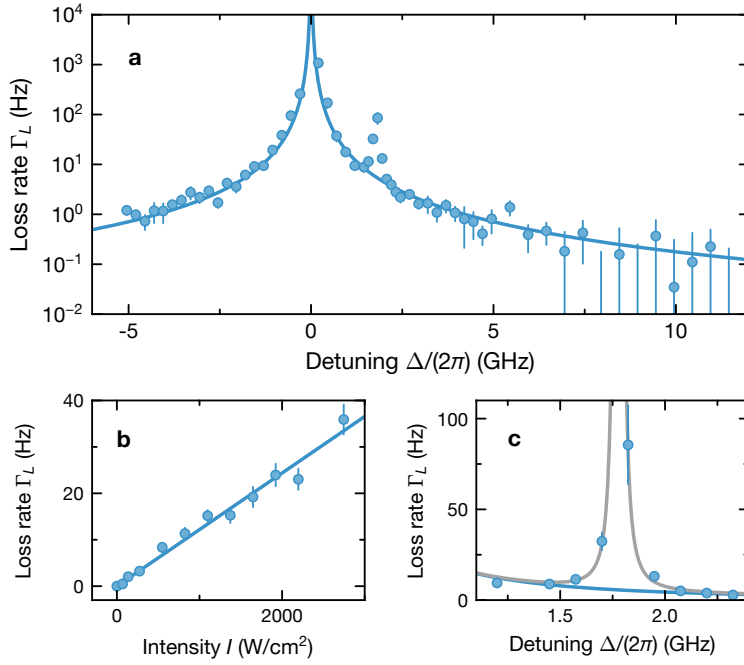


**Figure 4.11.**: Lifetime of ground-state molecules near the  $X \leftrightarrow b$  transition. **(a)** Observed loss rate  $\Gamma_L$  of molecules in  $|0\rangle$  subjected to 866-nm light at an intensity of  $1150 \text{ W/cm}^2$  (blue circles). The loss rate at  $I = 0$  was subtracted from these data points. The blue line is a fit of Equation (4.7) with  $\omega_0$  and  $\Gamma_e$  as the fit parameters, where data points between  $\Delta = 2\pi \times 1.5 \text{ GHz}$  and  $\Delta = 2\pi \times 2.5 \text{ GHz}$  were excluded to avoid biasing the fit. Error bars denote the standard error of the fit. **(b)** Intensity dependence of the loss rate at  $\Delta = 2\pi \times 1 \text{ GHz}$ . The solid line is a linear fit. **(c)** Secondary loss peak. The grey line is a Lorentzian fit with the previously determined lineshape of the main peak added as a background term. This fit which was used to determine the centre frequency and linewidth of this peak.

At first, the analysis of these data yielded puzzling results, with the loss rate  $\Gamma_L$  an order of magnitude larger than should be expected from plugging  $\Gamma$  into Equation (4.7). We excluded the possibility of a two-photon process causing this by measuring a curve of  $\Gamma_L$  versus  $I$ , which we found to be linear, as expected for a one-photon loss process (see Figure 4.11b). It turned out that our initial assumption that  $\Gamma \approx \Gamma_e$  does not hold for this molecule, rather we measured a much larger value  $\Gamma_e = 13.0(5)$  kHz. This is because the dominant decay channels from  $|b^3\Pi_0, v' = 0, R' = 1\rangle$  lead to the  $a^3\Sigma^+$  manifold, making the lifetime of the excited state much shorter than it would be for a two-level system. This was confirmed by a calculation by Ming Li using the optical potential method, which yielded  $\Gamma_e = 11.1$  kHz [553].

At  $\Delta = 2\pi \times 1.78(5)$  GHz we observed a second, smaller loss peak with an effective linewidth  $\sqrt{\Gamma\Gamma_e} = 2\pi \times 185(20)$  Hz. We hypothesise that this could be a transition to a state in the  $|b^3\Pi_{0-}\rangle$  manifold. Figure 4.11(c) shows the relevant frequency range around  $\Delta = 2\pi \times 1.8$  GHz. Still, at all detunings relevant for rotational-state dependent trapping, the loss rates low enough that lifetimes of more than 1 s can be achieved in a 866-nm trap with a depth of  $k_B \times 1$   $\mu$ K.

## 4.8. Potential applications

This demonstration of near-resonant optical dipole trapping of molecules opens up many exciting possibilities. Some of these are relatively simple, and have previously been implemented with atoms, while others are quite challenging or unique to molecular systems.

The availability of tune-out frequencies for both rotational levels enables selective addressing of molecules in one of these states. For example, a microwave sweep could be used to transfer molecules at the edge of a 3D lattice, which are hotter on average, into an untrapped state. This would enable evaporative cooling in lattices, where getting rid of hot particles is usually difficult. It is conceivable that polar molecules could be cooled exclusively via long-range interaction in a 3D lattice, without ever colliding at short range. Multiple molecules hopping onto the same lattice site could be prevented by Pauli blocking [308] or dipole blocking [206]. However, recent unpublished calculations by Yuqi Wang, Tao Shi and Su Yi at the Chinese Academy of Sciences show that the thermalisation in such a situation is likely to be impractically slow due to slow diffusion of strongly interacting molecules in the lattice.

The magic frequency is most important for reaching long coherence time of rotational superpositions. This is highly relevant, for example, for proposals to use rotational states to encode qubits [375]. There are many ways to achieve a magic condition, such as tuning the power and polarisation of the laser field as has been demonstrated in previous experiments [319, 572–574]. However, this alone is not enough to reach coherence times above a few milliseconds, as there are complicated effects resulting from rotation-hyperfine coupling as well as higher-order polarisability terms. Controlling polarisation to a higher precision than a few degrees is usually not practical due to temperature- and stress-dependent birefringence which is present in almost all optical components. This is much less problematic when working at the magic frequency. Taking the second-order term into account,

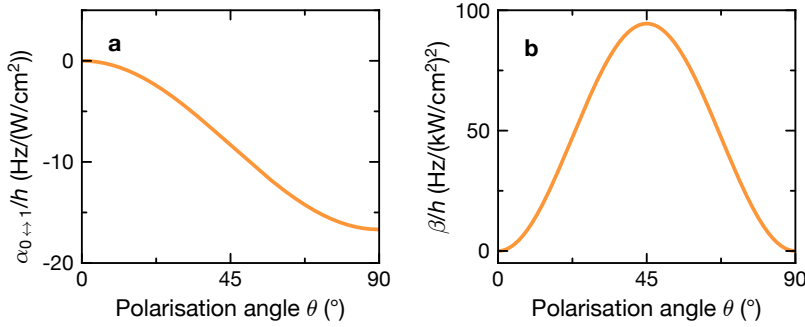


**Figure 4.12.:** Dependence of (a) differential polarisability  $\alpha_{0\leftrightarrow 1}$  and (b) second-order polarisability  $\beta$  on the polarisation angle  $\theta$  at the magic detuning with a dc electric field of 86 V/cm.

the differential light shift  $\delta\omega_{0\leftrightarrow 1}$  can be approximately described by [381]

$$\delta\omega_{0\leftrightarrow 1} = \frac{1}{\hbar}(\alpha_{0\leftrightarrow 1}(\theta)I + \beta(E, \theta)I^2 + \mathcal{O}(I^3)), \quad (4.14)$$

where  $\beta$  is the second-order polarisability of  $|1\rangle$ , and  $E$  is the magnitude of the dc electric field. An approximation for  $\beta$  can be derived by considering the contribution from four-photon couplings to the  $|X^1\Sigma^+, v = 0, R = 1, m_R = \pm 1\rangle$  states and back. It reads

$$\beta(E, \theta) = \frac{5B_{\text{rot}}}{3d^2E^2}(\alpha_1(0) - \alpha_1(\pi/2))^2 \sin^2(2\theta). \quad (4.15)$$

Figure 4.12 shows that the resulting angle-dependence of  $\alpha_{0\leftrightarrow 1}$  and  $\beta$  both vanish, and both have a vanishing slope at  $\theta = 0$ . Hence, they are first-order insensitive to polarisation fluctuations, allowing for improved stability.

An exciting possibility comes from lattices at an “antimagic” frequency, where two rotational states experience opposite polarisability. Such conditions should occur at detunings  $-2\pi \times 9.9$  GHz,  $2\pi \times 1.4$  GHz, and  $2\pi \times 7.5$  GHz. If an equal mixture of the two states could be created in an antimagic lattice, this would lead to molecules in  $R = 0$  and  $R = 1$  being trapped alternatingly in the intensity minima and maxima, leading to a lattice constant of half the usual value. In addition, the dipole-dipole interaction between these two states is very strong and can be chosen to be attractive or repulsive by choosing the value of  $m_R$ . This could allow the creation of fascinating new quantum phases, though the technical challenges in realising such strongly-interacting and high-density gases are certainly great.

The close proximity of the tune-out and magic frequencies allows dynamic switching or even continuous modulation between trap configurations with arbitrary ratios of polarisability experienced by different rotational states. This is unique to molecules, because typical rotational splittings of a few gigahertz are in a sweet spot that other systems do

not have: they are small enough to allow fast tuning of lasers between different magic or tune-out conditions, but large enough to allow working at reasonably large detunings. This may open up new possibilities for Floquet engineering of topological states in dipolar spin systems [580] or other novel methods of dynamic control of quantum systems.

Another problem that a near-resonant dipole trap naturally solves is that of creating a repulsive dipole potential. For atoms, this is often implemented with 532-nm light, but this is unlikely to work for any bialkali molecules. For example, for NaK, this frequency corresponds to transitions into the  $C^1\Sigma^+$  manifold [578], which is strongly coupled to the ground state. The proximity of many transitions with large linewidths is likely to cause prohibitively large photon-scattering rates. At the  $X \leftrightarrow b$  transition, strongly repulsive dipole forces can easily be achieved by working at a positive detuning of a few hundred megahertz. This has allowed us to realise the repulsive box trap described in the following chapter.

*It ain't what you don't know that gets you into trouble.  
It's what you know for sure that just ain't so.*

—Attributed to Mark Twain.

## 5. Collisions of ground-state molecules

What happens when two ground-state molecules collide in the ultracold regime? This question is highly relevant and deceptively simple. In the case of chemically stable molecules, where all reactions involving two partners are endothermic, one would naturally expect that all collisions have to be elastic. In fact, half of the alkali dimers are chemically stable in two-body collisions [238], but in spite of this, the presence of universal two-body loss has been consistently observed with the stable species RbCs, NaRb, and both bosonic and fermionic NaK [293, 388–390, 548]. Here, “universal” means that every collision event where two molecules reach the short-range part of their interaction potential leads to the loss of both participants. The collision dynamics are then independent of the details of the short-range potential. Comparisons with the chemically reactive species CaF and KRp have shown that their loss rates are similar [230, 233, 403, 429]. This puzzling observation is interesting in itself, but the presence of two-body loss has also created significant problems, making it imperative for the advancement of the field to keep collisions under control (see Section 2.6.2).

In this chapter, I show a comprehensive study of the collisions between  $^{23}\text{Na}^{40}\text{K}$  molecules at different temperatures, magnetic and electric fields, light intensities, and in different hyperfine states. The results show that, quite surprisingly, the loss remains universal under all observed conditions. There are, by now, a number of new ideas on how to explain these observations, but no clear consensus has emerged yet. This chapter is based on the publication [307].

### 5.1. Sticky complexes

#### 5.1.1. RRKM theory

So how is it possible for a collision without any energetically allowed reactions to lead to the loss of both involved molecules? The generally accepted answer is that a four-body *sticky complex* can be formed, which is long-lived enough to collide with a third particle. In the first version of this proposal, it was suggested that this third particle could be another molecule [391–393], but later, more accurate calculations showed that this was

unlikely to happen at typical densities [394–396]. Instead, it is more likely that the four-body complex scatters photons at a high rate, leading to it either leaving the trap due to the recoil momentum, or changing its internal state into something that can not decay back into two ground-state molecules. Until recently, all experiments with ultracold molecules have taken place in optical dipole traps at intensities where it was predicted that almost every formed complex gets lost in this way. Hence, a logical course of action is to trap molecules in the dark and observe if the two-body loss is reduced.

Here, a sticky complex is a metastable four-body bound state which can be formed in ultracold collisions. In contrast to intermediate complexes formed in other chemical reactions, which typically have lifetimes on the order of picoseconds, they can live substantially longer [403, 404]. This is because, in a close-range collision, two molecules enter a part of their mutual interaction potential that is quite deep, up to 1000s of  $\text{cm}^{-1}$  below the asymptotic energy of separated molecules. This energy can then be distributed, allowing the molecules to go into a large number of rovibrationally excited states. If this happens, the molecules can not leave the attractive potential, because they first need to randomly go back to their respective two-body ground states for this to be energetically allowed. As originally proposed by Mayle *et al.* [391, 392], the lifetime of a sticky complex,  $\tau_{\text{stick}}$ , can be estimated using Rice–Ramsperger–Kassel–Marcus (RRKM) theory:

$$\tau_{\text{stick}} \approx \tau_{\text{RRKM}} = \frac{2\pi\hbar\rho_s}{N_s}. \quad (5.1)$$

Here,  $N_s$  is the number of energetically available outgoing quantum states, with  $N_s = 1$  for nonreactive molecules, and  $\rho_s$  is its density of states of the complex. While this estimation makes it possible to calculate complex lifetimes, it requires some simplifying assumptions, notably that the dynamics inside the close-range potential are chaotic, which is not obviously justifiable. Nevertheless, recent experiments with  $^{40}\text{K}^{87}\text{Rb}$  and  $^{87}\text{Rb}^{133}\text{Cs}$  described in References [401, 402, 404] have found values for  $\tau_{\text{stick}}$  which match remarkably well with the RKKM predictions.

For the case of  $^{23}\text{Na}^{40}\text{K}$ , the theory predicts a lifetime of  $\tau_{\text{RRKM}} = 18\,\mu\text{s}$  [395] and a photon-scattering rate of sticky complexes of  $452\,\text{Hz}/(\text{W}/\text{cm}^2)$  at a wavelength of 1064 nm. With the typical intensity inside a dipole trap, which is on the order of  $1\,\text{kW}/\text{cm}^2$ , this should lead to almost every sticky complex undergoing at least one scattering event during its lifetime. On the other hand, reducing the intensity to  $1\,\text{W}/\text{cm}^2$  should increase the survival probability to 99%, as shown in Figure 5.1.

### 5.1.2. The recollision hypothesis

In the case of identical fermions, it is possible that an additional effect has to be considered when calculating complex lifetimes. During the process of its dissociation, when two molecules separate, they have to overcome the  $p$ -wave barrier again to leave the bound state [581, 582]. Depending on the collision energy, the probability of tunnelling through this barrier can become quite small, with almost all molecules being reflected back into the short-range potential (see Figure 5.2). The sticky complex is then formed multiple

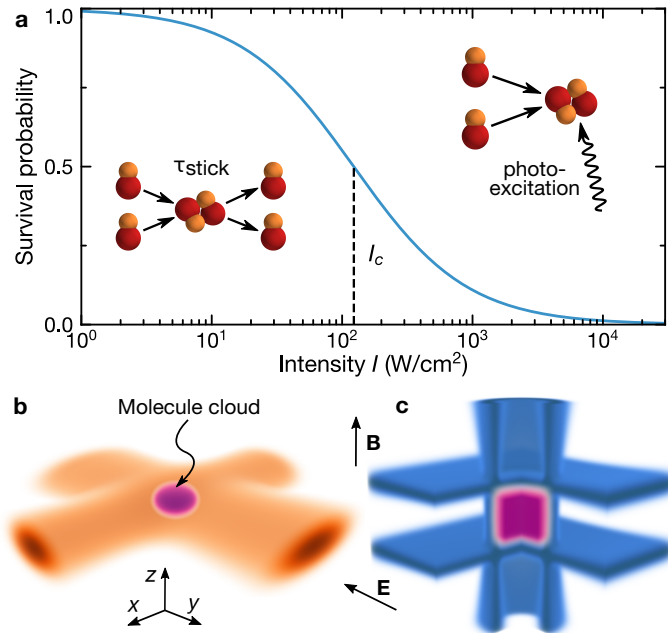


**Figure 5.1.:** Overview of sticky collisions and the experimental setup. (a) Probability for two molecules to survive a collision at a given intensity of 1064-nm light according to Reference [395]. Every collision results in the formation of a sticky complex, which is subsequently lost by photon scattering if the light intensity is high. At low intensity, the complex can decay back into ground-state molecules after a mean sticking time  $\tau_{\text{stick}}$ . At the critical intensity  $I_c$ , the survival probability is 50%. (b) Standard attractive crossed dipole trap consisting of two elliptical beams of wavelength 1064 nm and 1550 nm. (c) Repulsive box trap at 866 nm with vertical cylinder beam and two horizontal elliptical beams. One quadrant is cut out for visibility. The arrows that indicate magnetic field and electric field are valid for both (b) and (c). To compensate gravity in the box trap, we use an electric field gradient along the  $z$ -direction.

times; at typical temperatures we expect about 270 times. For bosons, where there is no *p*-wave barrier, the effect of recollisions should be significantly smaller, with complexes being formed on average three times before dissociating.

## 5.2. Loss in a bright trap

In the first part of the experiments described here, we performed a thorough characterisation of collisions at high light intensity in a standard red-detuned dipole trap setup. The results were compared to theory in order to serve as a reference point for the low-intensity measurements described later. We created molecules in the absolute ground state as described in Section 3.1.2. This was done in the combined 1064/1550-nm crossed dipole trap shown in Figure 5.1(b) at trap frequencies of  $(\omega_x, \omega_y, \omega_z) = 2\pi \times (57(1), 89(2), 205(3)) \text{ Hz}$  and a trap depth of  $k_B \times 6 \mu\text{K}$ .

### 5.2.1. Data analysis

In order to extract loss coefficients from experimentally measured curves of molecule number versus time, it is necessary to understand the density distribution of the sample and its change over time. In a harmonic trap, this is also strongly dependent on the sample's temperature, which is time-dependent itself. Considering these effects, the average density of a thermal sample is given by

$$n = N \left( \frac{m\bar{\omega}^2}{4\pi k_B \bar{T}} \right)^{3/2}, \quad (5.2)$$

where  $N$  is the total molecule number,  $m$  is the molecule mass,  $\bar{\omega} = (\omega_x \omega_y \omega_z)^{1/3}$  is the geometric mean trap frequency, and  $\bar{T}$  is the geometric average of the temperatures in the three directions. With this, the loss curve can be modelled as

$$\frac{dN}{dt} = (-KT_{\text{avg}}n - \Gamma_{\text{sc}})N, \quad (5.3)$$

with the arithmetic mean temperature  $T_{\text{avg}}$ , the two-body loss coefficient  $K$ , and the one-body loss rate  $\Gamma_{\text{sc}}$ . For fermions, which collide predominantly via *p*-wave interactions as long as the average kinetic energy is much lower than the height of the *p*-wave barrier, it is reasonable to assume that  $K$  is temperature-independent [233]. Here, we make the additional simplifying assumption that, with the small temperature changes during the holding time, only the influence of temperature on density is relevant, but the inelastic collision rate coefficient, which is defined as

$$\beta_{\text{inel}} = KT_{\text{avg}}, \quad (5.4)$$

is approximately constant during a single measurement. Finally, we assume that the sample is always in thermal equilibrium, with equal temperature in each spatial direction.

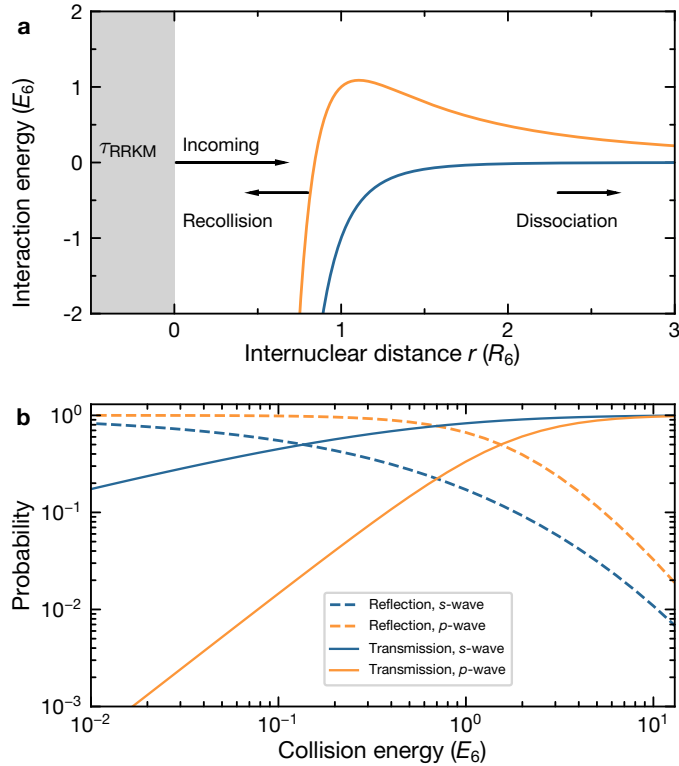


**Figure 5.2.:** Overview of the recollision hypothesis. **(a)** Effective radial potential of the van-der-Waals interaction between two molecules for *s*-wave (blue) and *p*-wave (orange) collisions. When the molecules reach  $r = 0$ , a complex with lifetime  $\tau_{\text{RRKM}}$  is formed. In order to dissociate, the incoming flux must be transmitted through the potential barrier. If it is instead reflected, the complex is formed again. **(b)** Probability for reflection (solid lines) and transmission (dashed lines) at the long-range potential. Lengths are given in units of  $R_6 = (2\mu C_6/\hbar^2)^{1/4} = 2.092 \bar{a} \approx 26.5 \text{ nm}$ , and energies in units of  $E_6 = \hbar^2/(2\mu R_6^2) \approx \hbar \times 220 \text{ kHz}$ . Here,  $C_6$  is the van-der-Waals coefficient [583], and  $\mu$  is the reduced mass of a molecule pair. These curves were calculated by Tijs Karman.

For identical fermions, this is not necessarily the case, especially since with an external electric field, the loss coefficient can be direction-dependent. However, under our experimental conditions, the differences between temperatures in all directions are on the same order as the systematic measurement error, so that assuming them to be equal makes sense. In the rest of the chapter, this equilibrium temperature is denoted  $T$  for simplicity.

For the time dependence of  $T$ , we assume a linear function

$$T(t) = T_0 + qt. \quad (5.5)$$

Again, there is no *ab initio* justification for this, but our data shows that it is a good empirical description (see Figure 5.3c). Because the one-body lifetime in far-detuned dipole traps is very long, it is also justified to assume here that  $\Gamma_{\text{sc}} \approx 0$ . With these assumptions, Equation (5.3) can be analytically solved, resulting in

$$N(t) = \frac{N_0}{1 + \frac{2\beta_{\text{inel}}N_0}{q(4\pi k_B/m\bar{\omega}^2)^{(3/2)}} \left( \frac{1}{\sqrt{T_0}} - \frac{1}{\sqrt{T_0+qt}} \right)}, \quad (5.6)$$

where  $N_0$  is the initial molecule number. Despite careful calibration and analysis, measuring densities accurately remains difficult, especially in harmonic traps. This is because the calibration of molecule number, trap frequency and temperature all affect the result strongly, resulting in potentially large systematic errors. We estimate that, in our case, the systematic error could be up to 50%.

## 5.2.2. Temperature dependence of collisions

To investigate the temperature-dependence of the two-body loss, we prepared molecule samples at initial temperatures between 300 nK and 900 nK. This was done by stopping the evaporation of the atomic mixture in the dipole trap at different trap depths before the molecule association. By ramping the dipole trap to a higher depth after the end of evaporation and holding the atoms before association, we ensured that the loss caused by evaporation is completely stopped before the beginning of the measurement. The results are shown in Figure 5.3 and confirm the expectation that  $K$  is approximately constant, i.e.,  $\beta_{\text{inel}} \propto T$ . For comparison, a multichannel quantum defect theory (MQDT) calculation using the universal condition results in  $\beta_{\text{inel}} = (11.48\bar{a})^3(k_B T/h)$  with the characteristic van-der-Waals length  $\bar{a} = 12.7 \text{ nm}$  [234, 583]. This is approximately two times smaller than the experimental result, which could indicate a systematic underestimation of the density. Hypothetically, it is also possible that the loss rates are actually above the universal threshold, which can occur if there are interference effects between incoming and reflected parts of the scattering wavefunction. Evidence of this has previously been observed for  $^{23}\text{Na}^{87}\text{Rb}$  and  $^{87}\text{Rb}^{133}\text{Cs}$  [389, 390, 584], and a clear observation was found with a  $^{23}\text{Na}^{6}\text{Li}+^{23}\text{Na}$  mixture [437]. However, in such a case, the curve of  $\beta_{\text{inel}}$  versus temperature or electric field should show scattering resonances of some form [274], which we did not observe in any experiment.

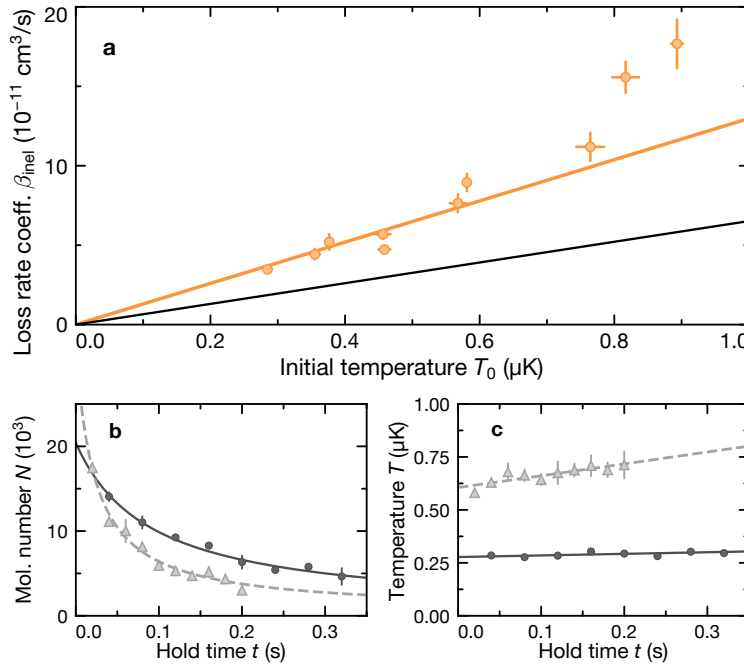


**Figure 5.3.:** Temperature dependence of two-body loss rate coefficient  $\beta_{\text{inel}}$ . (a) Measured  $\beta_{\text{inel}}$  versus initial temperature of the molecule sample in the crossed dipole trap. The orange line is a linear fit which yields  $K = 13.0(8) \times 10^{-11} \text{ cm}^3/\mu\text{Ks}$ . For comparison, the black line shows the MQDT result  $K = 6.52 \times 10^{-11} \text{ cm}^3/\mu\text{Ks}$ . The error bars represent the standard deviation of the fit. (b) Example data for molecule number versus hold time for two different initial temperatures (triangles and circles) and two-body loss fits (solid and dashed lines) according to Equation (5.6). (c) Example data for temperature versus hold time for the same two data sets as in (b). In subfigures (b) and (c), error bars correspond to the standard error of the mean.

### 5.2.3. Dipolar collisions

In the next series of measurements, we left the temperature constant at about 500 nK and varied the external dc electric field to probe the dependence of the collision rate on the dipole moment. The field is expected to have a strong effect, as the attraction between molecules in head-to-tail orientation weakens the *p*-wave barrier and strongly increases the collision rate. In contrast, in the other two directions, the dipole-dipole interaction is repulsive, thus preventing short-range collisions and reducing the loss rate. The dc electric field was created with an upgraded version of the setup described in Reference [525]. Due to the addition of more powerful but equally stable high-voltage amplifiers (609E-6, Trek), we were able to create fields of up to 1600 V/cm, compared to the previous limit of 160 V/cm.

The electric field at the molecule's position resulting from a given voltage applied to the electrodes depends strongly on the electrode geometry, which is hard to measure precisely. Therefore, a direct calibration of voltage from the Stark shift of the molecules is likely to be more accurate than a simulation. To obtain this calibration, we applied small voltages of up to 100 V to the electrodes, both in the horizontal and vertical directions. At such small fields, the Stark shift is nearly quadratic, and can be expressed as [206]

$$U = -\frac{\zeta E^2}{2}. \quad (5.7)$$

The constant  $\zeta = d_0^2/(3B_{\text{rot}}) = 221.5 \text{ Hz}/(\text{V}/\text{cm})^2$  can be accurately calculated from the known molecule-frame dipole moment  $d_0$  and the rotational constant. This expression was then compared to measurements of the Stark shift shown in Figure 5.4 to obtain the electric field. In addition, the data shows that the residual electric field is below 1 V when the voltage is turned off. This can very likely be considered negligible.

Figure 5.5(a) shows the observed dependence  $\beta_{\text{inel}}(E)$  compared to a numerical coupled-channel calculation described in Reference [307]. As expected, the loss rate strongly increased at higher fields. The discrepancies between experiment and theory may again be caused by the systematic error of the density, but it is also possible that the electric field is not sufficiently stable at very high voltages, where charging of the glass cell may occur. We also compared the observed heating rate  $q$  to a simplified version of the model established in the supplemental material of Reference [233]. In the case where the initial temperature is much larger than the total heating, this model predicts linear heating with a rate

$$\frac{q}{T_0^2 n_0} = \frac{\beta_{\text{inel}}}{12T_0} \quad (5.8)$$

with the initial average density  $n_0$ . As shown in Figure 5.5(b), this model agrees qualitatively with our data without any fit parameters.

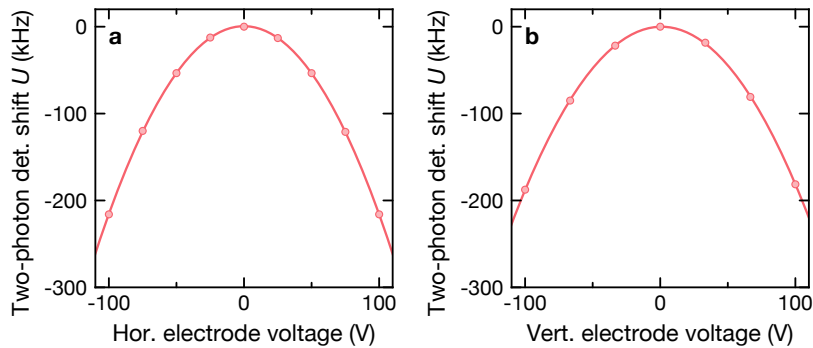


**Figure 5.4.:** Electric-field calibration at the molecule position. The Stark shift on ground-state molecules is measured from the shift of STIRAP two-photon detuning at various voltages applied to the electrodes. Given on the x-axis is the absolute value of the voltage applied to each electrode. A quadratic expression is fitted and compared to Equation (5.7). **(a)** Horizontal direction. Here, the fit yields a conversion factor of  $0.442(20) \text{ cm}^{-1}$  between applied voltage and resulting field. **(b)** Vertical direction. Here, the conversion factor is  $0.408(24) \text{ cm}^{-1}$ . In both directions, the fits indicate residual fields of  $< 1 \text{ V/cm}$  when no voltage is applied.

### 5.3. Temporally dark dipole trap

Red-detuned, attractive dipole traps require significant light intensity to confine molecules, making it hard to probe low-intensity trapping conditions in such a trap. There is, however, a simple way to circumvent this problem: the dipole trap does not need to be on all the time. The light can be periodically switched off and on (“chopped”) at a fixed frequency, as long as it is much larger than the harmonic trap frequency. The trapped particles then experience a time-averaged potential. If the trap can be off for a time on the order of  $\tau_{\text{stick}}$ , not all sticky complexes will be destroyed during this time, leading to smaller time-averaged loss rates. This was first observed with  $^{87}\text{Rb}^{133}\text{Cs}$  by Gregory *et al.* [401], and soon after also with  $^{40}\text{K}^{87}\text{Rb}$  by Liu *et al.* [404]. According to the RRKM-theory predictions, measuring this effect with  $^{23}\text{Na}^{40}\text{K}$  should actually be much easier than with  $^{87}\text{Rb}^{133}\text{Cs}$ , which has a much longer  $\tau_{\text{RRKM}}$  of  $253 \mu\text{s}$ .

There are two technical challenges associated with creating chopped dipole traps: first, the light intensity needs to be reduced below the critical value  $I_c$ , which is the intensity where half the complexes are expected to scatter at least one photon during their lifetime. Since  $I_c$  is typically three to four orders of magnitude below the dipole-trap intensity, this requires a control system with a sufficient dynamic range. Second, it is hard to completely avoid heating and loss of molecules caused by the chopping itself, especially at low frequencies.

For  $^{87}\text{Rb}^{133}\text{Cs}$  with its quite low  $I_c$  of  $0.7 \text{ W/cm}^2$  [401], solving the first problem is difficult: the Durham group achieved sufficiently low intensities only by blocking their beam with a mechanical chopper wheel. For NaK, the expected critical intensities at

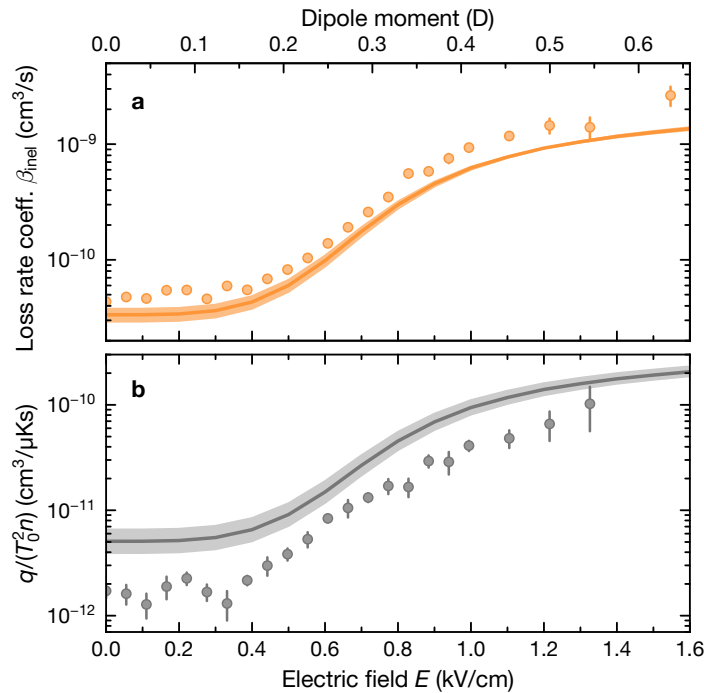


**Figure 5.5.:** Electric-field dependence of collisions in the red-detuned dipole trap. **(a)** Measured curve of  $\beta_{\text{inel}}$  versus the magnitude of the dc electric field  $E$  in the red-detuned crossed dipole trap. These data were taken at temperatures between 480nK and 620nK. The solid line is a parameter-free quantum close-coupling calculation at 550nK, provided by Goulven Quéméner. **(b)** Measured normalised heating rate  $q/(T_0^2 n)$  compared to the prediction from Equation (5.8). In both (a) and (b), the error bars correspond to the standard deviation of the fit and the shaded area around the theory curves takes the highest and lowest observed temperatures into account.

the two wavelengths we use are  $I_{c,1064} = 123 \text{ W/cm}^2$  and  $I_{c,1550} = 623 \text{ W/cm}^2$  [395], so this should be much less problematic. The second problem can not be solved, but circumvented by comparing the lifetime in the chopped trap with a control experiment where an additional, unchopped high-intensity beam dubbed the “kill-beam” is added. This beam is strong enough to cause excitation of all complexes, but the losses caused by chopping are the same in both cases. In our case, the kill-beam wavelength is 1064 nm.

In our experiments, we chopped both the 1064-nm and the 1550-nm dipole trap by periodically switching the rf power of the AOMs that control the intensity of the corresponding laser beams. This modulation was done with a duty cycle of 50%. During the modulation, the intensity during the on-times was doubled so as to keep the time-averaged value constant. Precisely determining the residual intensity during the off-time is difficult, since photodetectors which are sensitive enough to detect leakage light are easily saturated during the on-time, causing slow response at the falling edge. By using photodiodes with logarithmically-scaled transimpedance amplification, we were able to determine a residual intensity of  $5 \text{ W/cm}^2$  for the 1064-nm beam, and  $0.1 \text{ W/cm}^2$  for the 1550-nm beam.

Similar to the experiments described in Chapter 4, the chopped-trap measurements were done with the previous version of the STIRAP setup, which produced molecules in the state  $|J=0, m_J=0, m_{I,\text{Na}}=-1/2, m_{I,\text{K}}=-4\rangle$  state, rather than in the absolute ground state  $|0, 0, 3/2, -4\rangle$ . Since the collisional behaviour can in principle depend on the hyperfine state, we then used two microwave  $\pi$ -pulses to transfer the molecules into the absolute ground state. This transfer is possible due to hyperfine-rotation coupling, which gives a predominantly  $|1, -1, 3/2, -4\rangle$  state some admixture of  $|1, 1, -1/2, -4\rangle$ . All dipole traps were turned off during the microwave pulses to avoid broadening of the transition by inhomogeneous light shifts. The transfer efficiency was about 86%. We then performed the lifetime measurements with ground-state molecules, and reversed the transfer before detection.

The simplest way to find an effect of light on molecule lifetime is to vary the chopping frequency  $f_{\text{chop}}$ . At frequencies where the off-time is much shorter than  $\tau_{\text{stick}}$ , no effect should be observed. At lower frequencies, there should be a noticeable difference between the cases with and without the kill-beam. The measurement was performed with chopping durations of 170 ms (for  $f_{\text{chop}} \leq 2.5 \text{ kHz}$ ) or 50 ms (for  $f_{\text{chop}} > 2.5 \text{ kHz}$ ). These times were chosen to be long enough that there is already significant molecule number decay after an equally long hold time without chopping to ensure that a change in complex lifetime actually shows up in the remaining molecule numbers. At these hold times, the remaining molecule numbers  $N_e$  without chopping were 45% and 70% of the initial values, respectively.

We then expected to observe an increase in the remaining molecule numbers, i.e.,  $N/N_e > 1$ , but did not see this in any experiment, see Figure 5.6(b). Furthermore, adding the kill-beam had no effect on the remaining molecule number at any chopping frequency. Changing the intensity  $I$  of the kill-beam at fixed chopping frequencies, as shown in Fig. 5.6(c), also had no effect. This was measured by chopping for 50 ms at  $f_{\text{chop}} = 2 \text{ kHz}$ , where a strong  $I$ -dependent effect is expected, and at  $f_{\text{chop}} = 25 \text{ kHz}$ , where the loss should be nearly independent of  $I$ .

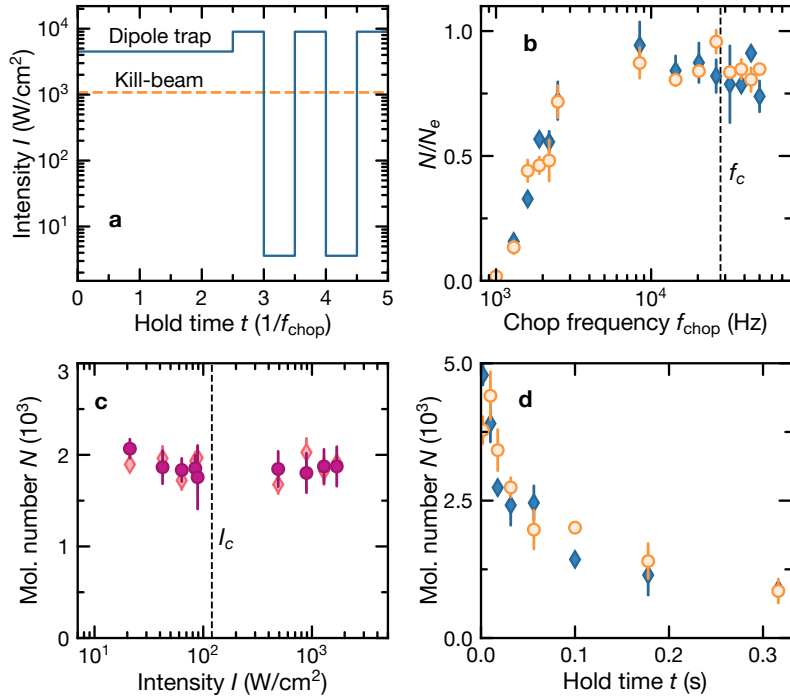


**Figure 5.6.:** Results from the chopped dipole trap. **(a)** Principle of the chopped trap. During the chopping duration (right half of the plot) the dipole-trap beam is periodically reduced to very low intensity. If the kill-beam is used, its intensity remains high all the time. **(b)** Normalised remaining molecule number versus chopping frequency with kill-beam at  $I = 1.08$  kW/cm $^2$  (orange circles) and without kill-beam (blue diamonds). The stronger loss at low trap frequencies is caused mostly by off-resonant parametric heating as the chopping frequency gets too close to the trap frequency. **(c)** Remaining molecule number versus kill-beam intensity at chopping frequencies of 2 kHz (bright diamonds) and 25 kHz (dark circles). The vertical dashed lines in (b) and (c) indicate the predicted critical values of  $f_c = 1/(2\tau_{\text{RRKM}})$  and  $I_{c,1064}$  from Reference [395]. **(d)** Comparison of loss of molecules in the excited hyperfine state  $|0,0,-1/2,-4\rangle$  with (orange) and without kill-beam (blue). Error bars represent the standard error of the mean of three to five repetitions.

Finally, we investigated if the result depends on the used hyperfine state by omitting the two-photon microwave transfer and directly using molecules in the state  $|0,0,-1/2,-4\rangle$ . As seen in Figure 5.6(d), the presence of the kill-beam again has no influence on the observed lifetime.

## 5.4. The box trap

Box-shaped, repulsive trapping potentials naturally solve the main problem of chopped traps when probing for light-induced complex loss. This is because they allow holding a sample in very low light intensity indefinitely without any modulation, which could cause confounding losses. Specifically, it is difficult to reduce the harmonic frequency of an attractive dipole trap below tens of Hertz, such that the longest dark times that can be realised in such a trap are limited to about 1 ms. This limitation is completely removed in a box trap. Box traps for atoms have become reasonable common in recent years, and are typically realised with high-power 532-nm laser beams [585–587].

However, doing the same thing for molecules is much more difficult, because it is hard to find any wavelength which simultaneously allows reaching strongly repulsive dipole forces and small off-resonant photon scattering rates. Rather, as one goes to short trapping wavelengths with a molecule, the forest of transitions almost never stops [578], making it very hard to find clearings where a sufficiently large blue detuning can be chosen. The only molecule other than NaK where this has been demonstrated is CaF, where a repulsive trap  $\sim 100$  GHz blue-detuned from a  $X^2\Sigma^+ \leftrightarrow B^2\Sigma^+$  transition was used to achieve improved laser cooling [588].

In our case, after we had investigated the  $X \leftrightarrow b$  transition and found the possibility to realise repulsive polarisabilities at wavelengths near 866 nm, we decided to use this technique to implement our box trap. Incidentally, using near-detuned trap light has another advantage for collision measurements: only a single rovibrational state is trapped, while atoms or molecules in other states fall out. This ensures that collisions with unassociated atoms or Feshbach molecules can not influence the results.

### 5.4.1. Optical setup

The trap is formed by light from a Ti:sapphire laser (MBR-110, Coherent) stabilised to a Fizeau-interferometer-based wavemeter (WS-7, HighFinesse). It runs at a frequency of 346.123 88 THz, which is 300 MHz, or approximately  $10^6$  linewidths, blue-detuned from the  $X \leftrightarrow b$  transition. The main challenge to then overcome is to shape this light into a hollow potential with lowest possible intensity on its inside. Importantly, the steeper the edges on the inside, the less time molecules spend penetrating into the walls. We create the box by splitting the laser light in two parts: the first part is formed into a hollow, cylinder-shaped “ring” beam which propagates along the vertical ( $z$ ) axis, the second part is turned into two strongly elliptical “cap” beams along the  $x$ - $y$ -plane, which close the cylinder on its top and bottom.

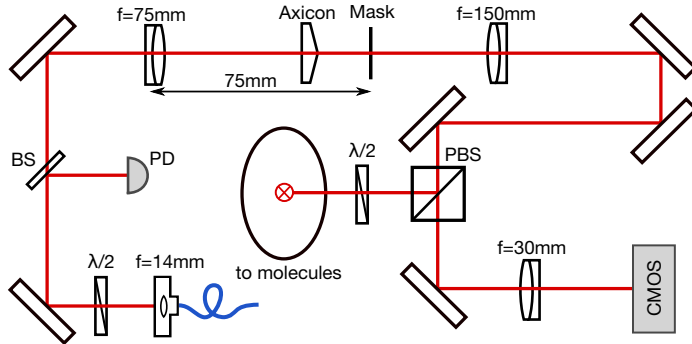


**Figure 5.7.:** Optical setup for generating the vertical ring beam. Light from an optical fibre with mode-field diameter  $5.3\text{ }\mu\text{m}$  is intensity-stabilised and shaped into a ring before being reflected downwards into a high-resolution objective (not shown) with effective focal length 30 mm. A clean ring shape is achieved by focusing the beam onto a circular mask target, with an axicon placed between the mask and the focusing lens. This is then imaged onto the molecule plane. A CMOS camera can be used to observe the beam shape to facilitate aligning the setup.

The ring beam is created in the optical setup shown in Figure 5.7, following the method described in Reference [589]. A more detailed description can be found in Renhao Tao's Master's thesis [590]. The laser beam is first fibre-coupled, intensity-stabilised and collimated before being focused by an achromatic lens of focal length 75 mm. Then follows the core of this setup, an axicon (AX251-B, Thorlabs). This cone-shaped optical element turns the Gaussian beam into a ring, which is focused onto a ring-shaped mask. This mask consists of a thin layer of chromium, coated onto a glass substrate by photolithography, and its purpose is to reduce the residual intensity in the centre of the ring beam. Finally, the ring is imaged onto the molecule plane with a telescope that shrinks its size by a factor 5, resulting in a radius of  $60\text{ }\mu\text{m}$  and a wall waist of  $7\text{ }\mu\text{m}$ . The last lens in this telescope is a high-resolution objective with a numerical aperture of 0.6, easily capable of projecting such edges. Shortly before reflection to the molecules, a part of the power can be split off and focused onto a camera to align and monitor the setup. An image of the ring beam taken by this camera is shown in Figure 5.8.

The cap beams propagate along the  $y$ -direction at a distance of  $75\text{ }\mu\text{m}$ . They are created by a combination of cylindrical lenses, which focus the beam along the  $z$ -direction, but collimate it along the  $x$ -direction (see Figure 5.9). Along the  $z$ -direction, each beam reaches a waist of  $8.5\text{ }\mu\text{m}$ . The difficult part here is to split this beam into two identically shaped ones at a very small distance. As this can not be accomplished in a stable and easy way with mirrors, we instead use a calcite beam displacer with a displacement of  $50\text{ }\mu\text{m}$  (PDC12005-AR800/400, Newlight Photonics). This optical element is made of strongly birefringent calcite and oriented in such a way that the vertically and horizontally polarised components of an input beam are split up and leave the displacer as two parallel, but displaced beams. As for the ring beam, a chromium mask located at the focal plane after the displacer blocks residual light between the two beams. Both beams are

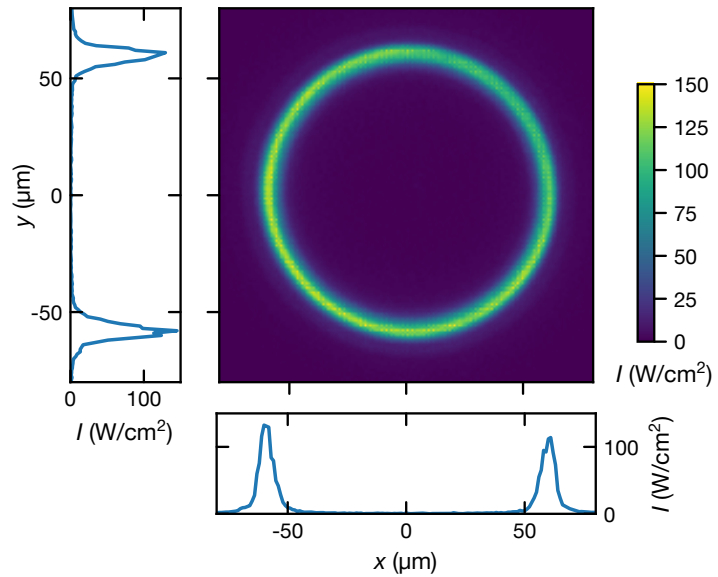


**Figure 5.8.:** Image of the ring beam. 2D cuts of the beam profile through the ring's centre are shown on the left and bottom. Note that, due to additional scattered light, which is not present at the molecule sample, and imaging noise, the residual intensity inside the trap is overestimated.

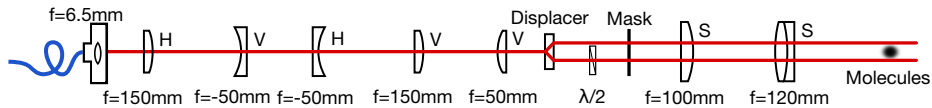


**Figure 5.9.:** Optical setup for generating the cap beams in the  $x$ - $y$ -plane. The input beam is simultaneously horizontally collimated and vertically focused onto a mask. Cylindrical lenses which affect the horizontal or vertical beam shape are labelled H or V, respectively. Spherical lenses are labelled S. A birefringent calcite beam displacer is used to split the beam into two components with orthogonal polarisation. Afterwards, a half-waveplate is used to make the two polarisations equal again. Another half-waveplate, used to control the power ratio of the two beams, and a photodiode used for intensity stabilisation, are not shown.

then imaged onto the molecules with another telescope with a magnification of 1.2.

In combination, the beams create a trap which is  $k_B \times 3\mu\text{K}$  deep at a detuning of 300 MHz. It is positioned such that molecules can be formed in the crossed dipole trap, then loaded into the box by adiabatically turning the crossed-trap power off.

### 5.4.2. Electric-field levitation

Due to the influence of gravity, molecules in the box at low temperatures spend most of their time close to the bottom cap beam, i.e., in a position where the light intensity is much larger than in the trap's centre. To avoid this, we can electrically levitate the molecules. This requires an electric background field to induce a finite lab-frame dipole moment, superimposed with a field gradient, which pulls the molecules upwards. This gradient is created by applying a voltage in a quadrupole configuration, i.e., opposite voltages of equal magnitude on the two diagonal electrode pairs. Using the electric-field calibration described previously, we can calculate the lab-frame dipole moment  $d$  and solve

$$mg = d \frac{dE}{dz}, \quad (5.9)$$

with the known gravitational acceleration  $g$  to calibrate the gradient resulting from a given voltage. For the calibration, we measured the point of optimal levitation, where the molecule lifetime is maximised, at multiple background fields (see Figure 5.10). As this calibration was done at background fields of up to 800 V/cm, it was necessary to use the full expression for  $d(E)$  rather than a quadratic approximation. When working with levitated molecules, the levitation gradient is turned on before the box-trap loading procedure, to prevent the molecules from falling.

### 5.4.3. Residual intensity in the box

Next, it is necessary to measure the level of background intensity experienced by the molecules *in situ*, to ensure that the trap is working as intended. We did this in two independent ways: first, we looked at the molecule lifetime and extracted one-body loss rates, which should be dominated by scattering of photons from the trap. The data for these measurements are shown in Figure 5.11. For the levitated box trap, this scattering rate was too small to observe it directly, so we compared measurements at detunings of 300 MHz and 600 MHz and used the known quadratic dependence of scattering rate on detuning to extract the intensity. From Equation (4.2) and the data given in Table 4.1, the photon-scattering rate at 300 MHz detuning is  $\gamma_{\text{sc}} = 0.17\text{ Hz}/(\text{W}/\text{cm}^2)$ . This resulted in a residual intensity of  $0.70(25)\text{ W}/\text{cm}^2$ . For the nonlevitated case, the intensity is much larger and could be measured directly. Here, we found  $6(2)\text{ W}/\text{cm}^2$ . Second, we performed microwave spectroscopy on the  $|0, 0, 3/2, -4\rangle \leftrightarrow |1, 1, 3/2, -4\rangle$  transition. The molecules are distributed over positions with different intensities in the trap, causing a deformation of the microwave resonance due to the light shift. In the absence of light, the

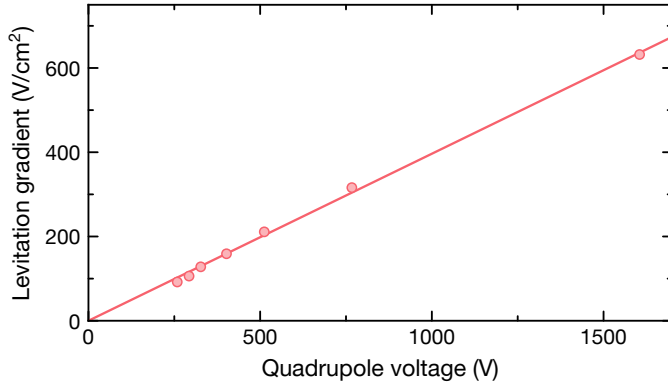


**Figure 5.10.:** Calibration of electric-field gradient along the vertical direction at the molecule position. We measured the point where the molecule lifetime is maximised in the box trap, which occurs when gravity is fully compensated by the levitation. Using the known gravitational acceleration and dipole moment, the linear fit yields a conversion factor of  $0.40\text{ cm}^{-2}$  between applied quadrupole voltage and measured gradient.

shape of the resulting feature after a microwave pulse of duration  $t$  is given by

$$N = N_0 \left( 1 - C \frac{\Omega_0^2}{\Omega_0^2 + \Delta^2} \sin^2 \left( \frac{t}{2} \sqrt{\Omega_0^2 + \Delta^2} \right) \right), \quad (5.10)$$

where  $N_0$  and  $N$  are the initial and remaining molecule number in the ground state, respectively,  $\Omega_0$  is the resonant Rabi frequency,  $\Delta$  is the microwave detuning, and  $C$  is the contrast. Taking the distortion of this shape by light shift into account requires a model of the trap shape. We obtain this from high-resolution images of the ring and cap beams. These can not directly be used to measure intensity in the centre, because of additional scattered light and the limited dynamic range of the camera, however we can subtract a constant offset from this shape and then numerically convolve the expected distribution of light shifts with Equation (5.10). Fitting the result of this convolution to data taken with the box-trap light at various powers, with  $N_0$ ,  $C$ , and the intensity offset as fit parameters, yields the mean intensity experienced by the molecules. In this fit,  $\Omega_0$  and  $t$  were fixed to the values which created a resonant  $\pi$ -pulse without the box-trap light. This resulted in residual intensities of  $0.63\text{ W/cm}^2$  for the levitated trap, and  $5.8\text{ W/cm}^2$  for the nonlevitated one, in agreement with the first method, see Figure 5.12. Finally, we determined upper bounds for the intensities at other wavelengths by measuring the size of all other laser beams aimed at the molecules, and their residual powers when switched off. A summary of all the measured residual intensities is given in Table 5.1.

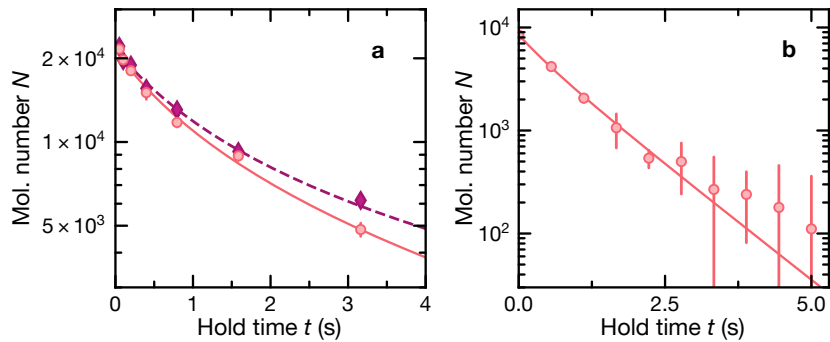


**Figure 5.11.:** Determination of one-body loss rate in the box trap. **(a)** Molecule loss in the levitated case, with box-trap detuning 300 MHz (600 MHz) shown as bright circles (dark diamonds). The solid and dashed lines show a simultaneous fit of Equation 5.12 to both data sets. **(b)** Nonlevitated case. The fit was used to determine  $\Gamma_{sc}$ . Error bars represent the standard error of the mean of three repetitions.

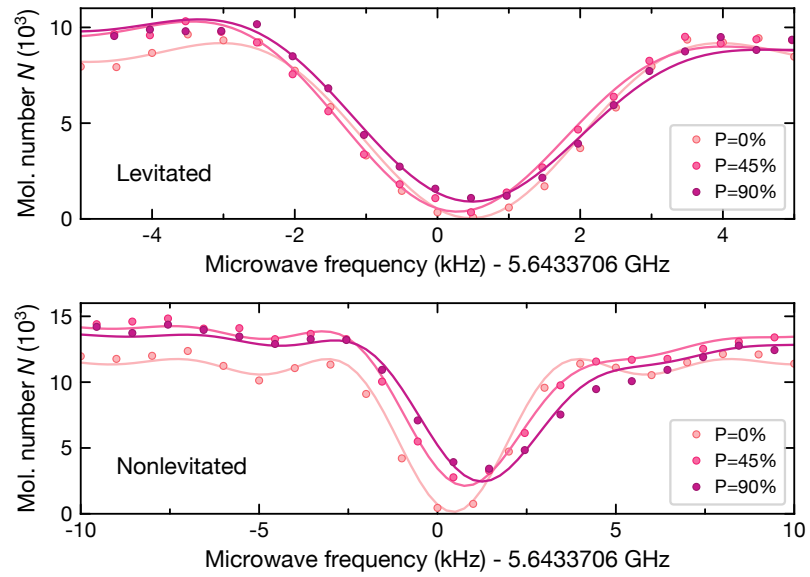


**Figure 5.12.:** Microwave spectroscopy for determination of the residual intensity in the box trap.  $P$  indicates the relative power setting of the box-trap light. The spectra were recorded after a 251- $\mu$ s microwave pulse, which corresponds to a  $\pi$ -pulse at zero detuning and  $P = 0$ . Each measurement was repeated at three different power setting for the box-trap light. For the reference measurements at zero power, the trap light was turned off quickly before the microwave pulse. The solid lines are fits to the convolution of Equation (5.10) with the numerically modelled light-shift distribution.

**Table 5.1.:** Residual intensity at the molecule position during the hold time in the box trap by wavelength.

Wavelength (nm)	Intensity (W/cm <sup>2</sup> )
1550	$25 \times 10^{-6}$
1064	$1.9 \times 10^{-3}$
866 (with levitation)	0.70(25)
866 (without levitation)	6(2)
805	$1.3 \times 10^{-3}$
767	$0.12 \times 10^{-3}$
589	$50 \times 10^{-6}$
567	$1.3 \times 10^{-3}$

## 5.5. Loss measurements in the box trap

### 5.5.1. Data analysis

As the density distribution in the box trap is nearly homogeneous, we observe no heating effect caused by colder molecules colliding more frequently, in contrast to the harmonic crossed dipole trap. Hence, Equation (5.2) simplifies to

$$n = \frac{N}{V}, \quad (5.11)$$

where  $V$  is the trap volume, which is numerically determined from the known intensity profile of the box. However, as the trap is operated with near-detuned light, the one-body loss due to photon scattering must be taken into account, such that the solution to Equation (5.3) becomes

$$N(t) = \frac{N_0 e^{-\Gamma_{sc} t}}{1 + \frac{N_0 \beta_{inel}}{V \Gamma_{sc}} (1 - e^{-\Gamma_{sc} t})}. \quad (5.12)$$

Quantifying the potential systematic error in the determination of loss coefficients in the box trap is difficult: because Feshbach molecules are not trapped, we can not distinguish between finite loading efficiency into the box trap, and STIRAP efficiency. The latter is likely to be slightly reduced, because the size of the STIRAP beam is comparable to the sample size in the box trap, such that molecules near the edge could be transferred with decreased efficiency. As we can not determine to what extent this is the case, we assume the STIRAP efficiency to be equal to the crossed-trap case and attribute all loss to the loading. This may cause a systematic error on the molecule number, and therefore also the density in the box. A further systematic effect is caused by the uncertainty of  $\Gamma_{sc}$ , which is much more important for the box trap. On the other hand, the systematic error caused by temperature is reduced compared to the crossed trap. In combination, we estimate that the systematic error of  $\beta_{inel}$  in the box trap is 50%, comparable to the

crossed trap.

Quantifying the lifetime and photon-scattering rate of sticky complexes from loss data requires a model of the relevant loss mechanisms. Here, we assume that two processes play a role in the two-body loss: photoexcitation, and complexes falling out of the trap, as they can neither be electrically levitated due to their small dipole moment [396], nor are they likely to experience a repulsive dipole force from the trap. The two processes are statistically independent, such that the probability of a sticky complex to survive and dissociate into diatomic molecules is

$$P_{\text{dis}} = (1 - P_t)(1 - P_{\text{sc}}). \quad (5.13)$$

Here,  $P_t$  is the probability to leave the trap and  $P_{\text{sc}}$  is the photon-scattering probability. The latter can be estimated by<sup>1</sup>

$$P_{\text{sc}} = \frac{\gamma_c I}{\gamma_c I + 1/\tau_{\text{stick}}}, \quad (5.14)$$

where  $\gamma_c$  denotes the complex photoexcitation rate, which was estimated to be  $\gamma_c = 452 \text{ Hz}/(\text{W}/\text{cm}^2)$  for 1064-nm light [395]. This rate may be somewhat higher at 866 nm, but the difference is likely small.

To estimate  $P_t$ , we assume that complexes are formed with a homogeneous initial density distribution  $\rho_i$  inside the box trap in thermal equilibrium with the molecules, and then undergo ballistic expansion in the gravitational field. For this estimate, we ignore the fact that complexes are more likely to be formed from hotter molecules, as the complex velocity is dominated by gravitational acceleration soon after their formation anyway. The ballistic expansion results in a known probability distribution for the position of a complex at time  $t$  after its formation. By setting  $t = \tau_{\text{stick}}$  and calculating the integral of this distribution over the box trap volume, we obtain  $P_t$  via

$$1 - P_t = \left( \int d\mathbf{x} \rho_i(\mathbf{x}) \right)^{-1} \times \int d\mathbf{x} \int d\mathbf{x}' \rho_i(\mathbf{x} - \mathbf{x}') \left( \frac{m}{2\pi k_B T \tau_{\text{stick}}^2} \right)^{3/2} \exp \left( -\frac{mr'^2}{2k_B T \tau_{\text{stick}}^2} \right) \Theta_{\text{box}}(\mathbf{x}). \quad (5.15)$$

Here,  $\Theta_{\text{box}}$  is a step function, which is 1 inside the box and 0 everywhere else. The integrand consists of three terms: the initial density distribution, a Maxwell-Boltzmann distribution which is convolved with the density to model the ballistic expansion, and the step function, which cuts off the part of the density distribution which has propagated outside the trap. The coordinate  $r'$  takes the gravitational acceleration into account:

$$r' = \sqrt{x'^2 + y'^2 + (z' + g\tau_{\text{stick}}^2/2)^2}. \quad (5.16)$$

In the case without levitation, instead of assuming  $\rho_i$  to be homogeneous, we use a thermal

---

<sup>1</sup>The corresponding equation (C1) in our paper [307] is incorrect.

distribution in the gravitational potential.

The bounds for  $\gamma_c$  and  $\tau_{\text{stick}}$  given in the following are then obtained as follows: we assume that all complexes are lost by photon-scattering, i.e.,  $P_{\text{sc}} = 1$ , in the case of very high kill-beam intensity, which gives us a reference loss rate. At low intensity, we model the expected reduction of loss rate as described above, modifying  $\tau_{\text{stick}}$  or  $\gamma_c$  until agreement with the lowest-intensity data point is achieved to within  $3\sigma$  uncertainty.

The effect of the recollisions described in Section 5.1.2 can easily be taken into account by multiplying the complex lifetime with the recollision factor if the collisions are purely  $p$ -wave, as is the case for identical fermions. In the case of an incoherent mixture of two hyperfine states of a fermionic molecule (see Section 5.5.4), it is more complicated because the complex lifetime depends on whether it was formed in an  $s$ -wave or a  $p$ -wave collision. We take both into account by using the MCQDT predictions for loss coefficients from Reference [234], and calculating the expected complex lifetime as a weighted average over  $s$ - and  $p$ -wave collisions with their respective complex lifetimes.

## 5.5.2. Light-intensity dependence of collisional loss

The most crucial measurement in the investigation of complex decay is the comparison of loss rate between the cases with and without kill-beam in the levitated box trap. As this is where the lowest intensity can be reached, this is the most sensitive way to probe the photoexcitation of sticky complexes. As shown in Figure 5.13, we observed no effect, with  $\beta_{\text{inel}}$  remaining constant down to intensities 200 times below the predicted  $I_c$ . Figure 5.14 shows the values of  $\gamma_c$  and  $\tau_{\text{stick}}$  which are excluded by these results.

In principle, the presence of external fields can lead to  $\tau_{\text{stick}}$  being increased by multiple orders of magnitude, because additional states can be sampled in the chaotic movement inside the sticky complex [395]. However, it is unclear how large electric or magnetic fields need to be for this effect to occur. To exclude a possible effect of the electric field on the complex lifetime, we measured the intensity-dependence of loss again without applying any voltage to the electrodes, see Figure 5.15. Because we found a precise determination of density to be impractical in this trap configuration, we did not extract  $\beta_{\text{inel}}$ , but rather the two-body loss rate  $L_2 = n\beta_{\text{inel}}$  from our data. In this case, complexes are formed mostly at the bottom of the trap, such that they fall out at a faster rate, making the measurement less sensitive. However, with the predicted  $\gamma_c$ , we can still conclude that  $\tau_{\text{stick}} > 1.4 \text{ ms}$  with  $3\sigma$  confidence.

We also probed the case of small magnetic fields, comparing the case of the crossed trap and boxed trap, as shown in Figure 5.16. Again, there was no difference between high- and low-intensity trapping within our measurement precision. We do observe increased loss at very low fields, both with and without the kill-beam, but this is likely unrelated to collisions. Rather, it indicates that the quantisation axis for the hyperfine states is no longer well-defined, leading to spin flips.

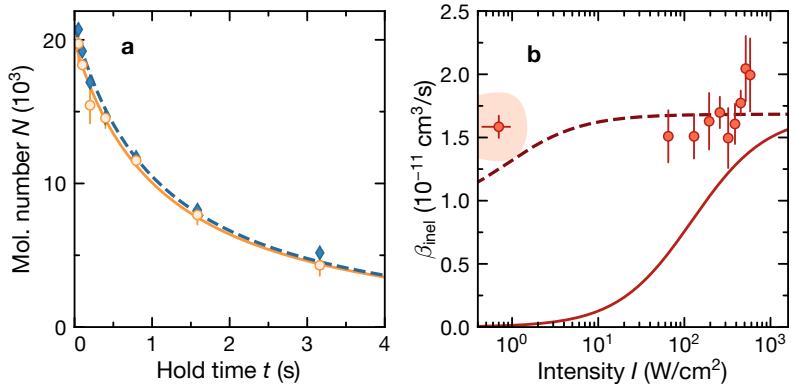


**Figure 5.13.:** Intensity-dependence of loss in the levitated box trap at an offset electric field of  $E = 411 \text{ V}/\text{cm}$ . **(a)** Comparison of loss with kill-beam off (blue diamonds) and on (orange circles) at an intensity of  $I = 276 \text{ W}/\text{cm}^2$ . The lines are fits of Equation (5.12) to determine  $\beta_{\text{inel}}$ . Error bars represent the standard error of the mean of three repetitions. **(b)** Dependence of  $\beta_{\text{inel}}$  on  $I$ . The solid line shows the expected value of  $\beta_{\text{inel}}$ , assuming  $\tau_{\text{stick}} = \tau_{\text{RRKM}}$ . The dashed line assumes  $\tau_{\text{stick}} = 2.6 \text{ ms}$ , which is the smallest value in agreement with the lowest-intensity point up to  $3\sigma$ . The shaded area indicates the  $3\sigma$  confidence region of the lowest-intensity data point. The error bars indicate the  $1\sigma$  uncertainty of the fit.

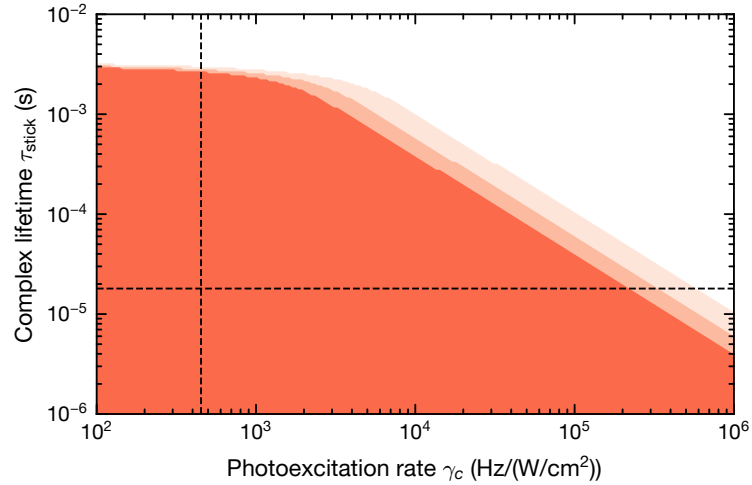


**Figure 5.14.:** Parameter space excluded by data taken in the levitated box. The shaded areas indicate regimes that are excluded with  $1\sigma$ ,  $2\sigma$ , and  $3\sigma$  confidence, with darker color corresponding to higher confidence. The predictions for  $\gamma_c$  and  $\tau_{\text{stick}}$  from Reference [395] are shown as dashed lines. Our method becomes insensitive at complex lifetimes above 3 ms because here, all complexes fall out of the trap regardless of photoexcitation probability.

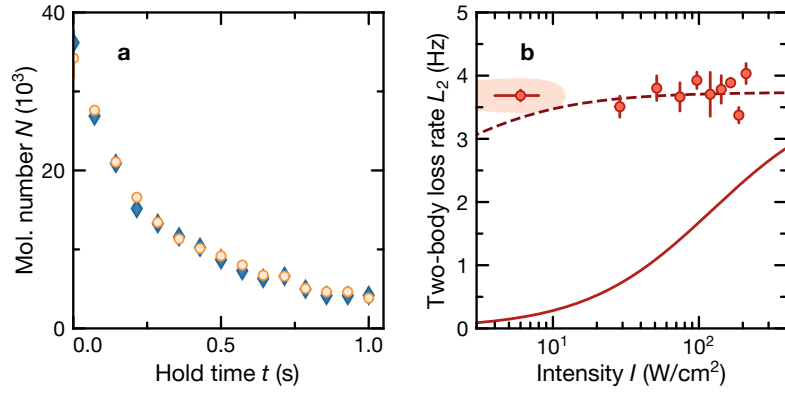


**Figure 5.15.:** Intensity-dependence of loss in the box trap without any electric field. (a) Comparison of loss with kill-beam off (blue diamonds) and on (orange circles) at an intensity of  $I = 204 \text{ W}/\text{cm}^2$ . Error bars represent the standard error of the mean of three repetitions. (b) Two-body loss rate  $L_2$  for different values of  $I$ . The solid (dashed) line indicates the expected loss rate assuming a  $\tau_{\text{stick}}$  of  $18 \mu\text{s}$  ( $1.4 \text{ ms}$ ). The shaded area indicates the  $3\sigma$  confidence region of the lowest-intensity data point.

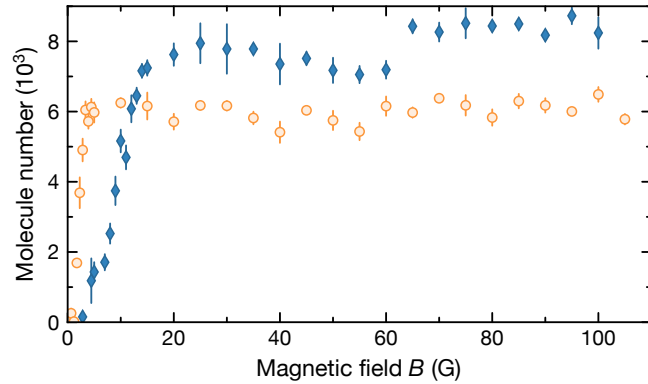


**Figure 5.16.:** Magnetic-field dependence of loss in the crossed trap (orange circles) and the box trap with levitation and without kill-beam (blue diamonds). Remaining molecule numbers were measured after a hold time of 150 ms in the crossed trap, or 352 ms in the box trap.

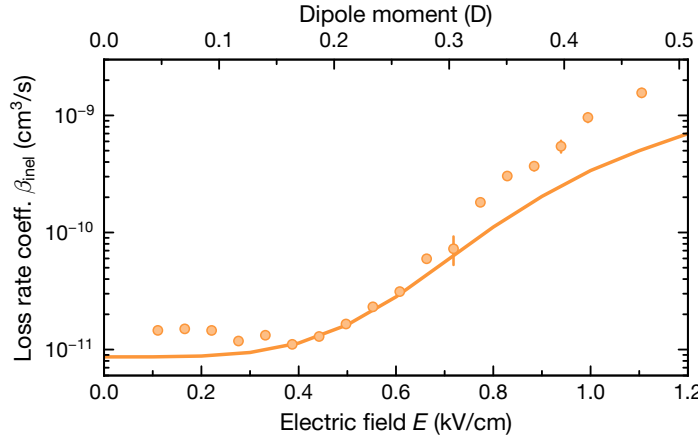


**Figure 5.17.:** Loss rate coefficient  $\beta_{\text{inel}}$  depending on external electric field  $E$  in the box trap with electric levitation at  $T = 140\text{nK}$ . The solid line is a parameter-free quantum close-coupling calculation by Goulven Quéméner. Error bars represent the  $1\sigma$  uncertainty of the fit.

### 5.5.3. Dipolar collisions

To exclude the possibility that resonances caused by nonuniversal scattering were hidden by photoinduced complex loss in the crossed trap, we repeated the measurements of the dependence of  $\beta_{\text{inel}}$  on the dc electric field in the box trap with levitation (see Figure 5.17). Like in the crossed trap, the loss rates were consistent with near-universal loss over the entire investigated range of electric fields. Note that there is a significant Stark shift of the  $X \leftrightarrow b$  transition, causing the detuning of the trap to change. At very high electric fields, we observed that this increased the photon-scattering rate, though at  $E < 1.2\text{kV/cm}$ , we did not see any change to  $\beta_{\text{inel}}$  when we doubled the box-trap detuning to 600 MHz. Data above this field were disregarded.

### 5.5.4. Enhanced sticking time due to p-wave barrier

All data shown up to this point were taken with samples of indistinguishable fermions, such that a strong effect of recollisions is to be expected due to the dominant  $p$ -wave character of the collisions. Indeed, when taking the estimated increase of the sticking time by a factor 270 into account, the theory is consistent with our results. If this really was the explanation for our surprising observations, the complex lifetime should be strongly reduced for  $s$ -wave collisions. By creating an incoherent mixture of molecules of the two lowest hyperfine states,  $|0, 0, 3/2, -4\rangle$  and  $|0, 0, 3/2, -3\rangle$ , we created a scenario where the fermions are no longer indistinguishable, and  $s$ -wave collisions become dominant, to test this hypothesis. In addition,  $\tau_{\text{RRKM}}$  is three times smaller for the  $s$ -wave case because of the reduced multiplicity of the total angular momentum in the collision.

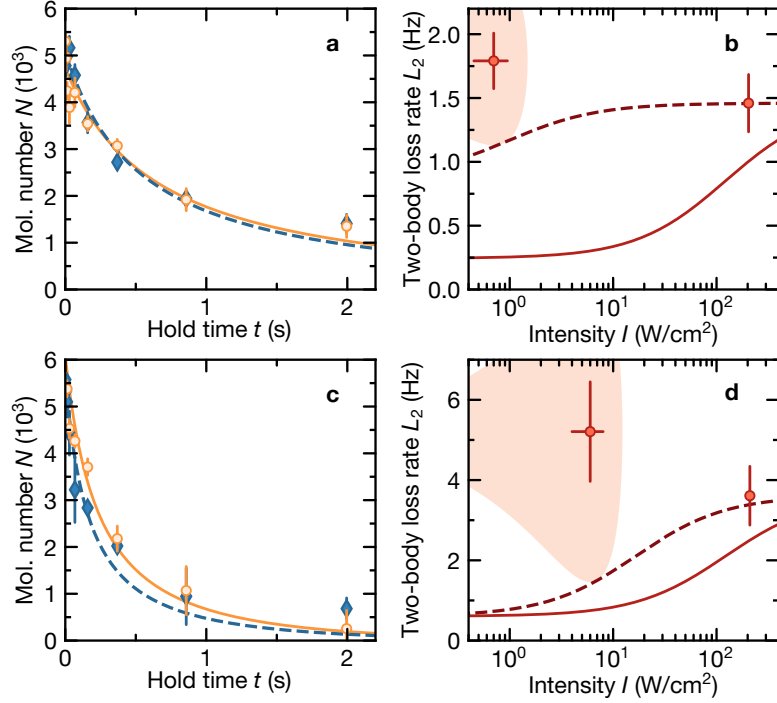


**Figure 5.18.:** Loss of an incoherent mixture of the states  $|0, 0, 3/2, -4\rangle$  and  $|0, 0, 3/2, -3\rangle$  in the box trap. **(a)** Loss curves with kill-beam at an intensity  $I = 204 \text{ W/cm}^2$  (orange circles) and without kill-beam (blue diamonds) in the box trap with electric levitation. The solid (dashed) line is a fit of Equation (5.12) to the data with kill-beam on (off). **(b)** Intensity dependence of two-body loss rate. The solid line shows the expected value, assuming  $\tau_{\text{stick}} = \tau_{\text{RRKM}}$ . The dashed line assumes  $\tau_{\text{stick}} = 2.3 \text{ ms}$ , which is the smallest value in agreement with the data up to  $3\sigma$ . **(c-d)** Like (a-b), but at zero electric field without levitation. Here, the smallest value of  $\tau_{\text{stick}}$  in  $3\sigma$ -agreement with the data is  $133 \mu\text{s}$ . In (a) and (c), error bars represent the standard error of the mean of three repetitions. In (b) and (d), they represent the standard deviation of the fit.

Starting from a pure ground-state sample, we made an incoherent mixture with two microwave pulses. The first pulse created a coherent superposition  $|0,0,3/2,-4\rangle + |1,1,3/2,-4\rangle$ , which is held until the dipole trap light has led to complete decoherence. The second pulse then transferred all population from  $|1,1,3/2,-4\rangle$  to  $|0,0,3/2,-3\rangle$ . In order to minimise residual population in the rotationally excited state, all dipole traps were switched off during the pulse duration. Figure 5.18 shows the comparison between high- and low-intensity trapping of the mixture, both with levitation and at zero electric field. As expected, the presence of *s*-wave collisions significantly increased the loss rate, but there was still no observable dependence on light intensity. Even when taking recollisions into account, the smallest values of  $\tau_{\text{stick}}$  which are consistent with our observations within  $3\sigma$ , are 2.3 ms for the levitated case and 133  $\mu$ s for the zero-field case. This means that, even though recollisions are probably one important piece to this puzzle, they are insufficient to explain the observations on their own.

## 5.6. Discussion

A natural first reaction to the results shown in this chapter is “This can’t be right.” After the refinement of the RRKM predictions [395, 396] and their experimental confirmation with both chemically stable and reactive molecules [401, 404], there was no good reason to believe the predictions could be off by orders of magnitude. Indeed, we were very doubtful about our own results at first, double-checking for possible loopholes again and again.

Finally, we decided to contact our colleagues in Hannover and Hong Kong and asked for their opinion. Not only had they all independently found comparable results with their molecular species ( $^{23}\text{Na}^{39}\text{K}$  and  $^{23}\text{Na}^{87}\text{Rb}$ ), they also couldn’t believe them and had all decided not to publish. Having cross-checked each other’s data, we decided to cooperate and submit our papers simultaneously [307, 405].

Since then, a number of further experiments have been performed, with highly interesting results. For example, it was found that the three-body complex formed in collisions between  $^{40}\text{K}^{87}\text{Rb}$  and  $^{87}\text{Rb}$  atoms lives five orders of magnitude longer than expected from RRKM [591]. The Hannover team observed a strong dependence on the initial hyperfine state in collisions between  $^{23}\text{Na}^{39}\text{K}$  and  $^{39}\text{K}$  atoms [432]. In a follow-up study to their original measurements with  $^{87}\text{Rb}^{133}\text{Cs}$ , the Durham team found a similarly hyperfine-state-dependent loss rate in molecule-molecule collisions [402].

With such strong evidence that the nuclear spin plays an important role, a reasonable idea is to choose molecules in the hyperfine ground state which is simultaneously spin-stretched, as is the case for  $^{87}\text{Rb}^{133}\text{Cs}$ . This is impossible for  $^{40}\text{K}^{87}\text{Rb}$  and  $^{23}\text{Na}^{40}\text{K}$ , where the ground state is not stretched. However, the results obtained with  $^{23}\text{Na}^{87}\text{Rb}$ , where universal loss was also found in the stretched hyperfine ground state, contradict this interpretation. In addition, the hyperfine state of  $^{40}\text{K}^{87}\text{Rb}$  is conserved in collisions, [592, 593], which should exclude any impact on sticking times, though this may be because the reactive collisions in this system last too short for hyperfine-state changes to occur.

Multiple proposals have been brought forth to explain the discrepancies between theory

and observations [406–410, 412, 413]. They investigate multiple possible reasons why the density of states in the sticky complex ( $\rho_s$  in Equation 5.1) could be increased, for example because of nuclear-spin involvement. There have also been suggestions that the statistical approach used in the RRKM theory may not be valid in certain cases and should be replaced with a different method [411].

With the crucial impact that the lack of understanding of ultracold collisions has had on the field for the last decade, it is undoubtedly necessary to experimentally test these new hypotheses, however this may not be easy. Probing even longer complex lifetimes with box traps is not likely to work, because at lifetimes above a few milliseconds, the complexes would have to be trapped so as to not just fly away. In principle, it would be possible to increase the box trap's size, but this seems rather impractical. Therefore, it appears likely that the only way to conclusively answer this question will be to construct a setup where the decay products themselves can be detected. Though this has been demonstrated for reactive molecules [403, 404, 594], to our knowledge there are no active attempts to do the same for chemically stable molecules yet. Another possible avenue is to further investigate molecule-atom collisions. While this topic has only been studied for a fairly short time, recent advances are quite impressive, and especially with the discovery of atom-molecule Feshbach resonances and sympathetic cooling [433–437, 595], this direction is certain to remain interesting.



*Experience keeps a dear school,  
yet fools will learn in no other.*

—Benjamin Franklin

## 6. Microwave shielding

Having, for the moment, exhausted our possibilities for understanding close-range collisions between molecules, we next focused our efforts on preventing them. We did this using the technique of *microwave shielding*, where a repulsive potential between colliding molecules is engineered with a high-power microwave field. This chapter describes our implementation of this method and the subsequent realisation of microwave-assisted evaporative cooling. It is based on the publication [596].

### 6.1. Motivation

Suppression of lossy collisions can be achieved in many ways, for example molecules can be confined in deep optical lattices as shown in References[295, 308, 309]. If they can not move through the lattice, collisions are strongly suppressed. However, this also stops interesting dynamics and makes it much harder to study things like Fermi–Hubbard models, which require tunnelling. It also hinders evaporative cooling, since high-energy molecules can not easily be removed from a lattice.

Therefore, a more interesting choice is to modify the interaction potential with external ac or dc fields. If this makes interaction sufficiently repulsive in all directions that molecules can not enter the lossy short-range potential, the problem is solved. There are multiple proposals on how to do this. The conceptually simplest is to apply a strong dc electric field and confine the molecules on a plane or tube orthogonal to the field direction, such that no attractive head-to-tail interactions can occur [206, 276–280]. This technique can be generalised to 3D systems of molecules with rotational angular momentum  $R = 1$  by choosing a specific, typically very large, electric-field value where a crossover between rotational states occurs [415–418]. This is known as *resonant shielding*. Both methods have recently been demonstrated with  $^{40}\text{K}^{87}\text{Rb}$  [414, 419, 420], but are not likely to work with the limitations of our experiment, as we can not reach sufficiently large and stable electric fields. For example, the resonant-shielding field for NaK is around 7 kV/cm [418], more than four times our current limit. In addition, NaK is expected to be harder to stabilise in this way due to its lower mass [277].

The other possibility is to prevent collisions using ac electromagnetic fields, either in the optical [427, 428] or microwave frequency ranges. This is analogous to shielding methods pioneered in the 1990s for atoms [63], and can be visualised in the following

way: ground-state molecules are illuminated with a light field which is blue-detuned from a transition to a rotationally excited state. In the case of optical shielding, a narrow transition should be chosen, for example to  $|b^3\Pi_0, R' = 1\rangle$ , in order to reduce photon scattering. For microwave shielding, it is the purely rotational  $R = 0 \leftrightarrow R' = 1$ . Because the interaction potential between the two levels with different  $R$  contains a repulsive branch, molecules approaching each other get closer to being resonant with the shielding light, which in the dressed-state picture means admixing more of the repulsive state.

Though optical shielding is simple to implement in principle, the problem is that it requires a fairly high intensity of near-detuned light, such that the detuning and Rabi frequency are on the same order of magnitude, around 100 MHz [427, 428]. This means that the molecules gain a significant admixture of the electronically excited state which can undergo spontaneous emission, leading to one-body loss. With a linewidth of 300 Hz for the  $|b^3\Pi_0, R' = 1\rangle$  state of  $^{23}\text{Na}^{40}\text{K}$ , a loss rate of 10 Hz or more should be expected, leading to inefficient evaporation. In contrast, the lifetime of purely rotationally excited levels against spontaneous emission is almost infinite, making microwave shielding the more promising option for our system.

## 6.2. Operating principle

Microwave shielding has been theoretically described in the publications [423–426, 597], and was recently experimentally demonstrated with pairs of  $^{40}\text{Ca}^{19}\text{F}$  molecules in optical tweezers [430]. It functions in the same basic way as optical shielding, however due to the differences between laser and microwave technology, the challenges in experimentally implementing it are very different. Molecules are initially in the absolute ground state  $|G\rangle = |R = 0, m_R = 0, \delta N_p\rangle = 0$ , where  $\delta N_p$  is the change of photon number in the microwave field. The presence of the circularly polarised microwave field then creates dressed states with some admixture of a rotationally excited state, for example  $|E\rangle = |1, -1, -1\rangle$ , where one  $\sigma^-$ -polarised photon has been absorbed by the molecule. In the limit of isolated molecules, the composition of the dressed states only depends on the Rabi frequency and the microwave detuning:

$$|+\rangle = \sin \phi |G\rangle + \cos \phi |E\rangle, \quad (6.1)$$

$$|-\rangle = \cos \phi |G\rangle - \sin \phi |E\rangle, \quad (6.2)$$

$$\tan 2\phi = -\frac{\Omega}{\Delta}. \quad (6.3)$$

All states with  $R = 1, m_R \neq -1$  are not coupled due to the choice of microwave polarisation, and are labelled as spectator states  $|0\rangle$ . Because the dressed states contain components of rotational states with opposite parity, the molecules in  $|+\rangle$  then experience dipole-dipole interactions with a time-averaged long-range potential

$$V = -\frac{d^2}{4\pi\epsilon_0} \frac{1-3\cos^2\theta}{12(1+(\Delta/\Omega)^2)r^3}, \quad (6.4)$$

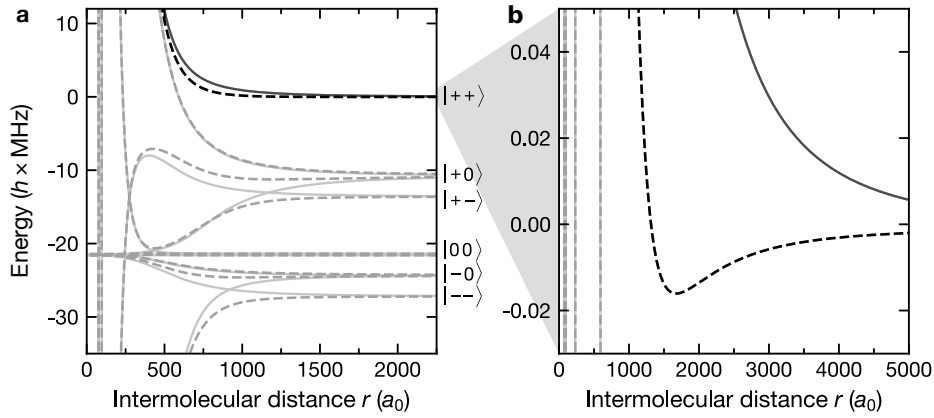


**Figure 6.1.:** Interaction potentials between the different dressed states of two NaK molecules. The dashed lines indicate collisions orthogonal to the microwave wavevector, the solid lines indicate parallel collisions. The  $p$ -wave barrier is not shown. **(a)** Overview of all combinations of dressed and spectator states. **(b)** Close-up of the repulsive  $|++\rangle$  channel where shielding is realised.

where  $\theta$  is the angle between the microwave wavevector and the intermolecular axis. Classically, this corresponds to the rotating molecules aligning themselves with the electric component of the microwave field at all times. In the limit of large Rabi frequencies, this rotation results in an effective lab-frame dipole moment of  $d = d_0/\sqrt{12}$ , corresponding to 0.785 D for NaK. Note that the interaction switches sign compared to the case of a static dipole moment, becoming repulsive along the microwave wavevector and attractive along the other two directions. At close range, the dynamics of the problem are changed by the mutual influence of the molecules (see Figure 6.1). In a collision, molecules in  $|+\rangle$  enter a strongly repulsive potential independently of their relative orientation. Hence, microwave shielding allows achieving strong dipolar interaction without a dc electric field, and suppressing lossy collisions at the same time.

### 6.3. Implementation with NaK

As the excited state for dressing, we choose  $|E\rangle = |1, -1, -1\rangle$ , which is coupled with  $|G\rangle$  via a  $\sigma^-$ -polarised microwave field. At a magnetic field  $B = 72.35$  G, which is typically used in the experiment, the resonance frequency of this transition is 5.643 413 7 GHz. As shown in Figure 6.2, the spectrum near this transition is complicated, but at sufficiently large power and detuning, it is nevertheless possible to create an almost pure  $|+\rangle$  state. Using  $\sigma^+$  polarisation and coupling to  $|1, 1, -1\rangle$  would also have worked, though we did not investigate this in detail.

To facilitate effective shielding, the microwave field must fulfil quite stringent requirements. First, the intensity must be high enough to reach Rabi frequencies of  $2\pi \times 10$  MHz

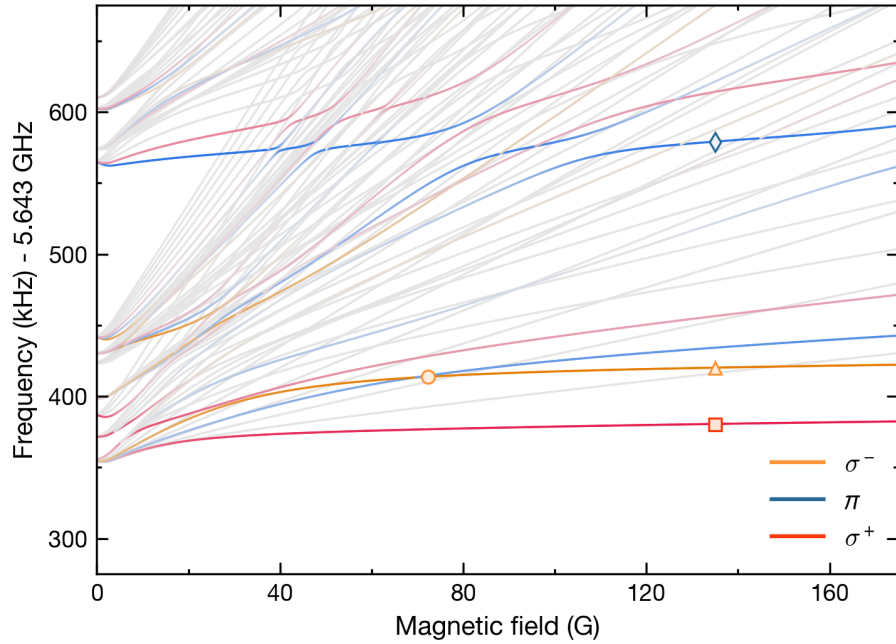


**Figure 6.2.:** Spectrum of microwave transitions depending on magnetic field. Each line corresponds to an excited state in the  $J = 1$  manifold, with orange indicating  $\sigma^-$  transitions, blue indicating  $\pi$  transitions, and red indicating  $\sigma^+$  transitions. Colour saturation is proportional to the transition dipole moment, meaning that grey states are unreachable with dipole transitions from the absolute ground state. The circle denotes the transition where microwave shielding is done. The square, triangle and diamond denote the transitions used to characterise the microwave polarisation. The data shown was calculated with the code described in Reference [598].

or more. This is relatively simple, as high-power, low-noise microwave amplifiers are readily available at frequencies around 5.6 GHz. Using a single 10-W amplifier (KU PA 510590, Kuhne), we were able to achieve  $\Omega = 2\pi \times 11$  MHz. Second, it is important to reach an extremely low level of phase noise, because noise at offset frequencies close to the Rabi frequency causes molecules to be transferred into the  $|-\rangle$  state where they are effectively lost. According to the supplemental material of Anderegg *et al.*'s paper [430], this process happens exponentially with a time constant

$$\tau = \frac{2}{\pi^2 \Omega^2 S_\phi(\Omega)}, \quad (6.5)$$

where  $S_\phi(\Omega)$  is the phase noise at an offset equal to the Rabi frequency. This means that, to realise lifetimes on the order of a second, the phase-noise level needs to be  $-164$  dBc/Hz at an offset of 10 MHz from the 5.6-GHz carrier, an extremely low level that is hard to reach even with the most advanced available technology.

The typical way to generate ultralow-noise microwaves is by locking an output oscillator to a reference-frequency source using a phase-locked loop (PLL) with a bandwidth of about 100 kHz. This means that the low-frequency noise below 100 kHz is determined mostly by the stability of the reference, while the high-frequency noise is given by the intrinsic noise of the output oscillator. Many microwave sources offer the option to use an external signal, for example from an ultrastable hydrogen maser, to replace the internal reference-frequency source and reduce low-frequency noise, however this is not useful in our case. Adding to this problem, ultralow-noise microwave oscillators are commonly used in military applications, and the best ones are difficult to obtain. For example, sapphire-loaded crystal oscillators can easily reach the desired noise level [599], but we are not aware of any suppliers on the civilian market.

To our knowledge, the best practically usable sources are the PSG series (Keysight) and the SMA-100B (Rohde&Schwarz), which use yttrium-iron-garnet (YIG) output oscillators. For the Keysight signal generators, there are multiple options available to reduce phase noise, but since they all improve the stability of the reference-frequency source, they are not expected to be helpful at offsets beyond the PLL bandwidth. On the other hand, the B-711 option available for the SMA-100B contains an upgrade of the output oscillator and indeed improves the phase-noise performance in the relevant frequency range. At a carrier frequency of 6 GHz and 10 MHz offset, these signal generators are specified to reach a noise level of  $-158$  to  $-160$  dBc/Hz. In our experiments, we initially used a Rohde&Schwarz SMF-100A (specified at  $-155$  dBc/Hz), which we later replaced with a Keysight E8267D ( $-158$  dBc/Hz). This led to an improvement in one-body lifetime by a factor two, in qualitative agreement with Equation 6.5. All the data shown here were taken with the E8267D.

Finally, a pure circular polarisation of the microwave field is important to avoid unwanted coupling with other excited states with  $m_R \neq -1$  [425, 426]. This can be quantified with the ellipticity angle

$$\xi = \arctan \left( \frac{E_{\sigma^+}}{E_{\sigma^-}} \right). \quad (6.6)$$

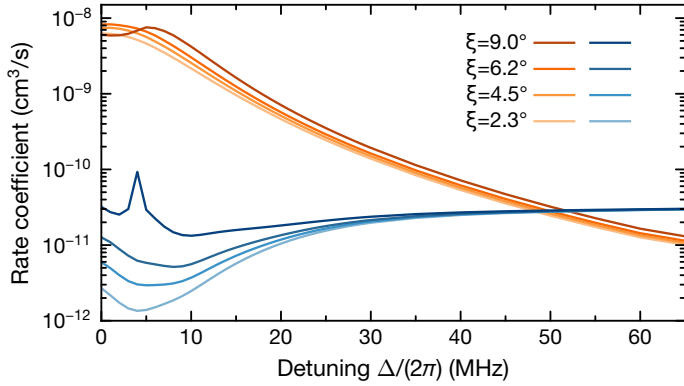


**Figure 6.3.:** Predicted elastic (orange) and inelastic (blue) collision rate coefficients at multiple values of the polarisation ellipticity angle  $\xi$ . These curves are the result of close-coupling simulations performed by Tijs Karman.

As long as the relevant coordinate system is given by the dc magnetic-field direction, there can also be  $\pi$ -components, but at sufficiently high microwave powers, the quantisation axis is given by the microwave wavevector. In this coordinate system, no  $\pi$ -components exist. As Figure 6.3 shows, there is a strong detrimental effect of polarisation impurity, so a small  $\xi$  is important. This requirement turned out to be the hardest to meet, as we found the polarisation to be sensitive to even small movements of any conductive objects near the molecule position. We initially attempted to compensate the effects of the environment by using a phased-array antenna consisting of four helices as described in Reference[430]. However tuning the phase relation between the four sub-antennas was an extremely tedious process and ultimately turned out to be ineffective, as the  $\sigma^+$  components could not be reduced enough. Instead, we settled on using a single helix antenna with five windings which was positioned such that its top end was 2.2 cm below the molecules, near the glass-cell wall. The polarisation purity was then tuned by carefully moving a cylindrical piece of metal foil which surrounds the antenna.

The setup for microwave generation is shown in Figure 6.4. It allows fast ramps of the output power via a voltage-controlled attenuator (VCA; D1954, General Microwave), which provides up to 65 dB of attenuation at an insertion loss of less than 3 dB. Since noise on the input voltage of the VCA causes unwanted amplitude modulation, this voltage is provided by an arbitrary waveform generator (33522A, Keysight), which is situated next to the VCA, reducing ground loops. In addition, there is a 100-kHz low-pass filter at the VCA input, further reducing high-frequency noise.

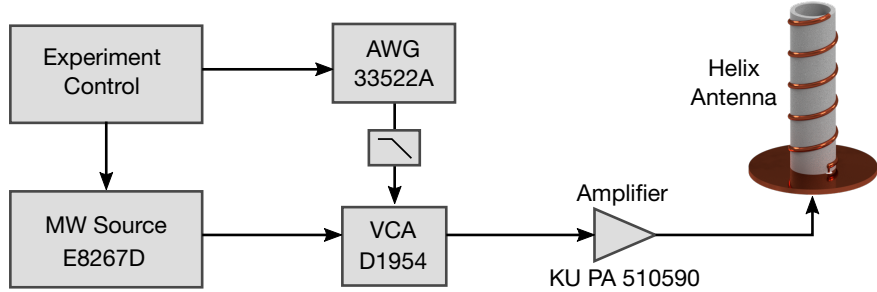


**Figure 6.4.:** Microwave-generation setup. The output signal from the microwave source is sent through a voltage-controlled attenuator (VCA) in order to create fast power ramps for the preparation of the dressed state. The 10-W amplifier has a gain of 35 dB and is run slightly below its saturation power. To avoid noise on the control channel of the VCA, its input signal comes directly from an arbitrary waveform generator (AWG) situated close by.

## 6.4. Shielding effectiveness

### 6.4.1. Data analysis

The great advantage of microwave shielding is that it not only prevents inelastic collisions; due to the effective dipole moment induced by the microwave field, it also creates elastic long-range collisions which allow thermalisation. Understanding the data thus requires a model that contains both elastic and inelastic collisions. This can be achieved with a generalised version of Equation (5.3), which is given by [233, 419]

$$\frac{dN}{dt} = \left( -K \frac{2T_h + T_v}{3} n - \Gamma_{sc} \right) N, \quad (6.7)$$

$$\frac{dT_h}{dt} = \frac{1}{12} K T_v T_h n + \frac{\Gamma_{th}}{3} (T_v - T_h), \quad (6.8)$$

$$\frac{dT_v}{dt} = \frac{1}{12} K (2T_h - T_v) T_v n - 2 \frac{\Gamma_{th}}{3} (T_v - T_h), \quad (6.9)$$

with the mean density defined, analogously to Equation (5.2), as

$$n = N \left( \frac{m \bar{\omega}^2}{4\pi k_B (T_h^2 T_v)^{1/3}} \right)^{3/2}. \quad (6.10)$$

In these expressions,  $T_v$  and  $T_h$  are the temperatures in the vertical and horizontal directions, respectively. Due to the cylindrical symmetry of the problem, it is reasonable to assume that temperatures in the two horizontal directions are equal. The rates of change for the two temperatures consist of two terms: the first corresponds to heating which is caused by a larger loss rate for the coldest molecules, which are situated in the highest-

density part of the trap. The second is a thermalisation term which leads to the temperatures in all directions equilibrating. The factor  $1/12$  in the heating rates comes from the fermionic quantum statistics. The rethermalisation rate  $\Gamma_{\text{th}}$  can be calculated from the elastic scattering cross section  $\sigma_{\text{el}}$  via

$$\Gamma_{\text{th}} = \frac{n\sigma_{\text{el}}v_{\text{col}}}{N_{\text{col}}}. \quad (6.11)$$

This expression depends on the mean collision velocity  $v_{\text{col}}$  and the number of collisions necessary for rethermalisation  $N_{\text{col}}$ . The former is given by

$$v_{\text{col}} = \sqrt{\frac{16k_B(2T_h + T_v)}{3\pi m}}. \quad (6.12)$$

The latter is dependent on the angle  $\theta$  between the microwave wavevector and the  $z$ -axis, and has been calculated to be [600]

$$N_{\text{col}} = \frac{112}{45 + 4\cos(2\theta) - 17\cos(4\theta)}. \quad (6.13)$$

From the experimental data, we obtain the time dependence of  $N$ ,  $T_v$ , and  $T_h$ , and fit a numerical solution of the equation system (6.7–6.9) to that. To keep the number of fit parameters at an acceptable level, the one-body loss rate  $\Gamma_{\text{sc}}$  is always fixed to 1.7 Hz, which was independently measured in a low-density sample. From this, the elastic and inelastic collision-rate coefficients can be calculated via

$$\beta_{\text{el}} = \sigma_{\text{el}}v_{\text{col}}, \quad (6.14)$$

$$\beta_{\text{inel}} = K \frac{2T_h + T_v}{3}. \quad (6.15)$$

## 6.4.2. Calibration measurements

We first characterised the microwave field by measuring Rabi frequencies of the transitions marked in Figure 6.2. For measuring polarisation purity, we chose three reasonably isolated transitions, one each with  $\sigma^-$ ,  $\pi$ , and  $\sigma^+$  character, and deduced the intensity in the respective component of the field from the observed Rabi frequency and the calculated transition dipole moment.

This was done at  $B = 135$  G, a compromise between the limits of our magnetic-field control system and isolating the different transitions as much as possible. At this field, the transitions are still much too close to each other to obtain clean Rabi oscillations at full microwave power, since off-resonant couplings would cause too much disturbance. We therefore reduced the power by about 60 dB, reaching  $\Omega \approx 2\pi \times 3$  kHz. According to the calculations obtained with the code described in [598], the transition dipole moments of the  $\sigma^-$ ,  $\pi$ , and  $\sigma^+$  transitions are  $0.989 d_0/\sqrt{3}$ ,  $0.789 d_0/\sqrt{3}$ , and  $0.875 d_0/\sqrt{3}$ , respectively. From the data, we then deduced the amplitude ratios  $E_{\sigma^+}/E_{\sigma^-} = 0.169(8)$  and  $E_{\pi}/E_{\sigma^-} = 0.169(8)$ .

With the weak microwave field in these measurements, the coordinate frame is given by the dc magnetic field, not the microwave wavevector, as evidenced by the finite  $\pi$  component. Indeed, it follows from this data that the microwave wavevector is tilted by  $20^\circ$  to  $30^\circ$  with respect to the dc field. Accounting for this, the possible values for the ellipticity angle  $\xi$  in the microwave coordinate frame are then between  $11.5^\circ$  and  $5.9^\circ$ . The presence of a large tilt is surprising, as one should expect the vertically aligned helix antenna to create a field which is close to parallel to the antenna direction. However we operate in the near-field regime and with many potentially disturbing conductive parts around the molecules, which may explain this effect. In the following, we assume  $N_{\text{col}} = 2.05$ , which is the predicted value at  $\theta = 29^\circ$ .

Next, we measured the reachable Rabi frequency at full microwave power for the shielding transition, i.e., the  $\sigma^-$  transition located at  $5.643\,413\,7\text{ GHz}$  for  $B = 72.35\text{ G}$ . As this can not be measured on resonance, we used multiple different detunings between  $2\pi \times 2\text{ MHz}$  and  $2\pi \times 25\text{ MHz}$ , and deduced a resonant Rabi frequency  $\Omega = 2\pi \times 11\text{ MHz}$  from the data. To create sufficiently short rectangle pulses of the microwave power for these measurements, we added a fast microwave switch (ZASWA-2-50DR+, Mini Circuits) before the amplifier, and disregarded data from the first  $5\,\mu\text{s}$ , where the response time of the amplifier limits the power.

### 6.4.3. Elastic and inelastic collision rates

For the measurements shown in this section, thermal molecule samples were prepared in the combined 1046/1550-nm crossed dipole trap, as described in Chapter 3. The trap frequencies were  $(\omega_x, \omega_y, \omega_z) = 2\pi \times (67, 99, 244)\text{ Hz}$  and the initial temperatures were around  $800\text{ nK}$ . The molecules were transferred into the dressed state  $|+\rangle$  by ramping the microwave field up from zero to full power within  $100\,\mu\text{s}$ . This ramp was performed by linearly changing the input voltage of the VCA, thus exponentially ramping the Rabi frequency. After a holding time at full microwave power, the ramp was reversed and the imaging procedure performed as usual. The inelastic collision rates were then measured by holding molecules in the trap for various times and at various microwave detunings  $\Delta$ , and fitting the resulting temperature and number curves as described above. As shown in Figure 6.5, the rates were close to the universal limit of  $\beta_{\text{inel}} = 4.9 \times 10^{-11}\text{ cm}^3/\text{s}$  for large  $\Delta$ , but could be suppressed to  $6.2(4) \times 10^{-12}\text{ cm}^3/\text{s}$  at the optimal value  $\Delta = 2\pi \times 8\text{ MHz}$ . Compared to the value measured without the presence of the microwave field,  $7.7(5) \times 10^{-11}\text{ cm}^3/\text{s}$ , this constitutes a reduction by an order of magnitude. Example data for the loss rates are shown in Figure 6.6(a).

The elastic scattering rates were measured by heating the trapped molecule sample along the  $z$ -direction and observing the thermalisation time. The heating was performed by modulating the 1064-nm beam sinusoidally at twice the vertical trap frequency for 100 oscillations, which caused a 30% increase in  $T_v$  at the beginning of the hold time. It can be seen in Figures 6.5 and 6.6(b) that the sample did not thermalise at large detunings, since the loss rate was larger than the thermalisation rate in this regime. However, at small  $\Delta$ , the dipolar interaction led to strong elastic collisions and the thermalisation rate increased

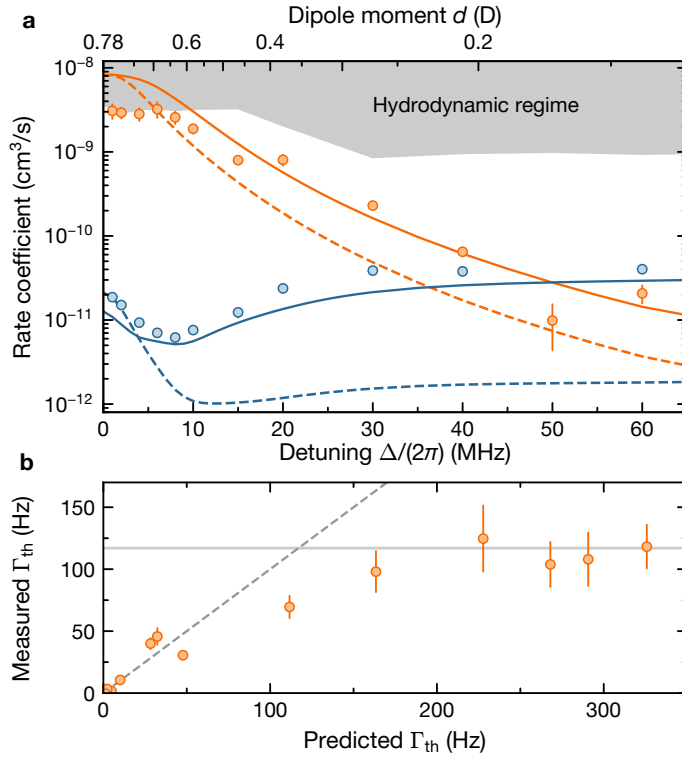


**Figure 6.5.:** Loss and thermalisation in a microwave-shielded thermal sample of NaK. (a) Elastic (orange) and inelastic (blue) scattering rate coefficients  $\beta_{\text{el}}$  and  $\beta_{\text{inel}}$  depending on the microwave detuning  $\Delta$ . All data were taken at  $\Omega = 2\pi \times 11 \text{ MHz}$  with molecules in the dressed state  $|+\rangle$ . The lines are coupled-channel calculations performed by Tijs Karman, which assume  $\xi = 6.2^\circ$ , at temperatures  $T = 800 \text{ nK}$  (solid) and  $T = 30 \text{ nK}$  (dashed). The area where the hydrodynamic regime limits the measured elastic rate coefficients is shown in grey. Its boundary is calculated via  $N_{\text{col}} \bar{\omega} / (2\pi n_0)$ . (b) Comparison between measured rethermalisation rate  $\Gamma_{\text{th}}$  and its expected value at the given dipolar interaction strength assuming that Equation (6.11) holds. The dashed line has a slope of 1, indicating that at weak interaction, this relation is a good description. At strong interaction, where the sample enters the hydrodynamic regime, the rate saturates and the solid line, which corresponds to  $\Gamma_{\text{th}} = \bar{\omega}$ , fits the data better.

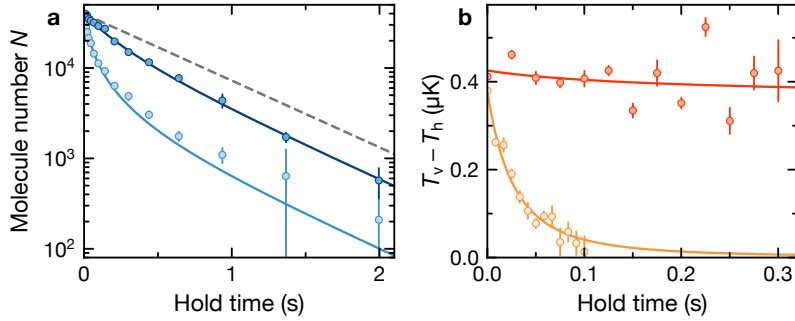


**Figure 6.6:** Example data for measurements of rate coefficients. **(a)** Measurements of loss rate, used to determine  $\beta_{\text{inel}}$ . Bright data points were taken without shielding, dark data points with optimal shielding at  $\Delta = 2\pi \times 8$  MHz. The solid lines are fits of Equations (6.7–6.9). The dashed line indicates the expected loss rate without any two-body loss, i.e.,  $\beta_{\text{inel}} = 0$ . **(b)** Measurements of thermalisation at  $\Delta = 2\pi \times 30$  MHz (orange) and at  $\Delta = 2\pi \times 80$  MHz (red). These are used to determine  $\beta_{\text{el}}$ . In the latter case,  $\beta_{\text{el}}$  is consistent with zero.

by at least two orders of magnitude.

At this point, we observed an unusual effect: most ultracold-gas samples are in the *ballistic regime*, which means that particles collide with the walls of the trap much more often than with each other. In this case, the thermalisation time is determined only by the collision rate. However, in the experiments with the largest elastic rates, the gas entered the *hydrodynamic regime*, where a particle undergoes many collisions before travelling through the trap once. In this regime, the thermalisation rate is limited by the propagation of collective excitations in the trap, which is given by the harmonic trap frequency. The measured rethermalisation rate thus saturated at a value corresponding to this trap frequency, as shown in Figure 6.5(b).

## 6.5. Evaporative cooling

For the data in this section, we used as a starting point the highest phase-space-density molecule sample we could create. As the inelastic collision rate coefficient scales strongly with temperature, this ensured the best possible evaporation efficiency. The main problem with creating ultracold samples of NaK is the difficulty in making the fermionic potassium and the bosonic sodium samples overlap, so that efficient magnetoassociation becomes possible. This is straightforward with thermal samples, but once the bosons condense, they form a very dense cloud in the centre of the trap, while degeneracy pressure stops the fermions from doing the same. We addressed this problem by adding a strongly focused dipole trap at a wavelength of 785.5 nm, which is near-resonant for potassium and confines it very strongly, but has a much smaller effect on sodium (see Figure 6.7). This specific wavelength was chosen because Feshbach and ground-state molecules exhibit

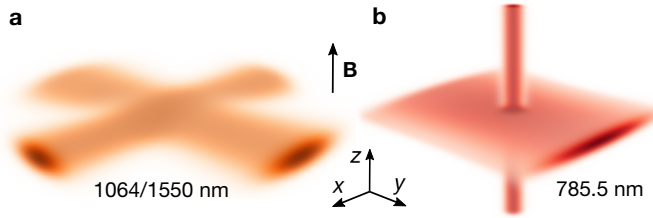


**Figure 6.7.:** Dipole traps used for preparing molecule samples. **(a)** Combined 1064/1550-nm trap as used for creating thermal samples. The 1064-nm and the 1550-nm beam propagate horizontally, and are both elliptical with an aspect ratio of two. **(b)** 785.5-nm trap used for compressing potassium. This trap consists of a strongly elliptical horizontal ‘lightsheet’ beam and a circular, vertical beam. For the creation of molecules from degenerate atoms, a combination of both traps is used.

the same polarisability there, reducing heating in the STIRAP transfer. By tuning the relative power between the dipole traps, we were able to match the density of bosons and fermions even at very low temperature, which led to significant improvement of the association efficiency. This turned out to be the key to reaching lower temperatures with  $^{23}\text{Na}^{40}\text{K}$ . These results are described in more detail in the publications [165, 386, 387].

For all following measurements, the starting samples were prepared at trap frequencies  $(\omega_x, \omega_y, \omega_z) = 2\pi \times (45, 67, 157) \text{ Hz}$  and at  $B = 72.35 \text{ G}$ .

### 6.5.1. Thermometry

Especially in the deeply degenerate regime, measuring the temperature of a molecule gas requires some care. For small samples, the signal-to-noise ratio of absorption images becomes low, and the fit function is very sensitive to the parameters, potentially leading to large errors. This is exacerbated when the time of flight before imaging is long, because this reduces the optical density of the sample. On the other hand, too short times of flight make the result strongly dependent on the trap shape, which is hard to measure precisely as well. As a compromise, we choose  $t_{\text{ToF}} = 10 \text{ ms}$ , and average over five to 20 images. To extract the temperature, the averaged images are fitted with a Fermi-Dirac distribution

$$n(x, z) = n_{\text{peak}} \text{Li}_2 \left[ -\mathcal{Z} \exp \left( -\frac{x^2}{2\sigma_x^2} - \frac{z^2}{\sigma_z^2} \right) \right], \quad (6.16)$$

with the peak density  $n_{\text{peak}}$ , the polylogarithmic function  $\text{Li}$ , the fugacity  $\mathcal{Z}$  and the cloud widths  $\sigma_{x/z}$ . The temperature in a given direction  $i$  then follows via the expression

$$\sigma_i = \frac{\sqrt{1 + \omega_i^2 t_{\text{ToF}}^2}}{\omega_i} \sqrt{\frac{k_B T_i}{m}}. \quad (6.17)$$

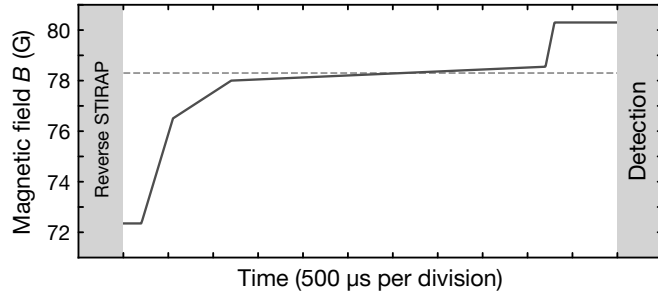


**Figure 6.8.:** Dissociation procedure for degenerate molecule samples. After reverse STIRAP, all dipole traps are immediately turned off, starting the time of flight. The magnetic field is first ramped quickly, then crosses the resonance at a very small ramp rate to minimise heating. Above the resonance, the field is then ramped quickly to 80.3 G, where the interspecies scattering length between sodium and potassium is zero. The dashed line marks the resonance position at 78.3 G.

In addition, we determine the reduced temperature, i.e.,  $T$  divided by the Fermi temperature  $T_F$ , from the fugacity:

$$\left(\frac{T}{T_F}\right)^3 = -\frac{1}{6\text{Li}_3(-\mathcal{Z})}. \quad (6.18)$$

Finally, we perform a check of the results above by fitting a Gaussian function to the thermal wings of the distribution. In this regime, the effect of Fermi-Dirac statistics is small, making this a good description. The temperature obtained with this method typically agreed with the one from the Fermi-Dirac fit within less than one standard deviation.

There is also a more fundamental problem with measuring the temperature of very cold molecule samples: the molecules need to be dissociated by means of reverse STIRAP and ramping over the Feshbach resonance before they can be imaged, so any heating caused by these processes will lead to an overestimation of  $T$ . The STIRAP process imparts a significant recoil energy of  $\hbar \times 1.7\text{kHz}$ . Luckily, not all of this is actually converted into heat, rather, it moves the entire cloud uniformly, causing oscillations. If the time of flight begins before these oscillations are fully damped out, the temperature in the centre-of-mass frame of the cloud rises only by some fraction of the imparted energy. This can also be reduced by adding a weak lattice potential orthogonally to the STIRAP direction as described in the supplemental material of Reference [385]. The effect of heating caused by ramping to the attractive side of the Feshbach resonance can be reduced by performing the ramp slowly, however this also leads to increased losses. We therefore devised a four-ramp scheme in which the field is ramped as quickly as possible away from the resonance, but crosses the resonance much more slowly (see Figure 6.8). In combination, the dissociation effects should lead to an overestimation of the fitted temperature by approximately 7 nK, which is not taken into account in any of the values given here.

## 6.5.2. Evaporation procedure and results

With optimal microwave shielding, we reach a ratio of elastic to inelastic collisions  $\beta_{\text{el}}/\beta_{\text{inel}} = 460(110)$ , which is limited by the onset of the hydrodynamic regime. At such a ratio, evaporative cooling should be quite efficient, however the very large elastic collision rate is not only an advantage. In fact, due to the limited thermalisation speed, the effective  $\beta_{\text{el}}/\beta_{\text{inel}}$  is much smaller during evaporation.

The hydrodynamic regime and its effect on thermalisation have been known for a long time: for example, caesium atoms exhibit a very large *s*-wave scattering length at most magnetic fields, and can easily enter the hydrodynamic regime [601]. For evaporative cooling, this is generally undesirable, because ideally, every particle that obtains a high enough kinetic energy should leave the trap. In the ballistic regime, this can happen anywhere within the volume of the sample, but in the hydrodynamic regime, it can only happen on its surface. Most particles with high energy will lose it again in a collision before they can leave the trap. Hence, for most evaporative cooling schemes, the scattering properties are chosen such that the gas always remains in the ballistic regime. For our case, this is not possible, as we can not reduce the elastic collision rate enough without impairing the shielding.

Starting with a nonthermalised sample of about  $2.5 \times 10^4$  ground-state molecules created from degenerate atoms, we ramped the dipole-trap power down exponentially for 150 ms, finally reaching trap frequencies down to  $2\pi \times (42, 56, 99)$  Hz in the most extreme case. We reduced the effect of the hydrodynamic regime by ramping the power of the vertical compression beam exponentially up during the process. This increased the trap frequency in two directions, limiting the reduction of thermalisation time when the other dipole traps are weakened.

We first investigated molecules held for 150 ms with shielding, but without changing the trap depth. In this case, the sample reached a final temperature of  $176(5)$  nK, corresponding to  $T/T_F = 1.00(3)$ , with  $1.43(5) \times 10^4$  molecules remaining. As this sample was fully thermalised, it can be used as a comparison point for the evaporation. Reducing the final trap depth clearly led to cooling, see Figure 6.9. In the optimal case, where we evaporated down to trap frequencies of  $2\pi \times (42, 56, 99)$  Hz, we reached  $T = 38(2)$  nK, corresponding to  $T/T_F = 0.47(2)$ . At this point, the evaporation was not completely stopped however, and the temperature reduced further if we held the sample for an additional 100 ms without changing the trap depth. After this, the temperature was reduced to  $21(5)$  nK or  $T/T_F = 0.36(9)$ . Figure 6.10 shows the images and the fits used to determine these temperatures.

In comparison, previous experiments have reached evaporative cooling of  $^{40}\text{K}^{87}\text{Rb}$  to  $1.4 T_F$  in 3D [419], and to  $0.6 T_F$  in 2D [414]. The improvement in our work was enabled by the large ratio of elastic to inelastic collisions that can be realised with microwave shielding. In addition, microwave shielding does not require high voltages in ultrahigh vacuum, which are difficult to control [318, 602]. High voltage can also be dangerous due to risk of electric shock as well as unintentional creation of X-rays [603]. While high-power microwaves come with their own difficulties and dangers, using them does not require any changes to existing vacuum setups, and they can be created straightforwardly

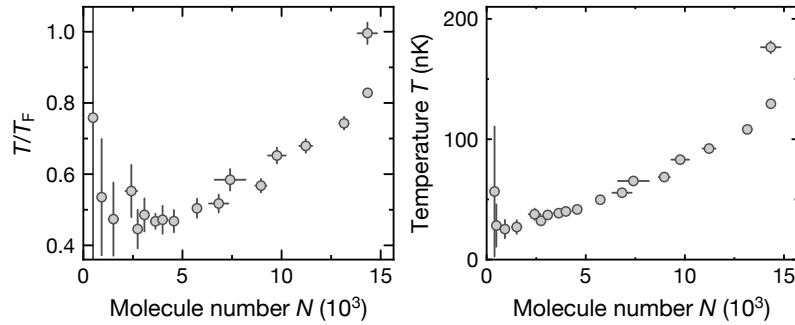


**Figure 6.9.:** Temperatures reached in the microwave-shielded evaporation process at various trap depths without additional holding time. **(a)** Reduced temperature, **(b)** Temperature. In both subfigures, the rightmost data point was taken without any reduction in trap depth. Lowering the trap depth then led to smaller atom numbers and cooling, until the molecule number became too small to reliably fit temperatures.

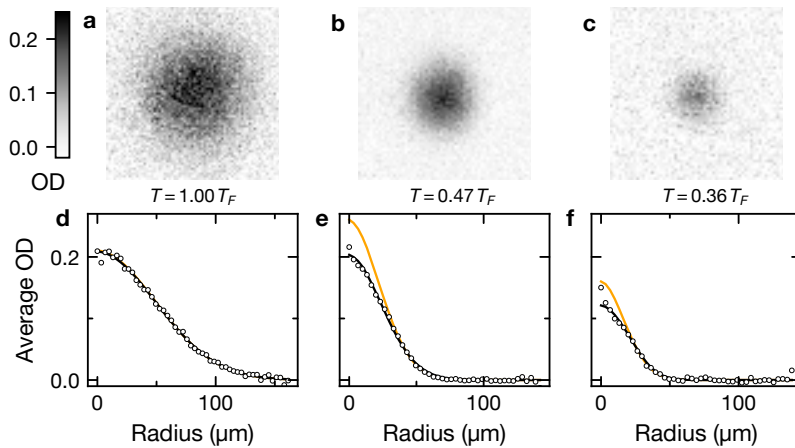


**Figure 6.10.:** Molecule clouds after microwave-assisted evaporation to various trap depths. OD stands for optical density. **(a-c):** Time-of-flight images averaged from multiple runs. **(d-f):** Azimuthally integrated optical densities extracted from these images. The black lines are polylogarithmic fits, the orange lines are Gaussian fits to the thermal wings of the sample. (a) and (d) correspond to  $T = 1.00 T_F$  (only thermalisation, no evaporation), (b) and (e) correspond to  $T = 0.47 T_F$  (evaporation without additional holding), and (c) and (d) correspond to  $T = 0.36 T_F$  (evaporation with additional holding).

with commercially available tools.

We hope to soon be able to improve our result further with a combination of upgrades: first, we plan to reduce the microwave phase noise by adding a narrowband filter at the output of the signal source. We hope that the one-body loss can thereby be suppressed below the background level caused by off-resonant scattering of dipole-trap photons and by background-gas collisions. Second, with improved antennas and a better understanding of the effect of the surroundings, it should be possible to reduce the polarisation ellipticity, hopefully gaining another factor three reduction in two-body loss. Third, the effect of the hydrodynamic regime on the evaporation efficiency could be reduced with a better trap geometry. With some combination of these, dipolar gases of molecules will hopefully soon cross the threshold where dipolar many-body physics become accessible.

*Not knowing when the dawn will come  
I open every door;  
Or has it feathers like a bird,  
Or billows like a shore?*

—Emily Dickinson

## 7. Next steps for dipolar many-body physics

With the aid of efficient, density-matched magnetoassociation [387] and microwave-assisted evaporation [596], we are now able to create samples of thousands of molecules at  $T/T_F = 0.36$  and  $T = 21\text{ nK}$ . The dipole moment can reach 0.64 D at optimal shielding conditions. With some technical improvements like higher microwave power, more efficient STIRAP, and better evaporation procedures, it is realistic to reach temperatures of  $T/T_F = 0.1$  and a dipole moment of 0.75 D. These conditions are a great starting point for the exploration of dipolar quantum matter.

### 7.1. Motivation

The behaviour of quantum many-body systems is notoriously difficult to predict from first principles. In the worst case, the computational effort required to simulate such systems on classical computers scales exponentially with their particle number. This means that in some cases, it is impossible to calculate the behaviour of a system governed by a known Hamiltonian even for moderate particle numbers on the order of 100. One particularly well-known and relevant case is the Fermi–Hubbard model, which is suspected to describe unconventional superconductivity. Though this model has been studied for decades, it remains unclear if its ground state is superconducting or not, and if it can provide an accurate description of existing high-temperature superconductors [604, 605]. Similar problems exist in other areas of condensed-matter physics and quantum chemistry [606].

A quantum simulator is a controllable quantum system which implements a given Hamiltonian, so that the system’s behaviour can be used to understand the Hamiltonian. The final goal of research on quantum simulators is to be able to choose any Hamiltonian and have a simulator available which can implement it. We are not quite there yet, however. Most current attempts to build quantum simulators are limited by too small system sizes and too high temperatures.

Long-range interacting quantum systems are in many ways even more difficult to understand than ones with short-range interaction. For example, systems with finite-range interactions behave in some sense locally, as there is a finite speed of information propagation given by the *Lieb–Robinson bound* [607]. For all practical purposes, this also applies

to systems of neutral atoms. However, for long-range interacting systems, this bound can be violated, as has been demonstrated with ions [608–610]. Furthermore, low-energy collisions in systems with short-range interactions can be described by a single parameter, the scattering length. This is no longer true for the dipole-dipole interaction with its  $1/r^3$  character, where multiple partial waves matter even in the low-energy limit [15, 611]. In the specific case of the dipole-dipole interaction, it is also important that it is anisotropic and can be simultaneously attractive and repulsive, depending on the relative spatial orientation of interacting particles. This allows the coexistence of phases which require attraction and repulsion. The interplay between these effects can lead to highly complex and fascinating behaviour, such as supersolidity. Dipolar systems have been theoretically investigated for almost 20 years, but only a very small number of results have ever been experimentally tested. Until now, only the regime of weak dipolar interactions has been accessible, mainly with magnetic atoms [147, 148, 506–510].

A list of theory papers, both in the weakly and strongly dipolar regimes, is given in Appendix B. In the following, I will investigate some selected predictions out of the large number of papers to judge their feasibility for experimental tests, both in our own experiment and in others, within the next few years. They can then serve as testbeds for techniques to control molecules and as proof-of-concept experiments for quantum simulation of dipolar matter.

## 7.2. Ground work

The emergence of dipolar quantum phases is driven by the dipole-dipole interaction and its relation to other energy scales in the system. These include the temperature, and, depending on the system, also others like the lattice hopping strength. The dipole-dipole interaction strength is commonly expressed in terms of the dipolar length  $a_d$ , which is defined as

$$a_d = \frac{md^2}{4\pi\epsilon_0\hbar^2}, \quad (7.1)$$

where  $d$  is the lab-frame dipole moment and  $m$  is the molecule mass. The dipolar lengths of NaK and KRb at various dipole moments are given in Tables 7.1 and 7.2.

Comparing  $a_d$  to the interparticle spacing yields the interaction strength. For fermions in a trap, the interparticle spacing is given by the inverse Fermi wavevector  $k_F^{-1}$ . It depends on the particle number and the geometry of the system. In the case of a fermionic 3D system at zero temperature in a harmonic trap, it is given by [612]

$$k_F = \sqrt{\frac{m\bar{\omega}(48N)^{1/3}}{\hbar}}, \quad (7.2)$$

with the geometric mean trap frequency  $\bar{\omega} = (\omega_x\omega_y\omega_z)^{1/3}$ .

In a lattice, energy scales are conveniently expressed in terms of lattice recoil energies. For NaK in a retro-reflected 1064-nm lattice, as used in our experiment, this is  $E_R =$

**Table 7.1.:** Dipolar characteristics of NaK. Nearest-neighbour (NN) interaction is given for 532 nm lattice spacing.

Dipole moment $d$	E field	Dipolar length $a_d$	NN interaction $U_{\text{NN}}$
0.50 D	1.2 kV/cm	235 nm	$h \times 251 \text{ Hz}$
0.75 D	1.8 kV/cm	529 nm	$h \times 564 \text{ Hz}$
1.00 D	2.7 kV/cm	941 nm	$h \times 1002 \text{ Hz}$
1.25 D	3.8 kV/cm	1470 nm	$h \times 1566 \text{ Hz}$
1.50 D	5.5 kV/cm	2116 nm	$h \times 2255 \text{ Hz}$
1.75 D	8.4 kV/cm	2881 nm	$h \times 3070 \text{ Hz}$
2.00 D	15 kV/cm	3763 nm	$h \times 4010 \text{ Hz}$

**Table 7.2.:** Dipolar characteristics of KRb. Nearest-neighbour (NN) interaction is given for 532 nm lattice spacing.

Dipole moment $d$	E field	Dipolar length $a_d$	NN interaction $U_{\text{NN}}$
0.10 D	2 kV/cm	19 nm	$h \times 10 \text{ Hz}$
0.20 D	5 kV/cm	76 nm	$h \times 40 \text{ Hz}$
0.30 D	9 kV/cm	171 nm	$h \times 90 \text{ Hz}$
0.45 D	45 kV/cm	384 nm	$h \times 203 \text{ Hz}$

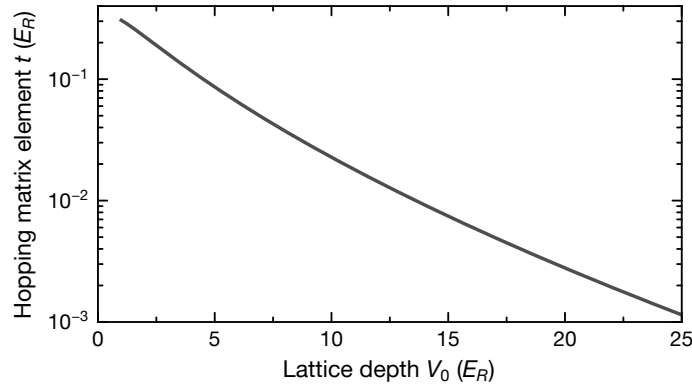


**Figure 7.1.:** Hopping matrix element in relation to lattice depth. Both quantities are given in units of lattice recoil energies. The curve was calculated using Equation (7.4).

$h \times 2.8\text{kHz}$ . The three important parameters are the interaction strength, the hopping matrix element, and the temperature. For an angle  $\theta$  between the intermolecular axis and the dc electric field, the interaction energy between molecules at a distance  $r$  reads

$$U(r, \theta) = \frac{d^2(1 - 3\cos^2 \theta)}{4\pi\epsilon_0 r^3}. \quad (7.3)$$

The interaction strength for long-range interacting systems is conveniently characterised by the nearest-neighbour interaction between maximally repulsive dipoles, which is  $U_{\text{NN}} = U(a, \pi/2)$  for the lattice spacing  $a$ . The hopping matrix element can be approximated as [613]

$$t = E_R \frac{4}{\sqrt{\pi}} \left( \frac{V_0}{E_R} \right)^{(3/4)} \exp \left( -2\sqrt{\frac{V_0}{E_R}} \right), \quad (7.4)$$

with the lattice depth  $V_0$ . Figure 7.1 shows the hopping matrix element predicted by this formula for a typical range of lattice depths. The formula is only valid for a single particle in a homogeneous lattice, since interactions and energy differences between different lattice sites can strongly modify the hopping.

When evaluating the temperatures in different types of traps and lattices, it is important to consider that additional confinement necessarily leads to increased temperature at constant entropy. This is unavoidable due to the reduced density of states [614]. In reality, the effect is even more pronounced if a gas is loaded into more confined geometries, because such a transfer can not be perfectly adiabatic [615].

### 7.3. Fermi-surface deformation

The presence of anisotropic interaction in a trapped Fermi gas deforms the Fermi surface. Along the repulsive direction, the cloud becomes narrower, as it is energetically less favourable for a particle to be on its edge, while the effect is reversed along the attractive direction [208, 616]. This is the conceptually simplest way to see the effect of the dipole-dipole interaction in a fermionic system, and it has been observed with magnetic atoms [508]. The strength of the deformation is proportional to the ratio of the interaction strength and the Fermi energy, which is [508]

$$\eta = \frac{n_{\text{peak}} d^2}{4\pi\epsilon_0 E_F}, \quad (7.5)$$

where  $n_{\text{peak}}$  is the peak density. The Fermi energy  $E_F$  of a zero-temperature Fermi gas in a harmonic trap is given by

$$E_F = \frac{\hbar^2 k_F^2}{2m} = \hbar\bar{\omega}(6N)^{1/3}. \quad (7.6)$$

A typical case for our experiment is  $N = 10^4$  and  $\bar{\omega} = 100\text{Hz}$ , such that  $E_F \approx h \times 4\text{kHz}$ , and a peak density on the order of  $n = 10^{12}\text{cm}^{-3}$ . This means at a dipole moment  $d = 1\text{D}$ ,

we would reach  $\eta = 0.04$ . This is almost three times larger than previously reached with erbium atoms, so it should be possible to measure this with molecules, too. However, it is difficult to prepare molecules in motional equilibrium, i.e., without any sloshing or breathing oscillations. As long as oscillations occur, they can mask the Fermi-surface deformation. In addition, degenerate samples with larger molecule number would be helpful to achieve the required signal-to-noise ratio to observe the effect clearly.

## 7.4. Dipolar Wigner crystal

One of the most carefully studied dipolar quantum phases is the *dipolar Wigner crystal* [204–206, 209, 617]. It comes about when confining dipoles to a 2D plane with a strong dipole moment orthogonal to the plane. In this situation, when the density is high enough, the repulsive interaction forces the particles into a spontaneously formed triangular lattice configuration. This phase has remained experimentally inaccessible because enormous interaction strength is required to reach it. The interaction strength can be given in terms of the dimensionless parameter  $n_{2D}a_d^2$ , where  $n_{2D}$  is the 2D density. For the case of bosons, the transition to the crystalline phase is predicted to occur at  $n_{2D}a_d^2 \approx 290$  [205]. For fermions, a slightly less extreme value of  $n_{2D}a_d^2 \approx 50$  is required [617]. With an ambitious lab-frame dipole moment of 1.25 D, this means  $n_{2D} = 2.3 \times 10^9 \text{ cm}^{-2}$  for fermions, or a gigantic  $n_{2D} = 1.3 \times 10^{10} \text{ cm}^{-2}$  for bosons.

For comparison, the current record density of dipolar molecules in 2D planes is held by JILA. In their paper [414], they reported  $N = 4000$  in a single 2D plane, and  $\omega_x = \omega_y = 2\pi \times 40 \text{ Hz}$ , resulting in an average density of  $6 \times 10^7 \text{ cm}^{-2}$ . While the peak density should be somewhat higher, this is still at least an order of magnitude too little. In addition, this density was reached with much smaller dipolar repulsion.

If sufficient densities can be reached, the stability of the gas might become a problem. The JILA experiment reported loss coefficients on the order of  $\beta = 1 \times 10^{-8} \text{ cm}^2/\text{s}$  under optimal conditions, which would limit the lifetime of a gas at the minimum necessary density to 50 ms. This way of estimating lifetime is of course very crude, as a gas with much larger dipolar length could be stabilised by repulsion. Using bosons or distinguishable fermions will likely make it easier to reach high densities as there is no *p*-wave barrier causing additional repulsion, however this also means that the two-body loss rate will be even higher. Experience shows that theoretical estimates for loss rates sometimes do not accurately describe real systems, so this question will likely only be answered by experiments.

Though it is not completely unrealistic to reach this phase, the challenges are substantial. Strong 2D confinement, high efficiency of loading single planes, and very large electric fields are necessary to attempt this. Even with all these in place, it will remain difficult to find a procedure to compress the molecules to the enormous required density without strong heating or loss. Finally, detecting the Wigner crystal is also likely to be challenging, because it will only form in the highest-density region in the centre of the confinement region, such that the non-crystallised parts at the edge of the sample will cause a large background signal for any imaging in momentum space. Imaging in posi-

tion space may be possible for sufficiently heavy molecules with strong interaction, where the lattice constant of the Wigner crystal could reach 700 nm or more, which quantum-gas microscopes can resolve.

Due to its relatively low mass and large rotational constant, NaK is not an ideal species for this endeavour. NaCs or NaRb would be more promising candidates if bosonic molecules can effectively be stabilised against collisions in 2D. Otherwise, heavy fermionic species like KCs or CsYb could be an option, if they can be cooled down far enough. If the Wigner crystal turns out to be unreachable, the phases described in Section 7.5 or the hexatic phases predicted in [618, 619] may be good alternatives.

## 7.5. Stripe phases and superfluidity in 2D bulk

The Wigner crystal is not the only way in which spontaneous symmetry breaking leads to new quantum phases for dipoles confined to 2D planes. In fact, other phases can occur at much lower interaction strengths, and are thus more easily accessible. For both bosons and fermions, stripe phases have been predicted [620–624], though in the case of bosons, it is still a point of contention whether the stripe phase is superfluid [625]. For fermions, a  $p$ -wave superfluid phase and a nematic crystal have also been predicted [623]. At the right conditions, stripe order and superfluidity can coexist, forming a supersolid [622]. In comparison to the Wigner crystal, which requires  $k_F a_d > 25$ , these phases exist already at  $k_F a_d \approx 2.5$ , though at a quite low critical temperature. According to the predictions in Reference [623], the system must be very degenerate at  $T_c \approx 0.025 T_F$  to reach them, though this limit could likely be increased a bit with stronger interactions.

Out of the predicted phases, only the nematic crystal can exist at an angle  $\theta = 90^\circ$  between the plane and the external field. The stripe phase becomes stronger at smaller angles and could probably best be observed at  $\theta \approx 60^\circ$ . The supersolid requires  $\theta < 45^\circ$ . This is experimentally relevant because it requires working in a sensitive regime: for  $\theta < 36^\circ$ , the system collapses due to the attractive interaction. Hence, the field angle needs to be precisely controlled, which is not possible for experiments which have only four rod electrodes, like ours. Experiments with more sophisticated electrode geometries should not have this problem, as demonstrated for example in Reference [626]. For interactions introduced via microwaves, a reliable way to control the direction has not been found yet, though there is no fundamental reason this should not be possible. The most critical requirement is thus temperature. Currently,  $T/T_F \approx 0.025$  is more than ten times lower than the record, and even if by means of stronger interaction the requirement can be eased a bit, this is still a tall order.

## 7.6. Rotational synchronisation

Achieving long coherence times between different rotational states of molecules is a significant challenge. This is due to the complicated coupling between molecules and external fields. First, an external electric field is required to isolate otherwise degenerate levels and achieve a proper two-level system. However, any inhomogeneity in this field leads to position-dependent shifts of the transition. Second, rotational states couple to the ac field of dipole traps differently, such that the transition is shifted depending on the trap intensity. Even if both of these effects are compensated to a high degree of precision by using a very homogeneous electric field and a magic dipole trap, the dipole-dipole interaction itself causes further transition shifts, such that long coherence times can only be achieved at very low density [381].

However, there is a way in which the interaction can be used to protect coherence rather than destroy it. This is known as a *condensate of rotational excitations*, or a rotational condensate for short. It was predicted by Kwasigroch and Cooper [627, 628] and is a quantum analogue to the famous experiment of synchronising metronomes on a table top. Initially, ground-state molecules are prepared on the sites of a square lattice with a weak electric field orthogonal to the lattice plane providing the quantisation axis. Using a resonant  $\pi/2$  microwave pulse, the molecules are then excited into an equal superposition of the ground state  $|0\rangle = |R = 0, m_R = 0\rangle$  and the first rotationally excited state  $|1\rangle = |1, 0\rangle$ . This yields the state

$$\prod_i \left( |0\rangle + e^{i\phi_i} |1\rangle \right). \quad (7.7)$$

where initially, all the  $\phi_i$  are equal. Because each molecule is essentially a two-level system with nearest-neighbour interaction, the Hamiltonian of this system can be written in the form of an spin-1/2 XY model [310, 628]:

$$H = \sum_{i \neq j} \frac{d_{01}^2}{8\pi\epsilon_0 |\mathbf{r}_i - \mathbf{r}_j|^3} (S_i^+ S_j^- + S_i^- S_j^+). \quad (7.8)$$

Here,  $S_i^\pm$  are the spin raising and lowering operators, and  $d_{01}$  is the dipole matrix element between the two rotational levels,  $d_{01} = \langle 0 | \mathbf{d} | 1 \rangle = d_0 / \sqrt{3}$ . Because of the choice of the quantisation axis orthogonal to the lattice plane, the relative angle between the dipole orientation is the same for all molecule pairs and the interaction depends only on the distance and the relative phases  $\phi_i$ . Because the interaction is maximally repulsive when all the  $\phi_i$  are equal, the system is initially in a state of maximum energy when all the molecules rotate in phase with each other. In the ideal case, there are no decay channels available where this energy can go, so the synchronous motion is protected from dephasing. When recasting the model in terms of hard-core bosons, where  $|0\rangle$  denotes an empty site and  $|1\rangle$  a particle, this looks the same as a BEC, hence the name of this phase.

The critical question for the experimental implementation is this: how much disorder can be in the system before it overcomes the synchronisation and destroys the coherence? In the case of a lattice filling of 10% or higher, the mean-field interaction energy per

particle is on the order of a few kilohertz, much larger than the relative shifts between neighbouring particles caused by external fields, which are on the order of tens of hertz. Therefore, the dominating source of disorder is the random filling of the lattice. Reference [628] treats the relation between filling and coherence time both analytically and numerically, finding that a phase transition occurs at a filling of about 15%. Below this number, it is expected that the coherence will reduce exponentially over time, but above it, a finite level of contrast should be observable in Ramsey experiments even after long times. Experimental imperfections could raise the critical filling slightly, but with previously demonstrated temperatures, it is reasonable to reach such filling in a square lattice. Hence, reaching the condensate appears to be realistic.

## 7.7. Dipolar XY and XXZ models

As described above, the rotational states of molecules on a lattice can be mapped onto spin-1/2 particles with  $1/r^3$  interaction. Generalising Equation (7.8) to cases with a potentially strong electric field along the  $z$  direction yields

$$H = \sum_{i \neq j} \frac{1}{8\pi\epsilon_0\hbar^2|\mathbf{r}_i - \mathbf{r}_j|^3} \left( d^2 S_i^z S_j^z + d_{01}^2 \left( S_i^x S_j^x + S_i^y S_j^y \right) \right). \quad (7.9)$$

In this situation, there are two different dipolar couplings: the first is caused by the dipole moment induced by the external field and gives the Ising term proportional to  $S_i^z S_j^z$ . The second is the coupling between the rotational ground and excited states and gives the XY term proportional to  $S_i^x S_j^x + S_i^y S_j^y$ . Note that for strong fields, the approximation that  $d_{01} = d_0/\sqrt{3}$  breaks down and  $d_{01}$  depends on the field [629].

For the case where  $d \neq 0$ , this corresponds to a dipolar XXZ model. By encoding the spin either as  $\{|0,0\rangle, |1,0\rangle\}$  or  $\{|0,0\rangle, |1,1\rangle\}$ , the sign of  $d_{01}$  is flipped, changing between favouring ferromagnetic or antiferromagnetic order. Peter *et al.* [630] investigated this and predicted four phases: XY (anti-)ferromagnetic and Ising (anti-)ferromagnetic. In the typical situation where  $d_{01} > 0$  and the external field is small, the ground state is an XY antiferromagnet, where neighbouring molecules rotate with a  $\pi$  phase shift. In some sense, this is the opposite of the rotational condensate, because here the interaction is maximally attractive. Reaching the phases where the Ising term dominates requires  $d > |d_{01}|$ . In the case of NaK,  $E = 6.1\text{ kV/cm}$  is needed for this, more than any current experiment can provide. Still, other species, especially those with small rotational constants, can reach this regime more easily and might soon be used to investigate the phase diagram of the dipolar XXZ model.

Even if a sufficiently strong Ising term can not be reached, the XY model with  $1/r^3$  interaction is already interesting. Specifically, it permits a ferromagnetic phase with true long-range order at finite temperatures. As a consequence of the Mermin-Wagner theorem, such a phase could not exist in the more common case of shorter-range interactions. For the antiferromagnetic case ( $d_{01} < 0$ ), there is instead a Kosterlitz-Thouless transition to a phase with quasi-long-range order at finite temperature [630].

Both the ferromagnetic and antiferromagnetic phases exhibit fascinating properties in terms of spin-wave propagation. In contrast to the typical  $\sim q^2$  dispersion relation with the quasimomentum  $q$ , the antiferromagnetic phase features a Goldstone mode with a linear  $\sim |q|$  dispersion. In the ferromagnetic case, the dipolar interaction changes the dispersion to the unusual case  $\sim \sqrt{|q|}$ . It is possible to observe this by exciting a spin wave and observing its propagation over time. Considering that even the short-range interacting case of this system has only been very recently realised with atoms [631], observing the dipolar case would constitute a major achievement.

As expected, this is not easy: the implementation with atoms featured a system size of  $\sim 10^4$  spins at a filling of at least 90% and a resolution corresponding to six lattice sites. With perfectly adiabatic loading of a 3D gas into a square lattice, reaching this filling would require starting at  $T/T_F = 0.14$ , so it is not too far away from the state of the art. Possibly a higher imaging resolution could reduce the system-size requirement somewhat, but high filling remains important, as any disorder would disturb the spin-wave propagation. Another challenge is the initial preparation of the spin wave. In Reference [631], a magnetic field gradient and a microwave pulse were used to create a spatially dependent excitation pattern. In principle, the same thing can be done with molecules using an electric field gradient, though this necessitates careful engineering of the correct field. Alternatively, a spatially dependent light shift, created with a spatial light modulator, could also fulfil this purpose.

## 7.8. Checkerboard and stripe phases on a square lattice

While the last two chapters focused on the situations that arise when molecules are pinned on their lattice sites, it is also interesting to investigate the physics that happens when the lattice becomes weaker and the molecules can move. This is known as the *extended Bose-Hubbard* (eBH) and *extended Fermi-Hubbard* (eFH) model. In simplified form, the eFH Hamiltonian for the case of a square lattice reads

$$H = t \sum_{\langle ij \rangle} (c_i^\dagger c_j + \text{h.c.}) + \sum_{i \neq j} \frac{U_{ij}}{2} n_i n_j. \quad (7.10)$$

Here,  $c_i^\dagger$  and  $c_i$  denote the fermionic creation and annihilation operators at site  $i$ ,  $n_i$  is the particle number operator, and  $\langle ij \rangle$  denotes all nearest-neighbour pairs. Hence, this Hamiltonian contains a hopping term with the rate  $t$ , and a dipolar interaction term proportional to the interaction energy  $U_{ij}$ . Note that dipole-assisted tunnelling and a position-dependent chemical potential can also play a role, but are not shown here for simplicity. More information on these terms as well as on beyond-nearest-neighbour interactions can be found in References [509, 632, 633]. In the bosonic case, there is also an on-site interaction term, but molecule pairs on a single lattice site will likely be so unstable that they should be avoided anyway, which could be done for example by making the long-range

interaction sufficiently repulsive.

Both the eBH and eFH models open up a multitude of possibilities for new exotic quantum phases, see for example the review by Dutta *et al.* [633]. Up to now, only a very limited regime has been experimentally accessible with magnetic atoms [507, 509]. An implementation with excitons in a solid-state system was also reported recently [634]. From the theory side, the case of a square lattice has been investigated most thoroughly, both with bosons [632, 635, 636] and fermions [637–641].

For the eFH, a number of quantum phases emerge which are characterised by their different charge order. At high temperature, no charge order exists, but when the interaction begins to overpower thermal fluctuations, long-range ordered *charge density wave* phases form. For a dipole moment orthogonal to the lattice ( $\theta = 90^\circ$ ), there is a checkerboard phase with alternating filled and empty sites, as well as higher-order fractionally filled phases (e.g., two empty sites for every filled one) at even stronger interaction [637]. This intuitively makes sense, as strong repulsion leads to maximised distance between particles. According to Gadsbølle and Bruun [639], the critical temperature  $T_c$  for the transition to the checkerboard phase depends on the nearest-neighbour interaction  $U$ . In the strong-interaction limit, which gives reasonable results when  $U_{NN} > 2t$ , they predict  $k_B T_c \approx 0.66 U_{NN}$ . At lower interaction strengths,  $T_c$  drops below this approximation. For a lattice with 532 nm spacing,  $U_{NN} = h \times 5 \text{ kHz}$  can be reached in principle, but with currently available electric fields,  $U_{NN} = h \times 1 \text{ kHz}$  is more realistic. This corresponds to  $T_c \approx 30 \text{ nK}$ , a temperature is certainly challenging but not impossible to reach. Using a smaller lattice wavelength or larger electric field could even raise the required temperature a bit more.

One other way to reach charge-density waves at higher temperatures is to make use of the dipolar interaction in head-to-tail orientation, which is twice as strong. This is realised when the dipole moment points along the lattice plane ( $\theta = 0$ ), and is parallel with one of the lattice directions. Stripes are then formed instead of a checkerboard, resulting in a critical temperature about two times higher [639]. However, with strong attractive interactions, the stability of this phase is questionable.

Similar phases have been predicted for the case of hard-core bosons, including superfluid and supersolid phases and multiple kinds of fractional-filling Mott insulator [635]. Here, the interesting regime is  $t/U_{NN} \approx 0.1$  and  $k_B T_c \approx t$ . This is likely somewhat harder to reach than in the fermionic case, requiring roughly three times lower temperatures at comparable dipole moment.

## 7.9. Supersolidity and superfluidity on cubic lattices or bilayers

Instead of tilting the dipole direction with respect to a 2D lattice, anisotropic interaction can also be engineered by using a 3D lattice or multiple square lattices on top of each other. Similar to the phases described in the previous chapter, the attractive interaction can lead to BCS pairing between fermions and  $p$ -wave superfluidity while the

repulsive interaction leads to crystalline ordering. When the ratio between attraction in the  $z$ -direction and repulsion in the  $x$ - $y$ -plane is right, a supersolid can form as a combination of a checkerboard phase in the  $x$ - $y$ -plane and a BCS state in the  $z$ -direction. This has been theoretically studied for fermionic dipoles in 3D lattices [642], and in bilayers [643, 644].

In principle, loading ultracold molecules into such a configuration is easier than creating purely 2D samples, since loading of single planes requires very stable control of the sample position and lattice phase along the stiff confinement direction. Reaching half-filling in a 3D lattice is probably doable. The critical temperature for both the superfluid and supersolid phase has been predicted to be  $k_B T_c \approx 0.07t$ , while  $t$  should be roughly equal to  $U_{NN}$ . For example, at  $t = U_{NN} = h \times 1 \text{ kHz}$ , it is expected that  $T_c \approx 3.4 \text{ nK}$  [642]. Considering that, even before lattice loading, the record-low temperature is above 20 nK, and the loading is expected to significantly increase this number, these phases seem for now clearly out of reach. In bilayers with an interlayer separation below 500 nm, the critical temperature is larger, however it is unclear how such small separations could be realised.

## 7.10. Topological superfluidity in 2D

BCS pairing on 2D planes can also be induced by an average attractive interaction due to a circularly polarised microwave field [645, 646]. In contrast to the case of an external dc electric field, this makes the interaction naturally attractive at long range if the microwave propagation is orthogonal to the lattice plane. Under these conditions, the interaction is isotropic so that no crystalline order or supersolidity is possible. At low enough temperatures, the interaction results in a topological phase transition to a  $p_x + ip_y$  superfluid.

Incidentally, we used the same kind of microwave field for the demonstration of shielding, so we know that molecules can be stable under these conditions. The critical temperature of the transition has been predicted to be [645]

$$T_c \approx \exp\left(-\frac{3\pi}{2k_F a_d}\right) T_F. \quad (7.11)$$

This result has to be taken with a grain of salt, as it comes from a weak-interaction approximation, which should be valid only up to  $k_F a_d \approx 2$ . Hence, the highest critical temperature that this model can predict is  $T_c \approx 0.1 T_F$ . Depending on the efficiency of loading into a 2D plane, this is between five and ten times lower than the current record. Still, it may be worth trying, as it seems reasonable that the critical temperature of this transition becomes higher at larger  $k_F a_d$ , even if this regime has not been theoretically investigated yet. Another idea is to add a shallow square lattice on top of the 2D trapping potential in order to increase the molecules' effective mass, leading to higher  $a_d$ .

## 7.11. Conclusion

The ideas described in this chapter showcase the great variety of dipolar quantum many-body physics, and yet the list only scratches the surface of what has been done. With the experimental progress that was made during recent years, some of these proposals can now, for the first time, be tried out. Without a doubt, this will lead to further fascinating discoveries, as experimentalists and theoreticians can now explore this field hand in hand. I hope that our experiment will be able to contribute to this exciting development. Looking at the past few years, in 2018 we still struggled to create 5000 thermal molecules, now we can get degenerate samples with twice the number, longer lifetime and a much higher dipole moment. Many further upgrades are planned or already ongoing, putting us into an excellent position to find new physics soon.

## A. List of heteronuclear alkali dimers

This appendix contains some basic information about the heteronuclear bialkali molecule species. For each of them, there is a list of references on experimental work with ultracold samples and attempts to create them. To the best of my ability, I attempted to be exhaustive and to mention every peer-reviewed paper on the subject.

Wherever possible, I gave the most recent experimentally measured value for the body-fixed dipole moment. The numbers given are always for the rovibrational ground-state of the  $X^1\Sigma$  manifold. There are also theoretical calculations, which are available for a larger variety of states, and are typically accurate to better than 10%, see for example [19, 647, 648]. Similarly, the given rotational constants are the most recent measured values except in those cases where, to my knowledge, no such measurements exist. The source for all given chemical stability values is [238].

### A.1. NaLi

Mixture investigated since 2002 by Wolfgang Ketterle's group at MIT. Work on molecules only significantly later; first Feshbach molecules reported in 2012. STIRAP demonstrated to "triplet ground state", i.e. lowest rovibrational level of the  $a^3\Sigma^+$  manifold of  $^{23}\text{Na}^6\text{Li}$ . The  $X^1\Sigma$  ground state and other isotopologues remain largely unexplored. Not very interesting for dipolar physics due to its small dipole moment. Research instead focused on collisions; pioneering work done on sympathetic cooling of molecules with atoms.

Quantum statistics: fermionic ( $^{23}\text{Na}^6\text{Li}$ ), bosonic ( $^{23}\text{Na}^7\text{Li}$ )

Body-fixed dipole moment: 0.463(2) D [649]

Ground-state rotational constant:  $2B_{\text{rot}} = h \times 22.8 \text{ GHz}$  [648]

Chemically stable: No

## Relevant references

- Creation of  ${}^6\text{Li}-{}^{23}\text{Na}$  mixture [162].
- Feshbach molecules via magnetoassociation [303].
- Photoassociation studies in preparation for STIRAP [305, 306].
- STIRAP to lowest triplet state [304].
- Observation of favourable atom-molecule collision properties and first demonstration of sympathetic cooling of molecules with atoms [433].
- Feshbach resonance found in the Na+NaLi system [437].

## A.2. LiK

Fermi-Fermi mixture of  $^6\text{Li} + ^{40}\text{K}$  investigated thoroughly in Munich, Amsterdam, and Innsbruck, mostly focused on polarons, atom-atom and atom-molecule collisions. Ground-state molecules of  $^6\text{Li}^{40}\text{K}$  have recently come into reach at Kai Dieckmann's group in Singapore, but ground-state samples have not yet been made. The other five isotopologues have not been systematically studied yet.

Quantum statistics: fermionic ( $^6\text{Li}^{39}\text{K}$ ,  $^6\text{Li}^{41}\text{K}$ ,  $^7\text{Li}^{40}\text{K}$ ), bosonic ( $^6\text{Li}^{40}\text{K}$ ,  $^7\text{Li}^{39}\text{K}$ ,  $^7\text{Li}^{41}\text{K}$ )

Body-fixed dipole moment: 3.45(10) D [649]

Ground-state rotational constant:  $2B_{\text{rot}} = h \times 15.6 \text{ GHz}$  [648]

Chemically stable: No

### Relevant references

- Studies of  $^6\text{Li} + ^{40}\text{K}$  mixture and Feshbach resonances [650–654].
- Feshbach molecules via magnetoassociation [655, 656].
- Weakly bound molecules via photoassociation [657].
- Feshbach resonances of the  $^6\text{Li} + ^{41}\text{K}$  mixture and  $^{41}\text{K}$  as sympathetic coolant for  $^6\text{Li}$  and  $^{40}\text{K}$  [658].
- Collision dynamics in mixtures of atoms and Feshbach molecules [659, 660].
- Impurities of  $^{40}\text{K}$  in a Fermi gas of  $^6\text{Li}$  [661]
- Magnetoassociation used to create singlet-dominated Feshbach molecules, STIRAP transitions found [546].
- Study of other potential STIRAP excited states [662].

## A.3. LiRb

Investigated at University of Tübingen, Purdue University and UC Berkeley. Feshbach resonances located for some isotope combinations, but association of Feshbach molecules not yet achieved due to problems with evaporation and sympathetic cooling.

Quantum statistics: fermionic ( ${}^6\text{Li}{}^{85}\text{Rb}$ ,  ${}^6\text{Li}{}^{87}\text{Rb}$ ), bosonic ( ${}^7\text{Li}{}^{85}\text{Rb}$ ,  ${}^7\text{Li}{}^{87}\text{Rb}$ )

Body-fixed dipole moment: 4.0(1) D [649]

Ground-state rotational constant:  $2B_{\text{rot}} = h \times 13.2\text{GHz}$  [648]

Chemically stable: No

### Relevant references

- Degenerate mixture of  ${}^6\text{Li}+{}^{87}\text{Rb}$  created [663].
- Investigation of Feshbach resonances and Efimov physics, with  ${}^6\text{Li}$  and  ${}^7\text{Li}$  [664–667].
- Photoassociation spectroscopy [668–671].

## A.4. LiCs

Highest body-fixed dipole moment of all alkali dimers, but never created in ground state. Investigated by Matthias Weidemüller's group in Heidelberg and by Cheng Chin's group at the University of Chicago. Difficulties for molecule creation caused by strong mass difference and uncontrollable interspecies interactions. Mixture was found to be ideal for investigation of Efimov physics, so most work in Li+Cs experiments was recently focused on this topic.

Quantum statistics: fermionic ( ${}^6\text{Li}{}^{133}\text{Cs}$ ), bosonic ( ${}^7\text{Li}{}^{133}\text{Cs}$ )

Body-fixed dipole moment: 5.52 D [647] (theory value, to my knowledge the best available experimental data is of insufficient quality.)

Ground-state rotational constant:  $2B_{\text{rot}} = h \times 11.6 \text{ GHz}$  [648]

Chemically stable: No

### Relevant references

- Molecule formation in MOT [672]
- Photoassociation into rovibrational ground state [673]
- Investigation of Feshbach resonances [674, 675]
- Studies of Efimov physics [676–678], see also reviews [679, 680].
- Doubly-degenerate mixture of  ${}^6\text{Li}$  and  ${}^{133}\text{Cs}$  [681].
- Fermion-mediated interactions between bosons in the degenerate mixture [682].

## A.5. NaK

Highest dipole moment among chemically stable fermions. Ground-state fermionic isotopeologue  $^{23}\text{Na}^{40}\text{K}$  produced first by Martin Zwierlein's group at MIT, later also at MPQ and USTC. Ground-state bosonic  $^{23}\text{Na}^{39}\text{K}$  first created in 2020 by Silke Ospelkaus' group at the University of Hannover. Only molecule produced in both a bosonic and a fermionic variant in the ground state so far.

Quantum statistics: fermionic ( $^{23}\text{Na}^{40}\text{K}$ ), bosonic ( $^{23}\text{Na}^{39}\text{K}$ ,  $^{23}\text{Na}^{41}\text{K}$ )

Body-fixed dipole moment: 2.72(6) D [683]

Ground-state rotational constant:  $2B_{\text{rot}} = h \times 5.6434594(20) \text{ GHz}$  [322]

Chemically stable: Yes

### Relevant references

- Studies of mixture and Feshbach resonances [298].
- Feshbach molecules via radiofrequency association [297].
- STIRAP to absolute ground state via  $c^3\Sigma^+ \sim B^1\Pi$  intermediate state [24, 299]. Reference [24] also contains overview of previous spectroscopic studies of NaK.
- Control of rotational and hyperfine levels via microwave excitation [322, 324]
- Systematic characterisation of Feshbach resonances in different spin states [684].
- Alternative STIRAP pathway via  $d^3\Pi \sim D^1\Pi$  intermediate state [524].
- Improvement of rotational coherence times with magic trap [381].
- Creation of ground-state molecules at USTC, using the  $c^3\Sigma^+ \sim B^1\Pi$  STIRAP scheme [526].
- Feshbach resonances between ground-state  $^{23}\text{Na}^{40}\text{K}$  and  $^{40}\text{K}$  atoms discovered and characterised [434, 436, 595]. Creation of Feshbach molecules using such a resonance [435].
- Microwave dressing changes collisional behaviour [685].
- Characterisation of tune-out and magic trapping conditions [553].
- Creation of Feshbach molecules and ground-state molecules of  $^{23}\text{Na}^{39}\text{K}$  at University of Hannover [547, 548, 686–688].

- Joint study of Hannover and Hong Kong teams on two-body loss in chopped dipole traps [405].
- First repulsive box trap of molecules, investigation of two-body loss [307].
- Magnetoassociation and simplified STIRAP [527].
- Hyperfine-dependent atom-molecule collisions [432].
- The role of many-body physics in magnetoassociation of degenerate Bose–Fermi mixtures [387].
- Three-body losses in atomic mixtures [386].
- Microwave shielding and evaporative cooling of ground-state  $^{23}\text{Na}^{40}\text{K}$  [596].

## A.6. NaRb

First creation of Feshbach molecules and STIRAP done by Dajun Wang's group at Chinese University of Hong Kong. Recently, the first molecular quantum-gas microscope was constructed by Waseem Bakr's group at Princeton using this species.

Quantum statistics: bosonic ( $^{23}\text{Na}^{85}\text{Rb}$ ,  $^{23}\text{Na}^{87}\text{Rb}$ )

Body-fixed dipole moment: 3.1(3) D [649]

Ground-state rotational constant:  $2B_{\text{rot}} = h \times 4.179\,325\,6(8)$  GHz [323]

Chemically stable: Yes

### Relevant references

- Doubly-degenerate mixture [689].
- Feshbach molecules via magnetoassociation [300].
- STIRAP to absolute ground state [301, 302].
- Demonstration of control over vibrational, rotational and hyperfine states, using STIRAP and microwave addressing [323].
- Studies of collision behaviour and its dependence on dipole moment and rotational states [388, 389, 690].
- Observation of collision resonances between Feshbach molecules [691].
- Imaging after photodisassociation [692].
- Joint study with Hannover team on two-body loss in chopped dipole traps [405].
- Spectroscopy of rovibrational ground state of  $b^3\Pi$  potential [693].
- Magic trapping for two rotational states in 1064-nm dipole trap [694].
- Long coherence time for hyperfine superpositions [380].
- First single-site resolved imaging of Feshbach molecules on a lattice demonstrated at Princeton [514].

## A.7. NaCs

Second-largest dipole moment among bialkali molecules. Created in ground state by Kang-Kuen Ni's group at Harvard by combining single atoms in optical tweezers. Association in free space by Sebastian Will's group at Columbia University.

Quantum statistics: bosonic ( $^{23}\text{Na}^{133}\text{Cs}$ )

Body-fixed dipole moment: 4.75(20) D [649]

Ground-state rotational constant:  $2B_{\text{rot}} = h \times 3.56 \text{ GHz}$  [648]

Chemically stable: Yes

### Relevant references

- Photoassociation experiments [174, 695, 696].
- Spectroscopic studies with ultracold samples [697].
- Combining one atom of each species in optical tweezer, subsequent magnetoassociation [365, 366, 368].
- Two-photon photoassociation in tweezer [369].
- Ground-state molecules via magnetoassociation and off-resonant Raman scattering [370].
- Free-space association from thermal gases and from overlapping BECs [512, 513].

## A.8. KRb

Mixture was investigated thoroughly already in the early 2000s. First ground-state molecule of  $^{40}\text{K}^{87}\text{Rb}$  created by Jun Ye's group at JILA in 2008. Since then, molecules studied there in two generations of experimental machines, many impressive successes. Also used by Kang-Kuen Ni's group at Harvard for studies of reactive collisions. Bosonic isotopologue  $^{41}\text{K}^{87}\text{Rb}$  created in ground state by Inouye group in Tokyo, but never reached ultracold temperatures.

Quantum statistics: fermionic ( $^{40}\text{K}^{85}\text{Rb}$ ,  $^{40}\text{K}^{87}\text{Rb}$ ), bosonic ( $^{39}\text{K}^{85}\text{Rb}$ ,  $^{39}\text{K}^{87}\text{Rb}$ ,  $^{41}\text{K}^{85}\text{Rb}$ ,  $^{41}\text{K}^{87}\text{Rb}$ )

Body-fixed dipole moment: 0.574(17) D [229]

Ground-state rotational constant:  $2B_{\text{rot}} = h \times 2.22790(1)$  GHz [230]

Chemically stable: No

### Relevant references

- Early photoassociation experiments with different isotopologues [168, 170–172].
- Studies of mixture and Feshbach resonances between 2002 and 2007 [164, 193–197, 201–203]
- Feshbach molecules in optical lattice via radiofrequency association [199].
- Feshbach molecules in dipole trap via radiofrequency association [225, 227].
- First STIRAP to absolute ground state, first ultracold molecule gas [27, 232, 698].
- Feshbach molecules of  $^{41}\text{K}^{87}\text{Rb}$  via new magnetic-field modulation technique [699].
- Rovibrational ground-state  $^{41}\text{K}^{87}\text{Rb}$  reached via photoassociation and STIRAP directly from MOT [236, 237].
- Photoassociation studies on  $^{39}\text{K}^{85}\text{Rb}$  [700].
- First studies of ultracold molecule collisions [233–235].
- Direct imaging of molecules [231].
- Ground-state molecules in 3D lattice, using magnetoassociation + STIRAP [308, 309].
- Improved magnetoassociation procedures [701].

- Coupling between trapping light and rotational structure [319].
- Studies of dynamics in lattice [310, 702].
- Preliminary investigations of direct molecule cooling [575].
- Simultaneous BEC of  $^{41}\text{K}$  and  $^{87}\text{Rb}$  [703].
- Variation of electron-proton mass ratio measured with factor 5 increased precision [475].
- First Fermi-degenerate molecules, but in non-thermal state [384, 385].
- First observation of products of ultracold collisions using ionisation and mass spectroscopy, studies on collision dynamics [403, 404, 591, 592, 594].
- First successful evaporation of ground-state molecules, using dipolar repulsion to avoid loss [414].
- Improvement of dipolar repulsion using rotational resonances [420]. Evaporative cooling in 3D demonstrated with this method [419].
- Reactions between molecules in multiple layers of a lattice [626].

## A.9. KCs

Only chemically stable fermionic bialikali species except NaK. Investigated at Hanns-Christoph N  gerl's group in Innsbruck. Doubly-degenerate mixture created with complex mixing scheme to avoid miscibility problems. STIRAP planned, but not yet demonstrated. New machine under construction in Simon Cornish's group at University of Durham.

Quantum statistics: fermionic ( $^{40}\text{K}^{133}\text{Cs}$ ), bosonic ( $^{39}\text{K}^{133}\text{Cs}$ ,  $^{41}\text{K}^{133}\text{Cs}$ )

Body-fixed dipole moment: 1.906 D [647] (theory value, to my knowledge the best available experimental data is of insufficient quality.)

Ground-state rotational constant:  $2B_{\text{rot}} = h \times 1.86 \text{ GHz}$  [648]

Chemically stable: Yes

### Relevant references

- Creation of doubly-degenerate mixture [704].
- Theoretical investigation of STIRAP [705].
- Observation of Feshbach resonances [706].

## A.10. RbCs

Second ultracold molecule and first bosonic one to be transferred to the ground state in 2014, after a long period of investigating mixture properties and Feshbach resonances. Ground-state  $^{87}\text{Rb}^{133}\text{Cs}$  successfully created within short time both in Hanns-Christoph Nägele's group (Innsbruck) and Simon Cornish's group (Durham). Important discoveries have been made with this species, including the first observation of reduced sticky-collision loss in a chopped trap.

Quantum statistics: bosonic ( $^{85}\text{Rb}^{133}\text{Cs}$ ,  $^{87}\text{Rb}^{133}\text{Cs}$ )

Body-fixed dipole moment: 1.17(6) D [293]

Ground-state rotational constant:  $2B_{\text{rot}} = h \times 0.980\,347\,988(90)$  GHz [321]

Chemically stable: Yes

### Relevant references

- Photoassociative production of molecules [173, 707–709].
- Two-pulse photoassociation into rovibrational ground state of  $X^1\Sigma^+$  [190].
- Investigation of Feshbach resonances [287].
- Creation of ultracold mixtures and molecular spectroscopy in preparation for ultracold ground-state molecules is done in parallel in Innsbruck and Durham [286, 288–290].
- Feshbach molecules via magnetoassociation [290–292].
- STIRAP to absolute ground state demonstrated via intermediate  $b^3\Pi_1 \sim A^1\Sigma^+$  state [293, 294].
- Details about STIRAP laser system and the transfer path [296, 551].
- Photoassociation spectroscopy of  $^{85}\text{Rb}^{133}\text{Cs}$  [710].
- Microwave addressing of rotational and hyperfine levels [321].
- Lattice scheme for efficient creation of molecules at low temperature [295].
- Coupling between trapping light, microwave fields and rotational structure [572, 573, 711, 712].
- Sticky collisions observed, reduction of loss rate seen in chopped dipole trap [390, 401].

- Photoassociation of  $^{85}\text{Rb}^{133}\text{Cs}$ ; microwave addressing of rotational states of this isotopologue [713].
- Long coherence time of hyperfine superpositions [379].
- Controlled production of atom pair in tweezer [714].
- Sticky collisions between multiple hyperfine levels and with atoms [402].

## B. Theory of dipolar many-body systems

**Table B.1.:** Theoretical investigations about quantum many-body systems with dipolar interactions. Note that for spin models, where particles can not tunnel, the quantum statistics typically do not matter. See also the overview articles by Baranov *et al.* [15], Trefzger *et al.* [715], and Dutta *et al.* [633]. Continued in Table B.2.

Geometry	Bosons	Fermions	Spin models
1D tube(s)	Dalla Torre <i>et al.</i> (2006) [716], Batrauni <i>et al.</i> (2006) [717], Sinha and Santos (2007) [718], Ruhman <i>et al.</i> (2012) [719], Rossini and Fazio (2012) [720], Knap <i>et al.</i> (2012) [721], Gammelmark and Zinner (2013) [722], Cartarius <i>et al.</i> (2017) [723], Biedron <i>et al.</i> (2018) [724], Hayashi <i>et al.</i> (2021) [725], Kraus <i>et al.</i> (2021) [726],	Quintanilla <i>et al.</i> (2009) [727], Huang and Wang (2009) [728], Carr <i>et al.</i> (2010) [729], Knap <i>et al.</i> (2012) [721]	Zhou <i>et al.</i> (2011) [730],
2D plane	Micheli <i>et al.</i> (2007) [206], Büchler <i>et al.</i> (2007) [204], Astrakharchik <i>et al.</i> (2007) [205], Mora <i>et al.</i> (2007) [731], Pupillo <i>et al.</i> (2008) [207], Macia <i>et al.</i> (2014) [732], Lechner <i>et al.</i> (2014) [619], Bruun and Nelson (2014) [618], Lu <i>et al.</i> (2015) [733], Bombin <i>et al.</i> (2019) [624], Cinti <i>et al.</i> (2020) [625], Shen and Quader (2021) [734]	Bruun and Taylor (2008) [209], Cooper and Shlyapnikov (2009) [645], Yamaguchi <i>et al.</i> (2010) [621], Sun <i>et al.</i> (2010) [620], Levinsen <i>et al.</i> (2011) [646], Matveeva and Giorgini (2012) [617], Lu and Shlyapnikov (2012) [735], Wu <i>et al.</i> (2015) [622], Wu <i>et al.</i> (2016) [623], Comparin <i>et al.</i> (2019) [736]	Bilitewski <i>et al.</i> (2021) [737]

**Table B.2.:** Continued from Table B.1.

Geometry	Bosons	Fermions	Spin models
Square lattice	Goral <i>et al.</i> (2002) [144], Sengupta <i>et al.</i> (2005) [738], Barnett <i>et al.</i> (2006) [739], Schmidt <i>et al.</i> (2008) [740], Danshita and Sá de Melo (2009) [741], Capogrosso-Sansone <i>et al.</i> (2010) [635], Sowiński <i>et al.</i> (2012) [632], Yao <i>et al.</i> (2011) [742], Bandyopadhyay <i>et al.</i> (2019) [636], Zhang <i>et al.</i> (2022) [743] Lake <i>et al.</i> (2022) [744]	Quintanilla <i>et al.</i> (2009) [727], Lin <i>et al.</i> (2010) [745], Mikelsons and Freericks (2011) [637], Kuns <i>et al.</i> (2011) [746], He and Hofstetter <i>et al.</i> (2011) [747], Gorshkov <i>et al.</i> (2011) [748, 749], Gadsbølle and Bruun (2012) [638], Gadsbølle and Bruun (2012) [639], Bhongale <i>et al.</i> (2012) [750], Bhongale <i>et al.</i> (2013) [751], Dutta <i>et al.</i> (2013) [752], van Loon <i>et al.</i> (2015) [640], Fedorov <i>et al.</i> (2016) [641]	Micheli <i>et al.</i> (2006) [212], Brennen <i>et al.</i> (2007) [753], Weimer (2011) [754], Peter <i>et al.</i> (2012) [630], Manmana <i>et al.</i> (2013) [755], Kwasigroch and Cooper (2014) [627], Kwasigroch and Cooper (2017) [628]
Triang. / hex. lat.	Pollet <i>et al.</i> (2010) [756], Yamamoto <i>et al.</i> (2012) [757]		Micheli <i>et al.</i> (2006) [212], Gorshkov <i>et al.</i> (2013) [758], Yao <i>et al.</i> (2018) [759], Fukui <i>et al.</i> (2022) [760]
Free space / 3D trap	Marinescu and You (1998) [140], Góral <i>et al.</i> (2000) [761], Santos <i>et al.</i> (2000) [141], Yi and You (2000) [142], Santos <i>et al.</i> (2003) [143], Schmidt <i>et al.</i> (2022) [762]	You and Marinescu (1999) [149], Baranov <i>et al.</i> (2002) [763], Miyakawa <i>et al.</i> (2008) [208], Fregoso <i>et al.</i> (2009) [764], Sun <i>et al.</i> (2010) [620], Lima and Pelster (2010) [765], Shi <i>et al.</i> (2010) [766], Zhao <i>et al.</i> (2010) [767], Wächtler <i>et al.</i> (2017) [768], Veljic <i>et al.</i> (2017) [616], Veljic <i>et al.</i> (2019) [769]	
Multiple 2D planes	Wang <i>et al.</i> (2006) [770] Lechner and Zoller (2013) [771]	Potter <i>et al.</i> (2010) [772], Pikovski <i>et al.</i> (2010) [643], Block <i>et al.</i> (2012) [773], Fedorov <i>et al.</i> (2016) [641]	
Multiple square lattices	Trefzger <i>et al.</i> (2009) [774]	Camacho-Guardian and Paredes (2015) [644], Domínguez-Castro and Paredes (2020) [775]	
3D lattice	Schuster <i>et al.</i> (2021) [776], Schuster <i>et al.</i> (2021) [777]	Zeng and Yin (2014) [642], Lake <i>et al.</i> (2022) [744]	Hazzard <i>et al.</i> (2014) [320]

# Bibliography

- [1] M. Nič, J. Jirát, B. Košata, A. Jenkins, and A. McNaught, eds. *IUPAC Compendium of Chemical Terminology*. IUPAC, 2009. DOI: [10.1351/goldbook](https://doi.org/10.1351/goldbook) (cit. on p. 1).
- [2] P. R. Bunker. “The Electronic Isotope Shift in Diatomic Molecules and the Partial Breakdown of the Born-Oppenheimer Approximation”. *J. Mol. Spectrosc.* (1968) (cit. on p. 1).
- [3] H. Lefebvre-Brion and R. W. Field. *The Spectra and Dynamics of Diatomic Molecules*. Elsevier, 2004 (cit. on pp. 1, 15, 17, 20, 93).
- [4] H. J. Wörner and F. Merkt. “Fundamentals of Electronic Spectroscopy”. In: *Handbook of High-resolution Spectroscopy*. John Wiley & Sons, 2011 (cit. on pp. 3, 9, 14, 15, 17, 18).
- [5] G. Herzberg. *Molecular Spectra and Molecular Structure I: Spectra of Diatomic Molecules*. D. Van Nostrand, 1950 (cit. on pp. 9, 15, 20).
- [6] W. Demtröder. *Molekülphysik*. Oldenbourg Verlag, 2003 (cit. on p. 9).
- [7] C. P. Koch, M. Lemeshko, and D. Sugny. “Quantum control of molecular rotation”. *Rev. Mod. Phys.* 91 (2019), p. 035005. DOI: [10.1103/revmodphys.91.035005](https://doi.org/10.1103/revmodphys.91.035005) (cit. on p. 9).
- [8] F. W. Byron and R. W. Fuller. *Mathematics of classical and quantum physics*. Dover Publications, New York, 1992 (cit. on p. 9).
- [9] J. Reinholt. *Quantentheorie der Moleküle*. Vieweg+Teubner Verlag, 2004. DOI: [10.1007/978-3-663-05739-0](https://doi.org/10.1007/978-3-663-05739-0) (cit. on pp. 9, 11).
- [10] R. S. Mulliken. “Report on Notation for Spectra of Diatomic Molecules”. *Phys. Rev.* 36 (1930), pp. 611–629 (cit. on p. 15).
- [11] J. T. Hougen. *The calculation of rotational energy levels and rotational line intensities in diatomic molecules*. National Bureau of Standards, 1970. DOI: [10.6028/NBS.MONO.115](https://doi.org/10.6028/NBS.MONO.115) (cit. on pp. 15, 20).
- [12] E. Nikitin and R. Zare. “Correlation diagrams for Hund’s coupling cases in diatomic molecules with high rotational angular momentum”. *Mol. Phys.* 82 (1994), pp. 85–100. DOI: [10.1080/00268979400100074](https://doi.org/10.1080/00268979400100074) (cit. on pp. 17, 19).
- [13] B. H. Bransden and C. J. Joachain. *Physics of atoms and molecules*. Prentice Hall, 2003 (cit. on p. 17).
- [14] R. G. Littlejohn. *The Stark Effect in Hydrogen and Alkali Atoms*. Lecture Notes, UC Berkeley. 2020 (cit. on p. 19).
- [15] M. A. Baranov, M. Dalmonte, G. Pupillo, and P. Zoller. “Condensed Matter Theory of Dipolar Quantum Gases”. *Chem. Rev.* 112 (2012), pp. 5012–5061. DOI: [10.1021/cr2003568](https://doi.org/10.1021/cr2003568) (cit. on pp. 21, 156, 181).

- [16] D. Hoffmann. “Johannes Stark – eine Persönlichkeit im Spannungsfeld von wissenschaftlicher Forschung und faschistischer Ideologie”. *Philosophie und Naturwissenschaften in Vergangenheit und Gegenwart* 22 (1982), pp. 90–100 (cit. on p. 22).
- [17] J. Stark. “The Pragmatic and the Dogmatic Spirit in Physics”. *Nature* 141 (1938), pp. 770–772 (cit. on p. 22).
- [18] W. Klemperer, K. K. Lehmann, J. K. G. Watson, and S. C. Wofsy. “Can molecules have permanent electric dipole moments?” *J. Phys. Chem.* 97 (1993), pp. 2413–2416. DOI: [10.1021/j100112a049](https://doi.org/10.1021/j100112a049) (cit. on p. 22).
- [19] M. Aymar and O. Dulieu. “Calculations of transition and permanent dipole moments of heteronuclear alkali dimers NaK, NaRb and NaCs”. *Mol. Phys.* 105 (2007), pp. 1733–1742. DOI: [10.1080/00268970701494016](https://doi.org/10.1080/00268970701494016) (cit. on pp. 26, 167).
- [20] I. Russier-Antoine, A. J. Ross, M. Aubert-Frécon, F. Martin, and P. Crozet. “An improved potential energy curve for the ground state of NaK”. *J. Phys. B: At., Mol. Opt. Phys.* 33 (2000), pp. 2753–2762. DOI: [10.1088/0953-4075/33/14/312](https://doi.org/10.1088/0953-4075/33/14/312) (cit. on p. 25).
- [21] A. Gerdes, M. Hobein, H. Knöckel, and E. Tiemann. “Ground state potentials of the NaK molecule”. *Eur. Phys. J. D* 49 (2008), pp. 67–73. DOI: [10.1140/epjd/e2008-00138-7](https://doi.org/10.1140/epjd/e2008-00138-7) (cit. on p. 25).
- [22] I. Temelkov, H. Knöckel, A. Pashov, and E. Tiemann. “Molecular beam study of the  $a^3\Sigma^+$  state of NaK up to the dissociation limit”. *Phys. Rev. A* 91 (2015), p. 032512. DOI: [10.1103/PhysRevA.91.032512](https://doi.org/10.1103/PhysRevA.91.032512) (cit. on p. 25).
- [23] H. Harker, P. Crozet, A. J. Ross, K. Richter, J. Jones, C. Faust, J. Huennekens, A. V. Stolyarov, H. Salami, and T. Bergeman. “Experimental and theoretical studies of the coupled  $A^1\Sigma^+$  and  $b^3\Pi$  states of NaK”. *Phys. Rev. A* 92 (2015), p. 012506. DOI: [10.1103/PhysRevA.92.012506](https://doi.org/10.1103/PhysRevA.92.012506) (cit. on pp. 25, 95).
- [24] J. W. Park, S. A. Will, and M. W. Zwierlein. “Two-photon pathway to ultracold ground state molecules of  $^{23}\text{Na}^{40}\text{K}$ ”. *New J. Phys.* 17 (2015), p. 075016. DOI: [10.1088/1367-2630/17/7/075016](https://doi.org/10.1088/1367-2630/17/7/075016) (cit. on pp. 25, 58, 72, 77, 83, 85, 86, 89, 172).
- [25] E. W. Streed, A. P. Chikkatur, T. L. Gustavson, M. Boyd, Y. Torii, D. Schneble, G. K. Campbell, D. E. Pritchard, and W. Ketterle. “Large atom number Bose-Einstein condensate machines”. *Rev. Sci. Instrum.* 77 (2006), p. 023106. DOI: [10.1063/1.2163977](https://doi.org/10.1063/1.2163977) (cit. on p. 25).
- [26] K. M. R. van der Stam, E. D. van Ooijen, R. Meppelink, J. M. Vogels, and P. van der Straten. “Large atom number Bose-Einstein condensate of sodium”. *Rev. Sci. Instrum.* 78 (2007), p. 013102. DOI: [10.1063/1.2424439](https://doi.org/10.1063/1.2424439) (cit. on p. 25).
- [27] K.-K. Ni, S. Ospelkaus, M. H. G. de Miranda, A. Pe’er, B. Neyenhuis, J. J. Zirbel, S. Kotochigova, P. S. Julienne, D. S. Jin, and J. Ye. “A High Phase-Space-Density Gas of Polar Molecules”. *Science* 322 (2008), pp. 231–235. DOI: [10.1126/science.1163861](https://doi.org/10.1126/science.1163861) (cit. on pp. 29, 49, 50, 89, 176).
- [28] J. C. Slater. *Introduction to Chemical Physics*. McGraw-Hill Book Company, Inc., 1939 (cit. on p. 29).
- [29] J. P. Gordon, H. J. Zeiger, and C. H. Townes. “The Maser—New Type of Microwave Amplifier, Frequency Standard, and Spectrometer”. *Phys. Rev.* 99 (1955), pp. 1264–1274 (cit. on p. 30).
- [30] C. H. Townes. *Production of Coherent Radiation by Atoms and Molecules*. Nobel Lecture at NobelPrize.org. <https://www.nobelprize.org/prizes/physics/1964/townes/lecture/>. 1964 (cit. on p. 30).
- [31] B. Friedrich and H. Schmidt-Böcking, eds. *Molecular Beams in Physics and Chemistry*. Springer International Publishing, 2021. DOI: [10.1007/978-3-030-63963-1](https://doi.org/10.1007/978-3-030-63963-1) (cit. on p. 30).
- [32] S. Y. T. van de Meerakker, H. L. Bethlem, and G. Meijer. “Taming molecular beams”. *Nat. Phys.* 4 (2008), pp. 595–602. DOI: [10.1038/nphys1031](https://doi.org/10.1038/nphys1031) (cit. on pp. 30, 36).

- [33] S. Y. T. van de Meerakker, H. L. Bethlem, N. Vanhaecke, and G. Meijer. “Manipulation and Control of Molecular Beams”. *Chem. Rev.* 112 (2012), pp. 4828–4878 (cit. on pp. 30, 36).
- [34] M. Lemeshko, R. V. Krems, J. M. Doyle, and S. Kais. “Manipulation of molecules with electromagnetic fields”. *Mol. Phys.* 111 (2013), pp. 1648–1682. DOI: [10.1080/00268976.2013.813595](https://doi.org/10.1080/00268976.2013.813595) (cit. on p. 30).
- [35] S. Chu, L. Hollberg, J. E. Bjorkholm, A. Cable, and A. Ashkin. “Three-dimensional viscous confinement and cooling of atoms by resonance radiation pressure”. *Phys. Rev. Lett.* 55 (1985), pp. 48–51. DOI: [10.1103/PhysRevLett.55.48](https://doi.org/10.1103/PhysRevLett.55.48) (cit. on p. 31).
- [36] W. D. Phillips and H. Metcalf. “Laser Deceleration of an Atomic Beam”. *Phys. Rev. Lett.* 48 (1982), pp. 596–599. DOI: [10.1103/PhysRevLett.48.596](https://doi.org/10.1103/PhysRevLett.48.596) (cit. on p. 31).
- [37] E. L. Raab, M. Prentiss, A. Cable, S. Chu, and D. E. Pritchard. “Trapping of Neutral Sodium Atoms with Radiation Pressure”. *Phys. Rev. Lett.* 59 (1987), pp. 2631–2634. DOI: [10.1103/PhysRevLett.59.2631](https://doi.org/10.1103/PhysRevLett.59.2631) (cit. on p. 31).
- [38] S. Chu. *The Manipulation of Neutral Particles*. Nobel Lecture at NobelPrize.org. <https://www.nobelprize.org/prizes/physics/1997/chu/lecture/>. 1997 (cit. on p. 31).
- [39] W. D. Phillips. “Nobel Lecture: Laser cooling and trapping of neutral atoms”. *Rev. Mod. Phys.* 70 (1998), pp. 721–741. DOI: [10.1103/RevModPhys.70.721](https://doi.org/10.1103/RevModPhys.70.721) (cit. on p. 31).
- [40] W. Ketterle. “Nobel lecture: When atoms behave as waves: Bose-Einstein condensation and the atom laser”. *Rev. Mod. Phys.* 74 (2002), pp. 1131–1151. DOI: [10.1103/RevModPhys.74.1131](https://doi.org/10.1103/RevModPhys.74.1131) (cit. on p. 31).
- [41] W. Ketterle, D. Durfee, and D. Stamper-Kurn. *Making, probing and understanding Bose-Einstein condensates*. 1999. arXiv: [cond-mat/9904034](https://arxiv.org/abs/cond-mat/9904034) (cit. on p. 31).
- [42] H. J. Metcalf and P. van der Straten. *Laser Cooling and Trapping of Neutral Atoms*. American Cancer Society, 2007. DOI: [10.1002/9783527600441.oe005](https://doi.org/10.1002/9783527600441.oe005). eprint: <https://onlinelibrary.wiley.com/doi/10.1002/9783527600441.oe005> (cit. on p. 31).
- [43] W. Ketterle and M. W. Zwierlein. *Making, probing and understanding ultracold Fermi gases*. 2008. arXiv: [0801.2500](https://arxiv.org/abs/0801.2500) (cit. on p. 31).
- [44] C. J. Pethick and H. Smith. *Bose-Einstein Condensation in Dilute Gases*. Cambridge University Press, 2008. DOI: [10.1017/cbo9780511802850](https://doi.org/10.1017/cbo9780511802850) (cit. on pp. 31, 38).
- [45] H. R. Thorsheim, J. Weiner, and P. S. Julienne. “Laser-induced photoassociation of ultracold sodium atoms”. *Phys. Rev. Lett.* 58 (1987), pp. 2420–2423. DOI: [10.1103/PhysRevLett.58.2420](https://doi.org/10.1103/PhysRevLett.58.2420) (cit. on pp. 31, 32).
- [46] P. L. Gould, P. D. Lett, P. S. Julienne, W. D. Phillips, H. R. Thorsheim, and J. Weiner. “Observation of associative ionization of ultracold laser-trapped sodium atoms”. *Phys. Rev. Lett.* 60 (1988), pp. 788–791. DOI: [10.1103/PhysRevLett.60.788](https://doi.org/10.1103/PhysRevLett.60.788) (cit. on p. 31).
- [47] A. L. Migdall, J. V. Prodan, W. D. Phillips, T. H. Bergeman, and H. J. Metcalf. “First Observation of Magnetically Trapped Neutral Atoms”. *Phys. Rev. Lett.* 54 (1985), pp. 2596–2599. DOI: [10.1103/PhysRevLett.54.2596](https://doi.org/10.1103/PhysRevLett.54.2596) (cit. on p. 31).
- [48] S. Chu, J. E. Bjorkholm, A. Ashkin, and A. Cable. “Experimental Observation of Optically Trapped Atoms”. *Phys. Rev. Lett.* 57 (1986), pp. 314–317. DOI: [10.1103/PhysRevLett.57.314](https://doi.org/10.1103/PhysRevLett.57.314) (cit. on p. 31).
- [49] J. Prodan, A. Migdall, W. D. Phillips, I. So, H. Metcalf, and J. Dalibard. “Stopping Atoms with Laser Light”. *Phys. Rev. Lett.* 54 (1985), pp. 992–995. DOI: [10.1103/PhysRevLett.54.992](https://doi.org/10.1103/PhysRevLett.54.992) (cit. on p. 31).

- [50] W. Ertmer, R. Blatt, J. L. Hall, and M. Zhu. “Laser Manipulation of Atomic Beam Velocities: Demonstration of Stopped Atoms and Velocity Reversal”. *Phys. Rev. Lett.* 54 (1985), pp. 996–999. DOI: [10.1103/PhysRevLett.54.996](https://doi.org/10.1103/PhysRevLett.54.996) (cit. on p. 31).
- [51] P. S. Julienne and J. Vigu  . “Cold collisions of ground- and excited-state alkali-metal atoms”. *Phys. Rev. A* 44 (1991), pp. 4464–4485. DOI: [10.1103/PhysRevA.44.4464](https://doi.org/10.1103/PhysRevA.44.4464) (cit. on p. 32).
- [52] E. Tiesinga, B. J. Verhaar, and H. T. C. Stoof. “Threshold and resonance phenomena in ultracold ground-state collisions”. *Phys. Rev. A* 47 (1993), pp. 4114–4122. DOI: [10.1103/PhysRevA.47.4114](https://doi.org/10.1103/PhysRevA.47.4114) (cit. on pp. 32, 34).
- [53] P. D. Lett, K. Helmerson, W. D. Phillips, L. P. Ratliff, S. L. Rolston, and M. E. Wagshul. “Spectroscopy of Na<sub>2</sub> by photoassociation of laser-cooled Na”. *Phys. Rev. Lett.* 71 (1993), pp. 2200–2203. DOI: [10.1103/PhysRevLett.71.2200](https://doi.org/10.1103/PhysRevLett.71.2200) (cit. on p. 32).
- [54] J. D. Miller, R. A. Cline, and D. J. Heinzen. “Photoassociation spectrum of ultracold Rb atoms”. *Phys. Rev. Lett.* 71 (1993), pp. 2204–2207. DOI: [10.1103/PhysRevLett.71.2204](https://doi.org/10.1103/PhysRevLett.71.2204) (cit. on p. 32).
- [55] C. J. Williams and P. S. Julienne. “Molecular hyperfine structure in the photoassociation spectroscopy of laser cooled atoms”. *J. Chem. Phys.* 101 (1994), pp. 2634–2637. DOI: [10.1063/1.467637](https://doi.org/10.1063/1.467637) (cit. on p. 33).
- [56] W. I. McAlexander, E. R. I. Abraham, N. W. M. Ritchie, C. J. Williams, H. T. C. Stoof, and R. G. Hulet. “Precise atomic radiative lifetime via photoassociative spectroscopy of ultracold lithium”. *Phys. Rev. A* 51 (1995), R871–R874 (cit. on p. 33).
- [57] H. Wang, P. L. Gould, and W. C. Stwalley. “Photoassociative spectroscopy of ultracold <sup>39</sup>K atoms in a high-density vapor-cell magneto-optical trap”. *Phys. Rev. A* 53 (1996), R1216–R1219. DOI: [10.1103/PhysRevA.53.R1216](https://doi.org/10.1103/PhysRevA.53.R1216) (cit. on p. 33).
- [58] E. R. I. Abraham, W. I. McAlexander, C. A. Sackett, and R. G. Hulet. “Spectroscopic Determination of the s-Wave Scattering Length of Lithium”. *Phys. Rev. Lett.* 74 (1995), pp. 1315–1318. DOI: [10.1103/PhysRevLett.74.1315](https://doi.org/10.1103/PhysRevLett.74.1315) (cit. on p. 33).
- [59] K. M. Jones, S. Maleki, L. P. Ratliff, and P. D. Lett. “Two-colour photoassociation spectroscopy of ultracold sodium”. *J. Phys. B: At., Mol. Opt. Phys.* 30 (1997), pp. 289–308. DOI: [10.1088/0953-4075/30/2/021](https://doi.org/10.1088/0953-4075/30/2/021) (cit. on p. 33).
- [60] C. C. Tsai, R. S. Freeland, J. M. Vogels, H. M. J. M. Boesten, B. J. Verhaar, and D. J. Heinzen. “Two-Color Photoassociation Spectroscopy of Ground State Rb<sub>2</sub>”. *Phys. Rev. Lett.* 79 (1997), pp. 1245–1248. DOI: [10.1103/PhysRevLett.79.1245](https://doi.org/10.1103/PhysRevLett.79.1245) (cit. on p. 33).
- [61] P. D. Lett, P. S. Julienne, and W. D. Phillips. “Photoassociative Spectroscopy of Laser-cooled atoms”. *Annu. Rev. Phys. Chem.* (1995) (cit. on p. 33).
- [62] W. C. Stwalley and H. Wang. “Photoassociation of Ultracold Atoms: A New Spectroscopic Technique”. *J. Mol. Spectrosc.* 195 (1999), pp. 194–228. DOI: [10.1006/jmsp.1999.7838](https://doi.org/10.1006/jmsp.1999.7838) (cit. on pp. 33, 36).
- [63] J. Weiner, V. S. Bagnato, S. Zilio, and P. S. Julienne. “Experiments and theory in cold and ultracold collisions”. *Rev. Mod. Phys.* 71 (1999), pp. 1–85. DOI: [10.1103/RevModPhys.71.1](https://doi.org/10.1103/RevModPhys.71.1) (cit. on pp. 33, 34, 139).
- [64] J. T. Bahns, W. C. Stwalley, and P. L. Gould. “Laser cooling of molecules: A sequential scheme for rotation, translation, and vibration”. *J. Chem. Phys.* 104 (1996), pp. 9689–9697. DOI: [10.1063/1.471731](https://doi.org/10.1063/1.471731) (cit. on p. 33).
- [65] J. M. Doyle, B. Friedrich, J. Kim, and D. Patterson. “Buffer-gas loading of atoms and molecules into a magnetic trap”. *Phys. Rev. A* 52 (1995), R2515–R2518. DOI: [10.1103/PhysRevA.52.R2515](https://doi.org/10.1103/PhysRevA.52.R2515) (cit. on p. 33).

- [66] Y. B. Band and P. S. Julienne. “Ultracold-molecule production by laser-cooled atom photoassociation”. *Phys. Rev. A* 51 (1995), R4317–R4320. DOI: [10.1103/PhysRevA.51.R4317](https://doi.org/10.1103/PhysRevA.51.R4317) (cit. on p. 33).
- [67] R. Côté and A. Dalgarno. “Mechanism for the production of vibrationally excited ultracold molecules of  $^7\text{Li}_2$ ”. *Chem. Phys. Lett.* 279 (1997), pp. 50–54. DOI: [10.1016/S0009-2614\(97\)00937-8](https://doi.org/10.1016/S0009-2614(97)00937-8) (cit. on p. 33).
- [68] H. Metcalf. “Colloquium: Strong optical forces on atoms in multifrequency light”. *Rev. Mod. Phys.* 89 (2017), p. 041001. DOI: [10.1103/RevModPhys.89.041001](https://doi.org/10.1103/RevModPhys.89.041001) (cit. on p. 33).
- [69] J. D. Weinstein, R. deCarvalho, T. Guillet, B. Friedrich, and J. M. Doyle. “Magnetic trapping of calcium monohydride molecules at millikelvin temperatures”. *Nature* 395 (1998), pp. 148–150. DOI: [10.1038/25949](https://doi.org/10.1038/25949) (cit. on pp. 33, 34).
- [70] A. Fioretti, D. Comparat, A. Crubellier, O. Dulieu, F. Masnou-Seeuws, and P. Pillet. “Formation of Cold  $\text{Cs}_2$  Molecules through Photoassociation”. *Phys. Rev. Lett.* 80 (1998), pp. 4402–4405. DOI: [10.1103/PhysRevLett.80.4402](https://doi.org/10.1103/PhysRevLett.80.4402) (cit. on p. 33).
- [71] T. Takekoshi, B. M. Patterson, and R. J. Knize. “Observation of Optically Trapped Cold Cesium Molecules”. *Phys. Rev. Lett.* 81 (1998), pp. 5105–5108. DOI: [10.1103/PhysRevLett.81.5105](https://doi.org/10.1103/PhysRevLett.81.5105) (cit. on p. 33).
- [72] T. Takekoshi, B. M. Patterson, and R. J. Knize. “Observation of cold ground-state cesium molecules produced in a magneto-optical trap”. *Phys. Rev. A* 59 (1999), R5–R7. DOI: [10.1103/PhysRevA.59.R5](https://doi.org/10.1103/PhysRevA.59.R5) (cit. on p. 33).
- [73] R. Grimm, M. Weidemüller, and Y. B. Ovchinnikov. “Optical Dipole Traps for Neutral Atoms”. In: *Advances In Atomic, Molecular, and Optical Physics*. Elsevier, 2000, pp. 95–170. DOI: [10.1016/s1049-250x\(08\)60186-x](https://doi.org/10.1016/s1049-250x(08)60186-x) (cit. on pp. 33, 93, 101).
- [74] N. Balakrishnan, R. C. Forrey, and A. Dalgarno. “Quenching of  $\text{H}_2$  Vibrations in Ultracold  $^3\text{He}$  and  $^4\text{He}$  Collisions”. *Phys. Rev. Lett.* 80 (1998), pp. 3224–3227. DOI: [10.1103/PhysRevLett.80.3224](https://doi.org/10.1103/PhysRevLett.80.3224) (cit. on p. 34).
- [75] N. Balakrishnan and A. Dalgarno. “Chemistry at ultracold temperatures”. *Chem. Phys. Lett.* 341 (2001), pp. 652–656. DOI: [10.1016/S0009-2614\(01\)00515-2](https://doi.org/10.1016/S0009-2614(01)00515-2) (cit. on p. 34).
- [76] S. Inouye, M. R. Andrews, J. Stenger, H.-J. Miesner, D. M. Stamper-Kurn, and W. Ketterle. “Observation of Feshbach resonances in a Bose–Einstein condensate”. *Nature* 392 (1998), pp. 151–154. DOI: [10.1038/32354](https://doi.org/10.1038/32354) (cit. on p. 34).
- [77] P. Courteille, R. S. Freeland, D. J. Heinzen, F. A. van Abeelen, and B. J. Verhaar. “Observation of a Feshbach Resonance in Cold Atom Scattering”. *Phys. Rev. Lett.* 81 (1998), pp. 69–72. DOI: [10.1103/PhysRevLett.81.69](https://doi.org/10.1103/PhysRevLett.81.69) (cit. on p. 36).
- [78] J. Stenger, S. Inouye, M. R. Andrews, H.-J. Miesner, D. M. Stamper-Kurn, and W. Ketterle. “Strongly Enhanced Inelastic Collisions in a Bose–Einstein Condensate near Feshbach Resonances”. *Phys. Rev. Lett.* 82 (1999), pp. 2422–2425. DOI: [10.1103/PhysRevLett.82.2422](https://doi.org/10.1103/PhysRevLett.82.2422) (cit. on p. 36).
- [79] F. A. van Abeelen and B. J. Verhaar. “Time-Dependent Feshbach Resonance Scattering and Anomalous Decay of a Na Bose–Einstein Condensate”. *Phys. Rev. Lett.* 83 (1999), pp. 1550–1553. DOI: [10.1103/PhysRevLett.83.1550](https://doi.org/10.1103/PhysRevLett.83.1550) (cit. on p. 36).
- [80] F. H. Mies, E. Tiesinga, and P. S. Julienne. “Manipulation of Feshbach resonances in ultracold atomic collisions using time-dependent magnetic fields”. *Phys. Rev. A* 61 (2000), p. 022721. DOI: [10.1103/PhysRevA.61.022721](https://doi.org/10.1103/PhysRevA.61.022721) (cit. on p. 36).
- [81] C. Chin, R. Grimm, P. Julienne, and E. Tiesinga. “Feshbach resonances in ultracold gases”. *Rev. Mod. Phys.* 82 (2010), pp. 1225–1286. DOI: [10.1103/RevModPhys.82.1225](https://doi.org/10.1103/RevModPhys.82.1225) (cit. on p. 36).

- [82] H. L. Bethlem, G. Berden, and G. Meijer. “Decelerating Neutral Dipolar Molecules”. *Phys. Rev. Lett.* 83 (1999), pp. 1558–1561. DOI: [10.1103/PhysRevLett.83.1558](https://doi.org/10.1103/PhysRevLett.83.1558) (cit. on pp. 36, 37).
- [83] J. A. Maddi, T. P. Dinneen, and H. Gould. “Slowing and cooling molecules and neutral atoms by time-varying electric-field gradients”. *Phys. Rev. A* 60 (1999), pp. 3882–3891. DOI: [10.1103/PhysRevA.60.3882](https://doi.org/10.1103/PhysRevA.60.3882) (cit. on p. 36).
- [84] J. M. Doyle and B. Friedrich. “Molecules are cool”. *Nature (London)* 401 (1999), p. 749 (cit. on p. 36).
- [85] H. L. Bethlem, G. Berden, A. J. A. van Roij, F. M. H. Crompvoets, and G. Meijer. “Trapping Neutral Molecules in a Traveling Potential Well”. *Phys. Rev. Lett.* 84 (2000), pp. 5744–5747. DOI: [10.1103/PhysRevLett.84.5744](https://doi.org/10.1103/PhysRevLett.84.5744) (cit. on p. 36).
- [86] H. L. Bethlem, A. J. A. van Roij, R. T. Jongma, and G. Meijer. “Alternate Gradient Focusing and Deceleration of a Molecular Beam”. *Phys. Rev. Lett.* 88 (2002), p. 133003. DOI: [10.1103/PhysRevLett.88.133003](https://doi.org/10.1103/PhysRevLett.88.133003) (cit. on p. 36).
- [87] H. L. Bethlem, G. Berden, F. M. H. Crompvoets, R. T. Jongma, A. J. A. van Roij, and G. Meijer. “Electrostatic trapping of ammonia molecules”. *Nature* 406 (2000), pp. 491–494. DOI: [10.1038/35020030](https://doi.org/10.1038/35020030) (cit. on p. 36).
- [88] F. M. Crompvoets, H. L. Bethlem, R. T. Jongma, and G. Meijer. “A prototype storage ring for neutral molecules”. *Nature* 411 (2001), pp. 174–176. DOI: [10.1038/35075537](https://doi.org/10.1038/35075537) (cit. on p. 36).
- [89] H. L. Bethlem, F. M. H. Crompvoets, R. T. Jongma, S. Y. T. van de Meerakker, and G. Meijer. “Deceleration and trapping of ammonia using time-varying electric fields”. *Phys. Rev. A* 65 (2002), p. 053416. DOI: [10.1103/PhysRevA.65.053416](https://doi.org/10.1103/PhysRevA.65.053416) (cit. on p. 36).
- [90] J. R. Bochinski, E. R. Hudson, H. J. Lewandowski, G. Meijer, and J. Ye. “Phase Space Manipulation of Cold Free Radical OH Molecules”. *Phys. Rev. Lett.* 91 (2003), p. 243001. DOI: [10.1103/PhysRevLett.91.243001](https://doi.org/10.1103/PhysRevLett.91.243001) (cit. on pp. 36, 51).
- [91] M. R. Tarbutt, H. L. Bethlem, J. J. Hudson, V. L. Ryabov, V. A. Ryzhov, B. E. Sauer, G. Meijer, and E. A. Hinds. “Slowing Heavy, Ground-State Molecules using an Alternating Gradient Decelerator”. *Phys. Rev. Lett.* 92 (2004), p. 173002. DOI: [10.1103/PhysRevLett.92.173002](https://doi.org/10.1103/PhysRevLett.92.173002) (cit. on pp. 36, 51).
- [92] S. K. Tokunaga, J. M. Dyne, E. A. Hinds, and M. R. Tarbutt. “Stark deceleration of lithium hydride molecules”. *New J. Phys.* 11 (2009), p. 055038. DOI: [10.1088/1367-2630/11/5/055038](https://doi.org/10.1088/1367-2630/11/5/055038) (cit. on p. 36).
- [93] H. L. Bethlem, M. R. Tarbutt, J. Küpper, D. Carty, K. Wohlfart, E. A. Hinds, and G. Meijer. “Alternating gradient focusing and deceleration of polar molecules”. *J. Phys. B: At., Mol. Opt. Phys.* 39 (2006), R263–R291. DOI: [10.1088/0953-4075/39/16/r01](https://doi.org/10.1088/0953-4075/39/16/r01) (cit. on p. 36).
- [94] A. N. Nikolov, E. E. Eyler, X. T. Wang, J. Li, H. Wang, W. C. Stwalley, and P. L. Gould. “Observation of Ultracold Ground-State Potassium Molecules”. *Phys. Rev. Lett.* 82 (1999), pp. 703–706. DOI: [10.1103/PhysRevLett.82.703](https://doi.org/10.1103/PhysRevLett.82.703) (cit. on p. 36).
- [95] A. N. Nikolov, J. R. Ensher, E. E. Eyler, H. Wang, W. C. Stwalley, and P. L. Gould. “Efficient Production of Ground-State Potassium Molecules at Sub-mK Temperatures by Two-Step Photoassociation”. *Phys. Rev. Lett.* 84 (2000), pp. 246–249. DOI: [10.1103/PhysRevLett.84.246](https://doi.org/10.1103/PhysRevLett.84.246) (cit. on p. 36).
- [96] M. H. Anderson, J. R. Ensher, M. R. Matthews, C. E. Wieman, and E. A. Cornell. “Observation of Bose-Einstein Condensation in a Dilute Atomic Vapor”. *Science* 269 (1995), pp. 198–201. DOI: [10.1126/science.269.5221.198](https://doi.org/10.1126/science.269.5221.198) (cit. on p. 38).
- [97] K. B. Davis, M.-O. Mewes, M. R. Andrews, N. J. van Druten, D. S. Durfee, D. M. Kurn, and W. Ketterle. “Bose-Einstein Condensation in a Gas of Sodium Atoms”. *Phys. Rev. Lett.* 75 (1995), pp. 3969–3973. DOI: [10.1103/PhysRevLett.75.3969](https://doi.org/10.1103/PhysRevLett.75.3969) (cit. on p. 38).

- [98] C. C. Bradley, C. A. Sackett, J. J. Tollett, and R. G. Hulet. “Evidence of Bose-Einstein Condensation in an Atomic Gas with Attractive Interactions”. *Phys. Rev. Lett.* 75 (1995), pp. 1687–1690. DOI: [10.1103/PhysRevLett.75.1687](https://doi.org/10.1103/PhysRevLett.75.1687) (cit. on p. 38).
- [99] A. J. Leggett. “Bose-Einstein condensation in the alkali gases: Some fundamental concepts”. *Rev. Mod. Phys.* 73 (2001), pp. 307–356. DOI: [10.1103/revmodphys.73.307](https://doi.org/10.1103/revmodphys.73.307) (cit. on p. 38).
- [100] J. Javanainen and M. Mackie. “Probability of photoassociation from a quasicontinuum approach”. *Phys. Rev. A* 58 (1998), R789–R792. DOI: [10.1103/PhysRevA.58.R789](https://doi.org/10.1103/PhysRevA.58.R789) (cit. on pp. 38, 44).
- [101] P. D. Drummond, K. V. Kheruntsyan, and H. He. “Coherent Molecular Solitons in Bose-Einstein Condensates”. *Phys. Rev. Lett.* 81 (1998), pp. 3055–3058. DOI: [10.1103/PhysRevLett.81.3055](https://doi.org/10.1103/PhysRevLett.81.3055) (cit. on p. 38).
- [102] E. Timmermans, P. Tommasini, R. Côté, M. Hussein, and A. Kerman. “Rarified Liquid Properties of Hybrid Atomic-Molecular Bose-Einstein Condensates”. *Phys. Rev. Lett.* 83 (1999), pp. 2691–2694. DOI: [10.1103/PhysRevLett.83.2691](https://doi.org/10.1103/PhysRevLett.83.2691) (cit. on p. 38).
- [103] J. Javanainen and M. Mackie. “Coherent photoassociation of a Bose-Einstein condensate”. *Phys. Rev. A* 59 (1999), R3186–R3189. DOI: [10.1103/PhysRevA.59.R3186](https://doi.org/10.1103/PhysRevA.59.R3186) (cit. on pp. 38, 44).
- [104] R. Wynar, R. S. Freeland, D. J. Han, C. Ryu, and D. J. Heinzen. “Molecules in a Bose-Einstein Condensate”. *Science* 287 (2000), pp. 1016–1019. DOI: [10.1126/science.287.5455.1016](https://doi.org/10.1126/science.287.5455.1016) (cit. on p. 38).
- [105] J. M. Hutson and P. Soldán. “Molecule formation in ultracold atomic gases”. *Int. Rev. Phys. Chem.* 25 (2006), pp. 497–526. DOI: [10.1080/01442350600921772](https://doi.org/10.1080/01442350600921772) (cit. on pp. 38, 39).
- [106] C. McKenzie et al. “Photoassociation of Sodium in a Bose-Einstein Condensate”. *Phys. Rev. Lett.* 88 (2002), p. 120403. DOI: [10.1103/PhysRevLett.88.120403](https://doi.org/10.1103/PhysRevLett.88.120403) (cit. on p. 38).
- [107] I. Bloch. “Ultracold quantum gases in optical lattices”. *Nat. Phys.* 1 (2005), pp. 23–30. DOI: [10.1038/nphys138](https://doi.org/10.1038/nphys138) (cit. on p. 38).
- [108] D. Jaksch, V. Venturi, J. I. Cirac, C. J. Williams, and P. Zoller. “Creation of a Molecular Condensate by Dynamically Melting a Mott Insulator”. *Phys. Rev. Lett.* 89 (2002), p. 040402. DOI: [10.1103/PhysRevLett.89.040402](https://doi.org/10.1103/PhysRevLett.89.040402) (cit. on p. 38).
- [109] E. A. Donley, N. R. Claussen, S. T. Thompson, and C. E. Wieman. “Atom–molecule coherence in a Bose-Einstein condensate”. *Nature* 417 (2002), pp. 529–533. DOI: [10.1038/417529a](https://doi.org/10.1038/417529a) (cit. on pp. 38, 39).
- [110] S. T. Thompson, E. Hodby, and C. E. Wieman. “Ultracold Molecule Production via a Resonant Oscillating Magnetic Field”. *Phys. Rev. Lett.* 95 (2005), p. 190404. DOI: [10.1103/PhysRevLett.95.190404](https://doi.org/10.1103/PhysRevLett.95.190404) (cit. on p. 38).
- [111] C. Chin, A. J. Kerman, V. Vuletić, and S. Chu. “Sensitive Detection of Cold Cesium Molecules Formed on Feshbach Resonances”. *Phys. Rev. Lett.* 90 (2003), p. 033201. DOI: [10.1103/PhysRevLett.90.033201](https://doi.org/10.1103/PhysRevLett.90.033201) (cit. on p. 39).
- [112] J. Cubizolles, T. Bourdel, S. J. J. M. F. Kokkelmans, G. V. Shlyapnikov, and C. Salomon. “Production of Long-Lived Ultracold Li<sub>2</sub> Molecules from a Fermi Gas”. *Phys. Rev. Lett.* 91 (2003), p. 240401. DOI: [10.1103/PhysRevLett.91.240401](https://doi.org/10.1103/PhysRevLett.91.240401) (cit. on p. 39).
- [113] K. E. Strecker, G. B. Partridge, and R. G. Hulet. “Conversion of an Atomic Fermi Gas to a Long-Lived Molecular Bose Gas”. *Phys. Rev. Lett.* 91 (2003), p. 080406. DOI: [10.1103/PhysRevLett.91.080406](https://doi.org/10.1103/PhysRevLett.91.080406) (cit. on p. 39).
- [114] C. A. Regal, C. Ticknor, J. L. Bohn, and D. S. Jin. “Creation of ultracold molecules from a Fermi gas of atoms”. *Nature* 424 (2003), pp. 47–50. DOI: [10.1038/nature01738](https://doi.org/10.1038/nature01738) (cit. on p. 39).

- [115] S. Jochim, M. Bartenstein, A. Altmeyer, G. Hendl, C. Chin, J. H. Denschlag, and R. Grimm. “Pure Gas of Optically Trapped Molecules Created from Fermionic Atoms”. *Phys. Rev. Lett.* 91 (2003), p. 240402. DOI: [10.1103/PhysRevLett.91.240402](https://doi.org/10.1103/PhysRevLett.91.240402) (cit. on pp. 39, 40).
- [116] T. Köhler, K. Góral, and P. S. Julienne. “Production of cold molecules via magnetically tunable Feshbach resonances”. *Rev. Mod. Phys.* 78 (2006), pp. 1311–1361. DOI: [10.1103/RevModPhys.78.1311](https://doi.org/10.1103/RevModPhys.78.1311) (cit. on p. 39).
- [117] S. J. Park, S. W. Suh, Y. S. Lee, and G.-H. Jeung. “Theoretical Study of the Electronic States of the Rb<sub>2</sub> Molecule”. *J. Mol. Spectrosc.* 207 (2001), pp. 129–135. DOI: [10.1006/jmsp.2001.8337](https://doi.org/10.1006/jmsp.2001.8337) (cit. on p. 39).
- [118] R. Haussmann. “Properties of a Fermi liquid at the superfluid transition in the crossover region between BCS superconductivity and Bose-Einstein condensation”. *Phys. Rev. B* 49 (1994), pp. 12975–12983. DOI: [10.1103/PhysRevB.49.12975](https://doi.org/10.1103/PhysRevB.49.12975) (cit. on p. 40).
- [119] M. Holland, S. J. J. M. F. Kokkelmans, M. L. Chiofalo, and R. Walser. “Resonance Superfluidity in a Quantum Degenerate Fermi Gas”. *Phys. Rev. Lett.* 87 (2001), p. 120406. DOI: [10.1103/PhysRevLett.87.120406](https://doi.org/10.1103/PhysRevLett.87.120406) (cit. on p. 40).
- [120] Y. Ohashi and A. Griffin. “BCS-BEC Crossover in a Gas of Fermi Atoms with a Feshbach Resonance”. *Phys. Rev. Lett.* 89 (2002), p. 130402. DOI: [10.1103/PhysRevLett.89.130402](https://doi.org/10.1103/PhysRevLett.89.130402) (cit. on p. 40).
- [121] C. Regal. “Experimental realization of BCS-BEC crossover physics with a Fermi gas of atoms”. PhD thesis. University of Colorado, 2005 (cit. on p. 40).
- [122] M. Bartenstein. “From Molecules to Cooper Pairs: Experiments in the BEC - BCS Crossover”. PhD thesis. Universität Innsbruck, 2005 (cit. on p. 40).
- [123] M. M. Parish. “The BCS–BEC Crossover”. In: *Cold Atoms*. Imperial College Press, 2014, pp. 179–197. DOI: [10.1142/9781783264766\\_0009](https://doi.org/10.1142/9781783264766_0009) (cit. on p. 40).
- [124] S. Jochim, M. Bartenstein, A. Altmeyer, G. Hendl, S. Riedl, C. Chin, J. H. Denschlag, and R. Grimm. “Bose-Einstein Condensation of Molecules”. *Science* 302 (2003), pp. 2101–2103. DOI: [10.1126/science.1093280](https://doi.org/10.1126/science.1093280) (cit. on p. 40).
- [125] M. W. Zwierlein, C. A. Stan, C. H. Schunck, S. M. F. Raupach, S. Gupta, Z. Hadzibabic, and W. Ketterle. “Observation of Bose-Einstein Condensation of Molecules”. *Phys. Rev. Lett.* 91 (2003), p. 250401. DOI: [10.1103/PhysRevLett.91.250401](https://doi.org/10.1103/PhysRevLett.91.250401) (cit. on p. 40).
- [126] K. Xu, T. Mukaiyama, J. R. Abo-Shaeer, J. K. Chin, D. E. Miller, and W. Ketterle. “Formation of Quantum-Degenerate Sodium Molecules”. *Phys. Rev. Lett.* 91 (2003), p. 210402. DOI: [10.1103/PhysRevLett.91.210402](https://doi.org/10.1103/PhysRevLett.91.210402) (cit. on p. 40).
- [127] M. Greiner, C. Regal, and D. S. Jin. “Emergence of a molecular Bose–Einstein condensate from a Fermi gas”. *Nature* 426 (2003), pp. 537–540. DOI: [10.1038/nature02199](https://doi.org/10.1038/nature02199) (cit. on pp. 40, 41).
- [128] S. Dürr, T. Volz, A. Marte, and G. Rempe. “Observation of Molecules Produced from a Bose-Einstein Condensate”. *Phys. Rev. Lett.* 92 (2004), p. 020406. DOI: [10.1103/PhysRevLett.92.020406](https://doi.org/10.1103/PhysRevLett.92.020406) (cit. on p. 40).
- [129] J. Herbig, T. Kraemer, M. Mark, T. Weber, C. Chin, H.-C. Nägerl, and R. Grimm. “Preparation of a Pure Molecular Quantum Gas”. *Science* 301 (2003), pp. 1510–1513. DOI: [10.1126/science.1088876](https://doi.org/10.1126/science.1088876) (cit. on p. 40).
- [130] T. Bourdel, L. Khaykovich, J. Cubizolles, J. Zhang, F. Chevy, M. Teichmann, L. Tarruell, S. J. J. M. F. Kokkelmans, and C. Salomon. “Experimental Study of the BEC-BCS Crossover Region in Lithium 6”. *Phys. Rev. Lett.* 93 (2004), p. 050401. DOI: [10.1103/PhysRevLett.93.050401](https://doi.org/10.1103/PhysRevLett.93.050401) (cit. on p. 40).

- [131] T. Mukaiyama, J. R. Abo-Shaeer, K. Xu, J. K. Chin, and W. Ketterle. “Dissociation and Decay of Ultracold Sodium Molecules”. *Phys. Rev. Lett.* 92 (2004), p. 180402. DOI: [10 . 1103 / PhysRevLett.92.180402](https://doi.org/10.1103/PhysRevLett.92.180402) (cit. on p. 40).
- [132] M. Bartenstein, A. Altmeyer, S. Riedl, S. Jochim, C. Chin, J. H. Denschlag, and R. Grimm. “Crossover from a Molecular Bose-Einstein Condensate to a Degenerate Fermi Gas”. *Phys. Rev. Lett.* 92 (2004), p. 120401. DOI: [10 . 1103 / PhysRevLett.92.120401](https://doi.org/10.1103/PhysRevLett.92.120401) (cit. on p. 40).
- [133] C. A. Regal, M. Greiner, and D. S. Jin. “Observation of Resonance Condensation of Fermionic Atom Pairs”. *Phys. Rev. Lett.* 92 (2004), p. 040403. DOI: [10 . 1103 / physrevlett.92.040403](https://doi.org/10.1103/physrevlett.92.040403) (cit. on p. 40).
- [134] M. W. Zwierlein, C. A. Stan, C. H. Schunck, S. M. F. Raupach, A. J. Kerman, and W. Ketterle. “Condensation of Pairs of Fermionic Atoms near a Feshbach Resonance”. *Phys. Rev. Lett.* 92 (2004), p. 120403. DOI: [10 . 1103 / physrevlett.92.120403](https://doi.org/10.1103/physrevlett.92.120403) (cit. on p. 40).
- [135] M. W. Zwierlein, C. H. Schunck, C. A. Stan, S. M. F. Raupach, and W. Ketterle. “Formation Dynamics of a Fermion Pair Condensate”. *Phys. Rev. Lett.* 94 (2005), p. 180401. DOI: [10 . 1103 / physrevlett.94.180401](https://doi.org/10.1103/physrevlett.94.180401) (cit. on p. 40).
- [136] S. Dürr, T. Volz, and G. Rempe. “Dissociation of ultracold molecules with Feshbach resonances”. *Phys. Rev. A* 70 (2004), p. 031601. DOI: [10 . 1103 / PhysRevA.70.031601](https://doi.org/10.1103/PhysRevA.70.031601) (cit. on p. 40).
- [137] D. S. Petrov, C. Salomon, and G. V. Shlyapnikov. “Weakly Bound Dimers of Fermionic Atoms”. *Phys. Rev. Lett.* 93 (2004), p. 090404. DOI: [10 . 1103 / PhysRevLett.93.090404](https://doi.org/10.1103/PhysRevLett.93.090404) (cit. on p. 40).
- [138] D. S. Petrov, C. Salomon, and G. V. Shlyapnikov. “Scattering properties of weakly bound dimers of fermionic atoms”. *Phys. Rev. A* 71 (2005), p. 012708. DOI: [10 . 1103 / PhysRevA.71.012708](https://doi.org/10.1103/PhysRevA.71.012708) (cit. on p. 40).
- [139] M. T. Cvitaš, P. Soldán, J. M. Hutson, P. Honvárt, and J.-M. Launay. “Ultracold Li + Li<sub>2</sub> Collisions: Bosonic and Fermionic Cases”. *Phys. Rev. Lett.* 94 (2005), p. 033201. DOI: [10 . 1103 / PhysRevLett.94.033201](https://doi.org/10.1103/PhysRevLett.94.033201) (cit. on p. 40).
- [140] M. Marinescu and L. You. “Controlling Atom-Atom Interaction at Ultralow Temperatures by dc Electric Fields”. *Physical Review Letters* 81 (1998), pp. 4596–4599. DOI: [10 . 1103 / PhysRevLett.81.4596](https://doi.org/10.1103/PhysRevLett.81.4596) (cit. on pp. 41, 182).
- [141] L. Santos, G. V. Shlyapnikov, P. Zoller, and M. Lewenstein. “Bose-Einstein Condensation in Trapped Dipolar Gases”. *Phys. Rev. Lett.* 85 (2000), pp. 1791–1794. DOI: [10 . 1103 / PhysRevLett.85.1791](https://doi.org/10.1103/PhysRevLett.85.1791) (cit. on pp. 41, 182).
- [142] S. Yi and L. You. “Trapped atomic condensates with anisotropic interactions”. *Phys. Rev. A* 61 (2000), p. 041604. DOI: [10 . 1103 / PhysRevA.61.041604](https://doi.org/10.1103/PhysRevA.61.041604) (cit. on pp. 41, 182).
- [143] L. Santos, G. V. Shlyapnikov, and M. Lewenstein. “Roton-Maxon Spectrum and Stability of Trapped Dipolar Bose-Einstein Condensates”. *Phys. Rev. Lett.* 90 (2003), p. 250403. DOI: [10 . 1103 / PhysRevLett.90.250403](https://doi.org/10.1103/PhysRevLett.90.250403) (cit. on pp. 41, 182).
- [144] K. Góral, L. Santos, and M. Lewenstein. “Quantum Phases of Dipolar Bosons in Optical Lattices”. *Phys. Rev. Lett.* 88 (2002), p. 170406. DOI: [10 . 1103 / PhysRevLett.88.170406](https://doi.org/10.1103/PhysRevLett.88.170406) (cit. on pp. 41, 182).
- [145] T. Lahaye, C. Menotti, L. Santos, M. Lewenstein, and T. Pfau. “The physics of dipolar bosonic quantum gases”. *Rep. Prog. Phys.* 72 (2009), p. 126401. DOI: [10 . 1088 / 0034-4885 / 72 / 12 / 126401](https://doi.org/10.1088/0034-4885/72/12/126401) (cit. on p. 41).
- [146] M. A. Baranov. “Theoretical progress in many-body physics with ultracold dipolar gases”. *Phys. Rep.* 464 (2008), pp. 71–111. DOI: <https://doi.org/10.1016/j.physrep.2008.04.007> (cit. on p. 41).

- [147] F. Böttcher, J.-N. Schmidt, J. Hertkorn, K. S. H. Ng, S. D. Graham, M. Guo, T. Langen, and T. Pfau. “New states of matter with fine-tuned interactions: quantum droplets and dipolar supersolids”. *Rep. Prog. Phys.* 84 (2021), p. 012403. DOI: [10.1088/1361-6633/abc9ab](https://doi.org/10.1088/1361-6633/abc9ab) (cit. on pp. 41, 69, 156).
- [148] L. Chomaz, I. Ferrier-Barbut, F. Ferlaino, B. Laburthe-Tolra, B. L. Lev, and T. Pfau. *Dipolar physics: A review of experiments with magnetic quantum gases*. 2022. arXiv: [2201.02672](https://arxiv.org/abs/2201.02672) (cit. on pp. 41, 69, 156).
- [149] L. You and M. Marinescu. “Prospects for p-wave paired Bardeen-Cooper-Schrieffer states of fermionic atoms”. *Phys. Rev. A* 60 (1999), pp. 2324–2329. DOI: [10.1103/PhysRevA.60.2324](https://doi.org/10.1103/PhysRevA.60.2324) (cit. on pp. 41, 182).
- [150] M. Baranov, L. Dobrek, K. Góral, L. Santos, and M. Lewenstein. “Ultracold Dipolar Gases — a Challenge for Experiments and Theory”. *Phys. Scr. T102* (2002), p. 74. DOI: [10.1238/physica.topical.102a00074](https://doi.org/10.1238/physica.topical.102a00074) (cit. on p. 41).
- [151] D. DeMille. “Quantum Computation with Trapped Polar Molecules”. *Phys. Rev. Lett.* 88 (2002), p. 067901. DOI: [10.1103/PhysRevLett.88.067901](https://doi.org/10.1103/PhysRevLett.88.067901) (cit. on p. 41).
- [152] M. S. Safranova, D. Budker, D. DeMille, D. F. J. Kimball, A. Derevianko, and C. W. Clark. “Search for new physics with atoms and molecules”. *Rev. Mod. Phys.* 90 (2018), p. 025008. DOI: [10.1103/RevModPhys.90.025008](https://doi.org/10.1103/RevModPhys.90.025008) (cit. on pp. 42, 68).
- [153] T. E. Chupp, P. Fierlinger, M. J. Ramsey-Musolf, and J. T. Singh. “Electric dipole moments of atoms, molecules, nuclei, and particles”. *Rev. Mod. Phys.* 91 (2019), p. 015001. DOI: [10.1103/revmodphys.91.015001](https://doi.org/10.1103/revmodphys.91.015001) (cit. on p. 42).
- [154] E. D. Commins, J. D. Jackson, and D. P. DeMille. “The electric dipole moment of the electron: An intuitive explanation for the evasion of Schiff’s theorem”. *Am. J. Phys.* 75 (2007), pp. 532–536. DOI: [10.1119/1.2710486](https://doi.org/10.1119/1.2710486) (cit. on p. 42).
- [155] O. P. Sushkov and V. V. Flambaum. “Parity breaking effects in diatomic molecules”. *Sov. Phys. JETP* 4 (1978), pp. 608–611 (cit. on p. 42).
- [156] E. A. Hinds. “Testing time reversal symmetry using molecules”. *Phys. Scr. T70* (1997), pp. 34–41 (cit. on p. 42).
- [157] D. DeMille, F. Bay, S. Bickman, D. Kawall, D. Krause, S. E. Maxwell, and L. R. Hunter. “Investigation of PbO as a system for measuring the electric dipole moment of the electron”. *Phys. Rev. A* 61 (2000), p. 052507. DOI: [10.1103/PhysRevA.61.052507](https://doi.org/10.1103/PhysRevA.61.052507) (cit. on p. 42).
- [158] B. E. Sauer, J. J. Hudson, M. R. Tarbutt, and E. A. Hinds. “Measuring the electron electric dipole moment in Ybf”. In: *AIP Conference Proceedings*. Vol. 596. AIP, 2001. DOI: [10.1063/1.1426794](https://doi.org/10.1063/1.1426794) (cit. on p. 42).
- [159] D. DeMille, F. Bay, S. Bickman, D. Kawall, L. Hunter, D. K. Jr., S. Maxwell, and K. Ulmer. “Search for the electric dipole moment of the electron using metastable PbO”. In: *AIP Conference Proceedings*. Vol. 596. AIP, 2001. DOI: [10.1063/1.1426795](https://doi.org/10.1063/1.1426795) (cit. on p. 42).
- [160] A. Mosk, S. Kraft, M. Mudrich, K. Singer, W. Wohllben, R. Grimm, and M. Weidmüller. “Mixture of ultracold lithium and cesium atoms in an optical dipole trap”. *Appl. Phys. B* 73 (2001), pp. 791–799. DOI: [10.1007/s003400100743](https://doi.org/10.1007/s003400100743) (cit. on p. 42).
- [161] G. Modugno, G. Ferrari, G. Roati, R. J. Brecha, A. Simoni, and M. Inguscio. “Bose-Einstein Condensation of Potassium Atoms by Sympathetic Cooling”. *Science* 294 (2001), pp. 1320–1322. DOI: [10.1126/science.1066687](https://doi.org/10.1126/science.1066687) (cit. on p. 42).
- [162] Z. Hadzibabic, C. A. Stan, K. Dieckmann, S. Gupta, M. W. Zwierlein, A. Görlitz, and W. Ketterle. “Two-Species Mixture of Quantum Degenerate Bose and Fermi Gases”. *Phys. Rev. Lett.* 88 (2002), p. 160401. DOI: [10.1103/PhysRevLett.88.160401](https://doi.org/10.1103/PhysRevLett.88.160401) (cit. on pp. 42, 168).

- [163] C. A. Stan, M. W. Zwierlein, C. H. Schunck, S. M. F. Raupach, and W. Ketterle. “Observation of Feshbach Resonances between Two Different Atomic Species”. *Phys. Rev. Lett.* 93 (2004), p. 143001. DOI: [10.1103/PhysRevLett.93.143001](https://doi.org/10.1103/PhysRevLett.93.143001) (cit. on p. 42).
- [164] S. Inouye, J. Goldwin, M. L. Olsen, C. Ticknor, J. L. Bohn, and D. S. Jin. “Observation of Heteronuclear Feshbach Resonances in a Mixture of Bosons and Fermions”. *Phys. Rev. Lett.* 93 (2004), p. 183201. DOI: [10.1103/PhysRevLett.93.183201](https://doi.org/10.1103/PhysRevLett.93.183201) (cit. on pp. 42, 43, 176).
- [165] M. Duda, X.-Y. Chen, R. Bause, A. Schindewolf, I. Bloch, and X.-Y. Luo. *Long-lived fermionic Feshbach molecules with tunable p-wave interactions*. In preparation (cit. on pp. 43, 64, 72, 150).
- [166] U. Schlöder, C. Silber, and C. Zimmermann. “Photoassociation of heteronuclear lithium”. *Appl. Phys. B* 73 (2001), pp. 801–805 (cit. on p. 43).
- [167] N. Vanhaecke, W. de Souza Melo, B. L. Tolra, D. Comparat, and P. Pillet. “Accumulation of Cold Cesium Molecules via Photoassociation in a Mixed Atomic and Molecular Trap”. *Phys. Rev. Lett.* 89 (2002), p. 063001. DOI: [10.1103/PhysRevLett.89.063001](https://doi.org/10.1103/PhysRevLett.89.063001) (cit. on p. 43).
- [168] H. Wang and W. C. Stwalley. “Ultracold photoassociative spectroscopy of heteronuclear alkali-metal diatomic molecules”. *J. Chem. Phys.* 108 (1998), pp. 5767–5771. DOI: [10.1063/1.475987](https://doi.org/10.1063/1.475987) (cit. on pp. 43, 176).
- [169] S. Azizi, M. Aymar, and O. Dulieu. “Prospects for the formation of ultracold ground state polar molecules from mixed alkali atom pairs”. *Eur. Phys. J. D* 31 (2004), pp. 195–203. DOI: [10.1140/epjd/e2004-00159-2](https://doi.org/10.1140/epjd/e2004-00159-2) (cit. on p. 43).
- [170] D. Wang, J. Qi, M. F. Stone, O. Nikolayeva, B. Hattaway, S. D. Gensemer, H. Wang, W. T. Zemke, P. L. Gould, E. E. Eyler, and W. C. Stwalley. “The photoassociative spectroscopy, photoassociative molecule formation, and trapping of ultracold  $^{39}\text{K}^{85}\text{Rb}$ ”. *Eur. Phys. J. D* 31 (2004), pp. 165–177. DOI: [10.1140/epjd/e2004-00162-7](https://doi.org/10.1140/epjd/e2004-00162-7) (cit. on pp. 43, 176).
- [171] D. Wang, J. Qi, M. F. Stone, O. Nikolayeva, H. Wang, B. Hattaway, S. D. Gensemer, P. L. Gould, E. E. Eyler, and W. C. Stwalley. “Photoassociative Production and Trapping of Ultracold KRb Molecules”. *Phys. Rev. Lett.* 93 (2004), p. 243005. DOI: [10.1103/PhysRevLett.93.243005](https://doi.org/10.1103/PhysRevLett.93.243005) (cit. on pp. 43, 176).
- [172] M. W. Mancini, G. D. Telles, A. R. L. Caires, V. S. Bagnato, and L. G. Marcassa. “Observation of Ultracold Ground-State Heteronuclear Molecules”. *Phys. Rev. Lett.* 92 (2004), p. 133203. DOI: [10.1103/PhysRevLett.92.133203](https://doi.org/10.1103/PhysRevLett.92.133203) (cit. on pp. 43, 176).
- [173] A. J. Kerman, J. M. Sage, S. Sainis, T. Bergeman, and D. DeMille. “Production and State-Selective Detection of Ultracold RbCs Molecules”. *Phys. Rev. Lett.* 92 (2004), p. 153001. DOI: [10.1103/PhysRevLett.92.153001](https://doi.org/10.1103/PhysRevLett.92.153001) (cit. on pp. 43, 179).
- [174] C. Haimberger, J. Kleinert, M. Bhattacharya, and N. P. Bigelow. “Formation and detection of ultracold ground-state polar molecules”. *Phys. Rev. A* 70 (2004), p. 021402. DOI: [10.1103/PhysRevA.70.021402](https://doi.org/10.1103/PhysRevA.70.021402) (cit. on pp. 43, 175).
- [175] K. M. Jones, E. Tiesinga, P. D. Lett, and P. S. Julienne. “Ultracold photoassociation spectroscopy: Long-range molecules and atomic scattering”. *Rev. Mod. Phys.* 78 (2006), pp. 483–535. DOI: [10.1103/RevModPhys.78.483](https://doi.org/10.1103/RevModPhys.78.483) (cit. on p. 44).
- [176] J. Ulmanis, J. Deiglmayr, M. Repp, R. Wester, and M. Weidemüller. “Ultracold Molecules Formed by Photoassociation: Heteronuclear Dimers, Inelastic Collisions, and Interactions with Ultrashort Laser Pulses”. *Chem. Rev.* 112 (2012), pp. 4890–4927 (cit. on pp. 44, 48).
- [177] J. Doyle, B. Friedrich, R. V. Krems, and F. Masnou-Seeuws. “Editorial: Quo vadis, cold molecules?” *Eur. Phys. J. D* 31 (2004), pp. 149–164. DOI: [10.1140/epjd/e2004-00151-x](https://doi.org/10.1140/epjd/e2004-00151-x) (cit. on p. 44).
- [178] M. D. Di Rosa. “Laser-cooling molecules”. *Eur. Phys. J. D* 31 (2004), pp. 395–402. DOI: [10.1140/epjd/e2004-00167-2](https://doi.org/10.1140/epjd/e2004-00167-2) (cit. on pp. 44, 51).

- [179] D. DeMille, D. R. Glenn, and J. Petricka. “Microwave traps for cold polar molecules”. *Eur. Phys. J. D* 31 (2004), pp. 375–384. DOI: [10.1140/epjd/e2004-00163-6](https://doi.org/10.1140/epjd/e2004-00163-6) (cit. on p. 44).
- [180] S. C. Wright, T. E. Wall, and M. R. Tarbutt. “Microwave trap for atoms and molecules”. *Phys. Rev. Research* 1 (2019), p. 033035. DOI: [10.1103/PhysRevResearch.1.033035](https://doi.org/10.1103/PhysRevResearch.1.033035) (cit. on p. 44).
- [181] W. C. Stwalley. “Efficient conversion of ultracold Feshbach-resonance-related polar molecules into ultracold ground state ( $X^1\Sigma^+ v=0, J=0$ ) molecules”. *Eur. Phys. J. D* 31 (2004), pp. 221–225. DOI: [10.1140/epjd/e2004-00147-6](https://doi.org/10.1140/epjd/e2004-00147-6) (cit. on p. 44).
- [182] U. Gaubatz, P. Rudecki, M. Becker, S. Schiemann, M. Külz, and K. Bergmann. “Population switching between vibrational levels in molecular beams”. *Chem. Phys. Lett.* 149 (1988), pp. 463–468. DOI: [10.1016/0009-2614\(88\)80364-6](https://doi.org/10.1016/0009-2614(88)80364-6) (cit. on p. 44).
- [183] K. Bergmann, H. Theuer, and B. W. Shore. “Coherent population transfer among quantum states of atoms and molecules”. *Rev. Mod. Phys.* 70 (1998), pp. 1003–1025. DOI: [10.1103/RevModPhys.70.1003](https://doi.org/10.1103/RevModPhys.70.1003) (cit. on p. 44).
- [184] K. Bergmann, N. V. Vitanov, and B. W. Shore. “Perspective: Stimulated Raman adiabatic passage: The status after 25 years”. *J. Chem. Phys.* 142 (2015), p. 170901. DOI: [10.1063/1.4916903](https://doi.org/10.1063/1.4916903) (cit. on p. 44).
- [185] N. V. Vitanov, A. A. Rangelov, B. W. Shore, and K. Bergmann. “Stimulated Raman adiabatic passage in physics, chemistry, and beyond”. *Rev. Mod. Phys.* 89 (2017), p. 015006. DOI: [10.1103/RevModPhys.89.015006](https://doi.org/10.1103/RevModPhys.89.015006) (cit. on p. 44).
- [186] K. Bergmann et al. “Roadmap on STIRAP applications”. *J. Phys. B: At., Mol. Opt. Phys.* 52 (2019), p. 202001. DOI: [10.1088/1361-6455/ab3995](https://doi.org/10.1088/1361-6455/ab3995) (cit. on p. 44).
- [187] M. Mackie, R. Kowalski, and J. Javanainen. “Bose-Stimulated Raman Adiabatic Passage in Photoassociation”. *Phys. Rev. Lett.* 84 (2000), pp. 3803–3806. DOI: [10.1103/PhysRevLett.84.3803](https://doi.org/10.1103/PhysRevLett.84.3803) (cit. on p. 44).
- [188] P. D. Drummond, K. V. Kheruntsyan, D. J. Heinzen, and R. H. Wynar. “Stimulated Raman adiabatic passage from an atomic to a molecular Bose-Einstein condensate”. *Phys. Rev. A* 65 (2002), p. 063619. DOI: [10.1103/PhysRevA.65.063619](https://doi.org/10.1103/PhysRevA.65.063619) (cit. on p. 44).
- [189] A. Vardi, M. Shapiro, and J. R. Anglin. “Comment on “Quasicontinuum modeling of photoassociation””. *Phys. Rev. A* 65 (2002), p. 027401. DOI: [10.1103/PhysRevA.65.027401](https://doi.org/10.1103/PhysRevA.65.027401) (cit. on p. 44).
- [190] J. M. Sage, S. Sainis, T. Bergeman, and D. DeMille. “Optical Production of Ultracold Polar Molecules”. *Phys. Rev. Lett.* 94 (2005), p. 203001. DOI: [10.1103/PhysRevLett.94.203001](https://doi.org/10.1103/PhysRevLett.94.203001) (cit. on pp. 45, 179).
- [191] K. Winkler, F. Lang, G. Thalhammer, P. v. d. Straten, R. Grimm, and J. H. Denschlag. “Coherent Optical Transfer of Feshbach Molecules to a Lower Vibrational State”. *Phys. Rev. Lett.* 98 (2007), p. 043201. DOI: [10.1103/PhysRevLett.98.043201](https://doi.org/10.1103/PhysRevLett.98.043201) (cit. on p. 45).
- [192] R. Roth. “Structure and stability of trapped atomic boson-fermion mixtures”. *Phys. Rev. A* 66 (2002), p. 013614. DOI: [10.1103/PhysRevA.66.013614](https://doi.org/10.1103/PhysRevA.66.013614) (cit. on p. 46).
- [193] S. Ospelkaus. “Quantum Degenerate Fermi-Bose Mixtures of  $^{40}\text{K}$  and  $^{87}\text{Rb}$ ”. PhD thesis. Universität Hamburg, 2006 (cit. on pp. 46, 176).
- [194] S. Ospelkaus, C. Ospelkaus, R. Dinter, J. Fuchs, M. Nakat, K. Sengstock, and K. Bongs. “Degenerate K-Rb Fermi-Bose gas mixtures with large particle numbers”. *J. Mod. Opt.* 54 (2007), pp. 661–673. DOI: [10.1080/09500340600777763](https://doi.org/10.1080/09500340600777763) (cit. on pp. 46, 176).
- [195] C. Ospelkaus, S. Ospelkaus, K. Sengstock, and K. Bongs. “Interaction-Driven Dynamics of  $^{40}\text{K}$ - $^{87}\text{Rb}$  Fermion-Boson Gas Mixtures in the Large-Particle-Number Limit”. *Phys. Rev. Lett.* 96 (2006), p. 020401. DOI: [10.1103/PhysRevLett.96.020401](https://doi.org/10.1103/PhysRevLett.96.020401) (cit. on pp. 46, 176).

- [196] S. Ospelkaus, C. Ospelkaus, L. Humbert, K. Sengstock, and K. Bongs. “Tuning of Heteronuclear Interactions in a Degenerate Fermi-Bose Mixture”. *Phys. Rev. Lett.* 97 (2006), p. 120403. DOI: [10.1103/PhysRevLett.97.120403](https://doi.org/10.1103/PhysRevLett.97.120403) (cit. on pp. 46, 176).
- [197] S. Ospelkaus, C. Ospelkaus, O. Wille, M. Succo, P. Ernst, K. Sengstock, and K. Bongs. “Localization of Bosonic Atoms by Fermionic Impurities in a Three-Dimensional Optical Lattice”. *Phys. Rev. Lett.* 96 (2006), p. 180403. DOI: [10.1103/PhysRevLett.96.180403](https://doi.org/10.1103/PhysRevLett.96.180403) (cit. on pp. 46, 176).
- [198] S. B. Papp and C. E. Wieman. “Observation of Heteronuclear Feshbach Molecules from a  $^{85}\text{Rb}$ - $^{87}\text{Rb}$  Gas”. *Phys. Rev. Lett.* 97 (2006), p. 180404. DOI: [10.1103/PhysRevLett.97.180404](https://doi.org/10.1103/PhysRevLett.97.180404) (cit. on p. 46).
- [199] C. Ospelkaus, S. Ospelkaus, L. Humbert, P. Ernst, K. Sengstock, and K. Bongs. “Ultracold Heteronuclear Molecules in a 3D Optical Lattice”. *Phys. Rev. Lett.* 97 (2006), p. 120402. DOI: [10.1103/PhysRevLett.97.120402](https://doi.org/10.1103/PhysRevLett.97.120402) (cit. on pp. 46, 59, 176).
- [200] J. Goldwin, S. B. Papp, B. DeMarco, and D. S. Jin. “Two-species magneto-optical trap with  $^{40}\text{K}$  and  $^{87}\text{Rb}$ ”. *Phys. Rev. A* 65 (2002), 021402(R). DOI: [10.1103/PhysRevA.65.021402](https://doi.org/10.1103/PhysRevA.65.021402) (cit. on p. 46).
- [201] G. Modugno, G. Roati, F. Riboli, F. Ferlaino, R. J. Brecha, and M. Inguscio. “Collapse of a Degenerate Fermi Gas”. *Science* 297 (2002), pp. 2240–2243. DOI: [10.1126/science.1077386](https://doi.org/10.1126/science.1077386) (cit. on pp. 46, 176).
- [202] M. Modugno, F. Ferlaino, F. Riboli, G. Roati, G. Modugno, and M. Inguscio. “Mean-field analysis of the stability of a K-Rb Fermi-Bose mixture”. *Phys. Rev. A* 68 (2003), p. 043626. DOI: [10.1103/PhysRevA.68.043626](https://doi.org/10.1103/PhysRevA.68.043626) (cit. on pp. 46, 176).
- [203] F. Ferlaino, C. D’Errico, G. Roati, M. Zaccanti, M. Inguscio, G. Modugno, and A. Simoni. “Feshbach spectroscopy of a K-Rb atomic mixture”. *Phys. Rev. A* 73 (2006), p. 040702. DOI: [10.1103/PhysRevA.73.040702](https://doi.org/10.1103/PhysRevA.73.040702) (cit. on pp. 46, 176).
- [204] H. P. Büchler, E. Demler, M. Lukin, A. Micheli, N. Prokof’ev, G. Pupillo, and P. Zoller. “Strongly Correlated 2D Quantum Phases with Cold Polar Molecules: Controlling the Shape of the Interaction Potential”. *Phys. Rev. Lett.* 98 (2007), p. 060404. DOI: [10.1103/PhysRevLett.98.060404](https://doi.org/10.1103/PhysRevLett.98.060404) (cit. on pp. 46, 47, 159, 181).
- [205] G. E. Astrakharchik, J. Boronat, I. L. Kurbakov, and Y. E. Lozovik. “Quantum Phase Transition in a Two-Dimensional System of Dipoles”. *Phys. Rev. Lett.* 98 (2007), p. 060405. DOI: [10.1103/PhysRevLett.98.060405](https://doi.org/10.1103/PhysRevLett.98.060405) (cit. on pp. 46, 159, 181).
- [206] A. Micheli, G. Pupillo, H. P. Büchler, and P. Zoller. “Cold polar molecules in two-dimensional traps: Tailoring interactions with external fields for novel quantum phases”. *Phys. Rev. A* 76 (2007), p. 043604. DOI: [10.1103/PhysRevA.76.043604](https://doi.org/10.1103/PhysRevA.76.043604) (cit. on pp. 46, 108, 118, 139, 159, 181).
- [207] G. Pupillo, A. Griessner, A. Micheli, M. Ortner, D.-W. Wang, and P. Zoller. “Cold Atoms and Molecules in Self-Assembled Dipolar Lattices”. *Phys. Rev. Lett.* 100 (2008), p. 050402. DOI: [10.1103/PhysRevLett.100.050402](https://doi.org/10.1103/PhysRevLett.100.050402) (cit. on pp. 46, 181).
- [208] T. Miyakawa, T. Sogo, and H. Pu. “Phase-space deformation of a trapped dipolar Fermi gas”. *Phys. Rev. A* 77 (2008), 061603(R). DOI: [10.1103/PhysRevA.77.061603](https://doi.org/10.1103/PhysRevA.77.061603) (cit. on pp. 46, 158, 182).
- [209] G. M. Bruun and E. Taylor. “Quantum Phases of a Two-Dimensional Dipolar Fermi Gas”. *Phys. Rev. Lett.* 101 (2008), p. 245301. DOI: [10.1103/PhysRevLett.101.245301](https://doi.org/10.1103/PhysRevLett.101.245301) (cit. on pp. 46, 159, 181).
- [210] P. Rabl and P. Zoller. “Molecular dipolar crystals as high-fidelity quantum memory for hybrid quantum computing”. *Phys. Rev. A* 76 (2007), p. 042308. DOI: [10.1103/PhysRevA.76.042308](https://doi.org/10.1103/PhysRevA.76.042308) (cit. on p. 47).

- [211] S. F. Yelin, K. Kirby, and R. Côté. “Schemes for robust quantum computation with polar molecules”. *Phys. Rev. A* 74 (2006), 050301(R). DOI: [10.1103/PhysRevA.74.050301](https://doi.org/10.1103/PhysRevA.74.050301) (cit. on p. 47).
- [212] A. Micheli, G. K. Brennen, and P. Zoller. “A toolbox for lattice-spin models with polar molecules”. *Nat. Phys.* 2 (2006), pp. 341–347. DOI: [10.1038/nphys287](https://doi.org/10.1038/nphys287) (cit. on pp. 47, 182).
- [213] P. Rabl, D. DeMille, J. M. Doyle, M. D. Lukin, R. J. Schoelkopf, and P. Zoller. “Hybrid Quantum Processors: Molecular Ensembles as Quantum Memory for Solid State Circuits”. *Phys. Rev. Lett.* 97 (2006), p. 033003. DOI: [10.1103/PhysRevLett.97.033003](https://doi.org/10.1103/PhysRevLett.97.033003) (cit. on p. 47).
- [214] V. V. Flambaum and M. G. Kozlov. “Enhanced Sensitivity to the Time Variation of the Fine-Structure Constant and  $m_p/m_e$  in Diatomic Molecules”. *Phys. Rev. Lett.* 99 (2007), p. 150801. DOI: [10.1103/PhysRevLett.99.150801](https://doi.org/10.1103/PhysRevLett.99.150801) (cit. on p. 47).
- [215] D. DeMille, S. B. Cahn, D. Murphree, D. A. Rahmlow, and M. G. Kozlov. “Using Molecules to Measure Nuclear Spin-Dependent Parity Violation”. *Phys. Rev. Lett.* 100 (2008), p. 023003. DOI: [10.1103/PhysRevLett.100.023003](https://doi.org/10.1103/PhysRevLett.100.023003) (cit. on p. 47).
- [216] O. Dulieu, M. Raoult, and E. Tiemann. “Cold molecules: a chemistry kitchen for physicists?” *J. Phys. B: At., Mol. Opt. Phys.* 39 (2006). DOI: [10.1088/0953-4075/39/19/E01](https://doi.org/10.1088/0953-4075/39/19/E01) (cit. on p. 47).
- [217] M. Mudrich, O. Bünermann, F. Stienkemeier, O. Dulieu, and M. Weidemüller. “Formation of cold bialkali dimers on helium nanodroplets”. *Eur. Phys. J. D* 31 (2004), pp. 291–299. DOI: [10.1140/epjd/e2004-00139-6](https://doi.org/10.1140/epjd/e2004-00139-6) (cit. on p. 47).
- [218] O. Allard, J. Nagl, G. Auböck, C. Callegari, and W. E. Ernst. “Investigation of KRb and Rb<sub>2</sub> formed on cold helium nanodroplets”. *J. Phys. B: At., Mol. Opt. Phys.* 39 (2006), S1169–S1181. DOI: [10.1088/0953-4075/39/19/S24](https://doi.org/10.1088/0953-4075/39/19/S24) (cit. on p. 47).
- [219] M. Mudrich and F. Stienkemeier. “Photoionisation of pure and doped helium nanodroplets”. *Int. Rev. Phys. Chem.* 33 (2014), pp. 301–339. DOI: [10.1080/0144235x.2014.937188](https://doi.org/10.1080/0144235x.2014.937188) (cit. on p. 47).
- [220] C. P. Koch, J. P. Palao, R. Kosloff, and F. Masnou-Seeuws. “Stabilization of ultracold molecules using optimal control theory”. *Phys. Rev. A* 70 (2004), p. 013402. DOI: [10.1103/PhysRevA.70.013402](https://doi.org/10.1103/PhysRevA.70.013402) (cit. on p. 48).
- [221] E. Luc-Koenig, R. Kosloff, F. Masnou-Seeuws, and M. Vatasescu. “Photoassociation of cold atoms with chirped laser pulses: Time-dependent calculations and analysis of the adiabatic transfer within a two-state model”. *Phys. Rev. A* 70 (2004), p. 033414. DOI: [10.1103/physreva.70.033414](https://doi.org/10.1103/physreva.70.033414) (cit. on p. 48).
- [222] B. L. Brown, A. J. Dicks, and I. A. Walmsley. “Coherent Control of Ultracold Molecule Dynamics in a Magneto-Optical Trap by Use of Chirped Femtosecond Laser Pulses”. *Phys. Rev. Lett.* 96 (2006), p. 173002. DOI: [10.1103/PhysRevLett.96.173002](https://doi.org/10.1103/PhysRevLett.96.173002) (cit. on p. 48).
- [223] C. P. Koch and M. Shapiro. “Coherent Control of Ultracold Photoassociation”. *Chem. Rev.* 112 (2012), pp. 4928–4948. DOI: [10.1021/cr2003882](https://doi.org/10.1021/cr2003882) (cit. on p. 48).
- [224] C. Koch. “Coherent Control of Cold Collisions”. In: O. Dulieu and A. Osterwalder, eds. *Cold Chemistry: Molecular Scattering and Reactivity Near Absolute Zero*. The Royal Society of Chemistry, 2018. Chap. 11, pp. 633–662 (cit. on p. 48).
- [225] J. J. Zirbel, K.-K. Ni, S. Ospelkaus, J. P. D’Incao, C. E. Wieman, J. Ye, and D. S. Jin. “Collisional Stability of Fermionic Feshbach Molecules”. *Phys. Rev. Lett.* 100 (2008), p. 143201. DOI: [10.1103/PhysRevLett.100.143201](https://doi.org/10.1103/PhysRevLett.100.143201) (cit. on pp. 48, 176).
- [226] J. J. Zirbel, K.-K. Ni, S. Ospelkaus, T. L. Nicholson, M. L. Olsen, P. S. Julienne, C. E. Wieman, J. Ye, and D. S. Jin. “Heteronuclear molecules in an optical dipole trap”. *Phys. Rev. A* 78 (2008), p. 013416. DOI: [10.1103/PhysRevA.78.013416](https://doi.org/10.1103/PhysRevA.78.013416) (cit. on pp. 48, 59).
- [227] J. Zirbel. “Ultracold Fermionic Feshbach Molecules”. PhD thesis. University of Colorado, 2008 (cit. on pp. 48, 49, 176).

- [228] S. Ospelkaus, K.-K. Ni, M. H. G. de Miranda, B. Neyenhuis, D. Wang, S. Kotochigova, P. S. Julienne, D. S. Jin, and J. Ye. “Ultracold polar molecules near quantum degeneracy”. *Faraday Discussions* (2009) (cit. on p. 49).
- [229] K.-K. Ni. “A Quantum Gas of Polar Molecules”. PhD thesis. University of Colorado, 2010 (cit. on pp. 49, 89, 176).
- [230] S. Ospelkaus, K.-K. Ni, G. Quéméner, B. Neyenhuis, D. Wang, M. H. G. de Miranda, J. L. Bohn, J. Ye, and D. S. Jin. “Controlling the Hyperfine State of Rovibronic Ground-State Polar Molecules”. *Phys. Rev. Lett.* 104 (2010), p. 030402. DOI: [10.1103/PhysRevLett.104.030402](https://doi.org/10.1103/PhysRevLett.104.030402) (cit. on pp. 49, 111, 176).
- [231] D. Wang, B. Neyenhuis, M. H. G. de Miranda, K.-K. Ni, S. Ospelkaus, D. S. Jin, and J. Ye. “Direct absorption imaging of ultracold polar molecules”. *Phys. Rev. A* 81 (2010), 061404(R). DOI: [10.1103/PhysRevA.81.061404](https://doi.org/10.1103/PhysRevA.81.061404) (cit. on pp. 49, 176).
- [232] K.-K. Ni, S. Ospelkaus, D. J. Nesbitt, J. Ye, and D. S. Jin. “A dipolar gas of ultracold molecules”. *Phys. Chem. Chem. Phys.* 11 (2009), pp. 9626–9639 (cit. on pp. 49, 176).
- [233] K.-K. Ni, S. Ospelkaus, D. Wang, G. Quéméner, B. Neyenhuis, M. H. G. de Miranda, J. L. Bohn, J. Ye, and D. S. Jin. “Dipolar collisions of polar molecules in the quantum regime”. *Nature* 464 (2010), pp. 1324–1328. DOI: [10.1038/nature08953](https://doi.org/10.1038/nature08953) (cit. on pp. 49, 111, 114, 118, 145, 176).
- [234] S. Ospelkaus, K.-K. Ni, D. Wang, M. H. G. de Miranda, B. Neyenhuis, G. Quéméner, P. S. Julienne, J. L. Bohn, D. S. Jin, and J. Ye. “Quantum-State Controlled Chemical Reactions of Ultracold Potassium-Rubidium Molecules”. *Science* 327 (2010), pp. 853–857. DOI: [10.1126/science.1184121](https://doi.org/10.1126/science.1184121) (cit. on pp. 49, 116, 131, 176).
- [235] M. H. G. de Miranda, A. Chotia, B. Neyenhuis, D. Wang, G. Quéméner, S. Ospelkaus, J. L. Bohn, J. Ye, and D. S. Jin. “Controlling the quantum stereodynamics of ultracold bimolecular reactions”. *Nat. Phys.* 7 (2011), p. 502. DOI: [10.1038/nphys1939](https://doi.org/10.1038/nphys1939) (cit. on pp. 49, 176).
- [236] K. Aikawa, D. Akamatsu, J. Kobayashi, M. Ueda, T. Kishimoto, and S. Inouye. “Toward the production of quantum degenerate bosonic polar molecules,  $^{41}\text{K}^{87}\text{Rb}$ ”. *New J. Phys.* 11 (2009) (cit. on pp. 49, 176).
- [237] K. Aikawa, D. Akamatsu, M. Hayashi, K. Oasa, J. Kobayashi, P. Naidon, T. Kishimoto, M. Ueda, and S. Inouye. “Coherent Transfer of Photoassociated Molecules into the Rovibrational Ground State”. *Phys. Rev. Lett.* 105 (2010), p. 203001. DOI: [10.1103/PhysRevLett.105.203001](https://doi.org/10.1103/PhysRevLett.105.203001) (cit. on pp. 49, 176).
- [238] P. S. Źuchowski and J. M. Hutson. “Reactions of ultracold alkali-metal dimers”. *Phys. Rev. A* 81 (2010), 060703(R). DOI: [10.1103/PhysRevA.81.060703](https://doi.org/10.1103/PhysRevA.81.060703) (cit. on pp. 50, 111, 167).
- [239] D. Egorov, T. Lahaye, W. Schöllkopf, B. Friedrich, and J. M. Doyle. “Buffer-gas cooling of atomic and molecular beams”. *Phys. Rev. A* 66 (2002), p. 043401. DOI: [10.1103/PhysRevA.66.043401](https://doi.org/10.1103/PhysRevA.66.043401) (cit. on p. 51).
- [240] S. E. Maxwell, N. Brahms, R. deCarvalho, D. R. Glenn, J. S. Helton, S. V. Nguyen, D. Patterson, J. Petricka, D. DeMille, and J. M. Doyle. “High-Flux Beam Source for Cold, Slow Atoms or Molecules”. *Phys. Rev. Lett.* 95 (2005), p. 173201. DOI: [10.1103/PhysRevLett.95.173201](https://doi.org/10.1103/PhysRevLett.95.173201) (cit. on p. 51).
- [241] N. R. Hutzler, H.-I. Lu, and J. M. Doyle. “The Buffer Gas Beam: An Intense, Cold, and Slow Source for Atoms and Molecules”. *Chem. Rev.* 112 (2012), pp. 4803–4827 (cit. on p. 51).
- [242] L. Scharfenberg, H. Haak, G. Meijer, and S. Y. T. van de Meerakker. “Operation of a Stark decelerator with optimum acceptance”. *Phys. Rev. A* 79 (2009), p. 023410. DOI: [10.1103/physreva.79.023410](https://doi.org/10.1103/physreva.79.023410) (cit. on p. 51).

- [243] A. Osterwalder, S. A. Meek, G. Hammer, H. Haak, and G. Meijer. “Deceleration of neutral molecules in macroscopic traveling traps”. *Phys. Rev. A* 81 (2010), p. 051401. DOI: [10.1103/physreva.81.051401](https://doi.org/10.1103/physreva.81.051401) (cit. on p. 51).
- [244] T. E. Wall, J. F. Kanem, J. M. Dyne, J. J. Hudson, B. E. Sauer, E. A. Hinds, and M. R. Tarbutt. “Stark deceleration of CaF molecules in strong- and weak-field seeking states”. *Phys. Chem. Chem. Phys.* 13 (2011), p. 18991. DOI: [10.1039/c1cp21254k](https://doi.org/10.1039/c1cp21254k) (cit. on p. 51).
- [245] S. A. Rangwala, T. Junglen, T. Rieger, P. W. H. Pinkse, and G. Rempe. “Continuous source of translationally cold dipolar molecules”. *Phys. Rev. A* 67 (2003), p. 043406. DOI: [10.1103/PhysRevA.67.043406](https://doi.org/10.1103/PhysRevA.67.043406) (cit. on p. 51).
- [246] E. Narevicius, A. Libson, M. F. Riedel, C. G. Parthey, I. Chavez, U. Even, and M. G. Raizen. “Coherent Slowing of a Supersonic Beam with an Atomic Paddle”. *Phys. Rev. Lett.* 98 (2007), p. 103201. DOI: [10.1103/PhysRevLett.98.103201](https://doi.org/10.1103/PhysRevLett.98.103201) (cit. on p. 51).
- [247] M. Viteau, A. Chotia, M. Allegrini, N. Bouloufa, O. Dulieu, D. Comparat, and P. Pillet. “Optical Pumping and Vibrational Cooling of Molecules”. *Science* 321 (2008), pp. 232–234. DOI: [10.1126/science.1159496](https://doi.org/10.1126/science.1159496) (cit. on p. 51).
- [248] E. Narevicius, C. G. Parthey, A. Libson, M. F. Riedel, U. Even, and M. G. Raizen. “Towards magnetic slowing of atoms and molecules”. *New J. Phys.* 9 (2007), pp. 96–96. DOI: [10.1088/1367-2630/9/4/096](https://doi.org/10.1088/1367-2630/9/4/096) (cit. on p. 51).
- [249] E. Tsikata, W. C. Campbell, M. T. Hummon, H.-I. Lu, and J. M. Doyle. “Magnetic trapping of NH molecules with 20 s lifetimes”. *New J. Phys.* 12 (2010), p. 065028. DOI: [10.1088/1367-2630/12/6/065028](https://doi.org/10.1088/1367-2630/12/6/065028) (cit. on p. 51).
- [250] J. Riedel, S. Hoekstra, W. Jäger, J. J. Gilijamse, S. Y. T. van de Meerakker, and G. Meijer. “Accumulation of Stark-decelerated NH molecules in a magnetic trap”. *Eur. Phys. J. D* 65 (2011), pp. 161–166. DOI: [10.1140/epjd/e2011-20082-7](https://doi.org/10.1140/epjd/e2011-20082-7) (cit. on p. 51).
- [251] E. Lavert-Ofir, S. Gersten, A. B. Henson, I. Shani, L. David, J. Narevicius, and E. Narevicius. “A moving magnetic trap decelerator: a new source of cold atoms and molecules”. *New J. Phys.* 13 (2011), p. 103030. DOI: [10.1088/1367-2630/13/10/103030](https://doi.org/10.1088/1367-2630/13/10/103030) (cit. on pp. 51, 62).
- [252] B. C. Sawyer, B. L. Lev, E. R. Hudson, B. K. Stuhl, M. Lara, J. L. Bohn, and J. Ye. “Magneto-electrostatic Trapping of Ground State OH Molecules”. *Phys. Rev. Lett.* 98 (2007), p. 253002. DOI: [10.1103/PhysRevLett.98.253002](https://doi.org/10.1103/PhysRevLett.98.253002) (cit. on p. 51).
- [253] B. C. Sawyer, B. K. Stuhl, D. Wang, M. Yeo, and J. Ye. “Molecular Beam Collisions with a Magnetically Trapped Target”. *Phys. Rev. Lett.* (2008). DOI: [10.1103/PhysRevLett.101.203203](https://doi.org/10.1103/PhysRevLett.101.203203) (cit. on p. 51).
- [254] G. Morigi, P. W. H. Pinkse, M. Kowalewski, and R. de Vivie-Riedle. “Cavity Cooling of Internal Molecular Motion”. *Phys. Rev. Lett.* 99 (2007), p. 073001. DOI: [10.1103/PhysRevLett.99.073001](https://doi.org/10.1103/PhysRevLett.99.073001) (cit. on p. 51).
- [255] B. L. Lev, A. Vukics, E. R. Hudson, B. C. Sawyer, P. Domokos, H. Ritsch, and J. Ye. “Prospects for the cavity-assisted laser cooling of molecules”. *Phys. Rev. A* 77 (2008), p. 023402. DOI: [10.1103/physreva.77.023402](https://doi.org/10.1103/physreva.77.023402) (cit. on p. 51).
- [256] B. K. Stuhl, B. C. Sawyer, D. Wang, and J. Ye. “Magneto-optical Trap for Polar Molecules”. *Phys. Rev. Lett.* 101 (2008), p. 243002. DOI: [10.1103/PhysRevLett.101.243002](https://doi.org/10.1103/PhysRevLett.101.243002) (cit. on pp. 51, 52, 60).
- [257] Y. Hao et al. “High accuracy theoretical investigations of CaF, SrF, and BaF and implications for laser-cooling”. *J. Chem. Phys.* 151 (2019), p. 034302. DOI: [10.1063/1.5098540](https://doi.org/10.1063/1.5098540) (cit. on p. 52).
- [258] E. S. Shuman, J. F. Barry, D. R. Glenn, and D. DeMille. “Radiative Force from Optical Cycling on a Diatomic Molecule”. *Phys. Rev. Lett.* 103 (2009), p. 223001. DOI: [10.1103/PhysRevLett.103.223001](https://doi.org/10.1103/PhysRevLett.103.223001) (cit. on pp. 52, 60).

- [259] E. S. Shuman, J. F. Barry, and D. DeMille. “Laser cooling of a diatomic molecule”. *Nature* 467 (2010), pp. 820–823. DOI: [10.1038/nature09443](https://doi.org/10.1038/nature09443) (cit. on pp. 52–54).
- [260] J. F. Barry. “Laser cooling and slowing of a diatomic molecule”. PhD thesis. Yale University, 2013 (cit. on p. 52).
- [261] B. K. Stuhl. “Ultracold molecules for the masses: evaporative cooling and magneto-optical trapping”. PhD thesis. University of Colorado, 2012 (cit. on pp. 52, 60).
- [262] J. J. Hudson, D. M. Kara, I. J. Smallman, B. E. Sauer, M. R. Tarbutt, and E. A. Hinds. “Improved measurement of the shape of the electron”. *Nature* 473 (2011), pp. 493–496. DOI: [10.1038/nature10104](https://doi.org/10.1038/nature10104) (cit. on p. 53).
- [263] B. C. Regan, E. D. Commins, C. J. Schmidt, and D. DeMille. “New Limit on the Electron Electric Dipole Moment”. *Phys. Rev. Lett.* 88 (2002), p. 071805. DOI: [10.1103/PhysRevLett.88.071805](https://doi.org/10.1103/PhysRevLett.88.071805) (cit. on p. 53).
- [264] J. G. Danzl, E. Haller, M. Gustavsson, M. J. Mark, R. Hart, N. Bouleuf, O. Dulieu, H. Ritsch, and H.-C. Nägerl. “Quantum Gas of Deeply Bound Ground State Molecules”. *Science* 321 (2008), pp. 1062–1066. DOI: [10.1126/science.1159909](https://doi.org/10.1126/science.1159909) (cit. on p. 54).
- [265] F. Lang, K. Winkler, C. Strauss, R. Grimm, and J. H. Denschlag. “Ultracold Triplet Molecules in the Rovibrational Ground State”. *Phys. Rev. Lett.* 101 (2008), p. 133005. DOI: [10.1103/PhysRevLett.101.133005](https://doi.org/10.1103/PhysRevLett.101.133005) (cit. on p. 54).
- [266] J. G. Danzl, M. J. Mark, E. Haller, M. Gustavsson, R. Hart, J. Aldegunde, J. M. Hutson, and H.-C. Nägerl. “An ultracold high-density sample of rovibronic ground-state molecules in an optical lattice”. *Nat. Phys.* 6 (2010), pp. 265–270. DOI: [10.1038/nphys1533](https://doi.org/10.1038/nphys1533) (cit. on p. 54).
- [267] H.-C. Nägerl, M. J. Mark, E. Haller, M. Gustavsson, R. Hart, and J. G. Danzl. “Ultracold and dense samples of ground-state molecules in lattice potentials”. *J. Phys. Conf. Ser.* 264 (2011), p. 012015. DOI: [10.1088/1742-6596/264/1/012015](https://doi.org/10.1088/1742-6596/264/1/012015) (cit. on p. 54).
- [268] K. Jag-Lauber. “Ultracold Homonuclear Cesium Molecules: Efficient Production, Collisional Properties and Stability Measurements”. PhD thesis. University of Innsbruck, 2018 (cit. on p. 54).
- [269] Z. Zhang, L. Chen, K. Yao, and C. Chin. “Transition from an atomic to a molecular Bose–Einstein condensate”. *Nature* 592 (2021), pp. 708–711. DOI: [10.1038/s41586-021-03443-0](https://doi.org/10.1038/s41586-021-03443-0) (cit. on p. 54).
- [270] L. D. Carr, D. DeMille, R. V. Krems, and J. Ye. “Cold and ultracold molecules: science, technology and applications”. *New J. Phys.* 11 (2009), p. 055049. DOI: [10.1088/1367-2630/11/5/055049](https://doi.org/10.1088/1367-2630/11/5/055049) (cit. on p. 54).
- [271] O. Dulieu and C. Gabbanini. “The formation and interactions of cold and ultracold molecules: new challenges for interdisciplinary physics”. *Rep. Progr. Phys.* 72 (2009), p. 086401. DOI: [10.1088/0034-4885/72/8/086401](https://doi.org/10.1088/0034-4885/72/8/086401) (cit. on p. 54).
- [272] B. Friedrich and J. M. Doyle. “Why are Cold Molecules so Hot?” *ChemPhysChem* 10 (2009), pp. 604–623. DOI: [10.1002/cphc.200800577](https://doi.org/10.1002/cphc.200800577) (cit. on p. 54).
- [273] D. S. Jin and J. Ye. “Polar molecules in the quantum regime”. *Physics Today* 64 (2011), pp. 27–31. DOI: [10.1063/1.3592002](https://doi.org/10.1063/1.3592002) (cit. on p. 55).
- [274] Z. Idziaszek, G. Quéméner, J. L. Bohn, and P. S. Julienne. “Simple quantum model of ultracold polar molecule collisions”. *Phys. Rev. A* 82 (2010), 020703(R). DOI: [10.1103/PhysRevA.82.020703](https://doi.org/10.1103/PhysRevA.82.020703) (cit. on pp. 55, 116).
- [275] Z. Idziaszek and P. S. Julienne. “Universal Rate Constants for Reactive Collisions of Ultracold Molecules”. *Phys. Rev. Lett.* 104 (2010), p. 113202. DOI: [10.1103/PhysRevLett.104.113202](https://doi.org/10.1103/PhysRevLett.104.113202) (cit. on p. 55).

- [276] G. Quéméner and J. L. Bohn. “Strong dependence of ultracold chemical rates on electric dipole moments”. *Phys. Rev. A* 81 (2010), p. 022702. DOI: [10.1103/PhysRevA.81.022702](https://doi.org/10.1103/PhysRevA.81.022702) (cit. on pp. 55, 139).
- [277] P. S. Julienne, T. M. Hanna, and Z. Idziaszek. “Universal ultracold collision rates for polar molecules of two alkali-metal atoms”. *Phys. Chem. Chem. Phys.* 13 (2011), p. 19114. DOI: [10.1039/c1cp21270b](https://doi.org/10.1039/c1cp21270b) (cit. on pp. 55, 139).
- [278] A. Micheli, Z. Idziaszek, G. Pupillo, M. A. Baranov, P. Zoller, and P. S. Julienne. “Universal Rates for Reactive Ultracold Polar Molecules in Reduced Dimensions”. *Phys. Rev. Lett.* 105 (2010), p. 073202. DOI: [10.1103/PhysRevLett.105.073202](https://doi.org/10.1103/PhysRevLett.105.073202) (cit. on pp. 55, 139).
- [279] G. Quéméner and J. L. Bohn. “Electric field suppression of ultracold confined chemical reactions”. *Phys. Rev. A* 81 (2010), 060701(R). DOI: [10.1103/PhysRevA.81.060701](https://doi.org/10.1103/PhysRevA.81.060701) (cit. on pp. 55, 139).
- [280] G. Quéméner and J. L. Bohn. “Dynamics of ultracold molecules in confined geometry and electric field”. *Phys. Rev. A* 83 (2011), p. 012705. DOI: [10.1103/PhysRevA.83.012705](https://doi.org/10.1103/PhysRevA.83.012705) (cit. on pp. 55, 139).
- [281] B. Zhu, G. Quéméner, A. M. Rey, and M. J. Holland. “Evaporative cooling of reactive polar molecules confined in a two-dimensional geometry”. *Phys. Rev. A* 88 (2013), p. 063405. DOI: [10.1103/PhysRevA.88.063405](https://doi.org/10.1103/PhysRevA.88.063405) (cit. on p. 55).
- [282] B. Zhu et al. “Suppressing the Loss of Ultracold Molecules Via the Continuous Quantum Zeno Effect”. *Phys. Rev. Lett.* 112 (2014), p. 070404. DOI: [10.1103/PhysRevLett.112.070404](https://doi.org/10.1103/PhysRevLett.112.070404) (cit. on p. 55).
- [283] G. Quéméner and P. S. Julienne. “Ultracold Molecules under Control!” *Chem. Rev.* 112 (2012), pp. 4949–5011. DOI: [10.1021/cr300092g](https://doi.org/10.1021/cr300092g) (cit. on p. 55).
- [284] G. Quéméner. “Ultracold collisions of molecules”. In: O. Dulieu and A. Osterwalder, eds. *Cold Chemistry: Molecular Scattering and Reactivity Near Absolute Zero*. The Royal Society of Chemistry, 2018. Chap. 12, pp. 579–632 (cit. on p. 55).
- [285] J. F. E. Croft, J. L. Bohn, and G. Quéméner. “Unified model of ultracold molecular collisions”. *Phys. Rev. A* 102 (2020), p. 033306. DOI: [10.1103/PhysRevA.102.033306](https://doi.org/10.1103/PhysRevA.102.033306) (cit. on p. 55).
- [286] A. Lercher, T. Takekoshi, M. Debatin, B. Schuster, R. Rameshan, F. Ferlaino, R. Grimm, and H.-C. Nägerl. “Production of a dual-species Bose-Einstein condensate of Rb and Cs atoms”. *Eur. Phys. J. D* 65 (2011), pp. 3–9. DOI: [10.1140/epjd/e2011-20015-6](https://doi.org/10.1140/epjd/e2011-20015-6) (cit. on pp. 55, 179).
- [287] K. Pilch, A. D. Lange, A. Prantner, G. Kerner, F. Ferlaino, H.-C. Nägerl, and R. Grimm. “Observation of interspecies Feshbach resonances in an ultracold Rb-Cs mixture”. *Phys. Rev. A* 79 (2009), p. 042718. DOI: [10.1103/PhysRevA.79.042718](https://doi.org/10.1103/PhysRevA.79.042718) (cit. on pp. 55, 179).
- [288] H. W. Cho, D. J. McCarron, D. L. Jenkin, M. P. Köppinger, and S. L. Cornish. “A high phase-space density mixture of  $^{87}\text{Rb}$  and  $^{133}\text{Cs}$ : towards ultracold heteronuclear molecules”. *Eur. Phys. J. D* 65 (2011), pp. 125–131. DOI: [10.1140/epjd/e2011-10716-1](https://doi.org/10.1140/epjd/e2011-10716-1) (cit. on pp. 55, 179).
- [289] D. J. McCarron, H. W. Cho, D. L. Jenkin, M. P. Köppinger, and S. L. Cornish. “Dual-species Bose-Einstein condensate of  $^{87}\text{Rb}$  and  $^{133}\text{Cs}$ ”. *Phys. Rev. A* 84 (2011), p. 011603. DOI: [10.1103/PhysRevA.84.011603](https://doi.org/10.1103/PhysRevA.84.011603) (cit. on pp. 55, 179).
- [290] M. Debatin, T. Takekoshi, R. Rameshan, L. Reichsöllner, F. Ferlaino, R. Grimm, R. Vexiau, N. Bouloufa, O. Dulieu, and H.-C. Nägerl. “Molecular spectroscopy for ground-state transfer of ultracold RbCs molecules”. *Phys. Chem. Chem. Phys.* 13 (2011), pp. 18926–18935. DOI: [10.1039/c1cp21769k](https://doi.org/10.1039/c1cp21769k) (cit. on pp. 55, 179).

- [291] T. Takekoshi, M. Debatin, R. Rameshan, F. Ferlaino, R. Grimm, H.-C. Nägerl, C. R. L. Sueur, J. M. Hutson, P. S. Julienne, S. Kotchigova, and E. Tiemann. “Towards the production of ultracold ground-state RbCs molecules: Feshbach resonances, weakly bound states, and the coupled-channel model”. *Phys. Rev. A* 85 (2012), p. 032506. DOI: [10.1103/physreva.85.032506](https://doi.org/10.1103/physreva.85.032506) (cit. on pp. 55, 179).
- [292] M. P. Köppinger, D. J. McCarron, D. L. Jenkin, P. K. Molony, H.-W. Cho, S. L. Cornish, C. R. Le Sueur, C. L. Blackley, and J. M. Hutson. “Production of optically trapped  $^{87}\text{Rb}$ Cs Feshbach molecules”. *Phys. Rev. A* 89 (2014), p. 033604. DOI: [10.1103/PhysRevA.89.033604](https://doi.org/10.1103/PhysRevA.89.033604) (cit. on pp. 55, 179).
- [293] T. Takekoshi, L. Reichsöllner, A. Schindewolf, J. M. Hutson, C. R. L. Sueur, O. Dulieu, F. Ferlaino, R. Grimm, and H.-C. Nägerl. “Ultracold Dense Samples of Dipolar RbCs Molecules in the Rovibrational and Hyperfine Ground State”. *Phys. Rev. Lett.* 113 (2014), p. 205301. DOI: [10.1103/PhysRevLett.113.205301](https://doi.org/10.1103/PhysRevLett.113.205301) (cit. on pp. 55, 58, 89, 111, 179).
- [294] P. K. Molony, P. D. Gregory, Z. Ji, B. Lu, M. P. Köppinger, C. R. L. Sueur, C. L. Blackley, J. M. Hutson, and S. L. Cornish. “Creation of Ultracold  $^{87}\text{Rb}$  $^{133}\text{Cs}$  Molecules in the Rovibrational Ground State”. *Phys. Rev. Lett.* 113 (2014), p. 255301. DOI: [10.1103/PhysRevLett.113.255301](https://doi.org/10.1103/PhysRevLett.113.255301) (cit. on pp. 55, 179).
- [295] L. Reichsöllner, A. Schindewolf, T. Takekoshi, R. Grimm, and H.-C. Nägerl. “Quantum Engineering of a Low-Entropy Gas of Heteronuclear Bosonic Molecules in an Optical Lattice”. *Phys. Rev. Lett.* 118 (2017), p. 073201. DOI: [10.1103/PhysRevLett.118.073201](https://doi.org/10.1103/PhysRevLett.118.073201) (cit. on pp. 56, 57, 139, 179).
- [296] P. D. Gregory, P. K. Molony, M. P. Köppinger, A. Kumar, Z. Ji, B. Lu, A. L. Marchant, and S. L. Cornish. “A simple, versatile laser system for the creation of ultracold ground state molecules”. *New J. Phys.* 17 (2015), p. 055006. DOI: [10.1088/1367-2630/17/5/055006](https://doi.org/10.1088/1367-2630/17/5/055006) (cit. on pp. 57, 179).
- [297] C.-H. Wu, J. W. Park, P. Ahmadi, S. Will, and M. W. Zwierlein. “Ultracold Fermionic Feshbach Molecules of  $^{23}\text{Na}$  $^{40}\text{K}$ ”. *Phys. Rev. Lett.* 109 (2012), p. 085301. DOI: [10.1103/PhysRevLett.109.085301](https://doi.org/10.1103/PhysRevLett.109.085301) (cit. on pp. 58, 72, 172).
- [298] J. W. Park, C.-H. Wu, I. Santiago, T. G. Tiecke, S. Will, P. Ahmadi, and M. W. Zwierlein. “Quantum degenerate Bose-Fermi mixture of chemically different atomic species with widely tunable interactions”. *Phys. Rev. A* 85 (2012), 051602(R). DOI: [10.1103/PhysRevA.85.051602](https://doi.org/10.1103/PhysRevA.85.051602) (cit. on pp. 58, 74, 172).
- [299] J. W. Park, S. A. Will, and M. W. Zwierlein. “Ultracold Dipolar Gas of Fermionic  $^{23}\text{Na}$  $^{40}\text{K}$  Molecules in Their Absolute Ground State”. *Phys. Rev. Lett.* 114 (2015), p. 205302. DOI: [10.1103/PhysRevLett.114.205302](https://doi.org/10.1103/PhysRevLett.114.205302) (cit. on pp. 58, 71, 77, 86, 89, 172).
- [300] F. Wang, X. He, X. Li, B. Zhu, J. Chen, and D. Wang. “Formation of ultracold NaRb Feshbach molecules”. *New J. Phys.* 17 (2015), p. 035003. DOI: [10.1088/1367-2630/17/3/035003](https://doi.org/10.1088/1367-2630/17/3/035003) (cit. on pp. 58, 174).
- [301] M. Guo, B. Zhu, B. Lu, X. Ye, F. Wang, R. Vexiau, N. Bouloufa-Maafa, G. Quéméner, O. Dulieu, and D. Wang. “Creation of an Ultracold Gas of Ground-State Dipolar  $^{23}\text{Na}$  $^{87}\text{Rb}$  Molecules”. *Phys. Rev. Lett.* 116 (2016), p. 205303. DOI: [10.1103/PhysRevLett.116.205303](https://doi.org/10.1103/PhysRevLett.116.205303) (cit. on pp. 58, 89, 174).
- [302] M. Guo, R. Vexiau, B. Zhu, B. Lu, N. Bouloufa-Maafa, O. Dulieu, and D. Wang. “High-resolution molecular spectroscopy for producing ultracold absolute-ground-state  $^{23}\text{Na}$  $^{87}\text{Rb}$  molecules”. *Phys. Rev. A* 96 (2017), p. 052505. DOI: [10.1103/PhysRevA.96.052505](https://doi.org/10.1103/PhysRevA.96.052505) (cit. on pp. 58, 89, 174).
- [303] M.-S. Heo, T. T. Wang, C. A. Christensen, T. M. Rvachov, D. A. Cotta, J.-H. Choi, Y.-R. Lee, and W. Ketterle. “Formation of ultracold fermionic NaLi Feshbach molecules”. *Phys. Rev. A* 86 (2012), 021602(R). DOI: [10.1103/PhysRevA.86.021602](https://doi.org/10.1103/PhysRevA.86.021602) (cit. on pp. 58, 168).

- [304] T. M. Rvachov, H. Son, A. T. Sommer, S. Ebadi, J. J. Park, M. W. Zwierlein, W. Ketterle, and A. O. Jamison. “Long-Lived Ultracold Molecules with Electric and Magnetic Dipole Moments”. *Phys. Rev. Lett.* 119 (2017), p. 143001. DOI: [10.1103/PhysRevLett.119.143001](https://doi.org/10.1103/PhysRevLett.119.143001) (cit. on pp. 58, 168).
- [305] T. M. Rvachov, H. Son, J. J. Park, P. M. Notz, T. T. Wang, M. W. Zwierlein, W. Ketterle, and A. O. Jamison. “Photoassociation of ultracold NaLi”. *Phys. Chem. Chem. Phys.* 20 (2018), pp. 4746–4751. DOI: [10.1039/c7cp08480c](https://doi.org/10.1039/c7cp08480c) (cit. on pp. 58, 168).
- [306] T. M. Rvachov, H. Son, J. J. Park, S. Ebadi, M. W. Zwierlein, W. Ketterle, and A. O. Jamison. “Two-photon spectroscopy of the NaLi triplet ground state”. *Phys. Chem. Chem. Phys.* 20 (2018), pp. 4739–4745. DOI: [10.1039/c7cp08481a](https://doi.org/10.1039/c7cp08481a) (cit. on pp. 58, 168).
- [307] R. Bause, A. Schindewolf, R. Tao, M. Duda, X.-Y. Chen, G. Quéméner, T. Karman, A. Christianen, I. Bloch, and X.-Y. Luo. “Collisions of ultracold molecules in bright and dark optical dipole traps”. *Phys. Rev. Research* 3 (2021), p. 033013. DOI: [10.1103/physrevresearch.3.033013](https://doi.org/10.1103/physrevresearch.3.033013) (cit. on pp. 58, 65, 111, 118, 130, 136, 173).
- [308] A. Chotia, B. Neyenhuis, S. A. Moses, B. Yan, J. P. Covey, M. Foss-Feig, A. M. Rey, D. S. Jin, and J. Ye. “Long-Lived Dipolar Molecules and Feshbach Molecules in a 3D Optical Lattice”. *Phys. Rev. Lett.* 108 (2012), p. 080405. DOI: [10.1103/PhysRevLett.108.080405](https://doi.org/10.1103/PhysRevLett.108.080405) (cit. on pp. 59, 108, 139, 176).
- [309] S. A. Moses, J. P. Covey, M. T. Miecnikowski, B. Yan, B. Gadway, J. Ye, and D. S. Jin. “Creation of a low-entropy quantum gas of polar molecules in an optical lattice”. *Science* 350 (2015), pp. 659–662. DOI: [10.1126/science.aac6400](https://doi.org/10.1126/science.aac6400) (cit. on pp. 59, 89, 139, 176).
- [310] B. Yan, S. A. Moses, B. Gadway, J. P. Covey, K. R. A. Hazzard, A. M. Rey, D. S. Jin, and J. Ye. “Observation of dipolar spin-exchange interactions with lattice-confined polar molecules”. *Nature* 501 (2013), pp. 521–525. DOI: [10.1038/nature12483](https://doi.org/10.1038/nature12483) (cit. on pp. 59, 161, 177).
- [311] N. Balakrishnan. “Perspective: Ultracold molecules and the dawn of cold controlled chemistry”. *J. Chem. Phys.* 145 (2016), p. 150901. DOI: [10.1063/1.4964096](https://doi.org/10.1063/1.4964096) (cit. on p. 59).
- [312] S. A. Moses, J. P. Covey, M. T. Miecnikowski, D. S. Jin, and J. Ye. “New frontiers for quantum gases of polar molecules”. *Nat. Phys.* 13 (2016), pp. 13–20. DOI: [10.1038/nphys3985](https://doi.org/10.1038/nphys3985) (cit. on p. 59).
- [313] B. Gadway and B. Yan. “Strongly interacting ultracold polar molecules”. *J. Phys. B: At., Mol. Opt. Phys.* 49 (2016), p. 152002. DOI: [10.1088/0953-4075/49/15/152002](https://doi.org/10.1088/0953-4075/49/15/152002) (cit. on p. 59).
- [314] J. L. Bohn, A. M. Rey, and J. Ye. “Cold molecules: Progress in quantum engineering of chemistry and quantum matter”. *Science* 357 (2017), pp. 1002–1010. DOI: [10.1126/science.aam6299](https://doi.org/10.1126/science.aam6299) (cit. on p. 59).
- [315] J. K. Freericks, M. M. Maśka, A. Hu, T. M. Hanna, C. J. Williams, P. S. Julienne, and R. Lemański. “Improving the efficiency of ultracold dipolar molecule formation by first loading onto an optical lattice”. *Phys. Rev. A* 81 (2010), 011605(R). DOI: [10.1103/PhysRevA.81.011605](https://doi.org/10.1103/PhysRevA.81.011605) (cit. on p. 59).
- [316] A. Safavi-Naini, M. L. Wall, and A. M. Rey. “Role of interspecies interactions in the preparation of a low-entropy gas of polar molecules in a lattice”. *Phys. Rev. A* 92 (2015), p. 063416. DOI: [10.1103/PhysRevA.92.063416](https://doi.org/10.1103/PhysRevA.92.063416) (cit. on p. 59).
- [317] S. A. Moses. “A quantum gas of polar molecules in an optical lattice”. PhD thesis. University of Colorado, 2016 (cit. on p. 59).
- [318] J. P. Covey. “Enhanced optical and electric manipulation of a quantum gas of KRb molecules”. PhD thesis. University of Colorado, 2017 (cit. on pp. 59, 152).
- [319] B. Neyenhuis, B. Yan, S. A. Moses, J. P. Covey, A. Chotia, A. Petrov, S. Kotochigova, J. Ye, and D. S. Jin. “Anisotropic Polarizability of Ultracold Polar  $^{40}\text{K}^{87}\text{Rb}$  Molecules”. *Phys. Rev. Lett.* 109 (2012), p. 230403. DOI: [10.1103/PhysRevLett.109.230403](https://doi.org/10.1103/PhysRevLett.109.230403) (cit. on pp. 59, 94, 108, 177).

- [320] K. R. A. Hazzard, B. Gadway, M. Foss-Feig, B. Yan, S. A. Moses, J. P. Covey, N. Y. Yao, M. D. Lukin, J. Ye, D. S. Jin, and A. M. Rey. “Many-Body Dynamics of Dipolar Molecules in an Optical Lattice”. *Phys. Rev. Lett.* 113 (2014), p. 195302. DOI: [10.1103/PhysRevLett.113.195302](https://doi.org/10.1103/PhysRevLett.113.195302) (cit. on pp. 59, 182).
- [321] P. D. Gregory, J. Aldegunde, J. M. Hutson, and S. L. Cornish. “Controlling the rotational and hyperfine state of ultracold  $^{87}\text{Rb}^{133}\text{Cs}$  molecules”. *Phys. Rev. A* 94 (2016), 041403(R). DOI: [10.1103/PhysRevA.94.041403](https://doi.org/10.1103/PhysRevA.94.041403) (cit. on pp. 59, 179).
- [322] S. A. Will, J. W. Park, Z. Z. Yan, H. Loh, and M. W. Zwierlein. “Coherent Microwave Control of Ultracold  $^{23}\text{Na}^{40}\text{K}$  Molecules”. *Phys. Rev. Lett.* 116 (2016), p. 225306. DOI: [10.1103/PhysRevLett.116.225306](https://doi.org/10.1103/PhysRevLett.116.225306) (cit. on pp. 59, 64, 172).
- [323] M. Guo, X. Ye, J. He, G. Quéméner, and D. Wang. “High-resolution internal state control of ultracold  $^{23}\text{Na}^{87}\text{Rb}$  molecules”. *Phys. Rev. A* 97 (2018), 020501(R). DOI: [10.1103/PhysRevA.97.020501](https://doi.org/10.1103/PhysRevA.97.020501) (cit. on pp. 59, 174).
- [324] J. W. Park, Z. Z. Yan, H. Loh, S. A. Will, and M. W. Zwierlein. “Second-scale nuclear spin coherence time of ultracold  $^{23}\text{Na}^{40}\text{K}$  molecules”. *Science* 357 (2017), pp. 372–375. DOI: [10.1126/science.aal5066](https://doi.org/10.1126/science.aal5066) (cit. on pp. 59, 172).
- [325] M. R. Tarbutt. “Magneto-optical trapping forces for atoms and molecules with complex level structures”. *New J. Phys.* 17 (2015), p. 015007. DOI: [10.1088/1367-2630/17/1/015007](https://doi.org/10.1088/1367-2630/17/1/015007) (cit. on p. 60).
- [326] J. F. Barry, E. S. Shuman, E. B. Norrgard, and D. DeMille. “Laser Radiation Pressure Slowing of a Molecular Beam”. *Phys. Rev. Lett.* 108 (2012), p. 103002. DOI: [10.1103/PhysRevLett.108.103002](https://doi.org/10.1103/PhysRevLett.108.103002) (cit. on p. 60).
- [327] M. T. Hummon, M. Yeo, B. K. Stuhl, A. L. Collopy, Y. Xia, and J. Ye. “2D Magneto-Optical Trapping of Diatomic Molecules”. *Phys. Rev. Lett.* 110 (2013), p. 143001. DOI: [10.1103/PhysRevLett.110.143001](https://doi.org/10.1103/PhysRevLett.110.143001) (cit. on p. 60).
- [328] M. Yeo, M. T. Hummon, A. L. Collopy, B. Yan, B. Hemmerling, E. Chae, J. M. Doyle, and J. Ye. “Rotational State Microwave Mixing for Laser Cooling of Complex Diatomic Molecules”. *Phys. Rev. Lett.* 114 (2015), p. 223003. DOI: [10.1103/PhysRevLett.114.223003](https://doi.org/10.1103/PhysRevLett.114.223003) (cit. on p. 60).
- [329] J. F. Barry, D. J. McCarron, E. B. Norrgard, M. H. Steinecker, and D. DeMille. “Magneto-optical trapping of a diatomic molecule”. *Nature* 512 (2014), pp. 286–289. DOI: [10.1038/nature13634](https://doi.org/10.1038/nature13634) (cit. on p. 60).
- [330] M. R. Tarbutt and T. C. Steinle. “Modeling magneto-optical trapping of CaF molecules”. *Phys. Rev. A* 92 (2015), p. 053401. DOI: [10.1103/PhysRevA.92.053401](https://doi.org/10.1103/PhysRevA.92.053401) (cit. on p. 60).
- [331] D. J. McCarron, E. B. Norrgard, M. H. Steinecker, and D. DeMille. “Improved magneto-optical trapping of a diatomic molecule”. *New J. Phys.* 17 (2015), p. 035014. DOI: [10.1088/1367-2630/17/3/035014](https://doi.org/10.1088/1367-2630/17/3/035014) (cit. on p. 60).
- [332] E. B. Norrgard, D. J. McCarron, M. H. Steinecker, M. R. Tarbutt, and D. DeMille. “Submillikelvin Dipolar Molecules in a Radio-Frequency Magneto-Optical Trap”. *Phys. Rev. Lett.* 116 (2016), p. 063004. DOI: [10.1103/PhysRevLett.116.063004](https://doi.org/10.1103/PhysRevLett.116.063004) (cit. on p. 60).
- [333] M. H. Steinecker, D. J. McCarron, Y. Zhu, and D. DeMille. “Improved Radio-Frequency Magneto-Optical Trap of SrF Molecules”. *ChemPhysChem* 17 (2016), pp. 3664–3669. DOI: [10.1002/cphc.201600967](https://doi.org/10.1002/cphc.201600967) (cit. on p. 60).
- [334] A. L. Collopy, S. Ding, Y. Wu, I. A. Finneran, L. Anderegg, B. L. Augenbraun, J. M. Doyle, and J. Ye. “3D Magneto-Optical Trap of Yttrium Monoxide”. *Phys. Rev. Lett.* 121 (2018), p. 213201. DOI: [10.1103/PhysRevLett.121.213201](https://doi.org/10.1103/PhysRevLett.121.213201) (cit. on p. 60).

- [335] V. Zhelyazkova, A. Cournol, T. E. Wall, A. Matsushima, J. J. Hudson, E. A. Hinds, M. R. Tarbutt, and B. E. Sauer. “Laser cooling and slowing of CaF molecules”. *Phys. Rev. A* 89 (2014), p. 053416. DOI: [10.1103/PhysRevA.89.053416](https://doi.org/10.1103/PhysRevA.89.053416) (cit. on p. 60).
- [336] S. Truppe, H. J. Williams, M. Hambach, L. Caldwell, N. J. Fitch, E. A. Hinds, B. E. Sauer, and M. R. Tarbutt. “Molecules cooled below the Doppler limit”. *Nat. Phys.* 13 (2017), pp. 1173–1176. DOI: [10.1038/nphys4241](https://doi.org/10.1038/nphys4241) (cit. on p. 60).
- [337] L. Anderegg, B. L. Augenbraun, E. Chae, B. Hemmerling, N. R. Hutzler, A. Ravi, A. Collopy, J. Ye, W. Ketterle, and J. M. Doyle. “Radio Frequency Magneto-Optical Trapping of CaF with High Density”. *Phys. Rev. Lett.* 119 (2017), p. 103201. DOI: [10.1103/PhysRevLett.119.103201](https://doi.org/10.1103/PhysRevLett.119.103201) (cit. on p. 60).
- [338] S. Truppe, H. J. Williams, N. J. Fitch, M. Hambach, T. E. Wall, E. A. Hinds, B. E. Sauer, and M. R. Tarbutt. “An intense, cold, velocity-controlled molecular beam by frequency-chirped laser slowing”. *New J. Phys.* 19 (2017), p. 022001. DOI: [10.1088/1367-2630/aa5ca2](https://doi.org/10.1088/1367-2630/aa5ca2) (cit. on p. 60).
- [339] H. J. Williams, S. Truppe, M. Hambach, L. Caldwell, N. J. Fitch, E. A. Hinds, B. E. Sauer, and M. R. Tarbutt. “Characteristics of a magneto-optical trap of molecules”. *New J. Phys.* 19 (2017), p. 113035. DOI: [10.1088/1367-2630/aa8e52](https://doi.org/10.1088/1367-2630/aa8e52) (cit. on p. 60).
- [340] D. McCarron. “Laser cooling and trapping molecules”. *J. Phys. B: At., Mol. Opt. Phys.* 51 (2018), p. 212001. DOI: [10.1088/1361-6455/aadfba](https://doi.org/10.1088/1361-6455/aadfba) (cit. on p. 61).
- [341] M. R. Tarbutt. “Laser cooling of molecules”. *Contemp. Phys.* 59 (2018), pp. 356–376. DOI: [10.1080/00107514.2018.1576338](https://doi.org/10.1080/00107514.2018.1576338) (cit. on p. 61).
- [342] H. J. Williams, L. Caldwell, N. J. Fitch, S. Truppe, J. Rodewald, E. A. Hinds, B. E. Sauer, and M. R. Tarbutt. “Magnetic Trapping and Coherent Control of Laser-Cooled Molecules”. *Phys. Rev. Lett.* 120 (2018), p. 163201. DOI: [10.1103/PhysRevLett.120.163201](https://doi.org/10.1103/PhysRevLett.120.163201) (cit. on p. 61).
- [343] D. J. McCarron, M. H. Steinecker, Y. Zhu, and D. DeMille. “Magnetic Trapping of an Ultracold Gas of Polar Molecules”. *Phys. Rev. Lett.* 121 (2018), p. 013202. DOI: [10.1103/PhysRevLett.121.013202](https://doi.org/10.1103/PhysRevLett.121.013202) (cit. on p. 61).
- [344] L. Anderegg, B. L. Augenbraun, Y. Bao, S. Burchesky, L. W. Cheuk, W. Ketterle, and J. M. Doyle. “Laser cooling of optically trapped molecules”. *Nat. Phys.* 14 (2018), pp. 890–893. DOI: [10.1038/s41567-018-0191-z](https://doi.org/10.1038/s41567-018-0191-z) (cit. on p. 61).
- [345] B. G. U. Englert, M. Mielenz, C. Sommer, J. Bayerl, M. Motsch, P. W. H. Pinkse, G. Rempe, and M. Zeppenfeld. “Storage and Adiabatic Cooling of Polar Molecules in a Microstructured Trap”. *Phys. Rev. Lett.* 107 (2011), p. 263003. DOI: [10.1103/PhysRevLett.107.263003](https://doi.org/10.1103/PhysRevLett.107.263003) (cit. on p. 61).
- [346] M. Zeppenfeld, B. G. U. Englert, R. Glöckner, A. Prehn, M. Mielenz, C. Sommer, L. D. van Buren, M. Motsch, and G. Rempe. “Sisyphus cooling of electrically trapped polyatomic molecules”. *Nature* 491 (2012), pp. 570–573. DOI: [10.1038/nature11595](https://doi.org/10.1038/nature11595) (cit. on p. 61).
- [347] A. Prehn, M. Ibrügger, R. Glöckner, G. Rempe, and M. Zeppenfeld. “Optoelectrical Cooling of Polar Molecules to Submillikelvin Temperatures”. *Phys. Rev. Lett.* 116 (2016), p. 063005. DOI: [10.1103/PhysRevLett.116.063005](https://doi.org/10.1103/PhysRevLett.116.063005) (cit. on p. 61).
- [348] A. Prehn, M. Ibrügger, G. Rempe, and M. Zeppenfeld. “High-Resolution “Magic”-Field Spectroscopy on Trapped Polyatomic Molecules”. *Phys. Rev. Lett.* 127 (2021), p. 173602. DOI: [10.1103/physrevlett.127.173602](https://doi.org/10.1103/physrevlett.127.173602) (cit. on p. 61).
- [349] S. Chervenkov, X. Wu, J. Bayerl, A. Rohlfes, T. Gantner, M. Zeppenfeld, and G. Rempe. “Continuous Centrifuge Decelerator for Polar Molecules”. *Phys. Rev. Lett.* 112 (2014), p. 013001. DOI: [10.1103/PhysRevLett.112.013001](https://doi.org/10.1103/PhysRevLett.112.013001) (cit. on p. 61).
- [350] X. Wu, T. Gantner, M. Koller, M. Zeppenfeld, S. Chervenkov, and G. Rempe. “A cryofuge for cold-collision experiments with slow polar molecules”. *Science* 358 (2017), pp. 645–648. DOI: [10.1126/science.aan3029](https://doi.org/10.1126/science.aan3029) (cit. on pp. 61, 63).

- [351] M. Koller, F. Jung, J. Phrompao, M. Zeppenfeld, I. M. Rabey, and G. Rempe. *Electric-field-controlled cold dipolar collisions between trapped CH<sub>3</sub>F molecules*. 2022. arXiv: [2204.12339](https://arxiv.org/abs/2204.12339) (cit. on p. 61).
- [352] H.-I. Lu, J. Rasmussen, M. J. Wright, D. Patterson, and J. M. Doyle. “A cold and slow molecular beam”. *Phys. Chem. Chem. Phys.* 13 (2011), p. 18986. DOI: [10.1039/c1cp21206k](https://doi.org/10.1039/c1cp21206k) (cit. on p. 61).
- [353] E. Narevicius, S. T. Bannerman, and M. G. Raizen. “Single-photon molecular cooling”. *New J. Phys.* 11 (2009), p. 055046. DOI: [10.1088/1367-2630/11/5/055046](https://doi.org/10.1088/1367-2630/11/5/055046) (cit. on p. 62).
- [354] H.-I. Lu, I. Kozyryev, B. Hemmerling, J. Piskorski, and J. M. Doyle. “Magnetic Trapping of Molecules via Optical Loading and Magnetic Slowing”. *Phys. Rev. Lett.* 112 (2014), p. 113006. DOI: [10.1103/PhysRevLett.112.113006](https://doi.org/10.1103/PhysRevLett.112.113006) (cit. on p. 62).
- [355] A. M. Jayich, A. C. Vutha, M. T. Hummon, J. V. Porto, and W. C. Campbell. “Continuous all-optical deceleration and single-photon cooling of molecular beams”. *Phys. Rev. A* 89 (2014), p. 023425. DOI: [10.1103/PhysRevA.89.023425](https://doi.org/10.1103/PhysRevA.89.023425) (cit. on p. 62).
- [356] N. Akerman, M. Karpov, L. David, E. Lavert-Ofir, J. Narevicius, and E. Narevicius. “Simultaneous deceleration of atoms and molecules in a supersonic beam”. *New J. Phys.* 17 (2015), p. 065015. DOI: [10.1088/1367-2630/17/6/065015](https://doi.org/10.1088/1367-2630/17/6/065015) (cit. on p. 62).
- [357] E. Narevicius, A. Libson, C. G. Parthey, I. Chavez, J. Narevicius, U. Even, and M. G. Raizen. “Stopping supersonic oxygen with a series of pulsed electromagnetic coils: A molecular coilgun”. *Phys. Rev. A* 77 (2008), p. 051401. DOI: [10.1103/physreva.77.051401](https://doi.org/10.1103/physreva.77.051401) (cit. on p. 62).
- [358] A. Wiederkehr, H. Schmutz, M. Motsch, and F. Merkt. “Velocity-tunable slow beams of cold O<sub>2</sub> in a single spin-rovibronic state with full angular-momentum orientation by multistage Zeeman deceleration”. *Mol. Phys.* 110 (2012), pp. 1807–1814. DOI: [10.1080/00268976.2012.681312](https://doi.org/10.1080/00268976.2012.681312) (cit. on p. 62).
- [359] P. Jansen, L. Semeria, L. E. Hofer, S. Scheidegger, J. A. Agner, H. Schmutz, and F. Merkt. “Precision Spectroscopy in Cold Molecules: The Lowest Rotational Interval of He<sub>2</sub><sup>+</sup> and Metastable He<sub>2</sub>”. *Phys. Rev. Lett.* 115 (2015), p. 133202. DOI: [10.1103/PhysRevLett.115.133202](https://doi.org/10.1103/PhysRevLett.115.133202) (cit. on p. 62).
- [360] Y. Liu, M. Vashishta, P. Djuricanin, S. Zhou, W. Zhong, T. Mitterreiner, D. Carty, and T. Momose. “Magnetic Trapping of Cold Methyl Radicals”. *Phys. Rev. Lett.* 118 (2017), p. 093201. DOI: [10.1103/PhysRevLett.118.093201](https://doi.org/10.1103/PhysRevLett.118.093201) (cit. on p. 62).
- [361] N. Akerman, M. Karpov, Y. Segev, N. Bibelnik, J. Narevicius, and E. Narevicius. “Trapping of Molecular Oxygen together with Lithium Atoms”. *Phys. Rev. Lett.* 119 (2017), p. 073204. DOI: [10.1103/PhysRevLett.119.073204](https://doi.org/10.1103/PhysRevLett.119.073204) (cit. on p. 62).
- [362] B. K. Stuhl, M. T. Hummon, M. Yeo, G. Quéméner, J. L. Bohn, and J. Ye. “Evaporative cooling of the dipolar hydroxyl radical”. *Nature* 492 (2012), pp. 396–400. DOI: [10.1038/nature11718](https://doi.org/10.1038/nature11718) (cit. on p. 62).
- [363] D. Reens, H. Wu, T. Langen, and J. Ye. “Controlling spin flips of molecules in an electromagnetic trap”. *Phys. Rev. A* 96 (2017), p. 063420. DOI: [10.1103/physreva.96.063420](https://doi.org/10.1103/physreva.96.063420) (cit. on p. 62).
- [364] A. M. Kaufman and K.-K. Ni. “Quantum science with optical tweezer arrays of ultracold atoms and molecules”. *Nat. Phys.* 17 (2021), pp. 1324–1333. DOI: [10.1038/s41567-021-01357-2](https://doi.org/10.1038/s41567-021-01357-2) (cit. on p. 63).
- [365] L. R. Liu, J. D. Hood, Y. Yu, J. T. Zhang, N. R. Hutzler, T. Rosenband, and K.-K. Ni. “Building one molecule from a reservoir of two atoms”. *Science* 360 (2018), pp. 900–903. DOI: [10.1126/science.aar7797](https://doi.org/10.1126/science.aar7797) (cit. on pp. 63, 175).
- [366] L. Liu, J. Hood, Y. Yu, J. Zhang, K. Wang, Y.-W. Lin, T. Rosenband, and K.-K. Ni. “Molecular Assembly of Ground-State Cooled Single Atoms”. *Phys. Rev. X* 9 (2019), p. 021039. DOI: [10.1103/PhysRevX.9.021039](https://doi.org/10.1103/PhysRevX.9.021039) (cit. on pp. 63, 175).

- [367] J. D. Hood, Y. Yu, Y.-W. Lin, J. T. Zhang, K. Wang, L. R. Liu, B. Gao, and K.-K. Ni. “Multichannel interactions of two atoms in an optical tweezer”. *Phys. Rev. Research* 2 (2020), p. 023108. DOI: [10.1103/PhysRevResearch.2.023108](https://doi.org/10.1103/PhysRevResearch.2.023108) (cit. on p. 63).
- [368] J. T. Zhang, Y. Yu, W. B. Cairncross, K. Wang, L. R. B. Picard, J. D. Hood, Y.-W. Lin, J. M. Hutson, and K.-K. Ni. “Forming a Single Molecule by Magnetoassociation in an Optical Tweezer”. *Phys. Rev. Lett.* 124 (2020), p. 253401. DOI: [10.1103/PhysRevLett.124.253401](https://doi.org/10.1103/PhysRevLett.124.253401) (cit. on pp. 63, 175).
- [369] Y. Yu, K. Wang, J. D. Hood, L. R. B. Picard, J. T. Zhang, W. B. Cairncross, J. M. Hutson, R. Gonzalez-Ferez, T. Rosenband, and K.-K. Ni. “Coherent Optical Creation of a Single Molecule”. *Phys. Rev. X* 11 (2021), p. 031061. DOI: [10.1103/PhysRevX.11.031061](https://doi.org/10.1103/PhysRevX.11.031061) (cit. on pp. 63, 175).
- [370] W. B. Cairncross, J. T. Zhang, L. R. B. Picard, Y. Yu, K. Wang, and K.-K. Ni. “Assembly of a Rovibrational Ground State Molecule in an Optical Tweezer”. *Phys. Rev. Lett.* 126 (2021), p. 123402. DOI: [10.1103/PhysRevLett.126.123402](https://doi.org/10.1103/PhysRevLett.126.123402) (cit. on pp. 63, 89, 175).
- [371] J. T. Zhang, L. R. B. Picard, W. B. Cairncross, K. Wang, Y. Yu, F. Fang, and K.-K. Ni. *An optical tweezer array of ground-state polar molecules*. 2021. arXiv: [2112.00991](https://arxiv.org/abs/2112.00991) (cit. on p. 63).
- [372] X. He, K. Wang, J. Zhuang, P. Xu, X. Gao, R. Guo, C. Sheng, M. Liu, J. Wang, J. Li, G. V. Shlyapnikov, and M. Zhan. “Coherently forming a single molecule in an optical trap”. *Science* 370 (2020), pp. 331–335. DOI: [10.1126/science.aba7468](https://doi.org/10.1126/science.aba7468) (cit. on p. 63).
- [373] L. Anderegg, L. W. Cheuk, Y. Bao, S. Burchesky, W. Ketterle, K.-K. Ni, and J. M. Doyle. “An optical tweezer array of ultracold molecules”. *Science* 365 (2019), pp. 1156–1158. DOI: [10.1126/science.aax1265](https://doi.org/10.1126/science.aax1265) (cit. on p. 63).
- [374] L. W. Cheuk, L. Anderegg, B. L. Augenbraun, Y. Bao, S. Burchesky, W. Ketterle, and J. M. Doyle. “A-Enhanced Imaging of Molecules in an Optical Trap”. *Phys. Rev. Lett.* 121 (2018), p. 083201. DOI: [10.1103/PhysRevLett.121.083201](https://doi.org/10.1103/PhysRevLett.121.083201) (cit. on p. 63).
- [375] K.-K. Ni, T. Rosenband, and D. D. Grimes. “Dipolar exchange quantum logic gate with polar molecules”. *Chem. Sci.* 9 (2018), pp. 6830–6838. DOI: [10.1039/c8sc02355g](https://doi.org/10.1039/c8sc02355g) (cit. on pp. 63, 108).
- [376] V. V. Albert, J. P. Covey, and J. Preskill. “Robust Encoding of a Qubit in a Molecule”. *Phys. Rev. X* 10 (2020). DOI: [10.1103/PhysRevX.10.031050](https://doi.org/10.1103/PhysRevX.10.031050) (cit. on p. 63).
- [377] M. Hughes, M. D. Frye, R. Sawant, G. Bhole, J. A. Jones, S. L. Cornish, M. R. Tarbutt, J. M. Hutson, D. Jaksch, and J. Mur-Petit. “Robust entangling gate for polar molecules using magnetic and microwave fields”. *Phys. Rev. A* 101 (2020), p. 062308. DOI: [10.1103/PhysRevA.101.062308](https://doi.org/10.1103/PhysRevA.101.062308) (cit. on p. 63).
- [378] K. Wang, C. P. Williams, L. R. B. Picard, N. Y. Yao, and K.-K. Ni. *Enriching the quantum toolbox of ultracold molecules with Rydberg atoms*. 2022. arXiv: [2204.05293](https://arxiv.org/abs/2204.05293) (cit. on p. 63).
- [379] P. D. Gregory, J. A. Blackmore, S. L. Bromley, J. M. Hutson, and S. L. Cornish. “Robust storage qubits in ultracold polar molecules”. *Nat. Phys.* (2021). DOI: [10.1038/s41567-021-01328-7](https://doi.org/10.1038/s41567-021-01328-7) (cit. on pp. 64, 180).
- [380] J. Lin, J. He, M. Jin, G. Chen, and D. Wang. *Seconds-scale coherence on nuclear spin transitions of ultracold polar molecules in 3D optical lattices*. 2021. arXiv: [2111.10013](https://arxiv.org/abs/2111.10013) (cit. on pp. 64, 174).
- [381] F. Seeßelberg, X.-Y. Luo, M. Li, R. Bause, S. Kotochigova, I. Bloch, and C. Gohle. “Extending Rotational Coherence of Interacting Polar Molecules in a Spin-Decoupled Magic Trap”. *Phys. Rev. Lett.* 121 (2018), p. 253401. DOI: [10.1103/PhysRevLett.121.253401](https://doi.org/10.1103/PhysRevLett.121.253401) (cit. on pp. 64, 94, 95, 97, 100, 101, 109, 161, 172).
- [382] L. Caldwell, H. J. Williams, N. J. Fitch, J. Aldegunde, J. M. Hutson, B. E. Sauer, and M. R. Tarbutt. “Long Rotational Coherence Times of Molecules in a Magnetic Trap”. *Phys. Rev. Lett.* 124 (2020), p. 063001. DOI: [10.1103/PhysRevLett.124.063001](https://doi.org/10.1103/PhysRevLett.124.063001) (cit. on p. 64).

- [383] S. Burchesky, L. Anderegg, Y. Bao, S. S. Yu, E. Chae, W. Ketterle, K.-K. Ni, and J. M. Doyle. “Rotational Coherence Times of Polar Molecules in Optical Tweezers”. *Phys. Rev. Lett.* 127 (2021), p. 123202. DOI: [10.1103/PhysRevLett.127.123202](https://doi.org/10.1103/PhysRevLett.127.123202) (cit. on p. 64).
- [384] L. De Marco, G. Valtolina, K. Matsuda, W. G. Tobias, J. P. Covey, and J. Ye. “A degenerate Fermi gas of polar molecules”. *Science* 363 (2019), pp. 853–856. DOI: [10.1126/science.aau7230](https://doi.org/10.1126/science.aau7230) (cit. on pp. 64, 177).
- [385] W. G. Tobias, K. Matsuda, G. Valtolina, L. D. Marco, J.-R. Li, and J. Ye. “Thermalization and Sub-Poissonian Density Fluctuations in a Degenerate Molecular Fermi Gas”. *Phys. Rev. Lett.* 124 (2020), p. 033401. DOI: [10.1103/PhysRevLett.124.033401](https://doi.org/10.1103/PhysRevLett.124.033401) (cit. on pp. 64, 151, 177).
- [386] X.-Y. Chen, M. Duda, A. Schindewolf, R. Bause, I. Bloch, and X.-Y. Luo. “Suppression of Unitary Three-Body Loss in a Degenerate Bose-Fermi Mixture”. *Phys. Rev. Lett.* 128 (2022), p. 153401. DOI: [10.1103/PhysRevLett.128.153401](https://doi.org/10.1103/PhysRevLett.128.153401) (cit. on pp. 64, 72, 73, 150, 173).
- [387] M. Duda, X.-Y. Chen, A. Schindewolf, R. Bause, J. von Milczewski, R. Schmidt, I. Bloch, and X.-Y. Luo. *Transition from a polaronic condensate to a degenerate Fermi gas of heteronuclear molecules*. 2021. arXiv: [2111.04301](https://arxiv.org/abs/2111.04301) (cit. on pp. 64, 72, 150, 155, 173).
- [388] M. Guo, X. Ye, J. He, M. L. González-Martínez, R. Vexiau, G. Quéméner, and D. Wang. “Dipolar Collisions of Ultracold Ground-State Bosonic Molecules”. *Phys. Rev. X* 8 (2018), p. 041044. DOI: [10.1103/PhysRevX.8.041044](https://doi.org/10.1103/PhysRevX.8.041044) (cit. on pp. 64, 111, 174).
- [389] X. Ye, M. Guo, M. L. González-Martínez, G. Quéméner, and D. Wang. “Collisions of ultracold  $^{23}\text{Na}^{87}\text{Rb}$  molecules with controlled chemical reactivities”. *Sci. Adv.* 4 (2018), eaq0083. DOI: [10.1126/sciadv.aaq0083](https://doi.org/10.1126/sciadv.aaq0083) (cit. on pp. 64, 89, 111, 116, 174).
- [390] P. D. Gregory, M. D. Frye, J. A. Blackmore, E. M. Bridge, R. Sawant, J. M. Hutson, and S. L. Cornish. “Sticky collisions of ultracold RbCs molecules”. *Nat. Commun.* 10 (2019), p. 3104. DOI: [10.1038/s41467-019-11033-y](https://doi.org/10.1038/s41467-019-11033-y) (cit. on pp. 64, 111, 116, 179).
- [391] M. Mayle, B. P. Ruzic, and J. L. Bohn. “Statistical aspects of ultracold resonant scattering”. *Phys. Rev. A* 85 (2012), p. 062712. DOI: [10.1103/PhysRevA.85.062712](https://doi.org/10.1103/PhysRevA.85.062712) (cit. on pp. 65, 111, 112).
- [392] M. Mayle, G. Quéméner, B. P. Ruzic, and J. L. Bohn. “Scattering of ultracold molecules in the highly resonant regime”. *Phys. Rev. A* 87 (2013), p. 012709. DOI: [10.1103/PhysRevA.87.012709](https://doi.org/10.1103/PhysRevA.87.012709) (cit. on pp. 65, 111, 112).
- [393] J. F. E. Croft and J. L. Bohn. “Long-lived complexes and chaos in ultracold molecular collisions”. *Phys. Rev. A* 89 (2014), p. 012714. DOI: [10.1103/PhysRevA.89.012714](https://doi.org/10.1103/PhysRevA.89.012714) (cit. on pp. 65, 111).
- [394] A. Christianen, T. Karman, R. A. Vargas-Hernández, G. C. Groenenboom, and R. V. Krems. “Six-dimensional potential energy surface for NaK–NaK collisions: Gaussian process representation with correct asymptotic form”. *J. Chem. Phys.* 150 (2019), p. 064106. DOI: [10.1063/1.5082740](https://doi.org/10.1063/1.5082740) (cit. on pp. 65, 112).
- [395] A. Christianen, M. W. Zwierlein, G. C. Groenenboom, and T. Karman. “Photoinduced Two-Body Loss of Ultracold Molecules”. *Phys. Rev. Lett.* 123 (2019), p. 123402. DOI: [10.1103/PhysRevLett.123.123402](https://doi.org/10.1103/PhysRevLett.123.123402) (cit. on pp. 65, 112, 113, 121, 122, 130–132, 136).
- [396] A. Christianen, T. Karman, and G. C. Groenenboom. “Quasiclassical method for calculating the density of states of ultracold collision complexes”. *Phys. Rev. A* 100 (2019), p. 032708. DOI: [10.1103/PhysRevA.100.032708](https://doi.org/10.1103/PhysRevA.100.032708) (cit. on pp. 65, 112, 130, 136).
- [397] R. V. Krems. “Cold controlled chemistry”. *Phys. Chem. Chem. Phys.* 10 (2008), p. 4079. DOI: [10.1039/b802322k](https://doi.org/10.1039/b802322k) (cit. on p. 65).
- [398] B. K. Stuhl, M. T. Hummon, and J. Ye. “Cold State-Selected Molecular Collisions and Reactions”. *Annu. Rev. Phys. Chem.* 65 (2014), pp. 501–518. DOI: [10.1146/annurev-physchem-040513-103744](https://doi.org/10.1146/annurev-physchem-040513-103744) (cit. on p. 65).

- [399] J. Onvlee, S. N. Vogels, and S. Y. T. van de Meerakker. “Unraveling Cold Molecular Collisions: Stark Decelerators in Crossed-Beam Experiments”. *ChemPhysChem* 17 (2016), pp. 3583–3595. DOI: [10.1002/cphc.201600604](https://doi.org/10.1002/cphc.201600604) (cit. on p. 65).
- [400] Y. Liu and L. Luo. “Molecular collisions: From near-cold to ultra-cold”. *Frontiers of Physics* 16 (2021). DOI: [10.1007/s11467-020-1037-6](https://doi.org/10.1007/s11467-020-1037-6) (cit. on p. 65).
- [401] P. D. Gregory, J. A. Blackmore, S. L. Bromley, and S. L. Cornish. “Loss of ultracold  $^{87}\text{Rb}^{133}\text{Cs}$  molecules via optical excitation of long-lived two-body collision complexes”. *Phys. Rev. Lett.* 124 (2020), p. 163402. DOI: [10.1103/PhysRevLett.124.163402](https://doi.org/10.1103/PhysRevLett.124.163402) (cit. on pp. 65, 112, 119, 136, 179).
- [402] P. D. Gregory, J. A. Blackmore, F. M. D, L. M. Fernley, S. L. Bromley, J. M. Hutson, and S. L. Cornish. “Molecule-molecule and atom-molecule collisions with ultracold RbCs molecules”. *New J. Phys.* 23 (2021), p. 125004. DOI: [10.1088/1367-2630/ac3c63](https://doi.org/10.1088/1367-2630/ac3c63) (cit. on pp. 65, 112, 136, 180).
- [403] M.-G. Hu, Y. Liu, D. D. Grimes, Y.-W. Lin, A. H. Gheorghe, R. Vexiau, N. Boulofa-Maafa, O. Dulieu, T. Rosenband, and K.-K. Ni. “Direct observation of bimolecular reactions of ultracold KRb molecules”. *Science* 366 (2019), pp. 1111–1115. DOI: [10.1126/science.aay9531](https://doi.org/10.1126/science.aay9531) (cit. on pp. 65, 111, 112, 137, 177).
- [404] Y. Liu, M.-G. Hu, M. A. Nichols, D. D. Grimes, T. Karman, H. Guo, and K.-K. Ni. “Photo-excitation of long-lived transient intermediates in ultracold reactions”. *Nat. Phys.* (2020). DOI: [10.1038/s41567-020-0968-8](https://doi.org/10.1038/s41567-020-0968-8) (cit. on pp. 65, 112, 119, 136, 137, 177).
- [405] P. Gersema, K. K. Voges, M. M. zum Alten Borgloh, L. Koch, T. Hartmann, A. Zenesini, S. Os-pelkaus, J. Lin, J. He, and D. Wang. “Probing photoinduced two-body loss of ultracold nonreactive bosonic  $^{23}\text{Na}^{87}\text{Rb}$  and  $^{23}\text{Na}^{39}\text{K}$  molecules”. *Phys. Rev. Lett.* 127 (2021), p. 163401. DOI: [10.1103/PhysRevLett.127.163401](https://doi.org/10.1103/PhysRevLett.127.163401) (cit. on pp. 65, 136, 173, 174).
- [406] J. Kłos, Q. Guan, H. Li, M. Li, E. Tiesinga, and S. Kotochigova. “Roaming pathways and survival probability in real-time collisional dynamics of cold and controlled bialkali molecules”. *Sci. Rep.* 11 (2021). DOI: [10.1038/s41598-021-90004-0](https://doi.org/10.1038/s41598-021-90004-0) (cit. on pp. 65, 137).
- [407] A. Christianen, G. C. Groenenboom, and T. Karman. “Lossy quantum defect theory of ultracold molecular collisions”. *Phys. Rev. A* 104 (2021), p. 043327. DOI: [10.1103/PhysRevA.104.043327](https://doi.org/10.1103/PhysRevA.104.043327) (cit. on pp. 65, 137).
- [408] G. Quéméner, J. F. E. Croft, and J. L. Bohn. “Electric field dependence of complex-dominated ultracold molecular collisions”. *Phys. Rev. A* 105 (2022), p. 013310. DOI: [10.1103/PhysRevA.105.013310](https://doi.org/10.1103/PhysRevA.105.013310) (cit. on pp. 65, 137).
- [409] M. D. Frye and J. M. Hutson. “Complexes formed in collisions between ultracold alkali-metal diatomic molecules and atoms”. *New Journal of Physics* 23 (2021), p. 125008. DOI: [10.1088/1367-2630/ac3ff8](https://doi.org/10.1088/1367-2630/ac3ff8) (cit. on pp. 65, 137).
- [410] K. Jachymski, M. Gronowski, and M. Tomza. *Collisional losses of ultracold molecules due to intermediate complex formation*. 2021. arXiv: [2110.07501](https://arxiv.org/abs/2110.07501) (cit. on pp. 65, 137).
- [411] J. F. E. Croft, J. L. Bohn, and G. Quéméner. *Anomalous Lifetimes of Ultracold Complexes Decaying into a Single Channel: What’s Taking So Long in There?* 2021. arXiv: [2111.09956](https://arxiv.org/abs/2111.09956) (cit. on pp. 65, 137).
- [412] J. K. Yao, C. A. Johnson, N. P. Mehta, and K. R. A. Hazzard. “Complex collisions of ultracold molecules: A toy model”. *Phys. Rev. A* 104 (2021), p. 053311. DOI: [10.1103/physreva.104.053311](https://doi.org/10.1103/physreva.104.053311) (cit. on pp. 65, 137).
- [413] M. P. Man, G. C. Groenenboom, and T. Karman. *Symmetry breaking in sticky collisions between ultracold molecules*. 2022. arXiv: [2203.13598](https://arxiv.org/abs/2203.13598) (cit. on pp. 65, 137).

- [414] G. Valtolina, K. Matsuda, W. G. Tobias, J.-R. Li, L. D. Marco, and J. Ye. “Dipolar evaporation of reactive molecules to below the Fermi temperature”. *Nature* 588 (2020), pp. 239–243. DOI: [10.1038/s41586-020-2980-7](https://doi.org/10.1038/s41586-020-2980-7) (cit. on pp. 65, 139, 152, 159, 177).
- [415] A. V. Avdeenkov, M. Kajita, and J. L. Bohn. “Suppression of inelastic collisions of polar  $^1\Sigma$  state molecules in an electrostatic field”. *Phys. Rev. A* 73 (2006), p. 022707. DOI: [10.1103/PhysRevA.73.022707](https://doi.org/10.1103/PhysRevA.73.022707) (cit. on pp. 66, 139).
- [416] G. Wang and G. Quéméner. “Tuning ultracold collisions of excited rotational dipolar molecules”. *New J. Phys.* 17 (2015), p. 035015. DOI: [10.1088/1367-2630/17/3/035015](https://doi.org/10.1088/1367-2630/17/3/035015) (cit. on pp. 66, 139).
- [417] G. Quéméner and J. L. Bohn. “Shielding  $^2\Sigma$  ultracold dipolar molecular collisions with electric fields”. *Phys. Rev. A* (2016). DOI: [10.1103/PhysRevA.93.012704](https://doi.org/10.1103/PhysRevA.93.012704) (cit. on pp. 66, 139).
- [418] M. L. González-Martínez, J. L. Bohn, and G. Quéméner. “Adimensional theory of shielding in ultracold collisions of dipolar rotors”. *Phys. Rev. A* 96 (2017), p. 032718. DOI: [10.1103/PhysRevA.96.032718](https://doi.org/10.1103/PhysRevA.96.032718) (cit. on pp. 66, 139).
- [419] J.-R. Li, W. G. Tobias, K. Matsuda, C. Miller, G. Valtolina, L. D. Marco, R. R. W. Wang, L. Lassablière, G. Quéméner, J. L. Bohn, and J. Ye. “Tuning of dipolar interactions and evaporative cooling in a three-dimensional molecular quantum gas”. *Nat. Phys.* (2021). DOI: [10.1038/s41567-021-01329-6](https://doi.org/10.1038/s41567-021-01329-6) (cit. on pp. 66, 139, 145, 152, 177).
- [420] K. Matsuda, L. D. Marco, J.-R. Li, W. G. Tobias, G. Valtolina, G. Quéméner, and J. Ye. “Resonant collisional shielding of reactive molecules using electric fields”. *Science* 370 (2020), pp. 1324–1327. DOI: [10.1126/science.abe7370](https://doi.org/10.1126/science.abe7370) (cit. on pp. 66, 139, 177).
- [421] A. V. Gorshkov, P. Rabl, G. Pupillo, A. Micheli, P. Zoller, M. D. Lukin, and H. P. Büchler. “Suppression of Inelastic Collisions Between Polar Molecules With a Repulsive Shield”. *Phys. Rev. Lett.* 101 (2008), p. 073201. DOI: [10.1103/PhysRevLett.101.073201](https://doi.org/10.1103/PhysRevLett.101.073201) (cit. on p. 66).
- [422] A. V. Avdeenkov. “Dipolar collisions of ultracold polar molecules in a microwave field”. *Phys. Rev. A* 86 (2012), p. 022707. DOI: [10.1103/PhysRevA.86.022707](https://doi.org/10.1103/PhysRevA.86.022707) (cit. on p. 66).
- [423] L. Lassablière and G. Quéméner. “Controlling the Scattering Length of Ultracold Dipolar Molecules”. *Phys. Rev. Lett.* 121 (2018), p. 163402. DOI: [10.1103/PhysRevLett.121.163402](https://doi.org/10.1103/PhysRevLett.121.163402) (cit. on pp. 66, 140).
- [424] T. Karman and J. M. Hutson. “Microwave Shielding of Ultracold Polar Molecules”. *Phys. Rev. Lett.* 121 (2018), p. 163401. DOI: [10.1103/PhysRevLett.121.163401](https://doi.org/10.1103/PhysRevLett.121.163401) (cit. on pp. 66, 140).
- [425] T. Karman and J. M. Hutson. “Microwave shielding of ultracold polar molecules with imperfectly circular polarization”. *Phys. Rev. A* 100 (2019), p. 052704. DOI: [10.1103/physreva.100.052704](https://doi.org/10.1103/physreva.100.052704) (cit. on pp. 66, 140, 143).
- [426] T. Karman. “Microwave shielding with far-from-circular polarization”. *Phys. Rev. A* 101 (2020), p. 042702. DOI: [10.1103/PhysRevA.101.042702](https://doi.org/10.1103/PhysRevA.101.042702) (cit. on pp. 66, 140, 143).
- [427] T. Xie, M. Lepers, R. Vexiau, A. Orbán, O. Dulieu, and N. Boulooufa-Maafa. “Optical Shielding of Destructive Chemical Reactions between Ultracold Ground-State NaRb Molecules”. *Phys. Rev. Lett.* 125 (2020), p. 153202. DOI: [10.1103/PhysRevLett.125.153202](https://doi.org/10.1103/PhysRevLett.125.153202) (cit. on pp. 66, 139, 140).
- [428] T. Xie, A. Orbán, E. Luc-Koenig, R. Vexiau, O. Dulieu, and N. Boulooufa-Maafa. “Engineering long-range interactions between ultracold atoms with light”. *J. Phys. B: At. Mol. Opt. Phys.* 55 (2022), p. 034001. DOI: [10.1088/1361-6455/ac4b40](https://doi.org/10.1088/1361-6455/ac4b40) (cit. on pp. 66, 139, 140).
- [429] L. W. Cheuk, L. Anderegg, Y. Bao, S. Burchesky, S. Yu, W. Ketterle, K.-K. Ni, and J. M. Doyle. “Observation of Collisions between Two Ultracold Ground-State CaF Molecules”. *Phys. Rev. Lett.* 125 (2020), p. 043401. DOI: [10.1103/PhysRevLett.125.043401](https://doi.org/10.1103/PhysRevLett.125.043401) (cit. on pp. 66, 111).

- [430] L. Anderegg, S. Burchesky, Y. Bao, S. S. Yu, T. Karman, E. Chae, K.-K. Ni, W. Ketterle, and J. M. Doyle. “Observation of microwave shielding of ultracold molecules”. *Science* 373 (2021), pp. 779–782. DOI: [10.1126/science.abg9502](https://doi.org/10.1126/science.abg9502) (cit. on pp. 66, 140, 143, 144).
- [431] S. Jurgilas, A. Chakraborty, C. J. H. Rich, L. Caldwell, H. J. Williams, N. J. Fitch, B. E. Sauer, M. D. Frye, J. M. Hutson, and M. R. Tarbutt. “Collisions between Ultracold Molecules and Atoms in a Magnetic Trap”. *Phys. Rev. Lett.* 126 (2021), p. 153401. DOI: [10.1103/PhysRevLett.126.153401](https://doi.org/10.1103/PhysRevLett.126.153401) (cit. on p. 66).
- [432] K. K. Voges, P. Gersema, T. Hartmann, S. Ospelkaus, and A. Zenesini. *Hyperfine dependent atom-molecule loss analyzed by the analytic solution of few-body loss equations*. 2021. arXiv: [2109.03605](https://arxiv.org/abs/2109.03605) (cit. on pp. 66, 136, 173).
- [433] H. Son, J. J. Park, W. Ketterle, and A. O. Jamison. “Collisional cooling of ultracold molecules”. *Nature* 580 (2020), pp. 197–200. DOI: [10.1038/s41586-020-2141-z](https://doi.org/10.1038/s41586-020-2141-z) (cit. on pp. 66, 137, 168).
- [434] H. Yang, D.-C. Zhang, L. Liu, Y.-X. Liu, J. Nan, B. Zhao, and J.-W. Pan. “Observation of magnetically tunable Feshbach resonances in ultracold  $^{23}\text{Na}^{40}\text{K} + ^{40}\text{K}$  collisions”. *Science* 363 (2019), pp. 261–264. DOI: [10.1126/science.aau5322](https://doi.org/10.1126/science.aau5322) (cit. on pp. 66, 70, 137, 172).
- [435] H. Yang, X.-Y. Wang, Z. Su, J. Cao, D.-C. Zhang, J. Rui, B. Zhao, C.-L. Bai, and J.-W. Pan. “Evidence for the association of triatomic molecules in ultracold  $^{23}\text{Na}^{40}\text{K} + ^{40}\text{K}$  mixtures”. *Nature* 602 (2022), pp. 229–233. DOI: [10.1038/s41586-021-04297-2](https://doi.org/10.1038/s41586-021-04297-2) (cit. on pp. 66, 70, 137, 172).
- [436] X.-Y. Wang, M. D. Frye, Z. Su, J. Cao, L. Liu, D.-C. Zhang, H. Yang, J. M. Hutson, B. Zhao, C.-L. Bai, and J.-W. Pan. “Magnetic Feshbach resonances in collisions of  $^{23}\text{Na}^{40}\text{K}$  with  $^{40}\text{K}$ ”. *New J. Phys.* 23 (2021), p. 115010. DOI: [10.1088/1367-2630/ac3318](https://doi.org/10.1088/1367-2630/ac3318) (cit. on pp. 66, 70, 137, 172).
- [437] H. Son, J. J. Park, Y.-K. Lu, A. O. Jamison, T. Karman, and W. Ketterle. “Control of reactive collisions by quantum interference”. *Science* 375 (2022), pp. 1006–1010. DOI: [10.1126/science.ab17257](https://doi.org/10.1126/science.ab17257) (cit. on pp. 66, 70, 116, 137, 168).
- [438] N. Nemitz, F. Baumer, F. Münchow, S. Tassy, and A. Görlitz. “Production of heteronuclear molecules in an electronically excited state by photoassociation in a mixture of ultracold Yb and Rb”. *Phys. Rev. A* 79 (2009), p. 061403. DOI: [10.1103/physreva.79.061403](https://doi.org/10.1103/physreva.79.061403) (cit. on p. 67).
- [439] F. Münchow, C. Bruni, M. Madalinski, and A. Görlitz. “Two-photon photoassociation spectroscopy of heteronuclear YbRb”. *Phys. Chem. Chem. Phys.* 13 (2011), p. 18734. DOI: [10.1039/c1cp21219b](https://doi.org/10.1039/c1cp21219b) (cit. on p. 67).
- [440] M. Borkowski, P. S. Żuchowski, R. Ciuryło, P. S. Julienne, D. Kędziera, Ł. Mentel, P. Tecmer, F. Münchow, C. Bruni, and A. Görlitz. “Scattering lengths in isotopologues of the RbYb system”. *Phys. Rev. A* 88 (2013), p. 052708. DOI: [10.1103/physreva.88.052708](https://doi.org/10.1103/physreva.88.052708) (cit. on p. 67).
- [441] A. Guttridge, S. A. Hopkins, S. L. Kemp, M. D. Frye, J. M. Hutson, and S. L. Cornish. “Interspecies thermalization in an ultracold mixture of Cs and Yb in an optical trap”. *Phys. Rev. A* 96 (2017), p. 012704. DOI: [10.1103/PhysRevA.96.012704](https://doi.org/10.1103/PhysRevA.96.012704) (cit. on p. 67).
- [442] A. Guttridge, S. A. Hopkins, M. D. Frye, J. J. McMerran, J. M. Hutson, and S. L. Cornish. “Production of ultracold Cs\*Yb molecules by photoassociation”. *Phys. Rev. A* 97 (2018), p. 063414. DOI: [10.1103/PhysRevA.97.063414](https://doi.org/10.1103/PhysRevA.97.063414) (cit. on p. 67).
- [443] A. Guttridge, M. D. Frye, B. C. Yang, J. M. Hutson, and S. L. Cornish. “Two-photon photoassociation spectroscopy of CsYb: Ground-state interaction potential and interspecies scattering lengths”. *Phys. Rev. A* 98 (2018), p. 022707. DOI: [10.1103/PhysRevA.98.022707](https://doi.org/10.1103/PhysRevA.98.022707) (cit. on p. 67).
- [444] P. S. Julienne. “Quo vadis now, cold molecules?” *Nat. Phys.* 14 (2018), pp. 873–874. DOI: [10.1038/s41567-018-0260-3](https://doi.org/10.1038/s41567-018-0260-3) (cit. on p. 67).

- [445] A. Ciamei, J. Szczepkowski, A. Bayerle, V. Barbé, L. Reichsöllner, S. M. Tzanova, C.-C. Chen, B. Pasquiou, A. Grochola, P. Kowalczyk, W. Jastrzebski, and F. Schreck. “The RbSr  $^2\Sigma^+$  ground state investigated via spectroscopy of hot and ultracold molecules”. *Phys. Chem. Chem. Phys.* (2018). DOI: [10.1039/C8CP03919D](https://doi.org/10.1039/C8CP03919D) (cit. on p. 67).
- [446] K. E. Wilson, A. Guttridge, J. Segal, and S. L. Cornish. “Quantum degenerate mixtures of Cs and Yb”. *Phys. Rev. A* 103 (2021), p. 033306. DOI: [10.1103/PhysRevA.103.033306](https://doi.org/10.1103/PhysRevA.103.033306) (cit. on p. 67).
- [447] P. S. Żuchowski, J. Aldegunde, and J. M. Hutson. “Ultracold RbSr Molecules Can Be Formed by Magnetoassociation”. *Phys. Rev. Lett.* 105 (2010), p. 153201. DOI: [10.1103/PhysRevLett.105.153201](https://doi.org/10.1103/PhysRevLett.105.153201) (cit. on p. 67).
- [448] V. Barbé, A. Ciamei, B. Pasquiou, L. Reichsöllner, F. Schreck, P. S. Żuchowski, and J. M. Hutson. “Observation of Feshbach resonances between alkali and closed-shell atoms”. *Nat. Phys.* 14 (2018), pp. 881–884. DOI: [10.1038/s41567-018-0169-x](https://doi.org/10.1038/s41567-018-0169-x) (cit. on p. 67).
- [449] B. C. Yang, M. D. Frye, A. Guttridge, J. Aldegunde, P. S. Żuchowski, S. L. Cornish, and J. M. Hutson. “Magnetic Feshbach resonances in ultracold collisions between Cs and Yb atoms”. *Phys. Rev. A* 100 (2019), p. 022704. DOI: [10.1103/PhysRevA.100.022704](https://doi.org/10.1103/PhysRevA.100.022704) (cit. on p. 67).
- [450] A. Devolder, E. Luc-Koenig, O. Atabek, M. Desouter-Lecomte, and O. Dulieu. “Proposal for the formation of ultracold deeply bound RbSr dipolar molecules by all-optical methods”. *Phys. Rev. A* 98 (2018), p. 053411. DOI: [10.1103/physreva.98.053411](https://doi.org/10.1103/physreva.98.053411) (cit. on p. 67).
- [451] A. Devolder, M. Desouter-Lecomte, O. Atabek, E. Luc-Koenig, and O. Dulieu. “Laser control of ultracold molecule formation: The case of RbSr”. *Phys. Rev. A* 103 (2021), p. 033301. DOI: [10.1103/physreva.103.033301](https://doi.org/10.1103/physreva.103.033301) (cit. on p. 67).
- [452] I. Kozyryev, L. Baum, K. Matsuda, and J. M. Doyle. “Proposal for Laser Cooling of Complex Polyatomic Molecules”. *ChemPhysChem* 17 (2016), pp. 3641–3648 (cit. on p. 67).
- [453] T. A. Isaev and R. Berger. “Polyatomic Candidates for Cooling of Molecules with Lasers from Simple Theoretical Concepts”. *Phys. Rev. Lett.* 116 (2016), p. 063006. DOI: [10.1103/PhysRevLett.116.063006](https://doi.org/10.1103/PhysRevLett.116.063006) (cit. on p. 67).
- [454] B. L. Augenbraun, J. M. Doyle, T. Zelevinsky, and I. Kozyryev. “Molecular Asymmetry and Optical Cycling: Laser Cooling Asymmetric Top Molecules”. *Phys. Rev. X* 10 (2020), p. 031022. DOI: [10.1103/PhysRevX.10.031022](https://doi.org/10.1103/PhysRevX.10.031022) (cit. on pp. 67, 70).
- [455] K. Wenz, I. Kozyryev, R. L. McNally, L. Aldridge, and T. Zelevinsky. “Large molasses-like cooling forces for molecules using polychromatic optical fields: A theoretical description”. *Phys. Rev. Research* 2 (2020), p. 043377. DOI: [10.1103/PhysRevResearch.2.043377](https://doi.org/10.1103/PhysRevResearch.2.043377) (cit. on p. 67).
- [456] I. Kozyryev, L. Baum, K. Matsuda, B. L. Augenbraun, L. Anderegg, A. P. Sedlack, and J. M. Doyle. “Sisyphus Laser Cooling of a Polyatomic Molecule”. *Phys. Rev. Lett.* 118 (2017), p. 173201. DOI: [10.1103/PhysRevLett.118.173201](https://doi.org/10.1103/PhysRevLett.118.173201) (cit. on p. 67).
- [457] I. Kozyryev, L. Baum, L. Aldridge, P. Yu, E. E. Eyler, and J. M. Doyle. “Coherent Bichromatic Force Deflection of Molecules”. *Phys. Rev. Lett.* 120 (2018), p. 063205. DOI: [10.1103/physrevlett.120.063205](https://doi.org/10.1103/physrevlett.120.063205) (cit. on p. 67).
- [458] B. L. Augenbraun, Z. D. Lasner, A. Frenett, H. Sawaoka, C. Miller, T. C. Steimle, and J. M. Doyle. “Laser-cooled polyatomic molecules for improved electron electric dipole moment searches”. *New J. Phys.* (2020). DOI: <http://dx.doi.org/10.1088/1367-2630/ab687b> (cit. on p. 67).
- [459] L. Baum, N. B. Vilas, C. Hallas, B. L. Augenbraun, S. Raval, D. Mitra, and J. M. Doyle. “1D Magneto-Optical Trap of Polyatomic Molecules”. *Phys. Rev. Lett.* 124 (2020), p. 133201. DOI: [10.1103/PhysRevLett.124.133201](https://doi.org/10.1103/PhysRevLett.124.133201) (cit. on p. 67).

- [460] D. Mitra, N. B. Vilas, C. Hallas, L. Anderegg, B. L. Augenbraun, L. Baum, C. Miller, S. Raval, and J. M. Doyle. “Direct laser cooling of a symmetric top molecule”. *Science* 369 (2020), pp. 1366–1369. DOI: [10 . 1126 / science . abc5357](https://doi.org/10.1126/science.abc5357). eprint: [https : / / science . sciencemag . org / content / 369 / 6509 / 1366 . full . pdf](https://science.sciencemag.org/content/369/6509/1366.full.pdf) (cit. on p. 67).
- [461] L. Baum, N. B. Vilas, C. Hallas, B. L. Augenbraun, S. Raval, D. Mitra, and J. M. Doyle. “Establishing a nearly closed cycling transition in a polyatomic molecule”. *Phys. Rev. A* 103 (2021), p. 043111. DOI: [10.1103/PhysRevA.103.043111](https://doi.org/10.1103/PhysRevA.103.043111) (cit. on p. 67).
- [462] B. L. Augenbraun, A. Frenett, H. Sawaoka, C. Hallas, N. B. Vilas, A. Nasir, Z. D. Lasner, and J. M. Doyle. “Zeeman-Sisyphus Deceleration of Molecular Beams”. *Phys. Rev. Lett.* 127 (2021), p. 263002. DOI: [10.1103/PhysRevLett.127.263002](https://doi.org/10.1103/PhysRevLett.127.263002) (cit. on p. 67).
- [463] N. B. Vilas, C. Hallas, L. Anderegg, P. Robichaud, A. Winnicki, D. Mitra, and J. M. Doyle. *Magneto-Optical Trapping and Sub-Doppler Cooling of a Polyatomic Molecule*. 2021. arXiv: [2112.08349](https://arxiv.org/abs/2112.08349) (cit. on p. 67).
- [464] P. Yu, L. W. Cheuk, I. Kozryev, and J. M. Doyle. “A scalable quantum computing platform using symmetric-top molecules”. *New J. Phys.* 21 (2019), p. 093049. DOI: [http://dx.doi.org/10.1088/1367-2630/ab428d](https://doi.org/10.1088/1367-2630/ab428d) (cit. on p. 67).
- [465] V. Andreev et al. “Improved limit on the electric dipole moment of the electron”. *Nature* 562 (2018), pp. 355–360. DOI: [10.1038/s41586-018-0599-8](https://doi.org/10.1038/s41586-018-0599-8) (cit. on pp. 67, 68).
- [466] J. Baron et al. “Order of Magnitude Smaller Limit on the Electric Dipole Moment of the Electron”. *Science* 343 (2013), pp. 269–272. DOI: [10.1126/science.1248213](https://doi.org/10.1126/science.1248213) (cit. on p. 67).
- [467] Z. Lasner. “Order-of-magnitude-tighter bound on the electron electric dipole moment”. PhD thesis. Yale University, 2019 (cit. on p. 67).
- [468] W. B. Cairncross, D. N. Gresh, M. Grau, K. C. Cossel, T. S. Roussy, Y. Ni, Y. Zhou, J. Ye, and E. A. Cornell. “Precision Measurement of the Electron’s Electric Dipole Moment Using Trapped Molecular Ions”. *Phys. Rev. Lett.* 119 (2017), p. 153001. DOI: [10.1103 / PhysRevLett . 119 . 153001](https://doi.org/10.1103/PhysRevLett.119.153001) (cit. on p. 67).
- [469] C. Cesarotti, Q. Lu, Y. Nakai, A. Parikh, and M. Reece. “Interpreting the electron EDM constraint”. *J. High Energy Phys.* 2019 (2019). DOI: [10.1007/jhep05\(2019\)059](https://doi.org/10.1007/jhep05(2019)059) (cit. on p. 68).
- [470] T. S. Roussy et al. “Experimental Constraint on Axionlike Particles over Seven Orders of Magnitude in Mass”. *Phys. Rev. Lett.* 126 (2021), p. 171301. DOI: [10.1103/physrevlett.126.171301](https://doi.org/10.1103/physrevlett.126.171301) (cit. on p. 68).
- [471] C. Chin and V. V. Flambaum. “Enhanced Sensitivity to Fundamental Constants In Ultracold Atomic and Molecular Systems near Feshbach Resonances”. *Phys. Rev. Lett.* 96 (2006), p. 230801. DOI: [10.1103 / PhysRevLett . 96 . 230801](https://doi.org/10.1103/PhysRevLett.96.230801) (cit. on p. 68).
- [472] T. Zelevinsky, S. Kotochigova, and J. Ye. “Precision Test of Mass-Ratio Variations with Lattice-Confining Ultracold Molecules”. *Phys. Rev. Lett.* 100 (2008), p. 043201. DOI: [10 . 1103 / PhysRevLett . 100 . 043201](https://doi.org/10.1103/PhysRevLett.100.043201) (cit. on p. 68).
- [473] C. Chin, V. V. Flambaum, and M. G. Kozlov. “Ultracold molecules: new probes on the variation of fundamental constants”. *New J. Phys.* 11 (2009), p. 055048. DOI: [10.1088/1367-2630/11/5/055048](https://doi.org/10.1088/1367-2630/11/5/055048) (cit. on p. 68).
- [474] M. Gacesa and R. Côté. “Photoassociation of ultracold molecules near a Feshbach resonance as a probe of the electron–proton mass ratio variation”. *J. Mol. Spectrosc.* 300 (2014), pp. 124–130. DOI: [10.1016 / j . jms . 2014 . 03 . 005](https://doi.org/10.1016/j.jms.2014.03.005) (cit. on p. 68).
- [475] J. Kobayashi, A. Ogino, and S. Inouye. “Measurement of the variation of electron-to-proton mass ratio using ultracold molecules produced from laser-cooled atoms”. *Nat. Commun.* (2019). DOI: [10.1038/s41467-019-11761-1](https://doi.org/10.1038/s41467-019-11761-1) (cit. on pp. 68, 177).

- [476] R. Oswald, A. Nevsky, V. Vogt, S. Schiller, N. L. Figueroa, K. Zhang, O. Tretiak, D. Antypas, D. Budker, A. Banerjee, and G. Perez. *Search for oscillations of fundamental constants using molecular spectroscopy*. 2021. arXiv: [2111.06883](https://arxiv.org/abs/2111.06883) (cit. on p. 68).
- [477] I. Kozryev, Z. Lasner, and J. M. Doyle. “Enhanced sensitivity to ultralight bosonic dark matter in the spectra of the linear radical SrOH”. *Phys. Rev. A* 103 (2021), p. 043313. DOI: [10.1103/PhysRevA.103.043313](https://doi.org/10.1103/PhysRevA.103.043313) (cit. on p. 68).
- [478] D. E. Maison, V. V. Flambaum, N. R. Hutzler, and L. V. Skripnikov. “Electronic structure of the ytterbium monohydroxide molecule to search for axionlike particles”. *Phys. Rev. A* 103 (2021), p. 022813. DOI: [10.1103/PhysRevA.103.022813](https://doi.org/10.1103/PhysRevA.103.022813) (cit. on p. 68).
- [479] W. B. Cairncross and J. Ye. “Atoms and molecules in the search for time-reversal symmetry violation”. *Nat. Rev. Phys.* 1 (2019), pp. 510–521. DOI: [10.1038/s42254-019-0080-0](https://doi.org/10.1038/s42254-019-0080-0) (cit. on p. 68).
- [480] D. Mitra, K. H. Leung, and T. Zelevinsky. “Quantum control of molecules for fundamental physics”. *Physical Review A* 105 (2022), p. 040101. DOI: [10.1103/PhysRevA.105.040101](https://doi.org/10.1103/PhysRevA.105.040101) (cit. on p. 68).
- [481] M. R. Tarbutt, B. E. Sauer, J. J. Hudson, and E. A. Hinds. “Design for a fountain of YbF molecules to measure the electron’s electric dipole moment”. *New J. Phys.* 15 (2013), p. 053034. DOI: [10.1088/1367-2630/15/5/053034](https://doi.org/10.1088/1367-2630/15/5/053034) (cit. on p. 68).
- [482] J. Lim, J. R. Almond, M. A. Trigatzis, J. A. Devlin, N. J. Fitch, B. Sauer, M. R. Tarbutt, and E. A. Hinds. “Laser Cooled YbF Molecules for Measuring the Electron’s Electric Dipole Moment”. *Phys. Rev. Lett.* 120 (2018), p. 123201. DOI: [10.1103/physrevlett.120.123201](https://doi.org/10.1103/physrevlett.120.123201) (cit. on p. 68).
- [483] N. J. Fitch, J. Lim, E. A. Hinds, B. E. Sauer, and M. R. Tarbutt. “Methods for measuring the electron’s electric dipole moment using ultracold YbF molecules”. *Quantum Sci. Technol.* 6 (2020), p. 014006. DOI: [10.1088/2058-9565/abc931](https://doi.org/10.1088/2058-9565/abc931) (cit. on p. 68).
- [484] X. Alauze, J. Lim, M. A. Trigatzis, S. Swarbrick, F. J. Collings, N. J. Fitch, B. E. Sauer, and M. R. Tarbutt. “An ultracold molecular beam for testing fundamental physics”. *Quantum Sci. Technol.* 6 (2021), p. 044005. DOI: [10.1088/2058-9565/ac107e](https://doi.org/10.1088/2058-9565/ac107e) (cit. on p. 68).
- [485] T. Chen, W. Bu, and B. Yan. “Structure, branching ratios, and a laser-cooling scheme for the  $^{138}\text{BaF}$  molecule”. *Phys. Rev. A* 94 (2016), p. 063415. DOI: [10.1103/physreva.94.063415](https://doi.org/10.1103/physreva.94.063415) (cit. on p. 68).
- [486] P. Aggarwal et al. “Measuring the electric dipole moment of the electron in BaF”. *Eur. Phys. J. D* 72 (2018). DOI: [10.1140/epjd/e2018-90192-9](https://doi.org/10.1140/epjd/e2018-90192-9) (cit. on p. 68).
- [487] R. Albrecht, M. Scharwaechter, T. Sixt, L. Hofer, and T. Langen. “Buffer-gas cooling, high-resolution spectroscopy, and optical cycling of barium monofluoride molecules”. *Phys. Rev. A* 101 (2020), p. 013413. DOI: [10.1103/physreva.101.013413](https://doi.org/10.1103/physreva.101.013413) (cit. on p. 68).
- [488] R. L. McNally, I. Kozryev, S. Vazquez-Carson, K. Wenz, T. Wang, and T. Zelevinsky. “Optical cycling, radiative deflection and laser cooling of barium monohydride ( $^{138}\text{Ba}^1\text{H}$ )”. *New J. Phys.* 22 (2020), p. 083047. DOI: [10.1088/1367-2630/aba3e9](https://doi.org/10.1088/1367-2630/aba3e9) (cit. on p. 68).
- [489] P. Aggarwal et al. “Deceleration and Trapping of SrF Molecules”. *Phys. Rev. Lett.* 127 (2021), p. 173201. DOI: [10.1103/PhysRevLett.127.173201](https://doi.org/10.1103/PhysRevLett.127.173201) (cit. on p. 68).
- [490] P. A. B. Haase et al. “Systematic study and uncertainty evaluation of  $P, T$ -odd molecular enhancement factors in BaF”. *J. Chem. Phys.* 155 (2021), p. 034309. DOI: [10.1063/5.0047344](https://doi.org/10.1063/5.0047344) (cit. on p. 68).
- [491] F. Kogel, M. Rockenhäuser, R. Albrecht, and T. Langen. “A laser cooling scheme for precision measurements using fermionic barium monofluoride ( $^{137}\text{Ba}^{19}\text{F}$ ) molecules”. *New J. Phys.* 23 (2021), p. 095003. DOI: [10.1088/1367-2630/ac1df2](https://doi.org/10.1088/1367-2630/ac1df2) (cit. on p. 68).

- [492] Y. Zhang, Z. Zeng, Q. Liang, W. Bu, and B. Yan. *Doppler cooling of buffer-gas-cooled Barium monofluoride molecules*. 2022. arXiv: [2201.04750](https://arxiv.org/abs/2201.04750) (cit. on p. 68).
- [493] I. Kozyryev and N. R. Hutzler. “Precision Measurement of Time-Reversal Symmetry Violation with Laser-Cooled Polyatomic Molecules”. *Phys. Rev. Lett.* 119 (2017), p. 133002. DOI: [10.1103/PhysRevLett.119.133002](https://doi.org/10.1103/PhysRevLett.119.133002) (cit. on p. 68).
- [494] N. R. Hutzler. “Polyatomic molecules as quantum sensors for fundamental physics”. *Quantum Sci. Technol.* 5 (2020), p. 044011. DOI: [10.1088/2058-9565/abb9c5](https://doi.org/10.1088/2058-9565/abb9c5) (cit. on p. 68).
- [495] B. L. Augenbraun, Z. D. Lasner, A. Frenett, H. Sawaoka, A. T. Le, J. M. Doyle, and T. C. Steinle. “Observation and laser spectroscopy of ytterbium monomethoxide,  $\text{YbOCH}_3$ ”. *Phys. Rev. A* 103 (2021), p. 022814. DOI: [10.1103/physreva.103.022814](https://doi.org/10.1103/physreva.103.022814) (cit. on p. 68).
- [496] S. F. Vázquez-Carson, Q. Sun, J. Dai, D. Mitra, and T. Zelevinsky. *Direct laser cooling of calcium monohydride molecules*. 2022. arXiv: [2203.04841](https://arxiv.org/abs/2203.04841) (cit. on p. 68).
- [497] M. Verma, A. M. Jayich, and A. C. Vutha. “Electron Electric Dipole Moment Searches Using Clock Transitions in Ultracold Molecules”. *Phys. Rev. Lett.* 125 (2020), p. 153201. DOI: [10.1103/physrevlett.125.153201](https://doi.org/10.1103/physrevlett.125.153201) (cit. on p. 68).
- [498] R. Mitra, V. S. Prasanna, R. F. G. Ruiz, T. K. Sato, M. Abe, Y. Sakemi, B. P. Das, and B. K. Sahoo. “Towards CP-violation studies on superheavy molecules: Theoretical and experimental perspectives”. *Phys. Rev. A* 104 (2021), p. 062801. DOI: [10.1103/PhysRevA.104.062801](https://doi.org/10.1103/PhysRevA.104.062801) (cit. on p. 68).
- [499] M. Śmiałkowski and M. Tomza. “Highly polar molecules consisting of a copper or silver atom interacting with an alkali-metal or alkaline-earth-metal atom”. *Phys. Rev. A* 103 (2021), p. 022802. DOI: [10.1103/physreva.103.022802](https://doi.org/10.1103/physreva.103.022802) (cit. on p. 68).
- [500] T. Fleig and D. DeMille. “Theoretical aspects of radium-containing molecules amenable to assembly from laser-cooled atoms for new physics searches”. *New J. Phys.* 23 (2021), p. 113039. DOI: [10.1088/1367-2630/ac3619](https://doi.org/10.1088/1367-2630/ac3619) (cit. on p. 68).
- [501] M. Tomza. “Interaction potentials, electric moments, polarizabilities, and chemical reactions of  $\text{YbCu}$ ,  $\text{YbAg}$ , and  $\text{YbAu}$  molecules”. *New J. Phys.* 23 (2021), p. 085003. DOI: [10.1088/1367-2630/ac1696](https://doi.org/10.1088/1367-2630/ac1696) (cit. on p. 68).
- [502] G. Uhlenberg, J. Dirscherl, and H. Walther. “Magneto-optical trapping of silver atoms”. *Phys. Rev. A* 62 (2000), p. 063404. DOI: [10.1103/PhysRevA.62.063404](https://doi.org/10.1103/PhysRevA.62.063404) (cit. on p. 68).
- [503] S. Aubin, E. Gomez, L. A. Orozco, and G. D. Sprouse. “High efficiency magneto-optical trap for unstable isotopes”. *Rev. Sci. Instrum.* 74 (2003), pp. 4342–4351. DOI: [10.1063/1.1606093](https://doi.org/10.1063/1.1606093) (cit. on p. 68).
- [504] J. Kłos, H. Li, E. Tiesinga, and S. Kotochigova. “Prospects for assembling ultracold radioactive molecules from laser-cooled atoms”. *New J. Phys.* 24 (2022), p. 025005. DOI: [10.1088/1367-2630/ac50ea](https://doi.org/10.1088/1367-2630/ac50ea) (cit. on p. 69).
- [505] T. Hayamizu, H. Haba, K. Nakamura, T. Aoki, H. Nagahama, K. S. Tanaka, N. Ozawa, M. Ohtsuka, and Y. Sakemi. “Development of Ultracold Francium Atomic Sources Towards the Permanent EDM Search”. *Few-Body Systems* 63 (2021). DOI: [10.1007/s00601-021-01710-4](https://doi.org/10.1007/s00601-021-01710-4) (cit. on p. 69).
- [506] J. Stuhler, A. Griesmaier, T. Koch, M. Fattori, T. Pfau, S. Giovanazzi, P. Pedri, and L. Santos. “Observation of Dipole-Dipole Interaction in a Degenerate Quantum Gas”. *Phys. Rev. Lett.* 95 (2005), p. 150406. DOI: [10.1103/physrevlett.95.150406](https://doi.org/10.1103/physrevlett.95.150406) (cit. on pp. 69, 156).
- [507] A. de Paz, A. Sharma, A. Chotia, E. Maréchal, J. H. Huckans, P. Pedri, L. Santos, O. Gorceix, L. Vernac, and B. Laburthe-Tolra. “Nonequilibrium Quantum Magnetism in a Dipolar Lattice Gas”. *Phys. Rev. Lett.* 111 (2013), p. 185305. DOI: [10.1103/PhysRevLett.111.185305](https://doi.org/10.1103/PhysRevLett.111.185305) (cit. on pp. 69, 156, 164).

- [508] K. Aikawa, S. Baier, A. Frisch, M. Mark, C. Ravensbergen, and F. Ferlaino. “Observation of Fermi surface deformation in a dipolar quantum gas”. *Science* 345 (2014), pp. 1484–1487. DOI: [10.1126/science.1255259](https://doi.org/10.1126/science.1255259) (cit. on pp. 69, 156, 158).
- [509] S. Baier, M. J. Mark, D. Petter, K. Aikawa, L. Chomaz, Z. Cai, M. Baranov, P. Zoller, and F. Ferlaino. “Extended Bose-Hubbard models with ultracold magnetic atoms”. *Science* 352 (2016), pp. 201–205. DOI: [10.1126/science.aac9812](https://doi.org/10.1126/science.aac9812) (cit. on pp. 69, 156, 163, 164).
- [510] M. Schmitt, M. Wenzel, F. Böttcher, I. Ferrier-Barbut, and T. Pfau. “Self-bound droplets of a dilute magnetic quantum liquid”. *Nature* 539 (2016), pp. 259–262. DOI: [10.1038/nature20126](https://doi.org/10.1038/nature20126) (cit. on pp. 69, 156).
- [511] A. Browaeys and T. Lahaye. “Many-body physics with individually controlled Rydberg atoms”. *Nat. Phys.* 16 (2020), pp. 132–142. DOI: [10.1038/s41567-019-0733-z](https://doi.org/10.1038/s41567-019-0733-z) (cit. on p. 69).
- [512] C. Warner, A. Z. Lam, N. Bigagli, H. C. Liu, I. Stevenson, and S. Will. “Overlapping Bose-Einstein Condensates of  $^{23}\text{Na}$  and  $^{133}\text{Cs}$ ”. *Phys. Rev. A* 104 (2021), p. 033302. DOI: [10.1103/PhysRevA.104.033302](https://doi.org/10.1103/PhysRevA.104.033302) (cit. on pp. 69, 175).
- [513] A. Z. Lam, N. Bigagli, C. Warner, E. Tiemann, I. Stevenson, and S. Will. *A High Phase-Space Density Gas of NaCs Feshbach Molecules*. 2022. arXiv: [2202.03355](https://arxiv.org/abs/2202.03355) (cit. on pp. 69, 175).
- [514] J. S. Rosenberg, L. Christakis, E. Guardado-Sánchez, Z. Z. Yan, and W. S. Bakr. *Observation of the Hanbury Brown and Twiss Effect with Ultracold Molecules*. 2021. arXiv: [2111.09426](https://arxiv.org/abs/2111.09426) (cit. on pp. 69, 174).
- [515] J. Schnabel, T. Kampschulte, S. Rupp, J. H. Denschlag, and A. Köhn. “Towards photoassociation processes of ultracold rubidium trimers”. *Phys. Rev. A* 103 (2021), p. 022820. DOI: [10.1103/physreva.103.022820](https://doi.org/10.1103/physreva.103.022820) (cit. on p. 70).
- [516] M. Gacesa, J. N. Byrd, J. Smucker, J. A. Montgomery, and R. Côté. “Photoassociation of ultracold long-range polyatomic molecules”. *Phys. Rev. Research* 3 (2021), p. 023163. DOI: [10.1103/PhysRevResearch.3.023163](https://doi.org/10.1103/PhysRevResearch.3.023163) (cit. on p. 70).
- [517] L. Caldwell, J. A. Devlin, H. Williams, N. J. Fitch, E. A. Hinds, B. E. Sauer, and M. R. Tarbutt. “Deep Laser Cooling and Efficient Magnetic Compression of Molecules”. *Phys. Rev. Lett.* 123 (2019), p. 033202. DOI: [10.1103/physrevlett.123.033202](https://doi.org/10.1103/physrevlett.123.033202) (cit. on p. 70).
- [518] S. Ding, Y. Wu, I. A. Finneran, J. J. Burau, and J. Ye. “Sub-Doppler Cooling and Compressed Trapping of YO Molecules at  $\mu\text{K}$  Temperatures”. *Phys. Rev. X* 10 (2020), p. 021049. DOI: [10.1103/physrevx.10.021049](https://doi.org/10.1103/physrevx.10.021049) (cit. on p. 70).
- [519] N. Fitch and M. Tarbutt. “Laser-cooled molecules”. In: *Advances In Atomic, Molecular, and Optical Physics*. Vol. 70. Elsevier, 2021, pp. 157–262. DOI: [10.1016/bs.aamop.2021.04.003](https://doi.org/10.1016/bs.aamop.2021.04.003). eprint: <https://arxiv.org/abs/2103.00968> (cit. on p. 70).
- [520] Y. Wu, J. J. Burau, K. Mehling, J. Ye, and S. Ding. “High Phase-Space Density of Laser-Cooled Molecules in an Optical Lattice”. *Phys. Rev. Lett.* 127 (2021), p. 263201. DOI: [10.1103/PhysRevLett.127.263201](https://doi.org/10.1103/PhysRevLett.127.263201) (cit. on p. 70).
- [521] N. Bigagli, D. W. Savin, and S. Will. *Laser Cooling Scheme for the Carbon Dimer ( $^{12}\text{C}_2$ )*. 2021. arXiv: [2112.10745](https://arxiv.org/abs/2112.10745) (cit. on p. 70).
- [522] N. Buchheim. “Dual-species apparatus for creating a dipolar quantum gas of  $^{23}\text{Na}^{40}\text{K}$  molecules”. PhD thesis. Ludwig-Maximilians-Universität München, 2015 (cit. on pp. 71, 74).
- [523] Z. Lu. “Towards many body physics with ultracold NaK molecules”. PhD thesis. Ludwig-Maximilians-Universität München, 2016 (cit. on pp. 71, 74).
- [524] F. Seeßelberg, N. Buchheim, Z.-K. Lu, T. Schneider, X.-Y. Luo, E. Tiemann, I. Bloch, and C. Gohle. “Modeling the adiabatic creation of ultracold polar  $^{23}\text{Na}^{40}\text{K}$  molecules”. *Phys. Rev. A* 97 (2018), p. 013405. DOI: [10.1103/PhysRevA.97.013405](https://doi.org/10.1103/PhysRevA.97.013405) (cit. on pp. 71, 72, 85, 89, 97, 172).

- [525] F. Seeßelberg. “Interacting gases of ultracold polar molecules”. PhD thesis. Ludwig-Maximilians-Universität München, 2019 (cit. on pp. 71, 74, 97, 118).
- [526] L. Liu, D.-C. Zhang, H. Yang, Y.-X. Liu, J. Nan, J. Rui, B. Zhao, and J.-W. Pan. “Observation of Interference between Resonant and Detuned STIRAP in the Adiabatic Creation of  $^{23}\text{Na}^{40}\text{K}$  Molecules”. *Phys. Rev. Lett.* 122 (2019), p. 253201. DOI: [10.1103/PhysRevLett.122.253201](https://doi.org/10.1103/PhysRevLett.122.253201) (cit. on pp. 71, 72, 77, 172).
- [527] R. Bause, A. Kamijo, X.-Y. Chen, M. Duda, A. Schindewolf, I. Bloch, and X.-Y. Luo. “Efficient conversion of closed-channel-dominated Feshbach molecules of  $^{23}\text{Na}^{40}\text{K}$  to their absolute ground state”. *Phys. Rev. A* 104 (2021), p. 043321. DOI: [10.1103/physreva.104.043321](https://doi.org/10.1103/physreva.104.043321) (cit. on pp. 71, 89, 173).
- [528] A. D. Lange, K. Pilch, A. Prantner, F. Ferlaino, B. Engeser, H.-C. Nägerl, R. Grimm, and C. Chin. “Determination of atomic scattering lengths from measurements of molecular binding energies near Feshbach resonances”. *Phys. Rev. A* 79 (2009), p. 013622. DOI: [10.1103/physreva.79.013622](https://doi.org/10.1103/physreva.79.013622) (cit. on pp. 72, 74).
- [529] A. Viel and A. Simoni. “Feshbach resonances and weakly bound molecular states of boson-boson and boson-fermion NaK pairs”. *Phys. Rev. A* 93 (2016), p. 042701. DOI: [10.1103/PhysRevA.93.042701](https://doi.org/10.1103/PhysRevA.93.042701) (cit. on p. 74).
- [530] M. L. Olsen. “Experiments with Feshbach molecules in a Bose–Fermi mixture”. PhD thesis. University of Colorado, 2008 (cit. on p. 77).
- [531] A. Kamijo. “A Laser System for Creating  $^{23}\text{Na}^{40}\text{K}$  Molecules in Their Absolute Ground-State”. MA thesis. Ludwig-Maximilians-Universität München, 2020 (cit. on p. 77).
- [532] R. W. P. Drever, J. L. Hall, F. V. Kowalski, J. Hough, G. M. Ford, A. J. Munley, and H. Ward. “Laser phase and frequency stabilization using an optical resonator”. *Appl. Phys. B* 31 (1983), pp. 97–105 (cit. on p. 79).
- [533] E. D. Black. “An introduction to Pound–Drever–Hall laser frequency stabilization”. *Am. J. Phys* 69 (2001), pp. 79–87. DOI: [10.1119/1.1286663](https://doi.org/10.1119/1.1286663) (cit. on p. 79).
- [534] M. J. Martin. “Quantum Metrology and Many-Body Physics: Pushing the Frontier of the Optical Lattice Clock”. PhD thesis. University of Colorado, 2013 (cit. on p. 79).
- [535] U. Sterr, T. Legero, T. Kessler, H. Schnatz, G. Grosche, O. Terra, and F. Riehle. “Ultrastable lasers: new developments and applications”. In: T. Ido and D. T. Reid, eds. *Time and Frequency Metrology II*. SPIE, 2009. DOI: [10.1117/12.825217](https://doi.org/10.1117/12.825217) (cit. on p. 80).
- [536] I. Ito, A. Silva, T. Nakamura, and Y. Kobayashi. “Stable CW laser based on low thermal expansion ceramic cavity with 49 mHz/s frequency drift”. *Opt. Express* 25 (2017), p. 26020. DOI: [10.1364/OE.25.026020](https://doi.org/10.1364/OE.25.026020) (cit. on p. 80).
- [537] M. Abdel-Hafiz et al. *Guidelines for developing optical clocks with  $10^{-18}$  fractional frequency uncertainty*. 2019. arXiv: [1906.11495](https://arxiv.org/abs/1906.11495) (cit. on p. 81).
- [538] N. Akerman, N. Navon, S. Kotler, Y. Glickman, and R. Ozeri. “Universal gate-set for trapped-ion qubits using a narrow linewidth diode laser”. *New J. Phys.* 17 (2015), p. 113060. DOI: [10.1088/1367-2630/17/11/113060](https://doi.org/10.1088/1367-2630/17/11/113060) (cit. on p. 81).
- [539] H. Levine, A. Keesling, A. Omran, H. Bernien, S. Schwartz, A. S. Zibrov, M. Endres, M. Greiner, V. Vuletić, and M. D. Lukin. “High-Fidelity Control and Entanglement of Rydberg-Atom Qubits”. *Phys. Rev. Lett.* 121 (2018), p. 123603. DOI: [10.1103/physrevlett.121.123603](https://doi.org/10.1103/physrevlett.121.123603) (cit. on p. 81).
- [540] M. L. Day, P. J. Low, B. White, R. Islam, and C. Senko. *Limits on atomic qubit control from laser noise*. 2021. arXiv: [2112.04946](https://arxiv.org/abs/2112.04946) (cit. on p. 81).
- [541] F. Schmid, J. Weitenberg, T. W. Hänsch, T. Udem, and A. Ozawa. “Simple phase noise measurement scheme for cavity-stabilized laser systems”. *Opt. Lett.* 44 (2019), pp. 2709–2712. DOI: [10.1364/OL.44.002709](https://doi.org/10.1364/OL.44.002709) (cit. on p. 81).

- [542] M. Fleischhauer, A. Imamoglu, and J. P. Marangos. “Electromagnetically induced transparency: Optics in coherent media”. *Rev. Mod. Phys.* 77 (2005), pp. 633–673. DOI: [10.1103/RevModPhys.77.633](https://doi.org/10.1103/RevModPhys.77.633) (cit. on p. 85).
- [543] D. Zhang. “Creation and Study of Ultracold  $^{23}\text{Na}^{40}\text{K}$  Ground-State Molecules”. PhD thesis. University of Science and Technology of China, 2019 (cit. on pp. 86, 88).
- [544] L. P. Yatsenko, V. I. Romanenko, B. W. Shore, and K. Bergmann. “Stimulated Raman adiabatic passage with partially coherent laser fields”. *Phys. Rev. A* 65 (2002), p. 043409. DOI: [10.1103/PhysRevA.65.043409](https://doi.org/10.1103/PhysRevA.65.043409) (cit. on p. 88).
- [545] L. P. Yatsenko, B. W. Shore, and K. Bergmann. “Detrimental consequences of small rapid laser fluctuations on stimulated Raman adiabatic passage”. *Phys. Rev. A* 89 (2014), p. 013831. DOI: [10.1103/PhysRevA.89.013831](https://doi.org/10.1103/PhysRevA.89.013831) (cit. on pp. 88, 90).
- [546] A. Yang, S. Botsis, S. Kumar, S. B. Pal, M. M. Lam, I. Čepaitė, A. Laugharn, and K. Dieckmann. “Singlet Pathway to the Ground State of Ultracold Polar Molecules”. *Phys. Rev. Lett.* 124 (2020), p. 133203. DOI: [10.1103/physrevlett.124.133203](https://doi.org/10.1103/physrevlett.124.133203) (cit. on pp. 89, 169).
- [547] K. K. Voges, P. Gersema, T. Hartmann, T. A. Schulze, A. Zenesini, and S. Ospelkaus. “A pathway to ultracold bosonic  $^{23}\text{Na}^{39}\text{K}$  ground state molecules”. *New J. Phys.* 21 (2019), p. 123034. DOI: [10.1088/1367-2630/ab5f31](https://doi.org/10.1088/1367-2630/ab5f31) (cit. on pp. 89, 172).
- [548] K. K. Voges, P. Gersema, M. M. zum Alten Borgloh, T. A. Schulze, T. Hartmann, A. Zenesini, and S. Ospelkaus. “Ultracold Gas of Bosonic  $^{23}\text{Na}^{39}\text{K}$  Ground-State Molecules”. *Phys. Rev. Lett.* 125 (2020), p. 083401. DOI: [10.1103/PhysRevLett.125.083401](https://doi.org/10.1103/PhysRevLett.125.083401) (cit. on pp. 89, 111, 172).
- [549] L. Liu. “Quantum Interference during the Adiabatic Passage on Forming  $^{23}\text{Na}^{40}\text{K}$  Ultracold Ground State Molecules”. PhD thesis. University of Science and Technology of China, 2019 (cit. on pp. 89, 90).
- [550] M. Guo. “An Ultracold Dipolar Gas of Ground-state  $^{23}\text{Na}^{87}\text{Rb}$  Molecules”. PhD thesis. The Chinese University of Hong Kong, 2017 (cit. on p. 89).
- [551] P. K. Molony, P. D. Gregory, A. Kumar, C. R. Le Sueur, J. M. Hutson, and S. L. Cornish. “Production of Ultracold  $^{87}\text{Rb}^{133}\text{Cs}$  in the Absolute Ground State: Complete Characterisation of the Stimulated Raman Adiabatic Passage Transfer”. *ChemPhysChem* 17 (2016), pp. 3811–3817. DOI: [10.1002/cphc.201600501](https://doi.org/10.1002/cphc.201600501) (cit. on pp. 89, 179).
- [552] L.-S. Ma, P. Jungner, J. Ye, and J. L. Hall. “Delivering the same optical frequency at two places: accurate cancellation of phase noise introduced by an optical fiber or other time-varying path”. *Opt. Lett.* 19 (1994), p. 1777. DOI: [10.1364/OL.19.001777](https://doi.org/10.1364/OL.19.001777) (cit. on pp. 90, 91).
- [553] R. Bause, M. Li, A. Schindewolf, X.-Y. Chen, M. Duda, S. Kotochigova, I. Bloch, and X.-Y. Luo. “Tune-Out and Magic Wavelengths for Ground-State  $^{23}\text{Na}^{40}\text{K}$  Molecules”. *Phys. Rev. Lett.* 125 (2020), p. 023201. DOI: [10.1103/PhysRevLett.125.023201](https://doi.org/10.1103/PhysRevLett.125.023201) (cit. on pp. 93, 101, 108, 172).
- [554] H. Katori, T. Ido, and M. Kuwata-Gonokami. “Optimal Design of Dipole Potentials for Efficient Loading of Sr Atoms”. *J. Phys. Soc. Jpn.* 68 (1999), pp. 2479–2482 (cit. on p. 94).
- [555] S. Kotochigova and D. DeMille. “Electric-field-dependent dynamic polarizability and state-insensitive conditions for optical trapping of diatomic polar molecules”. *Phys. Rev. A* 82 (2010), p. 063421. DOI: [10.1103/PhysRevA.82.063421](https://doi.org/10.1103/PhysRevA.82.063421) (cit. on pp. 94, 95).
- [556] Q. Guan, S. L. Cornish, and S. Kotochigova. “Magic conditions for multiple rotational states of bialkali molecules in optical lattices”. *Phys. Rev. A* 103 (2021), p. 043311. DOI: [10.1103/PhysRevA.103.043311](https://doi.org/10.1103/PhysRevA.103.043311) (cit. on p. 94).
- [557] J. Ye, H. J. Kimble, and H. Katori. “Quantum State Engineering and Precision Metrology Using State-Insensitive Light Traps”. *Science* 320 (2008), pp. 1734–1738. DOI: [10.1126/science.1148259](https://doi.org/10.1126/science.1148259) (cit. on p. 94).

- [558] S. S. Kondov, C.-H. Lee, K. H. Leung, C. Liedl, I. Majewska, R. Moszynski, and T. Zelevinsky. “Molecular lattice clock with long vibrational coherence”. *Nat. Phys.* 15 (2019), pp. 1118–1122. DOI: [10.1038/s41567-019-0632-3](https://doi.org/10.1038/s41567-019-0632-3) (cit. on p. 94).
- [559] K. H. Leung, I. Majewska, H. Bekker, C.-H. Lee, E. Tiberi, S. S. Kondov, R. Moszynski, and T. Zelevinsky. “Transition Strength Measurements to Guide Magic Wavelength Selection in Optically Trapped Molecules”. *Phys. Rev. Lett.* 125 (2020), p. 153001. DOI: [10.1103/PhysRevLett.125.153001](https://doi.org/10.1103/PhysRevLett.125.153001) (cit. on p. 94).
- [560] L. J. LeBlanc and J. H. Thywissen. “Species-specific optical lattices”. *Phys. Rev. A* 75 (2007), p. 053612. DOI: [10.1103/PhysRevA.75.053612](https://doi.org/10.1103/PhysRevA.75.053612) (cit. on p. 94).
- [561] B. Arora, M. S. Safranova, and C. W. Clark. “Tune-out wavelengths of alkali-metal atoms and their applications”. *Phys. Rev. A* 84 (2011), p. 043401. DOI: [10.1103/PhysRevA.84.043401](https://doi.org/10.1103/PhysRevA.84.043401) (cit. on p. 94).
- [562] S. Kotochigova and E. Tiesinga. “Controlling polar molecules in optical lattices”. *Phys. Rev. A* 73 (2006), 041405R. DOI: [10.1103/PhysRevA.73.041405](https://doi.org/10.1103/PhysRevA.73.041405) (cit. on p. 94).
- [563] Y. Wang, X. Zhang, T. A. Corcovilos, A. Kumar, and D. S. Weiss. “Coherent Addressing of Individual Neutral Atoms in a 3D Optical Lattice”. *Phys. Rev. Lett.* 115 (2015), p. 043003. DOI: [10.1103/PhysRevLett.115.043003](https://doi.org/10.1103/PhysRevLett.115.043003) (cit. on p. 94).
- [564] A. Rubio-Abadal, J.-Y. Choi, J. Zeiher, S. Hollerith, J. Rui, I. Bloch, and C. Gross. “Many-Body Delocalization in the Presence of a Quantum Bath”. *Phys. Rev. X* 9 (2019), p. 041014. DOI: [10.1103/PhysRevX.9.041014](https://doi.org/10.1103/PhysRevX.9.041014) (cit. on p. 94).
- [565] J. Catani, G. Barontini, G. Lamporesi, F. Rabatti, G. Thalhammer, F. Minardi, S. Stringari, and M. Inguscio. “Entropy Exchange in a Mixture of Ultracold Atoms”. *Phys. Rev. Lett.* 103 (2009), p. 140401. DOI: [10.1103/PhysRevLett.103.140401](https://doi.org/10.1103/PhysRevLett.103.140401) (cit. on p. 94).
- [566] W. F. Holmgren, R. Trubko, I. Hromada, and A. D. Cronin. “Measurement of a Wavelength of Light for Which the Energy Shift for an Atom Vanishes”. *Phys. Rev. Lett.* 109 (2012), p. 243004. DOI: [10.1103/PhysRevLett.109.243004](https://doi.org/10.1103/PhysRevLett.109.243004) (cit. on p. 94).
- [567] C. D. Herold, V. D. Vaidya, X. Li, S. L. Rolston, J. V. Porto, and M. S. Safranova. “Precision Measurement of Transition Matrix Elements via Light Shift Cancellation”. *Phys. Rev. Lett.* 109 (2012), p. 243003. DOI: [10.1103/PhysRevLett.109.243003](https://doi.org/10.1103/PhysRevLett.109.243003) (cit. on p. 94).
- [568] A. Petrov, C. Makrides, and S. Kotochigova. “External field control of spin-dependent rotational decoherence of ultracold polar molecules”. *Mol. Phys.* 111 (2013), pp. 1731–1737. DOI: [10.1080/00268976.2013.777812](https://doi.org/10.1080/00268976.2013.777812) (cit. on p. 94).
- [569] B. Henson, R. Khakimov, R. Dall, K. Baldwin, L.-Y. Tang, and A. Truscott. “Precision Measurement for Metastable Helium Atoms of the 413 nm Tune-Out Wavelength at Which the Atomic Polarizability Vanishes”. *Phys. Rev. Lett.* 115 (2015), p. 043004. DOI: [10.1103/PhysRevLett.115.043004](https://doi.org/10.1103/PhysRevLett.115.043004) (cit. on p. 94).
- [570] W. Kao, Y. Tang, N. Q. Burdick, and B. L. Lev. “Anisotropic dependence of tune-out wavelength near Dy 741-nm transition”. *Opt. Express* 25 (2017), p. 3411. DOI: [10.1364/OE.25.003411](https://doi.org/10.1364/OE.25.003411) (cit. on p. 94).
- [571] A. Heinz, A. J. Park, N. Šantić, J. Trautmann, S. G. Porsev, M. S. Safranova, I. Bloch, and S. Blatt. “State-Dependent Optical Lattices for the Strontium Optical Qubit”. *Phys. Rev. Lett.* 124 (2020), p. 203201. DOI: [10.1103/PhysRevLett.124.203201](https://doi.org/10.1103/PhysRevLett.124.203201) (cit. on p. 94).
- [572] P. D. Gregory, J. A. Blackmore, J. Aldeguende, J. M. Hutson, and S. L. Cornish. “ac Stark effect in ultracold polar  $^{87}\text{Rb}^{133}\text{Cs}$  molecules”. *Phys. Rev. A* 96 (2017), 021402(R). DOI: [10.1103/PhysRevA.96.021402](https://doi.org/10.1103/PhysRevA.96.021402) (cit. on pp. 94, 108, 179).

- [573] J. A. Blackmore, L. Caldwell, P. D. Gregory, E. M. Bridge, R. Sawant, J. Aldegunde, J. Mur-Petit, D. Jaksch, J. M. Hutson, B. E. Sauer, M. R. Tarbutt, and S. L. Cornish. “Ultracold molecules for quantum simulation: rotational coherences in CaF and RbCs”. *Quantum Sci. Technol.* 4 (2018), p. 014010. DOI: [10.1088/2058-9565/aaee35](https://doi.org/10.1088/2058-9565/aaee35) (cit. on pp. 94, 108, 179).
- [574] T. Rosenband, D. D. Grimes, and K.-K. Ni. “Elliptical polarization for molecular Stark shift compensation in deep optical traps”. *Opt. Express* 26 (2018), p. 19821. DOI: [10.1364/oe.26.019821](https://doi.org/10.1364/oe.26.019821) (cit. on pp. 94, 108).
- [575] J. Kobayashi, K. Aikawa, K. Oasa, and S. Inouye. “Prospects for narrow-line cooling of KRb molecules in the rovibrational ground state”. *Phys. Rev. A* 89 (2014), 021401(R). DOI: [10.1103/PhysRevA.89.021401](https://doi.org/10.1103/PhysRevA.89.021401) (cit. on pp. 95, 177).
- [576] M. Li, A. Petrov, C. Makrides, E. Tiesinga, and S. Kotochigova. “Pendular trapping conditions for ultracold polar molecules enforced by external electric fields”. *Phys. Rev. A* 95 (2017), p. 063422. DOI: [10.1103/PhysRevA.95.063422](https://doi.org/10.1103/PhysRevA.95.063422) (cit. on p. 95).
- [577] M. E. Gehm, K. M. O’Hara, T. A. Savard, and J. Thomas. “Dynamics of noise-induced heating in atom traps”. *Phys. Rev. A* 58 (1998), pp. 3914–3921. DOI: [10.1103/PhysRevA.58.3914](https://doi.org/10.1103/PhysRevA.58.3914) (cit. on p. 98).
- [578] R. Vexiau, D. Borsalino, M. Lepers, A. Orbán, M. Aymar, O. Dulieu, and N. Bouloufa-Maafa. “Dynamic dipole polarizabilities of heteronuclear alkali dimers: optical response, trapping and control of ultracold molecules”. *Int. Rev. Phys. Chem.* 36 (2017), pp. 709–750. DOI: [10.1080/0144235X.2017.1351821](https://doi.org/10.1080/0144235X.2017.1351821) (cit. on pp. 101, 110, 123).
- [579] M. Safranova, B. Arora, and C. Clark. “Frequency-dependent polarizabilities of alkali-metal atoms from ultraviolet through infrared spectral regions”. *Phys. Rev. A* 73 (2006), p. 022505. DOI: [10.1103/PhysRevA.73.022505](https://doi.org/10.1103/PhysRevA.73.022505) (cit. on p. 101).
- [580] T. Schuster, S. Gazit, J. E. Moore, and N. Y. Yao. “Floquet Hopf Insulators”. *Phys. Rev. Lett.* 123 (2019), p. 266803. DOI: [10.1103/PhysRevLett.123.266803](https://doi.org/10.1103/PhysRevLett.123.266803) (cit. on p. 110).
- [581] B. Gao. “Universal Model for Exoergic Bimolecular Reactions and Inelastic Processes”. *Phys. Rev. Lett.* 105 (2010), p. 263203. DOI: [10.1103/PhysRevLett.105.263203](https://doi.org/10.1103/PhysRevLett.105.263203) (cit. on p. 112).
- [582] G.-R. Wang, T. Xie, Y. Huang, W. Zhang, and S.-L. Cong. “Quantum defect theory for the van der Waals plus dipole-dipole interaction”. *Phys. Rev. A* 86 (2012), p. 062704. DOI: [10.1103/PhysRevA.86.062704](https://doi.org/10.1103/PhysRevA.86.062704) (cit. on p. 112).
- [583] M. Lepers, R. Vexiau, M. Aymar, N. Bouloufa-Maafa, and O. Dulieu. “Long-range interactions between polar alkali-metal diatoms in external electric fields”. *Phys. Rev. A* 88 (2013), p. 032709. DOI: [10.1103/PhysRevA.88.032709](https://doi.org/10.1103/PhysRevA.88.032709) (cit. on pp. 115, 116).
- [584] Y.-P. Bai, J.-L. Li, G.-R. Wang, and S.-L. Cong. “Model for investigating quantum reflection and quantum coherence in ultracold molecular collisions”. *Phys. Rev. A* 100 (2019), p. 012705. DOI: [10.1103/PhysRevA.100.012705](https://doi.org/10.1103/PhysRevA.100.012705) (cit. on p. 116).
- [585] A. L. Gaunt, T. F. Schmidutz, I. Gotlibovych, R. P. Smith, and Z. Hadzibabic. “Bose-Einstein Condensation of Atoms in a Uniform Potential”. *Phys. Rev. Lett.* 110 (2013), p. 200406. DOI: [10.1103/PhysRevLett.110.200406](https://doi.org/10.1103/PhysRevLett.110.200406) (cit. on p. 123).
- [586] B. Mukherjee, Z. Yan, P. B. Patel, Z. Hadzibabic, T. Yefsah, J. Struck, and M. W. Zwierlein. “Homogeneous Atomic Fermi Gases”. *Phys. Rev. Lett.* 118 (2017), p. 123401. DOI: [10.1103/PhysRevLett.118.123401](https://doi.org/10.1103/PhysRevLett.118.123401) (cit. on p. 123).
- [587] N. Navon, R. P. Smith, and Z. Hadzibabic. “Quantum gases in optical boxes”. *Nature Physics* 17 (2021), pp. 1334–1341. DOI: [10.1038/s41567-021-01403-z](https://doi.org/10.1038/s41567-021-01403-z) (cit. on p. 123).
- [588] Y. Lu, C. M. Holland, and L. W. Cheuk. “Molecular Laser-Cooling in a Dynamically Tunable Repulsive Optical Trap”. *arXiv* (2021) (cit. on p. 123).

- [589] I. Manek, Y. Ovchinnikov, and R. Grimm. “Generation of a hollow laser beam for atom trapping using an axicon”. *Opt. Commun.* 147 (1998), pp. 67–70. DOI: [10.1016/s0030-4018\(97\)00645-7](https://doi.org/10.1016/s0030-4018(97)00645-7) (cit. on p. 124).
- [590] R. Tao. “Near-resonant Dipole Traps and Lattices for Ultracold Molecules”. MA thesis. Ludwig-Maximilians-Universität München, 2020 (cit. on p. 124).
- [591] M. A. Nichols, Y.-X. Liu, L. Zhu, M.-G. Hu, Y. Liu, and K.-K. Ni. “Detection of Long-Lived Complexes in Ultracold Atom-Molecule Collisions”. *Phys. Rev. X* 12 (2022), p. 011049. DOI: [10.1103/PhysRevX.12.011049](https://doi.org/10.1103/PhysRevX.12.011049) (cit. on pp. 136, 177).
- [592] M.-G. Hu, Y. Liu, M. A. Nichols, L. Zhu, G. Quéméner, O. Dulieu, and K.-K. Ni. “Nuclear spin conservation enables state-to-state control of ultracold molecular reactions”. *Nat. Chem.* (2020). DOI: [10.1038/s41557-020-00610-0](https://doi.org/10.1038/s41557-020-00610-0) (cit. on pp. 136, 177).
- [593] G. Quéméner, M.-G. Hu, Y. Liu, M. A. Nichols, L. Zhu, and K.-K. Ni. “Model for nuclear spin product-state distributions of ultracold chemical reactions in magnetic fields”. *Phys. Rev. A* 104 (2021), p. 052817. DOI: [10.1103/PhysRevA.104.052817](https://doi.org/10.1103/PhysRevA.104.052817) (cit. on p. 136).
- [594] Y. Liu, M.-G. Hu, M. A. Nichols, D. Yang, D. Xie, H. Guo, and K.-K. Ni. “Precision test of statistical dynamics with state-to-state ultracold chemistry”. *Nature* 593 (2021), pp. 379–384. DOI: [10.1038/s41586-021-03459-6](https://doi.org/10.1038/s41586-021-03459-6) (cit. on pp. 137, 177).
- [595] X.-Y. Wang, Z. Su, J. Cao, H. Yang, B. Zhao, C.-L. Bai, and J.-W. Pan. “Production of an ultracold mixture of  $^{23}\text{Na}^{40}\text{K}$  and  $^{40}\text{K}$ ”. *Science China Physics, Mechanics & Astronomy* 65 (2021). DOI: [10.1007/s11433-021-1816-8](https://doi.org/10.1007/s11433-021-1816-8) (cit. on pp. 137, 172).
- [596] A. Schindewolf, R. Bause, X.-Y. Chen, M. Duda, T. Karman, I. Bloch, and X.-Y. Luo. *Evaporation of microwave-shielded polar molecules to quantum degeneracy*. 2022. arXiv: [2201.05143](https://arxiv.org/abs/2201.05143) (cit. on pp. 139, 155, 173).
- [597] T. Karman, Z. Z. Yan, and M. Zwierlein. “Resonant and first-order dipolar interactions between ultracold molecules in static and microwave electric fields”. *Phys. Rev. A* 105 (2022), p. 013321. DOI: [10.1103/PhysRevA.105.013321](https://doi.org/10.1103/PhysRevA.105.013321) (cit. on p. 140).
- [598] J. A. Blackmore. “Coherence and Collisions in Ultracold  $^{87}\text{Rb}^{133}\text{Cs}$  Molecules”. PhD thesis. Durham University, 2020 (cit. on pp. 142, 146).
- [599] T. M. Fortier et al. “Sub-femtosecond absolute timing jitter with a 10 GHz hybrid photonic-microwave oscillator”. *Applied Physics Letters* 100 (2012), p. 231111. DOI: [10.1063/1.4726122](https://doi.org/10.1063/1.4726122) (cit. on p. 143).
- [600] R. R. W. Wang and J. L. Bohn. “Anisotropic thermalization of dilute dipolar gases”. *Phys. Rev. A* 103 (2021), p. 063320. DOI: [10.1103/physreva.103.063320](https://doi.org/10.1103/physreva.103.063320) (cit. on p. 146).
- [601] Z.-Y. Ma, A. M. Thomas, C. J. Foot, and S. L. Cornish. “The evaporative cooling of a gas of caesium atoms in the hydrodynamic regime”. *Journal of Physics B: Atomic, Molecular and Optical Physics* 36 (2003), pp. 3533–3540. DOI: [10.1088/0953-4075/36/16/313](https://doi.org/10.1088/0953-4075/36/16/313) (cit. on p. 152).
- [602] M. W. Gempel, T. Hartmann, T. A. Schulze, K. K. Voges, A. Zenesini, and S. Ospelkaus. “Versatile electric fields for the manipulation of ultracold NaK molecules”. *New J. Phys.* 18 (2016), p. 045017. DOI: [10.1088/1367-2630/18/4/045017](https://doi.org/10.1088/1367-2630/18/4/045017) (cit. on p. 152).
- [603] A. West, Z. Lasner, D. DeMille, E. West, C. Panda, J. Doyle, G. Gabrielse, A. Kryskow, and C. Mitchell. “An Underappreciated Radiation Hazard from High Voltage Electrodes in Vacuum”. *Health Physics* 112 (2017), pp. 33–41 (cit. on p. 152).
- [604] P. A. Lee, N. Nagaosa, and X.-G. Wen. “Doping a Mott insulator: Physics of high-temperature superconductivity”. *Rev. Modern Phys.* 78 (2006), pp. 17–85. DOI: [10.1103/revmodphys.78.17](https://doi.org/10.1103/revmodphys.78.17) (cit. on p. 155).

- [605] M. Qin, C.-M. Chung, H. Shi, E. Vitali, C. Hubig, U. Schollwöck, S. R. White, and S. Z. and. “Absence of Superconductivity in the Pure Two-Dimensional Hubbard Model”. *Phys. Rev. X* 10 (2020), p. 031016. DOI: [10.1103/physrevx.10.031016](https://doi.org/10.1103/physrevx.10.031016) (cit. on p. 155).
- [606] E. Altman et al. “Quantum Simulators: Architectures and Opportunities”. *PRX Quantum* 2 (2021), p. 017003. DOI: [10.1103/PRXQuantum.2.017003](https://doi.org/10.1103/PRXQuantum.2.017003) (cit. on p. 155).
- [607] E. H. Lieb and D. W. Robinson. “The finite group velocity of quantum spin systems”. *Communications in Mathematical Physics* 28 (1972), pp. 251–257. DOI: [10.1007/bf01645779](https://doi.org/10.1007/bf01645779) (cit. on p. 155).
- [608] P. Richerme, Z.-X. Gong, A. Lee, C. Senko, J. Smith, M. Foss-Feig, S. Michalakis, A. V. Gorshkov, and C. Monroe. “Non-local propagation of correlations in quantum systems with long-range interactions”. *Nature* 511 (2014), pp. 198–201. DOI: [10.1038/nature13450](https://doi.org/10.1038/nature13450) (cit. on p. 156).
- [609] M. C. Tran, A. Y. Guo, Y. Su, J. R. Garrison, Z. Eldredge, M. Foss-Feig, A. M. Childs, and A. V. Gorshkov. “Locality and Digital Quantum Simulation of Power-Law Interactions”. *Phys. Rev. X* 9 (2019), p. 031006. DOI: [10.1103/physrevx.9.031006](https://doi.org/10.1103/physrevx.9.031006) (cit. on p. 156).
- [610] M. C. Tran, A. Y. Guo, C. L. Baldwin, A. Ehrenberg, A. V. Gorshkov, and A. Lucas. “Lieb–Robinson Light Cone for Power-Law Interactions”. *Phys. Rev. Lett.* 127 (2021), p. 160401. DOI: [10.1103/physrevlett.127.160401](https://doi.org/10.1103/physrevlett.127.160401) (cit. on p. 156).
- [611] L. D. Landau and E. M. Lifshitz. *Quantum Mechanics – Non-relativistic Theory*. Pergamon Press, 1965 (cit. on p. 156).
- [612] S. Giorgini, L. P. Pitaevskii, and S. Stringari. “Theory of ultracold atomic Fermi gases”. *Rev. Mod. Phys.* 80 (2008), pp. 1215–1274. DOI: [10.1103/revmodphys.80.1215](https://doi.org/10.1103/revmodphys.80.1215) (cit. on p. 156).
- [613] E. Duchon, Y. L. Loh, and N. Trivedi. “Optical lattice emulators: Bose– and Fermi–Hubbard models”. In: K. H. Bennemann and J. B. Ketterson, eds. *Novel Superfluids*. Vol. 2. Oxford University Press, 2014. Chap. 17, pp. 194–257 (cit. on p. 158).
- [614] P. B. Blakie, A. Bezett, and P. Buonsante. “Degenerate Fermi gas in a combined harmonic-lattice potential”. *Phys. Rev. A* 75 (2007), p. 063609. DOI: [10.1103/PhysRevA.75.063609](https://doi.org/10.1103/PhysRevA.75.063609) (cit. on p. 158).
- [615] J. L. Ville, T. Bienaimé, R. Saint-Jalm, L. Corman, M. Aidelsburger, L. Chomaz, K. Kleinlein, D. Perconte, S. Nascimbène, J. Dalibard, and J. Beugnon. “Loading and compression of a single two-dimensional Bose gas in an optical accordion”. *Phys. Rev. A* 95 (2017), p. 013632. DOI: [10.1103/physreva.95.013632](https://doi.org/10.1103/physreva.95.013632) (cit. on p. 158).
- [616] V. Veljić, A. Balaž, and A. Pelster. “Time-of-flight expansion of trapped dipolar Fermi gases: From the collisionless to the hydrodynamic regime”. *Phys. Rev. A* 95 (2017), p. 053635. DOI: [10.1103/physreva.95.053635](https://doi.org/10.1103/physreva.95.053635) (cit. on pp. 158, 182).
- [617] N. Matveeva and S. Giorgini. “Liquid and Crystal Phases of Dipolar Fermions in Two Dimensions”. *Phys. Rev. Lett.* 109 (2012), p. 200401. DOI: [10.1103/PhysRevLett.109.200401](https://doi.org/10.1103/PhysRevLett.109.200401) (cit. on pp. 159, 181).
- [618] W. Lechner, H.-P. Büchler, and P. Zoller. “Role of Quantum Fluctuations in the Hexatic Phase of Cold Polar Molecules”. *Phys. Rev. Lett.* 112 (2014), p. 255301. DOI: [10.1103/PhysRevLett.112.255301](https://doi.org/10.1103/PhysRevLett.112.255301) (cit. on pp. 160, 181).
- [619] G. M. Bruun and D. R. Nelson. “Quantum hexatic order in two-dimensional dipolar and charged fluids”. *Phys. Rev. B* 89 (2014), p. 094112. DOI: [10.1103/physrevb.89.094112](https://doi.org/10.1103/physrevb.89.094112) (cit. on pp. 160, 181).
- [620] K. Sun, C. Wu, and S. D. Sarma. “Spontaneous inhomogeneous phases in ultracold dipolar Fermi gases”. *Phys. Rev. B* 82 (2010), p. 075105. DOI: [10.1103/PhysRevB.82.075105](https://doi.org/10.1103/PhysRevB.82.075105) (cit. on pp. 160, 181, 182).

- [621] Y. Yamaguchi, T. Sogo, T. Ito, and T. Miyakawa. “Density-wave instability in a two-dimensional dipolar Fermi gas”. *Phys. Rev. A* 82 (2010), p. 013643. DOI: [10.1103/PhysRevA.82.013643](https://doi.org/10.1103/PhysRevA.82.013643) (cit. on pp. 160, 181).
- [622] Z. Wu, J. K. Block, and G. M. Bruun. “Coexistence of density wave and superfluid order in a dipolar Fermi gas”. *Phys. Rev. B* 91 (2015), p. 224504. DOI: [10.1103/physrevb.91.224504](https://doi.org/10.1103/physrevb.91.224504) (cit. on pp. 160, 181).
- [623] Z. Wu, J. K. Block, and G. M. Bruun. “Liquid crystal phases of two-dimensional dipolar gases and Berezinskii-Kosterlitz-Thouless melting”. *Sci. Rep.* 6 (2016). DOI: [10.1038/srep19038](https://doi.org/10.1038/srep19038) (cit. on pp. 160, 181).
- [624] R. Bombín, F. Mazzanti, and J. Boronat. “Berezinskii-Kosterlitz-Thouless transition in two-dimensional dipolar stripes”. *Phys. Rev. A* 100 (2019), p. 063614. DOI: [10.1103/PhysRevA.100.063614](https://doi.org/10.1103/PhysRevA.100.063614) (cit. on pp. 160, 181).
- [625] F. Cinti and M. Boninsegni. “Comment on “Berezinskii-Kosterlitz-Thouless transition in two-dimensional dipolar stripes””. *Phys. Rev. A* 102 (2020), p. 047301. DOI: [10.1103/PhysRevA.102.047301](https://doi.org/10.1103/PhysRevA.102.047301) (cit. on pp. 160, 181).
- [626] W. G. Tobias, K. Matsuda, J.-R. Li, C. Miller, A. N. Carroll, T. Bilitewski, A. M. Rey, and J. Ye. “Reactions between layer-resolved molecules mediated by dipolar spin exchange”. *Science* 375 (2022), pp. 1299–1303. DOI: [10.1126/science.abn8525](https://doi.org/10.1126/science.abn8525) (cit. on pp. 160, 177).
- [627] M. P. Kwasigroch and N. R. Cooper. “Bose-Einstein condensation and many-body localization of rotational excitations of polar molecules following a microwave pulse”. *Phys. Rev. A* 90 (2014), 021605(R). DOI: [10.1103/PhysRevA.90.021605](https://doi.org/10.1103/PhysRevA.90.021605) (cit. on pp. 161, 182).
- [628] M. P. Kwasigroch and N. R. Cooper. “Synchronization transition in dipole-coupled two-level systems with positional disorder”. *Phys. Rev. A* 96 (2017), p. 053610. DOI: [10.1103/PhysRevA.96.053610](https://doi.org/10.1103/PhysRevA.96.053610) (cit. on pp. 161, 162, 182).
- [629] M. L. Wall, K. R. A. Hazzard, and A. M. Rey. *Quantum Magnetism with Ultracold Molecules*. arXiv: [1406.4758](https://arxiv.org/abs/1406.4758) (cit. on p. 162).
- [630] D. Peter, S. Müller, S. Wessel, and H. P. Büchler. “Anomalous Behavior of Spin Systems with Dipolar Interactions”. *Phys. Rev. Lett.* 109 (2012), p. 025303. DOI: [10.1103/PhysRevLett.109.025303](https://doi.org/10.1103/PhysRevLett.109.025303) (cit. on pp. 162, 182).
- [631] P. N. Jepsen, J. Amato-Grill, I. Dimitrova, W. W. Ho, E. Demler, and W. Ketterle. “Spin transport in a tunable Heisenberg model realized with ultracold atoms”. *Nature* 588 (2020), pp. 403–407. DOI: [10.1038/s41586-020-3033-y](https://doi.org/10.1038/s41586-020-3033-y) (cit. on p. 163).
- [632] T. Sowiński, O. Dutta, P. Hauke, L. Tagliacozzo, and M. Lewenstein. “Dipolar Molecules in Optical Lattices”. *Phys. Rev. Lett.* 108 (2012), p. 115301. DOI: [10.1103/PhysRevLett.108.115301](https://doi.org/10.1103/PhysRevLett.108.115301) (cit. on pp. 163, 164, 182).
- [633] O. Dutta, M. Gajda, P. Hauke, M. Lewenstein, D.-S. Lühmann, B. A. Malomed, T. Sowiński, and J. Zakrzewski. “Non-standard Hubbard models in optical lattices: a review”. *Rep. Prog. Phys.* 78 (2015), p. 066001. DOI: [10.1088/0034-4885/78/6/066001](https://doi.org/10.1088/0034-4885/78/6/066001) (cit. on pp. 163, 164, 181).
- [634] C. Lagoin, U. Bhattacharya, T. Grass, R. Chhajlany, T. Salamon, K. Baldwin, L. Pfeiffer, M. Lewenstein, M. Holzmann, and F. Dubin. *Checkerboard solid of dipolar excitons in a two-dimensional lattice*. 2022. arXiv: [2201.03311](https://arxiv.org/abs/2201.03311) (cit. on p. 164).
- [635] B. Capogrosso-Sansone, C. Trefzger, M. Lewenstein, P. Zoller, and G. Pupillo. “Quantum Phases of Cold Polar Molecules in 2D Optical Lattices”. *Phys. Rev. Lett.* 104 (2010), p. 125301. DOI: [10.1103/PhysRevLett.104.125301](https://doi.org/10.1103/PhysRevLett.104.125301) (cit. on pp. 164, 182).
- [636] S. Bandyopadhyay, R. Bai, S. Pal, K. Suthar, R. Nath, and D. Angom. “Quantum phases of canted dipolar bosons in a two-dimensional square optical lattice”. *Phys. Rev. A* 100 (2019), p. 053623. DOI: [10.1103/PhysRevA.100.053623](https://doi.org/10.1103/PhysRevA.100.053623) (cit. on pp. 164, 182).

- [637] K. Mikelsons and J. K. Freericks. “Density-wave patterns for fermionic dipolar molecules on a square optical lattice: Mean-field-theory analysis”. *Phys. Rev. A* 83 (2011), p. 043609. DOI: [10.1103/PhysRevA.83.043609](https://doi.org/10.1103/PhysRevA.83.043609) (cit. on pp. 164, 182).
- [638] A.-L. Gadsbølle and G. M. Bruun. “Harmonically trapped dipolar fermions in a two-dimensional square lattice”. *Phys. Rev. A* 85 (2012), 021604(R). DOI: [10.1103/PhysRevA.85.021604](https://doi.org/10.1103/PhysRevA.85.021604) (cit. on pp. 164, 182).
- [639] A.-L. Gadsbølle and G. M. Bruun. “Dipolar fermions in a two-dimensional lattice at nonzero temperature”. *Phys. Rev. A* 86 (2012), p. 033623. DOI: [10.1103/PhysRevA.86.033623](https://doi.org/10.1103/PhysRevA.86.033623) (cit. on pp. 164, 182).
- [640] E. G. C. P. van Loon, M. I. Katsnelson, and M. Lemeshko. “Ultralong-range order in the Fermi-Hubbard model with long-range interactions”. *Phys. Rev. B* 92 (2015), 081106(R). DOI: [10.1103/PhysRevB.92.081106](https://doi.org/10.1103/PhysRevB.92.081106) (cit. on pp. 164, 182).
- [641] A. K. Fedorov, S. I. Matveenko, V. I. Yudson, and G. V. Shlyapnikov. “Novel p-wave superfluids of fermionic polar molecules”. *Sci. Rep.* 6 (2016). DOI: [10.1038/srep27448](https://doi.org/10.1038/srep27448) (cit. on pp. 164, 182).
- [642] T.-S. Zeng and L. Yin. “Supersolidity of a dipolar Fermi gas in a cubic optical lattice”. *Phys. Rev. B* 89 (2014), p. 174511. DOI: [10.1103/physrevb.89.174511](https://doi.org/10.1103/physrevb.89.174511) (cit. on pp. 165, 182).
- [643] A. Pikovski, M. Klawunn, G. V. Shlyapnikov, and L. Santos. “Interlayer Superfluidity in Bilayer Systems of Fermionic Polar Molecules”. *Phys. Rev. Lett.* 105 (2010), p. 215302. DOI: [10.1103/PhysRevLett.105.215302](https://doi.org/10.1103/PhysRevLett.105.215302) (cit. on pp. 165, 182).
- [644] A. Camacho-Guardian and R. Paredes. “Supersolid phases of dipolar fermions in a two-dimensional-lattice bilayer array”. *Phys. Rev. A* 94 (2016), p. 043638. DOI: [10.1103/PhysRevA.94.043638](https://doi.org/10.1103/PhysRevA.94.043638) (cit. on pp. 165, 182).
- [645] N. R. Cooper and G. V. Shlyapnikov. “Stable Topological Superfluid Phase of Ultracold Polar Fermionic Molecules”. *Phys. Rev. Lett.* 103 (2009), p. 155302. DOI: [10.1103/PhysRevLett.103.155302](https://doi.org/10.1103/PhysRevLett.103.155302) (cit. on pp. 165, 181).
- [646] J. Levinsen, N. R. Cooper, and G. V. Shlyapnikov. “Topological  $p_x + ip_y$  superfluid phase of fermionic polar molecules”. *Phys. Rev. A* 84 (2011), p. 013603. DOI: [10.1103/physreva.84.013603](https://doi.org/10.1103/physreva.84.013603) (cit. on pp. 165, 181).
- [647] M. Aymar and O. Dulieu. “Calculation of accurate permanent dipole moments of the lowest  $1,3\Sigma^+$  states of heteronuclear alkali dimers using extended basis sets”. *J. Chem. Phys.* 122 (2005), p. 204302. DOI: [10.1063/1.1903944](https://doi.org/10.1063/1.1903944) (cit. on pp. 167, 171, 178).
- [648] J. Deiglmayr, M. Aymar, R. Wester, M. Weidemüller, and O. Dulieu. “Calculations of static dipole polarizabilities of alkali dimers: Prospects for alignment of ultracold molecules”. *J. Chem. Phys.* 129 (2008), p. 064309. DOI: [10.1063/1.2960624](https://doi.org/10.1063/1.2960624) (cit. on pp. 167, 169–171, 175, 178).
- [649] P. J. Dagdigian and L. Wharton. “Molecular Beam Electric Deflection and Resonance Spectroscopy of the Heteronuclear Alkali Dimers:  $^{39}\text{K}^7\text{Li}$ ,  $\text{Rb}^7\text{Li}$ ,  $^{39}\text{K}^{23}\text{Na}$ ,  $\text{Rb}^{23}\text{Na}$ , and  $^{133}\text{Cs}^{23}\text{Na}$ ”. *J. Chem. Phys.* 57 (1972), pp. 1487–1496. DOI: [10.1063/1.1678429](https://doi.org/10.1063/1.1678429) (cit. on pp. 167, 169, 170, 174, 175).
- [650] M. Taglieber, A.-C. Voigt, T. Aoki, T. W. Hänsch, and K. Dieckmann. “Quantum Degenerate Two-Species Fermi-Fermi Mixture Coexisting with a Bose-Einstein Condensate”. *Phys. Rev. Lett.* 100 (2008), p. 010401. DOI: [10.1103/PhysRevLett.100.010401](https://doi.org/10.1103/PhysRevLett.100.010401) (cit. on p. 169).
- [651] E. Wille et al. “Exploring an Ultracold Fermi-Fermi Mixture: Interspecies Feshbach Resonances and Scattering Properties of  $^6\text{Li}$  and  $^{40}\text{K}$ ”. *Phys. Rev. Lett.* 100 (2008), p. 053201. DOI: [10.1103/PhysRevLett.100.053201](https://doi.org/10.1103/PhysRevLett.100.053201) (cit. on p. 169).
- [652] L. Costa, J. Brachmann, A.-C. Voigt, C. Hahn, M. Taglieber, T. W. Hänsch, and K. Dieckmann. “s-Wave Interaction in a Two-Species Fermi-Fermi Mixture at a Narrow Feshbach Resonance”. *Phys. Rev. Lett.* 105 (2010), p. 123201. DOI: [10.1103/PhysRevLett.105.123201](https://doi.org/10.1103/PhysRevLett.105.123201) (cit. on p. 169).

- [653] T. G. Tiecke, M. R. Goosen, A. Ludewig, S. D. Gensemer, S. Kraft, S. J. J. M. F. Kokkelmans, and J. T. M. Walraven. “Broad Feshbach Resonance in the  ${}^6\text{Li}$ - ${}^{40}\text{K}$  Mixture”. *Phys. Rev. Lett.* 104 (2010), p. 053202. DOI: [10.1103/PhysRevLett.104.053202](https://doi.org/10.1103/PhysRevLett.104.053202) (cit. on p. 169).
- [654] D. Naik, A. Trenkwalder, C. Kohstall, F. M. Spiegelhalder, M. Zaccanti, G. Hendl, F. Schreck, R. Grimm, T. M. Hanna, and P. S. Julienne. “Feshbach resonances in the  ${}^6\text{Li}$ - ${}^{40}\text{K}$  Fermi-Fermi mixture: elastic versus inelastic interactions”. *Eur. Phys. J. D* 65 (2011), pp. 55–65. DOI: [10.1140/epjd/e2010-10591-2](https://doi.org/10.1140/epjd/e2010-10591-2) (cit. on p. 169).
- [655] A.-C. Voigt, M. Taglieber, L. Costa, T. Aoki, W. Wieser, T. W. Hänsch, and K. Dieckmann. “Ultracold Heteronuclear Fermi-Fermi Molecules”. *Phys. Rev. Lett.* 102 (2009), p. 020405. DOI: [10.1103/PhysRevLett.102.020405](https://doi.org/10.1103/PhysRevLett.102.020405) (cit. on p. 169).
- [656] F. M. Spiegelhalder, A. Trenkwalder, D. Naik, G. Kerner, E. Wille, G. Hendl, F. Schreck, and R. Grimm. “All-optical production of a degenerate mixture of  ${}^6\text{Li}$  and  ${}^{40}\text{K}$  and creation of heteronuclear molecules”. *Phys. Rev. A* 81 (2010), p. 043637. DOI: [10.1103/PhysRevA.81.043637](https://doi.org/10.1103/PhysRevA.81.043637) (cit. on p. 169).
- [657] A. Ridinger, S. Chaudhuri, T. Salez, D. R. Fernandes, N. Bouloufa, O. Dulieu, C. Salomon, and F. Chevy. “Photoassociative creation of ultracold heteronuclear  ${}^6\text{Li}$ - ${}^{40}\text{K}$  molecules”. *Europhys. Lett.* 96 (2011), p. 33001. DOI: [10.1209/0295-5075/96/33001](https://doi.org/10.1209/0295-5075/96/33001) (cit. on p. 169).
- [658] C.-H. Wu, I. Santiago, J. W. Park, P. Ahmadi, and M. W. Zwierlein. “Strongly interacting isotopic Bose-Fermi mixture immersed in a Fermi sea”. *Phys. Rev. A* 84 (2011), p. 011601. DOI: [10.1103/physreva.84.011601](https://doi.org/10.1103/physreva.84.011601) (cit. on p. 169).
- [659] M. Jag, M. Zaccanti, M. Cetina, R. S. Lous, F. Schreck, R. Grimm, D. S. Petrov, and J. Levinsen. “Observation of a Strong Atom-Dimer Attraction in a Mass-Imbalanced Fermi-Fermi Mixture”. *Phys. Rev. Lett.* 112 (2014), p. 075302. DOI: [10.1103/PhysRevLett.112.075302](https://doi.org/10.1103/PhysRevLett.112.075302) (cit. on p. 169).
- [660] M. Jag, M. Cetina, R. S. Lous, R. Grimm, J. Levinsen, and D. S. Petrov. “Lifetime of Feshbach dimers in a Fermi-Fermi mixture of  ${}^6\text{Li}$  and  ${}^{40}\text{K}$ ”. *Phys. Rev. A* 94 (2016), p. 062706. DOI: [10.1103/PhysRevA.94.062706](https://doi.org/10.1103/PhysRevA.94.062706) (cit. on p. 169).
- [661] M. Cetina, M. Jag, R. S. Lous, I. Fritzsche, J. T. M. Walraven, R. Grimm, J. Levinsen, M. M. Parish, R. Schmidt, M. Knap, and E. Demler. “Ultrafast many-body interferometry of impurities coupled to a Fermi sea”. *Science* 354 (2016), pp. 96–99. DOI: [10.1126/science.aaf5134](https://doi.org/10.1126/science.aaf5134) (cit. on p. 169).
- [662] S. Botsi, A. Yang, M. M. Lam, S. B. Pal, S. Kumar, M. Debatin, and K. Dieckmann. “Empirical LiK excited state potentials: connecting short range and near dissociation expansions”. *Physical Chemistry Chemical Physics* 24 (2022), pp. 3933–3940. DOI: [10.1039/d1cp04707h](https://doi.org/10.1039/d1cp04707h) (cit. on p. 169).
- [663] C. Silber, S. Günther, C. Marzok, B. Deh, P. W. Courteille, and C. Zimmermann. “Quantum-Degenerate Mixture of Fermionic Lithium and Bosonic Rubidium Gases”. *Phys. Rev. Lett.* 95 (2005), p. 170408. DOI: [10.1103/PhysRevLett.95.170408](https://doi.org/10.1103/PhysRevLett.95.170408) (cit. on p. 170).
- [664] B. Deh, C. Marzok, C. Zimmermann, and P. W. Courteille. “Feshbach resonances in mixtures of ultracold  ${}^6\text{Li}$  and  ${}^{87}\text{Rb}$  gases”. *Phys. Rev. A* 77 (2008), 010701(R). DOI: [10.1103/PhysRevA.77.010701](https://doi.org/10.1103/PhysRevA.77.010701) (cit. on p. 170).
- [665] C. Marzok, B. Deh, C. Zimmermann, P. W. Courteille, E. Tiemann, Y. V. Vanne, and A. Saenz. “Feshbach resonances in an ultracold  ${}^7\text{Li}$  and  ${}^{87}\text{Rb}$  mixture”. *Phys. Rev. A* 79 (2009), p. 012717. DOI: [10.1103/PhysRevA.79.012717](https://doi.org/10.1103/PhysRevA.79.012717) (cit. on p. 170).
- [666] B. Deh, W. Gunton, B. G. Klappauf, Z. Li, M. Semczuk, J. V. Dongen, and K. W. Madison. “Giant Feshbach resonances in  ${}^6\text{Li}$ - ${}^{85}\text{Rb}$  mixtures”. *Phys. Rev. A* 82 (2010), p. 020701. DOI: [10.1103/physreva.82.020701](https://doi.org/10.1103/physreva.82.020701) (cit. on p. 170).

- [667] R. A. W. Maier, M. Eisele, E. Tiemann, and C. Zimmermann. “Efimov Resonance and Three-Body Parameter in a Lithium-Rubidium Mixture”. *Phys. Rev. Lett.* 115 (2015), p. 043201. DOI: [10.1103/PhysRevLett.115.043201](https://doi.org/10.1103/PhysRevLett.115.043201) (cit. on p. 170).
- [668] S. Dutta, D. S. Elliott, and Y. P. Chen. “Formation of ultracold LiRb molecules by photoassociation near the  $\text{Li}(2s^2S_{1/2}) + \text{Rb}(5p^2P_{1/2})$  asymptote”. *Europhys. Lett.* 104 (2013), p. 63001. DOI: [10.1209/0295-5075/104/63001](https://doi.org/10.1209/0295-5075/104/63001) (cit. on p. 170).
- [669] D. B. Blasing, I. C. Stevenson, J. Pérez-Ríos, D. S. Elliott, and Y. P. Chen. “Short-range photoassociation of LiRb”. *Phys. Rev. A* 94 (2016), p. 062504. DOI: [10.1103/PhysRevA.94.062504](https://doi.org/10.1103/PhysRevA.94.062504) (cit. on p. 170).
- [670] I. C. Stevenson, D. B. Blasing, Y. P. Chen, and D. S. Elliott. “Production of ultracold ground-state LiRb molecules by photoassociation through a resonantly coupled state”. *Phys. Rev. A* 94 (2016), p. 062510. DOI: [10.1103/physreva.94.062510](https://doi.org/10.1103/physreva.94.062510) (cit. on p. 170).
- [671] S. Dutta, J. Pérez-Ríos, D. S. Elliott, and Y. P. Chen. “Two-photon photoassociation spectroscopy of an ultracold heteronuclear molecule”. *Phys. Rev. A* 95 (2017), p. 013405. DOI: [10.1103/PhysRevA.95.013405](https://doi.org/10.1103/PhysRevA.95.013405) (cit. on p. 170).
- [672] S. D. Kraft, P. Staanum, J. Lange, L. Vogel, R. Wester, and M. Weidemüller. “Formation of ultracold LiCs molecules”. *J. Phys. B: At. Mol. Opt. Phys.* 39 (2006), S993–S1000. DOI: [10.1088/0953-4075/39/19/s13](https://doi.org/10.1088/0953-4075/39/19/s13) (cit. on p. 171).
- [673] J. Deiglmayr, A. Grochola, M. Repp, K. Mörtlbauer, C. Glück, J. Lange, O. Dulieu, R. Wester, and M. Weidemüller. “Formation of Ultracold Polar Molecules in the Rovibrational Ground State”. *Phys. Rev. Lett.* 101 (2008), p. 133004. DOI: [10.1103/PhysRevLett.101.133004](https://doi.org/10.1103/PhysRevLett.101.133004) (cit. on p. 171).
- [674] S.-K. Tung, C. Parker, J. Johansen, C. Chin, Y. Wang, and P. S. Julienne. “Ultracold mixtures of atomic  ${}^6\text{Li}$  and  ${}^{133}\text{Cs}$  with tunable interactions”. *Phys. Rev. A* 87 (2013), p. 010702. DOI: [10.1103/physreva.87.010702](https://doi.org/10.1103/physreva.87.010702) (cit. on p. 171).
- [675] M. Repp, R. Pires, J. Ulmanis, R. Heck, E. D. Kuhnle, M. Weidemüller, and E. Tiemann. “Observation of interspecies  ${}^6\text{Li}-{}^{133}\text{Cs}$  Feshbach resonances”. *Phys. Rev. A* 87 (2013), p. 010701. DOI: [10.1103/physreva.87.010701](https://doi.org/10.1103/physreva.87.010701) (cit. on p. 171).
- [676] S.-K. Tung, K. Jiménez-García, J. Johansen, C. V. Parker, and C. Chin. “Geometric Scaling of Efimov States in a  ${}^6\text{Li}-{}^{133}\text{Cs}$  Mixture”. *Phys. Rev. Lett.* 113 (2014), p. 240402. DOI: [10.1103/PhysRevLett.113.240402](https://doi.org/10.1103/PhysRevLett.113.240402) (cit. on p. 171).
- [677] J. Ulmanis, S. Häfner, R. Pires, E. D. Kuhnle, Y. Wang, C. H. Greene, and M. Weidemüller. “Heteronuclear Efimov Scenario with Positive Intraspecies Scattering Length”. *Phys. Rev. Lett.* 117 (2016), p. 153201. DOI: [10.1103/PhysRevLett.117.153201](https://doi.org/10.1103/PhysRevLett.117.153201) (cit. on p. 171).
- [678] J. Johansen, B. J. DeSalvo, K. Patel, and C. Chin. “Testing universality of Efimov physics across broad and narrow Feshbach resonances”. *Nat. Phys.* 13 (2017), pp. 731–735. DOI: [10.1038/nphys4130](https://doi.org/10.1038/nphys4130) (cit. on p. 171).
- [679] F. Ferlaino, A. Zenesini, M. Berninger, B. Huang, H.-C. Nägerl, and R. Grimm. “Efimov Resonances in Ultracold Quantum Gases”. *Few-Body Systems* 51 (2011), pp. 113–133. DOI: [10.1007/s00601-011-0260-7](https://doi.org/10.1007/s00601-011-0260-7) (cit. on p. 171).
- [680] P. Naidon and S. Endo. “Efimov physics: a review”. *Rep. Progr. Phys.* 80 (2017), p. 056001. DOI: [10.1088/1361-6633/aa50e8](https://doi.org/10.1088/1361-6633/aa50e8) (cit. on p. 171).
- [681] B. J. DeSalvo, K. Patel, J. Johansen, and C. Chin. “Observation of a Degenerate Fermi Gas Trapped by a Bose-Einstein Condensate”. *Phys. Rev. Lett.* 119 (2017), p. 233401. DOI: [10.1103/PhysRevLett.119.233401](https://doi.org/10.1103/PhysRevLett.119.233401) (cit. on p. 171).

- [682] B. J. DeSalvo, K. Patel, G. Cai, and C. Chin. “Observation of fermion-mediated interactions between bosonic atoms”. *Nature* 568 (2019), pp. 61–64. DOI: [10.1038/s41586-019-1055-0](https://doi.org/10.1038/s41586-019-1055-0) (cit. on p. 171).
- [683] A. Gerdes, O. Dulieu, H. Knöckel, and E. Tiemann. “Stark effect measurements on the NaK molecule”. *Eur. Phys. J. D* 65 (2011), pp. 105–111. DOI: [10.1140/epjd/e2011-20048-9](https://doi.org/10.1140/epjd/e2011-20048-9) (cit. on p. 172).
- [684] M.-J. Zhu, H. Yang, L. Liu, D.-C. Zhang, Y.-X. Liu, J. Nan, J. Rui, B. Zhao, J.-W. Pan, and E. Tiemann. “Feshbach loss spectroscopy in an ultracold  $^{23}\text{Na}$ - $^{40}\text{K}$  mixture”. *Phys. Rev. A* 96 (2017), p. 062705. DOI: [10.1103/PhysRevA.96.062705](https://doi.org/10.1103/PhysRevA.96.062705) (cit. on p. 172).
- [685] Z. Z. Yan, J. W. Park, Y. Ni, H. Loh, S. Will, T. Karman, and M. Zwierlein. “Resonant Dipolar Collisions of Ultracold Molecules Induced by Microwave Dressing”. *Phys. Rev. Lett.* 125 (2020), p. 063401. DOI: [10.1103/PhysRevLett.125.063401](https://doi.org/10.1103/PhysRevLett.125.063401) (cit. on p. 172).
- [686] T. A. Schulze, T. Hartmann, K. K. Voges, M. W. Gempel, E. Tiemann, A. Zenesini, and S. Ospelkaus. “Feshbach spectroscopy and dual-species Bose-Einstein condensation of  $^{23}\text{Na}$ - $^{39}\text{K}$  mixtures”. *Phys. Rev. A* 97 (2018), p. 023623. DOI: [10.1103/physreva.97.023623](https://doi.org/10.1103/physreva.97.023623) (cit. on p. 172).
- [687] T. Hartmann, T. A. Schulze, K. K. Voges, P. Gersema, M. W. Gempel, E. Tiemann, A. Zenesini, and S. Ospelkaus. “Feshbach resonances in  $^{23}\text{Na}$  +  $^{39}\text{K}$  mixtures and refined molecular potentials for the NaK molecule”. *Phys. Rev. A* 99 (2019), p. 032711. DOI: [10.1103/PhysRevA.99.032711](https://doi.org/10.1103/PhysRevA.99.032711) (cit. on p. 172).
- [688] K. K. Voges, P. Gersema, T. Hartmann, T. A. Schulze, A. Zenesini, and S. Ospelkaus. “Formation of ultracold weakly bound dimers of bosonic  $^{23}\text{Na}$ - $^{39}\text{K}$ ”. *Phys. Rev. A* 101 (2020), p. 042704. DOI: [10.1103/physreva.101.042704](https://doi.org/10.1103/physreva.101.042704) (cit. on p. 172).
- [689] F. Wang, X. Li, D. Xiong, and D. Wang. “A double species  $^{23}\text{Na}$  and  $^{87}\text{Rb}$  Bose-Einstein condensate with tunable miscibility via an interspecies Feshbach resonance”. *J. Phys. B: At., Mol. Opt. Phys.* 49 (2015), p. 015302. DOI: [10.1088/0953-4075/49/1/015302](https://doi.org/10.1088/0953-4075/49/1/015302) (cit. on p. 174).
- [690] J. He, X. Ye, J. Lin, M. Guo, G. Quéméner, and D. Wang. “Observation of resonant dipolar collisions in ultracold  $^{23}\text{Na}$ - $^{87}\text{Rb}$  rotational mixtures”. *Phys. Rev. Research* 3 (2021), p. 013016. DOI: [10.1103/PhysRevResearch.3.013016](https://doi.org/10.1103/PhysRevResearch.3.013016) (cit. on p. 174).
- [691] F. Wang, X. Ye, M. Guo, D. Blume, and D. Wang. “Observation of resonant scattering between ultracold heteronuclear Feshbach molecules”. *Phys. Rev. A* 100 (2019), p. 042706. DOI: [10.1103/PhysRevA.100.042706](https://doi.org/10.1103/PhysRevA.100.042706) (cit. on p. 174).
- [692] F. Jia, Z. Guo, L. Li, and D. Wang. “Detection of NaRb Feshbach molecules by photodissociation”. *Phys. Rev. A* 102 (2020), p. 043327. DOI: [10.1103/physreva.102.043327](https://doi.org/10.1103/physreva.102.043327) (cit. on p. 174).
- [693] J. He, J. Lin, R. Vexiau, N. Bouloufa-Maafa, O. Dulieu, and D. Wang. “Characterization of the lowest electronically excited-state ro-vibrational level of  $^{23}\text{Na}$ - $^{87}\text{Rb}$ ”. *New J. Phys.* 23 (2021), p. 115003. DOI: [10.1088/1367-2630/ac2dad](https://doi.org/10.1088/1367-2630/ac2dad) (cit. on p. 174).
- [694] J. Lin, J. He, X. Ye, and D. Wang. “Anisotropic polarizability of ultracold ground-state  $^{23}\text{Na}$ - $^{87}\text{Rb}$  molecules”. *Phys. Rev. A* 103 (2021), p. 023332. DOI: [10.1103/physreva.103.023332](https://doi.org/10.1103/physreva.103.023332) (cit. on p. 174).
- [695] C. Haimberger, J. Kleinert, P. Zabawa, A. Wakim, and N. P. Bigelow. “Formation of ultracold, highly polar  $X^1\Sigma^+$  NaCs molecules”. *New J. Phys.* 11 (2009), p. 055042. DOI: [10.1088/1367-2630/11/5/055042](https://doi.org/10.1088/1367-2630/11/5/055042) (cit. on p. 175).
- [696] P. Zabawa, A. Wakim, A. Neukirch, C. Haimberger, N. P. Bigelow, A. V. Stolyarov, E. A. Pazyuk, M. Tamanis, and R. Ferber. “Near-dissociation photoassociative production of deeply bound NaCs molecules”. *Phys. Rev. A* 82 (2010), p. 040501. DOI: [10.1103/physreva.82.040501](https://doi.org/10.1103/physreva.82.040501) (cit. on p. 175).

- [697] A. Grochola, P. Kowalczyk, J. Szczepkowski, W. Jastrzebski, A. Wakim, P. Zabawa, and N. P. Bigelow. “Spin-forbidden  $c^3\Sigma^+$  ( $\Omega = 1$ ) transition in NaCs: Investigation of the  $\Omega = 1$  state in hot and cold environments”. *Phys. Rev. A* 84 (2011), p. 012507. DOI: [10.1103/PhysRevA.84.012507](https://doi.org/10.1103/PhysRevA.84.012507) (cit. on p. 175).
- [698] S. Ospelkaus, A. Pe’er, K.-K. Ni, J. J. Zirbel, B. Neyenhuis, S. Kotochigova, P. S. Julienne, J. Ye, and D. S. Jin. “Efficient state transfer in an ultracold dense gas of heteronuclear molecules”. *Nat. Phys.* 4 (2008), pp. 622–626. DOI: [10.1038/nphys997](https://doi.org/10.1038/nphys997) (cit. on p. 176).
- [699] C. Weber, G. Barontini, J. Catani, G. Thalhammer, M. Inguscio, and F. Minardi. “Association of ultracold double-species bosonic molecules”. *Phys. Rev. A* 78 (2008), p. 061601. DOI: [10.1103/PhysRevA.78.061601](https://doi.org/10.1103/PhysRevA.78.061601) (cit. on p. 176).
- [700] J. T. Kim, D. Wang, E. E. Eyler, P. L. Gould, and W. C. Stwalley. “Spectroscopy of  $^{39}\text{K}^{85}\text{Rb}$  triplet excited states using ultracold  $a^3\Sigma$  state molecules formed by photoassociation”. *New J. Phys.* 11 (2009), p. 055020. DOI: [10.1088/1367-2630/11/5/055020](https://doi.org/10.1088/1367-2630/11/5/055020) (cit. on p. 176).
- [701] T. D. Cumby, R. A. Shewmon, M.-G. Hu, J. D. Perreault, and D. S. Jin. “Feshbach-molecule formation in a Bose-Fermi mixture”. *Phys. Rev. A* 87 (2013), p. 012703. DOI: [10.1103/PhysRevA.87.012703](https://doi.org/10.1103/PhysRevA.87.012703) (cit. on p. 176).
- [702] J. P. Covey, S. A. Moses, M. Gärttner, A. Safavi-Naini, M. T. Miecnikowski, Z. Fu, J. Schachenmayer, P. S. Julienne, A. M. Rey, D. S. Jin, and J. Ye. “Doublon dynamics and polar molecule production in an optical lattice”. *Nat. Commun.* 7 (2016), p. 11279. DOI: [10.1038/ncomms11279](https://doi.org/10.1038/ncomms11279) (cit. on p. 177).
- [703] A. Burchianti, C. D’Errico, S. Rosi, A. Simoni, M. Modugno, C. Fort, and F. Minardi. “Dual-species Bose-Einstein condensate of  $^{41}\text{K}$  and  $^{87}\text{Rb}$  in a hybrid trap”. *Phys. Rev. A* 98 (2018), p. 063616. DOI: [10.1103/physreva.98.063616](https://doi.org/10.1103/physreva.98.063616) (cit. on p. 177).
- [704] M. Gröbner, P. Weinmann, F. Meinert, K. Lauber, E. Kirilov, and H.-C. Nägerl. “A new quantum gas apparatus for ultracold mixtures of K and Cs and KCs ground-state molecules”. *J. Mod. Opt.* 63 (2016), pp. 1829–1839. DOI: [10.1080/09500340.2016.1143051](https://doi.org/10.1080/09500340.2016.1143051) (cit. on p. 178).
- [705] D. Borsalino, R. Vexiau, M. Aymar, E. Luc-Koenig, O. Dulieu, and N. Bouhoufa-Maafa. “Prospects for the formation of ultracold polar ground state KCs molecules via an optical process”. *J. Phys. B: At. Mol. Opt. Phys.* 49 (2016), p. 055301. DOI: [10.1088/0953-4075/49/5/055301](https://doi.org/10.1088/0953-4075/49/5/055301) (cit. on p. 178).
- [706] M. Gröbner, P. Weinmann, E. Kirilov, H.-C. Nägerl, P. S. Julienne, C. R. L. Sueur, and J. M. Hutson. “Observation of interspecies Feshbach resonances in an ultracold  $^{39}\text{K}$ - $^{133}\text{Cs}$  mixture and refinement of interaction potentials”. *Phys. Rev. A* 95 (2017), p. 022715. DOI: [10.1103/PhysRevA.95.022715](https://doi.org/10.1103/PhysRevA.95.022715) (cit. on p. 178).
- [707] T. Bergeman, A. J. Kerman, J. Sage, S. Sainis, and D. DeMille. “Prospects for production of ultracold  $X^1\Sigma^+$  RbCs molecules”. *Eur. Phys. J. D* 31 (2004), pp. 179–188. DOI: [10.1140/epjd/e2004-00155-6](https://doi.org/10.1140/epjd/e2004-00155-6) (cit. on p. 179).
- [708] C. Gabbanini and O. Dulieu. “Formation of ultracold metastable RbCs molecules by short-range photoassociation”. *Phys. Chem. Chem. Phys.* 13 (2011), p. 18905. DOI: [10.1039/c1cp21497g](https://doi.org/10.1039/c1cp21497g) (cit. on p. 179).
- [709] Z. Ji, H. Zhang, J. Wu, J. Yuan, Y. Yang, Y. Zhao, J. Ma, L. Wang, L. Xiao, and S. Jia. “Photoassociative formation of ultracold RbCs molecules in the  $(2)^3\Pi$  state”. *Phys. Rev. A* 85 (2012), p. 013401. DOI: [10.1103/PhysRevA.85.013401](https://doi.org/10.1103/PhysRevA.85.013401) (cit. on p. 179).
- [710] T. Shimasaki, J.-T. Kim, and D. DeMille. “Production of RbCs Molecules in the Rovibronic Ground State via Short-Range Photoassociation to the  $2^1\Pi_1$ ,  $2^3\Pi_1$ , and  $3^3\Sigma_1^+$  States”. *ChemPhysChem* (2016). DOI: [10.1002/cphc.201600933](https://doi.org/10.1002/cphc.201600933) (cit. on p. 179).

- [711] J. A. Blackmore, R. Sawant, P. D. Gregory, S. L. Bromley, J. Aldegunde, J. M. Hutson, and S. L. Cornish. “Controlling the ac Stark effect of RbCs with dc electric and magnetic fields”. *Phys. Rev. A* 102 (2020), p. 053316. DOI: [10.1103/PhysRevA.102.053316](https://doi.org/10.1103/PhysRevA.102.053316) (cit. on p. 179).
- [712] J. A. Blackmore, P. D. Gregory, S. L. Bromley, and S. L. Cornish. “Coherent manipulation of the internal state of ultracold  $^{87}\text{Rb}^{133}\text{Cs}$  molecules with multiple microwave fields”. *Phys. Chem. Chem. Phys.* 22 (2020), pp. 27529–27538. DOI: [10.1039/d0cp04651e](https://doi.org/10.1039/d0cp04651e) (cit. on p. 179).
- [713] Z. Ji, T. Gong, Y. He, J. M. Hutson, Y. Zhao, L. Xiao, and S. Jia. “Microwave coherent control of ultracold ground-state molecules formed by short-range photoassociation”. *Phys. Chem. Chem. Phys.* 22 (2020), pp. 13002–13007. DOI: [10.1039/d0cp01191f](https://doi.org/10.1039/d0cp01191f) (cit. on p. 180).
- [714] R. V. Brooks, S. Spence, A. Guttridge, A. Alampouli, A. Rakonjac, L. A. McArd, J. M. Hutson, and S. L. Cornish. “Preparation of one  $^{87}\text{Rb}$  and one  $^{133}\text{Cs}$  atom in a single optical tweezer”. *New J. Phys.* 23 (2021), p. 065002. DOI: [10.1088/1367-2630/ac0000](https://doi.org/10.1088/1367-2630/ac0000) (cit. on p. 180).
- [715] C. Trefzger, C. Menotti, B. Capogrosso-Sansone, and M. Lewenstein. “Ultracold dipolar gases in optical lattices”. *J. Phys. B: At., Mol. Opt. Phys.* 44 (2011), p. 193001. DOI: [10.1088/0953-4075/44/19/193001](https://doi.org/10.1088/0953-4075/44/19/193001) (cit. on p. 181).
- [716] E. G. Dalla Torre, E. Berg, and E. Altman. “Hidden Order in 1D Bose Insulators”. *Phys. Rev. Lett.* 97 (2006), p. 260401. DOI: [10.1103/PhysRevLett.97.260401](https://doi.org/10.1103/PhysRevLett.97.260401) (cit. on p. 181).
- [717] G. G. Batrouni, F. Hébert, and R. T. Scalettar. “Supersolid Phases in the One-Dimensional Extended Soft-Core Bosonic Hubbard Model”. *Phys. Rev. Lett.* 97 (2006), p. 087209. DOI: [10.1103/PhysRevLett.97.087209](https://doi.org/10.1103/PhysRevLett.97.087209) (cit. on p. 181).
- [718] S. Sinha and L. Santos. “Cold Dipolar Gases in Quasi-One-Dimensional Geometries”. *Phys. Rev. Lett.* 99 (2007), p. 140406. DOI: [10.1103/PhysRevLett.99.140406](https://doi.org/10.1103/PhysRevLett.99.140406) (cit. on p. 181).
- [719] J. Ruhman, E. G. D. Torre, S. D. Huber, and E. Altman. “Nonlocal order in elongated dipolar gases”. *Phys. Rev. B* 85 (2012), p. 125121. DOI: [10.1103/PhysRevB.85.125121](https://doi.org/10.1103/PhysRevB.85.125121) (cit. on p. 181).
- [720] D. Rossini and R. Fazio. “Phase diagram of the extended Bose–Hubbard model”. *New J. Phys.* 14 (2012), p. 065012. DOI: [10.1088/1367-2630/14/6/065012](https://doi.org/10.1088/1367-2630/14/6/065012) (cit. on p. 181).
- [721] M. Knap, E. Berg, M. Ganahl, and E. Demler. “Clustered Wigner-crystal phases of cold polar molecules in arrays of one-dimensional tubes”. *Phys. Rev. B* 86 (2012), p. 064501. DOI: [10.1103/PhysRevB.86.064501](https://doi.org/10.1103/PhysRevB.86.064501) (cit. on p. 181).
- [722] S. Gammelmark and N. T. Zinner. “Dipoles on a two-leg ladder”. *Phys. Rev. B* 88 (2013), p. 245135. DOI: [10.1103/PhysRevB.88.245135](https://doi.org/10.1103/PhysRevB.88.245135) (cit. on p. 181).
- [723] F. Cartarius, A. Minguzzi, and G. Morigi. “Multimode Bose-Hubbard model for quantum dipolar gases in confined geometries”. *Phys. Rev. A* 95 (2017), p. 063603. DOI: [10.1103/PhysRevA.95.063603](https://doi.org/10.1103/PhysRevA.95.063603) (cit. on p. 181).
- [724] K. Biedroń, M. Łącki, and J. Zakrzewski. “Extended Bose-Hubbard model with dipolar and contact interactions”. *Phys. Rev. B* 97 (2018), p. 245102. DOI: [10.1103/physrevb.97.245102](https://doi.org/10.1103/physrevb.97.245102) (cit. on p. 181).
- [725] A. Hayashi, S. Mondal, T. Mishra, and B. P. Das. *Competing insulating phases of dipolar bosons in a dimerized optical lattice*. 2021. arXiv: [2111.02224](https://arxiv.org/abs/2111.02224) (cit. on p. 181).
- [726] R. Kraus, T. Chanda, J. Zakrzewski, and G. Morigi. *Quantum phases of dipolar bosons in one-dimensional optical lattices*. 2021. arXiv: [2112.10386](https://arxiv.org/abs/2112.10386) (cit. on p. 181).
- [727] J. Quintanilla, S. T. Carr, and J. J. Betouras. “Metanematic, smectic, and crystalline phases of dipolar fermions in an optical lattice”. *Phys. Rev. A* 79 (2009), p. 031601. DOI: [10.1103/physreva.79.031601](https://doi.org/10.1103/physreva.79.031601) (cit. on pp. 181, 182).

- [728] Y.-P. Huang and D.-W. Wang. “Quantum phase diagrams of fermionic dipolar gases in a planar array of one-dimensional tubes”. *Phys. Rev. A* 80 (2009), p. 053610. DOI: [10.1103/physreva.80.053610](https://doi.org/10.1103/physreva.80.053610) (cit. on p. 181).
- [729] S. T. Carr, J. Quintanilla, and J. J. Betouras. “Lifshitz transitions and crystallization of fully polarized dipolar fermions in an anisotropic two-dimensional lattice”. *Phys. Rev. B* 82 (2010), p. 045110. DOI: [10.1103/PhysRevB.82.045110](https://doi.org/10.1103/PhysRevB.82.045110) (cit. on p. 181).
- [730] Y. L. Zhou, M. Ortner, and P. Rabl. “Long-range and frustrated spin-spin interactions in crystals of cold polar molecules”. *Phys. Rev. A* 84 (2011), p. 052332. DOI: [10.1103/physreva.84.052332](https://doi.org/10.1103/physreva.84.052332) (cit. on p. 181).
- [731] C. Mora, O. Parcollet, and X. Waintal. “Quantum melting of a crystal of dipolar bosons”. *Phys. Rev. B* 76 (2007), p. 064511. DOI: [10.1103/PhysRevB.76.064511](https://doi.org/10.1103/PhysRevB.76.064511) (cit. on p. 181).
- [732] A. Macia, J. Boronat, and F. Mazzanti. “Phase diagram of dipolar bosons in two dimensions with tilted polarization”. *Phys. Rev. A* 90 (2014), 061601(R). DOI: [10.1103/PhysRevA.90.061601](https://doi.org/10.1103/PhysRevA.90.061601) (cit. on p. 181).
- [733] Z.-K. Lu, Y. Li, D. S. Petrov, and G. V. Shlyapnikov. “Stable Dilute Supersolid of Two-Dimensional Dipolar Bosons”. *Phys. Rev. Lett.* 115 (2015), p. 075303. DOI: [10.1103/PhysRevLett.115.075303](https://doi.org/10.1103/PhysRevLett.115.075303) (cit. on p. 181).
- [734] P. Shen and K. F. Quader. “Finite-temperature instabilities of a two-dimensional dipolar Bose gas at arbitrary tilt angle”. *Phys. Rev. A* 103 (2021), p. 043317. DOI: [10.1103/physreva.103.043317](https://doi.org/10.1103/physreva.103.043317) (cit. on p. 181).
- [735] Z.-K. Lu and G. V. Shlyapnikov. “Fermi liquid of two-dimensional polar molecules”. *Phys. Rev. A* 85 (2012), p. 023614. DOI: [10.1103/PhysRevA.85.023614](https://doi.org/10.1103/PhysRevA.85.023614) (cit. on p. 181).
- [736] T. Comparin, R. Bombín, M. Holzmann, F. Mazzanti, J. Boronat, and S. Giorgini. “Two-dimensional mixture of dipolar fermions: Equation of state and magnetic phases”. *Phys. Rev. A* 99 (2019), p. 043609. DOI: [10.1103/PhysRevA.99.043609](https://doi.org/10.1103/PhysRevA.99.043609) (cit. on p. 181).
- [737] T. Bilitewski, L. D. Marco, J.-R. Li, K. Matsuda, W. G. Tobias, G. Valtolina, J. Ye, and A. M. Rey. “Dynamical Generation of Spin Squeezing in Ultracold Dipolar Molecules”. *Phys. Rev. Lett.* 126 (2021), p. 113401. DOI: [10.1103/physrevlett.126.113401](https://doi.org/10.1103/physrevlett.126.113401) (cit. on p. 181).
- [738] P. Sengupta, L. P. Pryadko, F. Alet, M. Troyer, and G. Schmid. “Supersolids versus Phase Separation in Two-Dimensional Lattice Bosons”. *Phys. Rev. Lett.* 94 (2005), p. 207202. DOI: [10.1103/PhysRevLett.94.207202](https://doi.org/10.1103/PhysRevLett.94.207202) (cit. on p. 182).
- [739] R. Barnett, D. Petrov, M. Lukin, and E. Demler. “Quantum Magnetism with Multicomponent Dipolar Molecules in an Optical Lattice”. *Phys. Rev. Lett.* 96 (2006), p. 190401. DOI: [10.1103/physrevlett.96.190401](https://doi.org/10.1103/physrevlett.96.190401) (cit. on p. 182).
- [740] K. P. Schmidt, J. Dorier, and A. M. Läuchli. “Solids and Supersolids of Three-Body Interacting Polar Molecules on an Optical Lattice”. *Phys. Rev. Lett.* 101 (2008), p. 150405. DOI: [10.1103/PhysRevLett.101.150405](https://doi.org/10.1103/PhysRevLett.101.150405) (cit. on p. 182).
- [741] I. Danshita and C. A. R. Sá de Melo. “Stability of Superfluid and Supersolid Phases of Dipolar Bosons in Optical Lattices”. *Phys. Rev. Lett.* 103 (2009), p. 225301. DOI: [10.1103/PhysRevLett.103.225301](https://doi.org/10.1103/PhysRevLett.103.225301) (cit. on p. 182).
- [742] N. Y. Yao, A. V. Gorshkov, C. R. Laumann, A. M. Läuchli, J. Ye, and M. D. Lukin. “Realizing Fractional Chern Insulators in Dipolar Spin Systems”. *Phys. Rev. Lett.* 110 (2013), p. 185302. DOI: [10.1103/PhysRevLett.110.185302](https://doi.org/10.1103/PhysRevLett.110.185302) (cit. on p. 182).
- [743] J. Zhang, C. Zhang, J. Yang, and B. Capogrosso-Sansone. *Supersolid phases of lattice dipoles tilted in three-dimensions*. 2022. arXiv: [2201.03756](https://arxiv.org/abs/2201.03756) (cit. on p. 182).
- [744] E. Lake, M. Hermele, and T. Senthil. *The dipolar Bose-Hubbard model*. 2022. arXiv: [2201.04132](https://arxiv.org/abs/2201.04132) (cit. on p. 182).

- [745] C. Lin, E. Zhao, and W. V. Liu. “Liquid crystal phases of ultracold dipolar fermions on a lattice”. *Phys. Rev. B* 81 (2010), p. 045115. DOI: [10.1103/PhysRevB.81.045115](https://doi.org/10.1103/PhysRevB.81.045115) (cit. on p. 182).
- [746] K. A. Kuns, A. M. Rey, and A. V. Gorshkov. “ $d$ -wave superfluidity in optical lattices of ultracold polar molecules”. *Phys. Rev. A* 84 (2011), p. 063639. DOI: [10.1103/PhysRevA.84.063639](https://doi.org/10.1103/PhysRevA.84.063639) (cit. on p. 182).
- [747] L. He and W. Hofstetter. “Supersolid phase of cold fermionic polar molecules in two-dimensional optical lattices”. *Phys. Rev. A* 83 (2011), p. 053629. DOI: [10.1103/physreva.83.053629](https://doi.org/10.1103/physreva.83.053629) (cit. on p. 182).
- [748] A. V. Gorshkov, S. R. Manmana, G. Chen, J. Ye, E. Demler, M. D. Lukin, and A. M. Rey. “Tunable Superfluidity and Quantum Magnetism with Ultracold Polar Molecules”. *Phys. Rev. Lett.* 107 (2011), p. 115301. DOI: [10.1103/PhysRevLett.107.115301](https://doi.org/10.1103/PhysRevLett.107.115301) (cit. on p. 182).
- [749] A. V. Gorshkov, S. R. Manmana, G. Chen, E. Demler, M. D. Lukin, and A. M. Rey. “Quantum magnetism with polar alkali-metal dimers”. *Phys. Rev. A* 84 (2011), p. 033619. DOI: [10.1103/physreva.84.033619](https://doi.org/10.1103/physreva.84.033619) (cit. on p. 182).
- [750] S. G. Bhongale, L. Mathey, S.-W. Tsai, C. W. Clark, and E. Zhao. “Bond Order Solid of Two-Dimensional Dipolar Fermions”. *Phys. Rev. Lett.* 108 (2012), p. 145301. DOI: [10.1103/PhysRevLett.108.145301](https://doi.org/10.1103/PhysRevLett.108.145301) (cit. on p. 182).
- [751] S. G. Bhongale, L. Mathey, S.-W. Tsai, C. W. Clark, and E. Zhao. “Unconventional spin-density waves in dipolar Fermi gases”. *Phys. Rev. A* 87 (2013), p. 043604. DOI: [10.1103/PhysRevA.87.043604](https://doi.org/10.1103/PhysRevA.87.043604) (cit. on p. 182).
- [752] O. Dutta, T. Sowiński, and M. Lewenstein. “Orbital physics of polar Fermi molecules”. *Phys. Rev. A* 87 (2013), p. 023619. DOI: [10.1103/physreva.87.023619](https://doi.org/10.1103/physreva.87.023619) (cit. on p. 182).
- [753] G. K. Brennen, A. Micheli, and P. Zoller. “Designing spin-1 lattice models using polar molecules”. *New J. Phys.* 9 (2007), pp. 138–138. DOI: [10.1088/1367-2630/9/5/138](https://doi.org/10.1088/1367-2630/9/5/138) (cit. on p. 182).
- [754] H. Weimer. “Quantum simulation of many-body spin interactions with ultracold polar molecules”. *Mol. Phys.* 111 (2013), pp. 1753–1758. DOI: [10.1080/00268976.2013.789567](https://doi.org/10.1080/00268976.2013.789567) (cit. on p. 182).
- [755] S. R. Manmana, E. M. Stoudenmire, K. R. A. Hazzard, A. M. Rey, and A. V. Gorshkov. “Topological phases in ultracold polar-molecule quantum magnets”. *Phys. Rev. B* 87 (2013), p. 081106. DOI: [10.1103/physrevb.87.081106](https://doi.org/10.1103/physrevb.87.081106) (cit. on p. 182).
- [756] L. Pollet, J. D. Picon, H. P. Büchler, and M. Troyer. “Supersolid Phase with Cold Polar Molecules on a Triangular Lattice”. *Phys. Rev. Lett.* 104 (2010), p. 125302. DOI: [10.1103/PhysRevLett.104.125302](https://doi.org/10.1103/PhysRevLett.104.125302) (cit. on p. 182).
- [757] D. Yamamoto, I. Danshita, and C. A. R. Sá de Melo. “Dipolar bosons in triangular optical lattices: Quantum phase transitions and anomalous hysteresis”. *Phys. Rev. A* 85 (2012), p. 021601. DOI: [10.1103/physreva.85.021601](https://doi.org/10.1103/physreva.85.021601) (cit. on p. 182).
- [758] A. V. Gorshkov, K. R. Hazzard, and A. M. Rey. “Kitaev honeycomb and other exotic spin models with polar molecules”. *Mol. Phys.* 111 (2013), pp. 1908–1916. DOI: [10.1080/00268976.2013.800604](https://doi.org/10.1080/00268976.2013.800604) (cit. on p. 182).
- [759] N. Y. Yao, M. P. Zaletel, D. M. Stamper-Kurn, and A. Vishwanath. “A quantum dipolar spin liquid”. *Nature Physics* 14 (2018), pp. 405–410. DOI: [10.1038/s41567-017-0030-7](https://doi.org/10.1038/s41567-017-0030-7) (cit. on p. 182).
- [760] K. Fukui, Y. Kato, J. Nasu, and Y. Motome. *Feasibility of Kitaev quantum spin liquids in ultracold polar molecules*. 2022. arXiv: [2204.06144](https://arxiv.org/abs/2204.06144) (cit. on p. 182).
- [761] K. Góral, K. Rzażewski, and T. Pfau. “Bose-Einstein condensation with magnetic dipole-dipole forces”. *Phys. Rev. A* 61 (2000), p. 051601. DOI: [10.1103/PhysRevA.61.051601](https://doi.org/10.1103/PhysRevA.61.051601) (cit. on p. 182).

- [762] M. Schmidt, L. Lassablière, G. Quéméner, and T. Langen. “Self-bound dipolar droplets and supersolids in molecular Bose-Einstein condensates”. *Phys. Rev. Research* 4 (2022), p. 013235. DOI: [10.1103/PhysRevResearch.4.013235](https://doi.org/10.1103/PhysRevResearch.4.013235) (cit. on p. 182).
- [763] M. A. Baranov, M. S. Mar’enko, V. S. Rychkov, and G. V. Shlyapnikov. “Superfluid pairing in a polarized dipolar Fermi gas”. *Phys. Rev. A* 66 (2002), p. 013606. DOI: [10.1103/physreva.66.013606](https://doi.org/10.1103/physreva.66.013606) (cit. on p. 182).
- [764] B. M. Fregoso, K. Sun, E. Fradkin, and B. L. Lev. “Biaxial nematic phases in ultracold dipolar Fermi gases”. *New J. Phys.* 11 (2009), p. 103003. DOI: [10.1088/1367-2630/11/10/103003](https://doi.org/10.1088/1367-2630/11/10/103003) (cit. on p. 182).
- [765] A. R. P. Lima and A. Pelster. “Collective motion of polarized dipolar Fermi gases in the hydrodynamic regime”. *Phys. Rev. A* 81 (2010), p. 021606. DOI: [10.1103/physreva.81.021606](https://doi.org/10.1103/physreva.81.021606) (cit. on p. 182).
- [766] T. Shi, J.-N. Zhang, C.-P. Sun, and S. Yi. “Singlet and triplet Bardeen-Cooper-Schrieffer pairs in a gas of two-species fermionic polar molecules”. *Phys. Rev. A* 82 (2010), p. 033623. DOI: [10.1103/physreva.82.033623](https://doi.org/10.1103/physreva.82.033623) (cit. on p. 182).
- [767] C. Zhao, L. Jiang, X. Liu, W. M. Liu, X. Zou, and H. Pu. “Hartree-Fock-Bogoliubov theory of dipolar Fermi gases”. *Phys. Rev. A* 81 (2010), p. 063642. DOI: [10.1103/physreva.81.063642](https://doi.org/10.1103/physreva.81.063642) (cit. on p. 182).
- [768] F. Wächtler, A. R. P. Lima, and A. Pelster. “Low-lying excitation modes of trapped dipolar Fermi gases: From the collisionless to the hydrodynamic regime”. *Phys. Rev. A* 96 (2017), p. 043608. DOI: [10.1103/physreva.96.043608](https://doi.org/10.1103/physreva.96.043608) (cit. on p. 182).
- [769] V. Veljić, A. Pelster, and A. Balaž. “Stability of quantum degenerate Fermi gases of tilted polar molecules”. *Phys. Rev. Research* 1 (2019), p. 012009. DOI: [10.1103/physrevresearch.1.012009](https://doi.org/10.1103/physrevresearch.1.012009) (cit. on p. 182).
- [770] D.-W. Wang, M. D. Lukin, and E. Demler. “Quantum Fluids of Self-Assembled Chains of Polar Molecules”. *Phys. Rev. Lett.* 97 (2006), p. 180413. DOI: [10.1103/PhysRevLett.97.180413](https://doi.org/10.1103/PhysRevLett.97.180413) (cit. on p. 182).
- [771] W. Lechner and P. Zoller. “From Classical to Quantum Glasses with Ultracold Polar Molecules”. *Phys. Rev. Lett.* 111 (2013), p. 185306. DOI: [10.1103/PhysRevLett.111.185306](https://doi.org/10.1103/PhysRevLett.111.185306) (cit. on p. 182).
- [772] A. C. Potter, E. Berg, D.-W. Wang, B. I. Halperin, and E. Demler. “Superfluidity and Dimerization in a Multilayered System of Fermionic Polar Molecules”. *Phys. Rev. Lett.* 105 (2010), p. 220406. DOI: [10.1103/PhysRevLett.105.220406](https://doi.org/10.1103/PhysRevLett.105.220406) (cit. on p. 182).
- [773] J. K. Block, N. T. Zinner, and G. M. Bruun. “Density wave instabilities of tilted fermionic dipoles in a multilayer geometry”. *New J. Phys.* 14 (2012), p. 105006. DOI: [10.1088/1367-2630/14/10/105006](https://doi.org/10.1088/1367-2630/14/10/105006) (cit. on p. 182).
- [774] C. Trefzger, C. Menotti, and M. Lewenstein. “Pair-Supersolid Phase in a Bilayer System of Dipolar Lattice Bosons”. *Phys. Rev. Lett.* 103 (2009), p. 035304. DOI: [10.1103/PhysRevLett.103.035304](https://doi.org/10.1103/PhysRevLett.103.035304) (cit. on p. 182).
- [775] G. A. Domínguez-Castro and R. Paredes. “Unconventional Superfluidity in Ultracold Dipolar Gases”. *J. Phys. Conf. Ser.* 1540 (2020), p. 012002. DOI: [10.1088/1742-6596/1540/1/012002](https://doi.org/10.1088/1742-6596/1540/1/012002) (cit. on p. 182).
- [776] T. Schuster, F. Flicker, M. Li, S. Kotochigova, J. E. Moore, J. Ye, and N. Y. Yao. “Realizing Hopf Insulators in Dipolar Spin Systems”. *Phys. Rev. Lett.* 127 (2021), p. 015301. DOI: [10.1103/PhysRevLett.127.015301](https://doi.org/10.1103/PhysRevLett.127.015301) (cit. on p. 182).

- [777] T. Schuster, F. Flicker, M. Li, S. Kotochigova, J. E. Moore, J. Ye, and N. Y. Yao. “Floquet engineering ultracold polar molecules to simulate topological insulators”. *Phys. Rev. A* 103 (2021), p. 063322. DOI: [10.1103/physreva.103.063322](https://doi.org/10.1103/physreva.103.063322) (cit. on p. 182).

# Acknowledgements

From the first day to the last of my PhD, everything that happened in the Molecules lab was teamwork, and it was a privilege to be a part of it. First and foremost, I therefore have to thank my team.

Marcel, you are my brother-in-science. Having joined the lab a few months after me, you quickly surpassed me (and everyone else) at machine-whispering. You coerced the last bit of performance out of the available equipment, even when confronted with the most daunting high-dimensional optimisation problems. I think I can go as far as to say that degenerate NaK would not have happened without you. You have also become a valued friend, both in the best times (doing stupid accents, talking about travel adventures) and in the worst (lending your support when the going got tough). Whatever you do, I wish all the best to you, to Denise, and to little Livi!

Xingyan, you are the third in the molecule brotherhood. You joined the lab as a Master student, already a better theoretician than the rest of us ever hoped to be. Exclaiming “Oh, it’s simple!”, you wrote down equations, in the air if no board was available, solving problems in a few seconds that took us mortals hours. Without a doubt, you caught the worst of the pandemic, being stuck in Wuhan for half a year following the outbreak, only to come back to Germany and go right back into lockdown. Not the ideal beginning for your PhD! Never to be discouraged, you contributed to our work even from your quarantine half a planet away, and quickly mastered the experiment after your return. Not to forget, your lessons on Chinese culture and language have really broadened my horizon, and I highly appreciated them.

Andreas, you are the most experienced lab member when it comes to molecules and you taught me a lot. More than one important dataset came out the way it did only because you reminded me to avoid some subtle mistake, or because you stayed up until the early morning to make use of the precious hours when the machine was stable. Your patience and attention to detail are second to none, and I don’t want to know how many embarrassing mistakes in our publications we would have missed without you. Thank you also for many spectacular cocktails!

Xinyu, you are the visionary of the team, and our unending source of motivation. You led us into the Age of a Thousand Plans, and no matter how bad things seemed, you always pushed on until the end. Though it was exhausting, in the end I must admit that it was worth it. And although I sometimes had a hard time accepting it, your wisdom and experience proved right more often than not.

During my time, we were lucky to be supported by many exceptionally talented and hard-working Master students: Scott, you built the 3D lattice setup and we spent my first few months together, inserting it into the experiment. I will always fondly remember these days where we learned how to properly route cables, as well as the short time we were flat mates at Olympiadorf. May you soon make degenerate titanium! Benedikt, you became a Bachelor student in our lab the same week I joined, then came back as a HiWi and again as a Master student. I guess you liked it with us, and we certainly liked having you around, not only for your impressive technical skills. Best of luck making strontium atom lasers in Amsterdam! Akira, we shared a very intense time implementing the STIRAP laser system you built. As this was done during the harshest lockdown in April and May 2020, there was only the two of us, and when we went home at night we were never sure if we would find MPQ shut down the next morning. That never happened though, and we went from some breadboards full of half-aligned optics to ground-state molecules in less than five weeks. I am still amazed by this feat, which was only possible due to your highly professional preparation. Renhao, you built our new vertical lattice and the box trap. Due to your creativity, precision and willingness to go the extra mile, both worked wonderfully. And although the box trap was dismantled after only a few months, it brought us our most unexpected result. Good luck to you too, both for your Rydberg atoms and as a PhD representative (in good Molecules tradition!)

The Molecules lab would never have gotten to where it is today without those who started it, who built the vacuum chamber and the laser systems, and who made the first ground-state molecules: Christoph, Niko, Zhenkai, and Frauke. I met all of you during my time as a Master student, and some again at the beginning of my PhD. Back then, the Molecules lab was still the ugly duckling at MPQ, and look at the swan it has become! Sadly, it took too long to grow up, and now you are no longer here to witness this. All the more reason to thank you for everything you have done.

Sebastian and Shrestha, you are the upcoming generation of Molecule PhDs. Soon you will take over, and I have to say I envy you a bit. The most exciting opportunities yet lie ahead, and you will be the ones to take them. Be fearless and be dedicated, and I have no doubt you will do great things!

The philosopher Laozi said “The best leader values his words, and uses them sparingly. When he has accomplished his task, the people say: Amazing, we did it, all by ourselves!” Immanuel, you have been such a leader to the Molecules team. When it counted, you had our back. Thank you also for giving me a second chance after my excursion into industry. Coming back was one of the best decisions of my life.

I would also like to thank the entire Bloch group, both at LMU and MPQ. You were always ready to help with any problem or to have a beer. We were all in this together, and I will surely miss the wonderful spirit of comradery that we shared. Special mention goes to Simon Hollerith for proofreading and for teaching me many fascinating things about music, to Sarah Hirthe for the design of the automatic rotation mount and for being the heart and soul of the group, and to Nikolaus Lorenz for help with the ULE-cavity vacuum setup. Thank you also to the technicians and engineers: Karsten, Anton, Olivia, Bodo, the team of the MPQ workshop, and the house technicians. No challenge was too great for you, and I often stood in awe of the elegance and quality of the many things you designed

or built for our lab. Finally, I thank the administrative team, Ildiko, Doreen, Valeria, and most importantly Kristina. You were always available for help, and I greatly appreciated your enthusiasm for organising social events and workshops, which even the pandemic could not stop.

One of the most exciting times of my PhD was September and October 2020, when we saw the molecules disappear from the box trap, and could not make sense of it. We doubted everything from the laser frequency to our own sanity, until we finally began to believe the “impossible” observation. Our theory collaborators Arthur Christianen, Tijs Karman, Goulven Quéméner, and Gerrit Groenenboom were with us in many Zoom conferences, leaving no stone unturned to figure out the mystery. Back then, we came up empty, but I’m sure this will not remain the case for much longer!

Over the years, we also received a lot of valuable input from Nadia Bouloufa-Maafa, Olivier Dulieu, Svetlana Kotochigova, Ming Li, Tao Shi, and Romain Vexiau. Our first STIRAP system, finding the transition to the  $b^3\Pi_0$  state, and choosing the right wavelength for potassium compression would not have been possible without you. Thanks to all of you!

The most difficult part of writing this dissertation was without a doubt the introduction and historical overview. Sometimes, I realised that reading papers could only take me so far, and I had to ask experts or eyewitnesses to get a feeling for the situations I wanted to describe. I was lucky to always get quick and helpful answers! For their invaluable help with this project, I thank (in alphabetical order) Andreas Bluhm, Arthur Christianen, Shiqian Ding, Scott Eustice, Fang Fang, Manuel Gerken, Christiane Koch, Silke Ospelkaus, Anbang Yang, and Martin Zeppenfeld. I also thank Lea Boßmann for taking time out of her extremely busy schedule to proofread my ramblings.

The Molecules’ success would not have been possible without all of you. It has been the greatest pleasure working with you.